2006:34

DOCTORAL THESIS

L

Synthesis and Characterization of Zeolite Films and Membranes

Magdalena Gualtieri

Luleå University of Technology
Department of Chemical Engineering and Geosciences
Division of Chemical Technology

2006:34 | ISSN: 1402-1544 | ISRN: LTU-DT -- 06/34 -- SE

Synthesis and Characterization of Zeolite Films and Membranes

Magdalena Gualtieri

September 2006

Department of Chemical Engineering and Geosciences
Division of Chemical Technology
Luleå University of Technology, Luleå, Sweden

ABSTRACT

In this work, a seeding technique was used to synthesize films and membranes of FAU, LTA and MFI type zeolites. In the first part, hydrothermal growth was performed without organic template molecules, which resulted in template-free zeolite films and membranes. The samples were characterized by Scanning Electron Microscopy, X-ray Powder Diffraction and permeation measurements with gaseous probe molecules. Thin films of FAU-type zeolite were prepared on polished single crystals. The thickness and morphology of the films could be controlled by varying the synthesis conditions. Preparation of LTA-type membranes was also attempted. However, the membranes cracked during drying at temperatures above room temperature. Template free MFI membranes with higher quality could be prepared. These membranes had a maximum separation factor α of 17.8 at 220 °C for a *n*-butane/*i*-butane mixture. Cracks formed at temperatures higher than 250 °C. Crack formation in zeolite membranes at high temperatures has also been reported by several other groups. Since no model for the crack formation process has been established in the literature, the second part of this work was devoted to study crack formation and to develop a model. Relatively thick (ca 1800 nm) α-alumina supported MFI films, prepared using organic template molecules (TPA^+), were selected for the study since data on crack formation in the form of SEM images and permeation measurements for these membranes had been obtained in earlier work by the group. These membranes were further studied by *in-situ* High Temperature X-ray Powder Diffraction experiments in the present work. In addition, MFI powder and a blank α-alumina support were also investigated. Data were collected with the aid of a Synchrotron radiation facility as well as with a conventional laboratory instrument for the temperature cycle 25-500-25 °C. The Rietveld method was used to determine the unit cell parameters of MFI and α-

alumina as well as the TPA^+ occupancy of MFI. The out-of-plane strain (i.e. strain in the direction perpendicular to the film surface) in the film and the support was calculated. In addition, the microstructure of the support was investigated by pattern decomposition and Williamson-Hall plots. In agreement with previous reports in the literature, it was found that the TPA-MFI structure contracts as a consequence of template removal and possibly also a structure intrinsic mechanism and the α-alumina support expands. Hence, a large thermal expansion mismatch occurs in the membranes during heating. An overall out-of-plane compressive strain was observed for the MFI film during heating, which indicates an in-plane tensile stress (i.e. in the direction parallel to the film surface) in the film. This result was explained by the larger expansion of the support, compared to the film. The α-alumina support was also found to be under an overall out-of-plane compressive strain at non-ambient temperatures, presumably due to zeolite in the pores of the support. The microstrain for the MFI coated α-alumina support increased during heating, and remained during cooling, which indicate the formation of structural defects in the support. Based on these results and results from earlier work, a model for crack formation was proposed: In the thick films (ca 1800 nm) studied in the present work, the crystals are well intergrown. During heating, the MFI crystals contracts and the α-alumina support expands. Consequently, a thermal stress develops in the composite which eventually leads to formation of cracks. In addition, part of the stress is also released via formation of structural defects in the α-alumina support. In thinner films (ca 500 nm), the crystals are less well intergrown and the thermal expansion mismatch between the crystals in the film and the support leads to opening of grain boundaries in the film rather than cracks.

LIST OF PUBLICATIONS

I **Synthesis of thin zeolite Y films on polished α-alumina wafers using a seeding technique**

Magdalena Lassinanti, Jonas Hedlund and Johan Sterte,

Porous Materials in Environmentally Friendly Processes, Editors. I. Kiricsi, G. Pál-Borbély, J.B.Nagy and H.G. Karge, Elsevier, Amsterdam, 181-187 (1999).

II **Faujasite-type films synthesized by seeding**

Magdalena Lassinantti, Jonas Hedlund and Johan Sterte

Microporous and Mesoporous Materials, 38 (2000) 25-34.

III **Preparation and evaluation of thin ZSM-5 membranes synthesized in the absence of organic template molecules**

Magdalena Lassinantti, Fredrik Jareman, Jonas Hedlund, Derek Creaser and Johan Sterte

Catalysis Today, 67 (2001) 109-119.

IV **Effects of synthesis parameters on intra-pore zeolite formation in zeolite A membranes**

Magdalena Lassinantti, Jonas Hedlund, Johan Sterte

Studies in Surface Science and Catalysis 135. Proceedings of the 13th international zeolite conference, Montpellier, France, 8-13 July, 20-P-10, 2001.

V **Accurate measurement of the thermal expansion of MFI zeolite membranes by *in-situ* HT-XRPD**

Magdalena Lassinantti Gualtieri, Alessandro F. Gualtieri, Jonas Hedlund, Fredrik Jareman, Johan Sterte and Monica Dapiaggi

Proc. 14th International Zeolite Conference. E. van Steen et al. Eds (2004) 703.

VI **The influence of heating rate on template removal in silicalite-1: an *in situ* HT-XRPD study**

Magdalena Lassinantti Gualtieri, Alessandro F. Gualtieri and Jonas Hedlund

Microporous and Mesoporous Materials, 89 (2005) 1-8.

VII **Crack formation in α-alumina supported MFI zeolite membranes studied by *in situ* High Temperature Synchrotron Powder Diffraction**

Magdalena Lassinantti Gualtieri, Alessandro F. Gualtieri, Charlotte Andersson, Jonas Hedlund, Fredrik Jareman, Matteo Leoni and Carlo Meneghini

Submitted to Journal of Membrane Science

INDEX

1. INTRODUCTION

1.1 What is a zeolite?

Zeolites are alumino-silicates with an open structure composed of a three-dimensional network of $[SiO_4]^{4-}$ and $[AlO_4]^{5-}$ tetrahedra sharing all the corners with each other. The pores are of molecular dimensions and are defined by the crystal structure. Zeolites may be found in nature as minerals and also synthesized in the laboratory. A general formula for the chemical composition may be expressed as:

$$\left(M^{+},0.5M^{2+}\right)_m\left[Al_mSi_{x-m}O_{2x}\right]\cdot nH_2O$$

where M = extra-framework cation. The exchange of silicon for aluminum in the framework results in a net negative charge, which must be compensated by extra-framework cations. In general, these may be any alkali, alkaline earth or rare earth cations as well as organic cations such as the tetrapropylammonium ion. In addition to the neutralizing cations, the voids (cages and channels) usually contain water or organic molecules that must be removed by heating in order to activate the material, i.e. render the pores of the structure available for guest molecules. Si may be substituted for other tetrahedrally coordinated elements such as B, Ti, Fe and Ga, forming zeolite-like materials. Hence further tailoring of the materials for a specific purpose is possible.

Depending on the structure, the size of the pores is in the range 3 to 13 Å [1]. Such pores are called *micropores* (i.e. d < 2 nm), according to the International Union of Pure and Applied Chemistry (IUPAC). The apertures are bounded by oxygen atoms of connected tetrahedras in rings involving 6, 8, 10 or 12 oxygen atoms. However, other factors such as the location, size and coordination of the extra-framework cations are also influencing pore size. A good example is zeolite A, in which the size of the pore openings can be tailored by using extra-framework cations of different sizes.

The interconnected regular three-dimensional network of micropores, the Si/Al ratio and the nature and content of the extra-framework cations are key factors determining the physical and chemical properties of zeolites. The well-defined micropores give the zeolites molecular sieving properties, i.e. if the molecule is larger than the pore size, it will not enter the structure. In fact, zeolites are also called “molecular sieves” which are structures able to separate molecules on size basis. As the Si/Al ratio decreases, the surface becomes more hydrophilic and more cations are needed to compensate the negative charges introduced by aluminum. The extra-framework cations are in many cases exchangeable, which allows for the introduction of acid sites bonded to the non-saturated oxygen atoms.

The framework topologies are represented by three capital letters, in accordance with the recommendations of the IUPAC committee on chemical nomenclature of zeolites.

Zeolites with three different topologies were investigated in this work; Zeolite Y (FAU), zeolite A (LTA) and ZSM-5/silicalite-1 (MFI). These structures are shown in Figure 1.

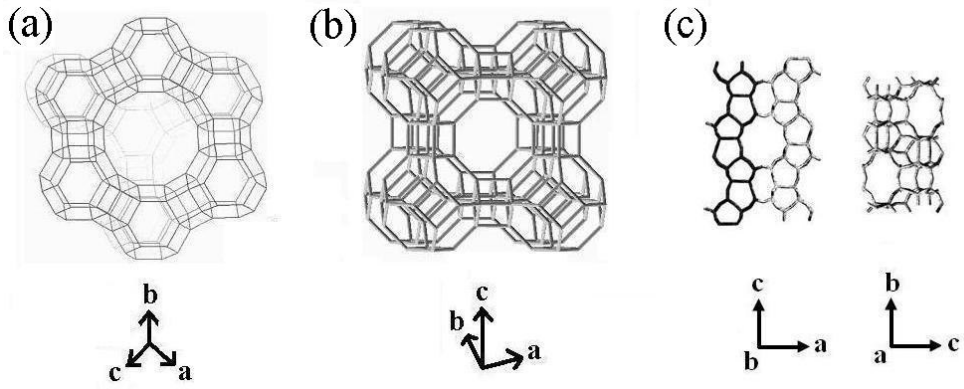

Figure 1. The framework of FAU, LTA and MFI is shown in (a), (b) and (c), respectively.

All of them have found important industrial applications and are therefore synthesized on a large scale. Zeolite Y and X are the synthetic analogues to the natural faujasite. The difference between these two zeolites is the Si/Al ratio, which is 1-1.5 and 1.5-3 in zeolite X and Y, respectively [2]. Zeolite A has a Si/Al ratio of ca. 1 [3]. ZSM-5 can be synthesized with Si/Al ratios in the range 5-100 [4]. Silicalite-1 is the aluminum-free form of ZSM-5, and is prepared using organic template molecules (discussed further in section 1.3). A zeolite mineral with the MFI topology, mutinaite, was also discovered [5].

The FAU- and LTA-type structures are cubic with a three-dimensional pore system (Figure 1a and b, respectively). The equidimensional channels intersect in a perpendicular fashion. The free aperture diameter for the channels is 8 and 4 Å in NaY [6] and NaA [3], respectively. MFI type materials have two stable symmetries: monoclinic and orthorhombic at low and high temperature, respectively. The phase transition is reversible and the transition temperature for HZSM-5 with a Si/Al ratio of 300 is ca 70 °C [7]. However, the temperature of transition depends on the Si/Al ratio [8] and the presence/absence of guest molecules such as water [8] and organic compounds [9]. MFI type zeolite has a two-dimensional pore system consisting of sinusoidal channels (5.1×5.5 Å) running in the a-direction and intersecting straight channels (5.3×5.6 Å) running along b [10] (Figure 1c).

1.2 Thermal expansion of zeolites

Generally, zeolites exhibit the unusual phenomenon of intrinsic negative thermal expansion (NTE), i.e. materials which contract on heating. The phenomenon is likely correlated to the nature of the channel system [11,12]. Zeolites with two-or three-dimensional channel systems show NTE which was suggested to result from structural expansion into the pores and channels during heating [11]. The positive thermal expansion observed in a few zeolites seems to

be encouraged by high density and one-dimensional pore systems [11,12]. Park et al. investigated the thermal behavior of as-synthesized and calcined forms of MFI, DOH, DDR and MTN [13]. The as-synthesized forms displayed a positive thermal expansion in the temperature range 120-298 K. The calcined materials were investigated in the temperature range 298-1200 K. An expansion of the structures was observed up to 370-520 K (with the exact temperature depending on the structure). Upon further heating, NTE of the materials was observed. The thermal behavior of TPA-MFI has been studied extensively [14-16]. The structure experiences a strong contraction in the temperature interval in which the template molecules are decomposed. The unit cell of the calcined framework is smaller than the as-synthesized one [14,15,17]. Attfield and Sleight used HT-XRPD data and Rietveld refinements to study the thermal behavior of siliceous FAU [18] in the temperature range 25-573 K. A constant thermal expansion of $-4.2\ 10^{-6}\ K^{-1}$ was observed (i.e. NTE). Tschaufeser and Parker [11] performed lattice dynamic calculation for various zeolites to evaluate the thermal expansion behavior. The NTE in FAU observed experimentally by Attfield and Sleight was in perfect agreement with the predicted values. However, the calculations for the Al substituted FAU failed to predict the experimental results from High Resolution Diffraction data reported by Couves et al. [19] who found that NAX expands upon heating above 200 K (the investigated temperature range was 25-293 K). A factor that possibly explained this discrepancy is the presence of water in the zeolite investigated by Couves et al. The charge compensating cations as well as adsorbed water affect the thermal expansion behavior of the zeolite. In particular, bonds between framework oxygen atoms and alkali or alkaline earth cations exhibit large positive thermal expansion. These cations may therefore provide a positive contribution to the thermal expansion of the zeolite. The dynamic lattice calculations by Tschaufeser and Parker show that the siliceous zeolites exhibit a larger NTE than the aluminum containing

analogues [11]. Colantuono et al. showed that the dehydration of zeolite A is accompanied by a strong contraction of the framework [20].

1.3 Zeolite crystallization

Zeolites are often crystallized by hydrothermal treatment of an aqueous synthesis mixture containing a silica source, an aluminum source and an alkali source. Upon mixing the components, a gel is normally precipitated. It is also possible to prepare highly alkaline zeolite precursor mixtures in the form of clear solutions [21].

The composition of the precursor mixture is important and controls the properties of the final product. The Si/Al ratio in the mixture influences the ratio in the zeolite product. Some zeolites, such as ZSM-5, crystallize in a very broad range of Si/Al ratios in the starting gel. For other structure types, such as zeolite A and the FAU-type zeolites, the range is very narrow. The hydroxide content of the system influences the nature of the species present in the reaction mixture, the concentration of the dissolved components, the charge of these species and the rate of hydrolysis or exchange between solid and liquid phases or between different species in solution. Thus, it is obvious that the alkalinity in the synthesis batch influences the final composition and structure type [22]. For example, as the silica species are more soluble than alumina species, an increased pH may favor the formation of zeolites with a lower Si/Al ratio [22]. The primary role of the inorganic cations added in the synthesis gel is to compensate the negative charge introduced in the framework by Al. However, they may also have a structure directing role, i.e. the addition of the cations results in the crystallization of a zeolite which otherwise would not have formed. One example of this is sodium in the crystallization of LTA and FAU [23]. These cations are frequently referred to as *templates* or *structure directing agents (SDA)*. Organic cations, such as tetrapropylammonium (TMA^+) and

tetrapropylammonium (TPA^+), may also be used as framework charge compensator and templates. Due to the large size of these compounds, the number of negative Al centers they can neutralize is limited. Hence, the Si/Al ratio can be increased in a given structure by exchanging the conventional alkali cations for organic ones in the synthesis mixture. For example, silicalite-1, the aluminum-free analog of ZSM-5, is obtained by large organic cations as templates. The most common SDA for the crystallization of MFI zeolite is TPA^+. The ions are found in the intersection of the straight and sinusoidal channels [24]. Figure 2 shows a sketch view of the MFI channel system, including the position of the TPA^+ ions. The template molecules block the pores of the zeolite structure and must be removed in order to activate the material. The zeolite activation is usually achieved by calcination, which entails decomposition of the organic molecules at temperature higher than 400 °C. The calcined structure is in protonated form. In the preparation of zeolites for use as acid catalysts, the use of organic cations instead of inorganic ones is an advantage since no exchange of the alkali ions for H^+ via the ammonium ion is necessary to obtain the catalytically active material. The reaction mechanism for

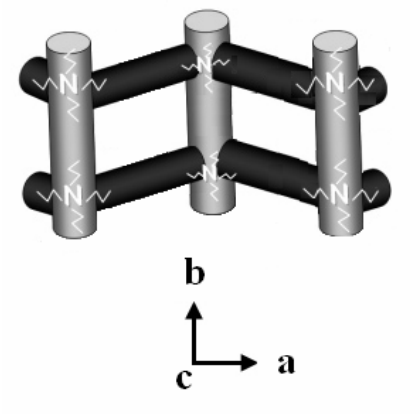

Figure 2. A sketch view of the MFI channel system showing the sinusoidal channels running along the a-direction, and the straight channels running along the b-direction. The TPA^+ template molecules are trapped in the channel intersections.

the TPA^+ decomposition during calcination of MFI type zeolite will be discussed further in section 1.4.

High temperature calcination processes may be unsuitable in many cases, for example for zeolite films prepared on temperature-sensitive supports. In addition, thermal stress may develop at elevated temperatures [15]. Some efforts have been made to find alternative routes for the template removal, in order to avoid these problems. Techniques that have been described in the literature are (i) ozone treatment at moderate temperatures [25], (ii) UV light exposure at near room temperature during which the organic template molecules are degraded and removed from the structure [26] and (iii) the use of structure directing agents degradable by acidic hydrolysis [27].

Other parameters influencing the zeolite synthesis are the purity of the chemicals used as well as the ageing time of the synthesis mixture prior to thermal treatment. For example, aluminum contamination limits the possibility to tailor the Si/Al ratio of the product. Ageing of the synthesis mixture prior to thermal treatment may decrease the duration of the crystallization, alter the size of the crystals in the final product and decrease the induction period [28]. It should be remarked that the chemistry of zeolite synthesis is very complex, and there is no simple way of predicting the optimal conditions for the synthesis of the desired product. However, for practical use, a collection of verified recipes for the crystallization of a large number of zeolite structures was published [29].

In addition to the composition of the synthesis mixture, there are a number of physical parameters that influence the zeolite crystallization. Synthesis time is a very important parameter to control the properties of the product. Crystallization curves representing the conversion of amorphous material to crystalline material as a function of synthesis time can be used to gain information about the reaction kinetics [30]. Such curves are obtained by plotting the amount of crystalline material(s) in the synthesis mixture as a function of synthesis time. Since the desired zeolite is often a metastable product, such curves may be used

to identify the synthesis time for maximum crystallinity and purity under certain conditions. Another important variable is the temperature, which has a direct influence on the crystallization kinetics [31]. In addition, metastable species are decomposed faster at higher temperatures. Stirring of the synthesis mixture modifies the local concentration of the reagents and may result in for example different crystallization kinetics or formation of a different phase [32]. The addition of seed crystals can be used to govern the nature of the final product. For example, Kumakiri et al. showed that depending on the topology of the seed crystals added in the synthesis mixture, both FAU and LTA type zeolite could be obtained as only product using the same synthesis conditions (temperature, duration and precursor solution) [33]. Kacierk et al. studied the growth of FAU using the addition of seeds in synthesis gel with various compositions [34]. It was found that FAU could be obtained as major product using the addition of seed crystals in a synthesis gel which gave zeolite NaP1 as major product in the absence of seeds.

1.4 TPA decomposition in MFI Zeolite

Pyrolytic decomposition of TPA occluded in the as-synthesized MFI structure has been studied extensively by thermal gravimetric analysis (TGA) [35-43], in some studies coupled to mass spectroscopy (MS) for *in-situ* monitoring of the decomposition products [36,42]. Other techniques that have been used are C-NMR [40-41], Si-NMR [39-40] and Infrared (IR) spectroscopy [41,44]. Based on the results from TGA-MS analyses, Parker et al. [36] proposed a model for the decomposition of ion-paired TPA^+ in MFI. According to this model, the first step is a Hofmann elimination reaction, with tripropylamine, propene and water as products (Reaction 1, see below). The second step is a β- elimination of each propyl group with ammonia as a final product (Reaction 2-4, see below).

1. $\left(C_3H_7\right)_4N^+ \cdot OH^- \rightarrow \left(C_3H_7\right)_3N + CH_3 - CH = CH_2 + H_2O$

2. $(C_3H_7)_3N \rightarrow (C_3H_7)_2NH + CH_3 - CH = CH_2$

3. $(C_3H_7)_2NH \rightarrow (C_3H_7)NH_2 + CH_3 - CH = CH_2$

4. $(C_3H_7)NH_2 \rightarrow NH_3 + CH_3 - CH = CH_2$

An analogous mechanism was suggested for the decomposition of TPA^+ ions compensating for the negative charges introduced by Al [36].

Generally, the decomposition of the TPA^+ in the zeolite structure is accompanied by several endothermal DTA peaks whose position, intensity and shape depend on the nature of organic template used [36,41], the amount and nature of trivalent elements incorporated in the structure [35-38], the synthesis medium (OH^-or F^-) [38,41] and the heating rate [43]. Earlier work has shown that TPA^+ ions neutralizing the framework negative charge introduced by Al are more strongly held (hence decompose at a higher temperature) than those not interacting with the (Si-O-Al)- groups [35-38]. The relative amount of TPA^+ decomposed at higher temperature is well correlated with the amount of negative charge of the framework which has to be neutralized by TPA^+ ions [35,38-39]. The low temperature peaks were first assigned to the presence of TPAOH in the zeolite channels [37-38,41]. Later it was suggested that in the commonly used synthesis conditions of MFI zeolite, a large amount of Si-O-R defect groups (R= H, M or TPA) are formed, which recombine under calcination to yield the final healed structure [44]. Hence, the lower temperature DTA peaks were also assigned to the TPA^+ ions, which neutralize the Si-O- negative charges of the defect groups [39-40]. El Hage-Al Asswad et al. assigned the high temperature peak observed in a MFI sample with a high Si/Al ratio to more "relaxed" TPA^+ ions balancing the negative charges introduced by the defect groups [40].

The calcination of the organic template under oxidizing condition is not studied to the same extent, compared to the calcination in an inert atmosphere. However, Gilbert et al. [43] used thermoanalytical techniques (TG, DTA, DTG)

to study the effect of heating rate and gas atmosphere (inert and oxidizing) on the template decomposition in TPA-silicalite-1. Endothermal DTA peaks were detected when the calcination was performed in an inert environment, as found previously (see above). However, under oxidizing conditions (air, oxygen, ozone and air mixture), the template decomposition reaction was found to be net exothermic as expected for an oxidation reaction. By FTIR spectroscopy, Geus and van Bekkum [14] observed the presence of propene in single MFI crystals after partial calcination in air. Hence, the initial Hofmann degradation reaction of TPA was confirmed during calcination in the presence of oxygen.

1.4.1 Defect formation in large MFI crystals

Template decomposition in large MFI crystals may result in intra-crystal cracks [14,45-46]. Soulard et al. studied the template decomposition in fluoride-synthesized MFI crystals by means of thermal analysis techniques (TG, DTG, DTA and DSC) and C-NMR [45]. The dependence of the positions and areas of the DSC peaks on the crystal size were explained by the formation of cracks in larger crystals (150×65×15 μm^3) during the initial Hofmann elimination reaction. In a later work, crack formation during template removal within single crystals with MFI topology (cube-shaped silicalite-1, fluoride-synthesized silicalite-1 and vanadium-containing silicalite-1) was investigated [14]. Light microscopy observations of cracks in the crystals at different stages of the calcination were explained with the aid of complementary results from *in-situ* micro-FTIR spectroscopy and thermogravimetry. For cube-shaped silicalite-1 crystals, the crystal size was correlated to the amount and nature of cracks formed during calcination. In large crystals (> 300 μm length) some straight cracks (not observed in smaller cubes) along the c-axis develop at 260 °C. The occurrence of straight cracks seemed related to the dehydration of the framework, as shown by FTIR spectroscopy and TG, during the initial Hofmann

elimination reaction of TPA (with tripropylamine and propene as products). Random cracking was observed in cube-shaped crystals larger than 150 μm (more severe in larger crystals) as well as fluoride- and vanadium-silicalite. The random cracking coincided with the temperature interval in which the further degradation of tripropylamine via β-elimination reactions occurs, according to FTIR spectroscopy results. Furthermore, a brown color developed within the crystals in that temperature interval. Hence, the author hypothesized that the development of random cracks may be related to the formation of carbonaceous species within the zeolite framework. Pachtova et al. studied the TPA removal in large silicalite-1 crystals of three different dimensions [46]. The calcination was effected in both air and nitrogen. According to *ex-situ* light microscopy, no cracks were observed in the smallest crystal (L_c = 130 μm) after calcination in air. In larger crystals, cracks developed in both air and nitrogen atmosphere. In the medium-sized crystals (L_c = 190 μm), cracks were found after complete template removal, whereas in the largest crystals (L_c = 230 μm) they already appeared after partial calcination. Hence, in concert with previous results [14], the formation of cracks was related to the crystal size. In practice, intra-crystal cracks would have a negative effect on the selectivity of a membrane (see next section). However, the crystals constituting zeolite films are generally elongated perpendicular to the surface (i.e. columnar) and not larger than 1 μm. Therefore, the studies discussed in this section does not necessarily suggest that intra-crystal cracks should be a problem in MFI membranes.

1.5 General about membranes

This section will give a short introduction to membrane technology and some terms frequently used in membrane science will be defined here, as they also will appear in this thesis.

A membrane is a selective permeable barrier, capable of separating components in a gas or a liquid stream in a continuous process. The selectivity is based on differences in physical or chemical properties of the components in the mixture. The driving force for flow through the membrane is a gradient in chemical potential such as a pressure gradient. The *feed* is the mixture to be separated and the *permeate* is the portion of the feed that diffuses through the membrane. The *retentate* is the portion of the feed that does not pass through the membrane. The terms *flux* and *permeance* are frequently encountered. The flux is defined as the flow (mass-, molar- or volumetric flow) per unit area and the permeance is calculated by dividing the flux with the partial pressure gradient over the membrane. Permeation experiments in which the feed is one single compound is referred to as *single permeation*. The ratio of the permeance of two compounds, measured in single permeation experiments, is called *permselectivity* (or *ideal selectivity*). The *separation factor* (or *separation selectivity*), $\alpha_{i,j}$, for a binary mixture of compound *i* and *j* with the molar fraction *x* is defined as:

$$\alpha_{i,j} = \frac{\left(\frac{x_i}{x_j}\right)_{Permeate}}{\left(\frac{x_i}{x_j}\right)_{Feed}} \tag{1.1}$$

A classification of membrane processes in general can be based on the phases of the feed and permeate as well as the driving force for diffusion through the membrane [47]. In microfiltration, ultrafiltration and reverse osmosis, both the feed and the permeate are in the liquid phase. In *pervaporation*, a liquid feed is fed to the membrane and the permeate side of the membrane is kept under vacuum. Hence, the permeate is in gas phase. In fact, the term “pervaporation” is a contraction of “permeation” and “evaporation” [48]. In *gas permeation*, both the feed and the permeate are in gas phase. The *Wicke-Kallenbach* setup is

frequently used, in which a partial pressure difference across the membrane act as the driving force for diffusion. The partial pressure difference is maintained by the use of a sweep gas (often He or N_2) on the permeate side. A difference in absolute pressure across the membrane, referred to as *transmembrane pressure*, can also be used as the driving force for diffusion.

1.6 Zeolite membranes

The thermal and chemical stability combined with high fluxes and selectivity are the main potential advantages of zeolite membranes over organic membranes and other inorganic ones [49-50]. Some groups have prepared free-standing zeolite films which were tested as membranes [51,52]. A major draw-back is that the films have to be thick (for example > 60 μm in [52]) to obtain enough mechanical strength for membrane applications. Consequently, the fluxes are low. In order to prepare thinner films with reasonable fluxes, the majority of zeolite membranes are prepared on porous supports. Generally, the zeolite is prepared as a continuous film on top of the support. However, some groups grow the zeolite in the pores of the support [53-56]. Molecules may be separated on the basis of difference in size and shape (molecular sieving), diffusivity and adsorption strength (preferential adsorption). In preferential adsorption, one component is more strongly adsorbed than others. In this case, larger molecules may permeate more readily than smaller molecules if both components are sufficiently small to enter the pores. The permeation of gases is temperature dependent which is explained by the variation of diffusivity and adsorption with temperature [57]. Zeolite membranes are generally used for processes in which one or both sides of the membrane are in gas phase (i.e pervaporation or gas separation). At the present, there is large research activity, which is reflected in the large number of published papers and filed patents, on this subject. Various zeolites with different pore size and aluminum content such as Faujasite type

structures [58-60], A-type structures [59,61-65] and Ferrierite type structures [66] were investigated in membrane applications. However, most literature concerning this field deals with MFI-type structures and a few examples are given in the reference list [60,67-73]. MFI is a particularly interesting structure type due to the pores with a diameter similar to the kinetic diameter of many industrially important molecules. The high thermal stability (>600 °C [74]) is another important characteristic of this structure. Furthermore, the Si may be substituted by other tetrahedrally coordinated atoms such as B, Al, Ti, Fe and Ga which introduces new properties. Such materials have recently been investigated in membrane applications [75-77].

Zeolite membranes have also a great potential as a component in membrane reactors [78]. A membrane reactor can be used to simultaneously carry out reaction and separation in a continuous process [79]. Zeolite membranes are commonly integrated in so-called packed bed membrane reactors (PBMR) and catalytic membrane reactors (CMR) (see Figure 3) [78]. The membrane may serve to increase the conversion of the equilibrium limited reaction by selective removal of one of the reaction products. Also, the reaction selectivity may be increased by controlled addition of a reactant through the membrane. In PBMR, the reaction is carried out in a packed bed of catalyst pellets or extrudates in the flow stream. In CMR on the other hand, the membrane serves as both a permselective barrier as well as reaction catalyst. For example, Van de Graaf et al. increased the conversion of propene into ethene, cis-2-butene and trans-2-butene by selectively removing trans-2-butene using a silicalite-1 membrane [80-81].

The majority of the applications proposed to date for zeolite membranes are of relatively large scale. For separation processes, excellent results (high fluxes and selectivity) were obtained for isomer separation such as xylenes [67,82]. A major current draw-back for industrialization of large-scale processes involving

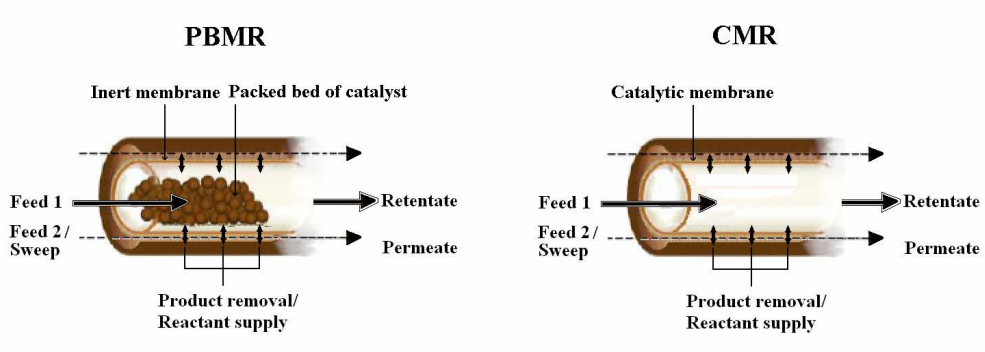

Figure 3. A sketch of a packed bed (a) and catalytic (b) membrane reactor.

zeolite membranes is the high costs for the membranes, mainly due to batch syntheses, expensive chemicals and supports [83]. In the recent years, increased interest was paid to zeolite membranes in small-scale applications [83,84].

A promising micro-scale application for zeolite membranes is sensors. The role of the zeolite is often to enhance the selectivity of an existing sensor by physically separate the interfering molecules from the ones that should be sensed [85-86]. Vilaseca and coworkers [85] studied a Pd-doped SnO_2 semiconductor gas sensor coated with different zeolite type films (LTA and MFI). The response to methane and propane was completely and partly suppressed when the sensor was covered with a film of zeolite LTA and MFI, respectively. The film hinders the diffusion of these molecules to the sensing layer as they do not readily adsorb in the zeolite. The ethanol response is almost not affected as this molecule effectively adsorb and diffuse in the zeolite. The presence of water in the gas stream has a negative effect on the response of all gases. However, the sensor response towards ethanol is still sufficient, as this molecule may compete with water for access to adsorption sites, and hence diffusion towards the sensing layer. Grahn et al. showed that zeolites also have a positive effect on the sensitivity of the sensor, due to effective adsorption of the analyte [87].

1.6.1 Synthesis of supported zeolite films

There are three main routes to synthesize continuous supported zeolite films. A common method is to treat the support directly with a molecular sieve precursor solution, called *in-situ* crystallization or direct synthesis in the literature. Different approaches are discussed in a report by Jansen et al. [88]. Direct synthesis relies on both nucleation and growth of molecular sieve crystals on the surface of the support. The surface chemistry of the support plays a crucial role in the nucleation step and the support must therefore be chosen carefully [89]. The second method, called the vapor phase transport method, was first described by Xu et al. [90]. MFI zeolite was crystallized from an amorphous dry aluminosilicate gel under the vapors of triethylamine (Et_3N), ethylenediamine (EDA) and water. Since then, the method has been used to synthesize membranes of various zeolites such as ANA, MOR, FER and MFI [91-92]. The third, and nowadays the most common method involves the growth of seed crystals attached to the support. When surface seeding is used, nucleation on the support surface is no longer necessary. Hence, the film growth is less sensitive to the support chemistry. An elegant way to obtain a continuous layer of discrete seed crystals is to use colloidal seed crystal sols as precursors. This approach was introduced about ten years ago, and the pioneering work was performed by our group [93-98] and the group of M. Tsapatsis [99-101]. Tsapatsis and coworkers deposited the seed layer by immersing the support in the seed crystal sol and then slowly remove it at a constant speed (also called dip-coating) [99-101]. This procedure has to be repeated several times in order to obtain a satisfactory surface coverage. They used the term “secondary growth” for the subsequent growth of the seed crystals and film formation.

In the method presented by our group, the support surface is modified in order to facilitate seed adsorption from a sol [69,73,93-97,102-107]. The seeds attached to the support are subsequently grown in a synthesis gel under hydrothermal conditions, ultimately forming a dense film. This technique is

denoted *the seed film method*. Figure 4 shows the basic principle of the method. Negatively charged colloidal molecular sieve crystals are electrostatically adsorbed on supports pretreated to render the surface positively charged. The pretreatment depends on the type of surface. Negatively charged surfaces are charge modified by adsorption of cationic polymer molecules. Gold is sulfidized in order to obtain a negatively charged surface prior to polymer adsorption. The seed film method was utilized to prepare films of a number of molecular sieve types such as MFI [94-95,98,102-103,105-106], LTA [97] and FAU [87,94] on various dense supports such as vegetal fibers [93], carbon fibers [98], gold [102], silicon [94,103], quartz [95,104-105], α-alumina [97] and stainless steel [104]. The seed film method was also used to prepare continuous zeolite films on porous α-alumina supports [69,73] and structured supports [107] which were tested as membranes and catalysts, respectively. In summary, zeolite film preparation by this method has proven to be very flexible. Several other methods

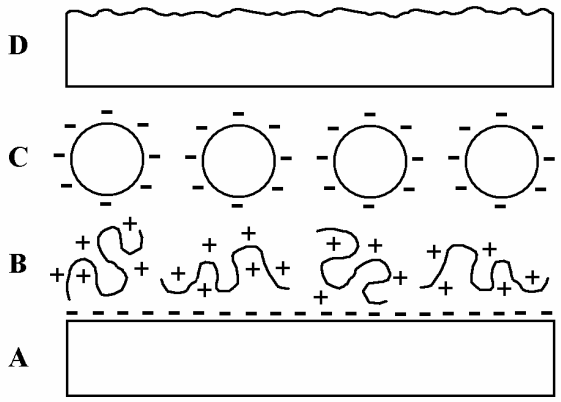

Figure 4. Principal steps in the seed-film method. The negatively charged support (A) is treated with cationic polymer molecules which are electrostatically adsorbed on the surface (B). Negatively charged seed crystals are adsorbed on the charge-reversed surface in a subsequent step (C). The seeded support is hydrothermally treated in a synthesis solution during which the seeds are grown into a dense film (D).

for the attachment of seed crystals to the surface have been reported, and some examples will be given here. Zeolite Y films were synthesized on tubular α-alumina supports using a seeding technique in which NaX zeolite crystals were mechanically placed on the support surface prior to hydrothermal growth in a synthesis solution [108]. The same seeding approach was utilized to synthesize zeolite A and faujasite membranes [59]. A chemical interaction-based seeding method was recently introduced by Ha et al. [109]. A silane coupling agent, which has two functional groups, is used to covalently link seeds to the support. In the first step, one functional group reacts with the support surface. In the second step, the other functional group reacts with the seed surface. This seeding technique was also adopted by other groups for the deposition of monolayers of seed crystals for further growth into dense films [67,110].

A combination of surface seeding and the vapor phase method was proposed by Tsay et al. [111]. A layer of colloidal MFI zeolite was deposited on a porous support, pre-coated with a silica layer. The composite was heated under saturated water vapor to obtain a zeolite film.

1.6.2 Texture in supported MFI films and effect on membrane performance

The effect of various synthesis parameters on crystal orientation in MFI films has been investigated by several groups [103,112-113]. The coverage of seed crystals [103,112] and the crystal size of the seeds [103] as well as the composition of the synthesis solution [113] were found to play a crucial role in the orientation of the crystals in the resulting film. The development of texture in MFI films prepared by seeding was recently discussed in a review by Hedlund and Jareman [114].

Preferred orientation of the crystals in MFI films is often developed due to *competitive growth* [103,112-114]. During competitive growth, the crystals with the fastest growing direction perpendicular to the surface will grow and surrounding crystals with different orientations will eventually be overgrown by

the faster-growing crystals. At the early stages of film growth, lateral growth of the crystals must also be considered in the model, as pointed out by Bons and Bons [115]. MFI crystals prepared with TPA as the structure directing agent, are often coffin shaped with the fastest growing direction along the c-axis [67]. Hence, according to the competitive growth model, the development of a c-oriented film is favored when randomly oriented seeds are grown in the presence of TPA. If the film is synthesized by growth of b-oriented twin crystals attached to the surface, an a-orientation of the crystals in the film will develop [103]. In this case the a-direction of the twin crystal is perpendicular to the support surface and these crystals can grow and form an a-oriented film. Lai et al. managed to preserve the initial b-orientation of seed crystals without twins by using trimer-TPA instead of the monomer TPA normally used for crystallization of MFI [67,110]. The use of trimer-TPA enhanced the relative growth rate of the b-direction of the seeds. Furthermore, the synthesis conditions for the preparation of the seed crystals were fine tuned to avoid the formation of twin crystals. The work by Lai et al. shows the importance of the structure directing agent for control of growth rates and also preferred orientation of the crystals in the film.

The orientation of the crystals in the MFI film is an important characteristic for zeolite films and membranes. The diameter of the channels running along b is slightly larger than the ones running along a (see section 1.1). In addition, no channels run along c. Hence, the diffusion of molecules through the crystals in the film should be dependent on crystal orientation. Jareman et al. determined the intrinsic diffusion coefficient of He, N_2, H_2 and SF_6 in masked MFI membranes with varying orientation of the zeolite crystals [116]. As opposed to lighter gases, the diffusion coefficient of SF_6 was dependent on preferred orientation, with a lower diffusivity for a more strongly a-oriented film. These results were explained by the relatively narrow pores running in the a-direction resulting in a lower diffusion coefficient for the bulky SF_6 molecule. As

discussed above, Lai et al. [67,110] prepared membranes with the b-axis oriented perpendicular to the support surface. The membranes were evaluated with xylene isomer separation experiments and high separation factors were observed. The authors attributed this to the fact that the straight channels in this case were oriented perpendicular to the membrane surface, allowing for faster molecular transport. A faster transport of para-xylene molecules through the membrane increases the separation factor if the transport of ortho-xylene (which mostly permeate through defects) remains constant. Furthermore, a lower density of defects such as cracks and open grain boundaries was mentioned as possible factor contributing to the high membrane quality.

1.6.3 Supports for zeolite membranes

Zeolite films for membrane applications are in most cases grown on porous supports for mechanical strength. The supports may be flat, tubular or multi-channel monoliths. Due to the high mechanical strength and chemical and thermal stability, α-alumina is most commonly used as support material. Other materials such as γ-alumina [15], steel [117] and carbon [118] are also utilized.

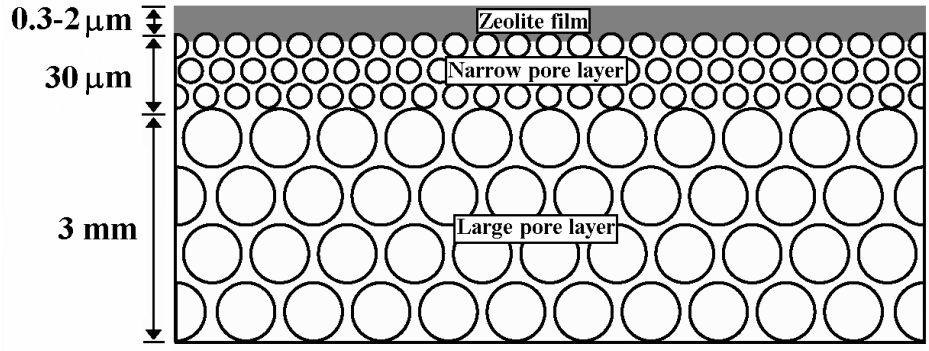

Figure 5. A sketch of the cross section of a zeolite film synthesized on an asymmetric porous support.

The pores of the support must be sufficiently small to facilitate formation of a continuous zeolite film. If the pores in the support are large, the support will have little mass transport resistance but a thick zeolite film is necessary in order to close the pores, which would reduce the flux through the membrane. Small pores allow the crystallization of a thin zeolite film but flux resistance is introduced from the support itself. Asymmetric supports combine the positive effects of small and large pores. A sketch of the cross section of an asymmetric support is shown in Figure 5. The indicated dimensions are typical for the samples studied in the present work. Such supports consist of two (or several) layers with different pore sizes. The top layer is thin with small pores. The bottom layer(s) have larger pores. Another advantage with asymmetric supports is that no continuous film will form on the bottom of the support.

Preferably, the difference in the thermal expansion between the support and the zeolite film should be small in order to minimize the risk of crack formation. Hence, the thermal behavior of the support may influence the quality of the film when the composite is exposed to temperatures deviating from the temperature of film synthesis.

1.6.4 Deposits in the support pores during film synthesis

Important features of a useful membrane are high permeability and selectivity. Synthesis of zeolite film on a porous support is often accompanied by the formation of siliceous species within the pores of the support [119-124]. The internal siliceous layer was shown to affect the membrane performance. Piera et al. achieved higher MeOH/O_2 and EtOH/O_2 selectivity for MFI membranes with a larger amount of zeolite inside the porous support [120]. However, the permeation of N_2 was much lower for membranes with intra-support layers than for membranes where most of the zeolite existed as a thin layer on the top of the support. Both flux and selectivity in the separation of *n*-butane/*i*-butane were highly enhanced in ZSM-5 membranes where the internal siliceous layer was

assumed to be both thinner and more crystalline [121]. The same group describes a method to reduce the amount of deposits in the support pores by carbonization of a mixture of furfuryl alcohol and tetraethylorthosilicate in the support prior to MFI film synthesis [122-123]. Both flux and selectivity in *n*-butane/*i*-butane separation experiments were improved by this treatment. Bernal et al. synthesized MFI type films on tubular porous support by a direct synthesis method [124]. By using different preparation procedures, the location of the crystalline material on the support could be controlled (mainly as a film on top of the support or in the pores of the support). *n*-Butane/*i*-butane separation experiments showed a higher maximum selectivity for the samples which lack of intra-support deposits. Kang and Gavalas grew MFI type zeolite inside the pores of a α-alumina support and the resulting composite was tested in single gas permeation experiments and in mixture separations (*n*-butane/*i*-butane) [125]. Several growth steps were required for a good separation factor in the mixture separation. Lai et al. [67,110] deposited a mesoporous silica layer, which acts as a barrier for the formation of zeolite in the interior of the support. Recently, a *two-step masking procedure* was developed [73]. The novel procedure protects the support and inhibits the formation of zeolite (or siliceous species) inside the support pores. A viscous polymer solution is applied on the top surface of the support and this polymer forms a protective layer. In the next step, the pores of the support are filled with molten wax. The polymer layer is dissolved and the exposed surface is seeded. The seeded support is hydrothermally treated in a synthesis solution during which the seeds are grown into a dense film. The wax present in the pores of the support in the as-synthesized membrane is removed during the calcination procedure. Masked MFI membranes were compared with unmasked membranes [82]. It was concluded that the membranes prepared on masked supports had higher selectivity and permeance.

The reason for the flux decrease observed as a consequence of intra-pore zeolite growth should partly be due to an increased total thickness of the zeolite layer which introduces additional mass transport resistance. In addition, the effective membrane surface also decreases due to the relatively low porosity of the support top layer. The combination of these two effects may thus reduce the flux significantly.

1.6.5 Defects in zeolite membranes

1.6.5.1 Classification of defects

Defects in membranes have a negative impact on the separation performance. Hence, it is of crucial importance to avoid formation of defects during synthesis and activation. *Pinholes* are holes propagating through the entire film, and can be avoided using suitable synthesis conditions [88]. *Grain boundaries* between neighboring crystals are an intrinsic feature of a polycrystalline film. If open, they will offer alternative pathways for the mixture to be separated and reduce the selectivity and increase the permeance [60]. The grain boundaries may open during calcination of as-synthesized membrane [15]. *Cracks* are possibly the most troublesome defect type and are frequently found in activated membranes [15,61,82-83,126-128].

1.6.5.2 Defect detection and characterization

Several techniques are used for the characterization of defects in zeolite membranes. A common technique is SEM, which allows the visualization of defects with a size greater than the resolution of the microscope at the surface of the film [82]. The permeance ratios (ideal selectivities) between light inorganic gases (H_2, N_2, He, SF_6) are frequently used as a measure of membrane quality. However, it was demonstrated that ideal selectivities are not reliable as a quality measure [82] and should only be used to compare similar membranes tested under identical conditions [82,129-130]. For the quality determination of MFI

membranes, separation experiments of hydrocarbon isomer mixtures such as the xylenes have also been used [82,67]. A recently developed technique is permporosimetry [82,131]. In this method, the permeance of a light gas is measured as a function of partial pressure of a condensable hydrocarbon in the feed. With increasing partial pressure, the hydrocarbon will first block the zeolite pores and at higher partial pressure also gradually condense in the defects and block these. Consequently, the permeance of the light gas will drop. Based on the data extracted from such experiments the size distribution and amount of defects can be determined [116,129,132]. A major advantage of permporosimetry over mixture separation experiments for defect characterization is that the technique is insensitive to the membrane pore size (i.e. zeolite type). Fluorescence Confocal Optical Microscopy (FCOM) was recently introduced as a tool for defect detection in MFI membranes [133]. The impregnation of various defects, such as open grain boundaries and cracks, with a fluorescent dye allows their detection and direct imaging along the thickness of the film. Hence, this technique offers a non-destructive imaging of defects in the membrane interior, which is not possible with conventional microscopy techniques.

1.6.5.3 Defect formation mechanisms

Activation of zeolite membranes at high temperature often results in the formation of defects. Geus and van Bekkum, early suggested that the thermal expansion mismatch between the support and the film was responsible for crack formation in MFI membranes [14]. Dong et al. [15] performed an HT-XRPD study on TPA-MFI films synthesized on porous α-alumina supports and Yttria-Zirconia (YZ) supports. The film prepared on the α-alumina support was shown to be of higher quality after calcination, compared to films synthesized on YZ supports. The authors proposed the following model for the observed quality differences: The crystals in the MFI film are not well-adhered to the YZ support

after synthesis. During template removal, the MFI structure shrinks. As the crystals are not firmly bonded to the support, they are free to move on the surface and remain in good contact. During a 6 h isotherm at 450 °C, chemical bonds are formed between the support and the film. Consequently, the film experiences a large compressive stress due to the constrained cooling (expansion of the film and contraction of the support) with crack formation as a result. For the α-alumina supported film on the other hand, the authors propose that the film is chemically bonded to the support after synthesis. The bonds to the support are stronger than between crystallites and the tensile strain imposed on the film during template removal, due to the difference in thermal expansion between the phases, is released via formation of open grain boundaries rather than cracks.

The model proposed by Dong et al. [15] does however not explain the occurrence of cracks in calcined α-alumina supported MFI membranes [15,61,83,126-128].

The orientation of the MFI crystals in the film was early recognized as an important factor for crack formation in silicalite-1 films [134]. den Exter et al. [134] studied silicalite-1 films prepared on dense silicon wafers containing silicon nitride windows that were removed after film synthesis, leaving the silicalite-1 film locally non-supported. Hence, the stress induced in the layer due to structural changes in the calcined material could be studied. According to XRD data, the crystallites constituting the films were (a, b)-oriented. Derived from crystallographic data [135] for as-synthesized and calcined silicalite-1, the authors reported that the change in the unit cell dimensions after calcination (*ex-situ* data) was –0.71, +1.05 and –0.105 % for the a, b and c axes, respectively. Based on these values and a quantitative estimation of a-and b-oriented crystallites in the film, the calcined crystal layer would show an expansion with respect to the as-synthesized film. In fact, a curving of the calcined crystal layer

was observed. The cracks observed in the film were attributed to the compressive stress in the calcined layer.

1.6.5.4 Methods to avoid crack formation during calcination

In early work, it was suggested that the calcination of supported MFI membranes should be performed at a temperature and heating rate not higher than 400 °C and 1°C/min, respectively [14]. It was shown that higher calcination temperature was not necessary to remove the template from the MFI structure, and would therefore only lead to increased thermal stress and crack formation. No explanation was however given for the recommended use of a slow heating rate. In later work, Jareman et al. studied the effect of heating rate on the quality of calcined MFI membranes (0.2-5 °C/min) with a film thickness of 500 nm [136]. No correlation between heating rate and quality was observed. In fact, cracks in MFI membranes have been observed after calcination with heating/cooling rates as low as 0.2-0.5 °C/min [82 and 110, respectively]. A potential factor for crack formation related to the heating rate is the presence of thermal gradients that possibly could form within the composite for high heating rates. However, such effects were not observed by Jareman et al. [136].

Some research groups presented alternative methods to conventional high-temperature calcination [25,26]. In a resent work, TPA-MFI membranes were treated with ozone at low temperature (200 °C) to remove the template molecules [25]. The membranes were also subjected to a temperature program normally used for calcination. The normal procedure caused cracks, while no cracks were found in membranes treated with ozone at moderate temperatures. Li et al. used a UV-ozone treatment at near-room temperature (local sample temperature ca 40-50 °C) to remove the template molecules (TPAOH) from thin MFI films [26]. FT-IR spectroscopy data confirmed the complete removal of the template. No cracks were observed by SEM in the films after template removal.

In some work, template-free synthesis procedures were employed for the preparation of MFI films and membranes [69,137-138]. Hence, no post-synthesis calcination was necessary to render the pores accessible to guest molecules.

Lai et al. [67] deposited a layer of mesoporous silica on the support prior to MFI zeolite film growth. These membranes showed excellent performance in xylene isomer separation, as already discussed in section 1.6.2. This was partly attributed to the presence of the silica layer which was claimed to eliminated stress-induced crack formation during calcination.

1.6.5.5 Defect reparation

A possible approach to minimize the effects of defects is to repair them. Yan et al. substantially increased the *n*-butane:*i*-butane ideal selectivity of a ZSM-5 membrane by a selective coke formation procedure that closed defects. The authors speculated that the intra-crystallite pores of the membrane were unaffected [123]. However, the increased selectivity was accompanied by a substantial flux decrease. Nair et al. sealed cracks in a MFI membrane with silica which substantially improved the membrane performance in xylene isomer separation experiments [60].

1.7 Description of principal characterization methods

This section will briefly present some of the characterization methods used in the present work.

1.7.1 Scanning Electron Microscopy (SEM)

SEM played a central role in the characterization of the films and membranes. The grain boundaries are readily observed with SEM which allows the determination of the approximate crystal size. The thickness of the films was

estimated from side view SEM images. Top view images allowed the detection of surface defects such as cracks, pinholes and unclosed films.

1.7.2 Permeation measurements

Permeation measurements with various probe molecules were used to estimate the quality (i.e. the presence/absence of defects) and the separation performance of the membranes. A perfect zeolite membrane acts as a barrier for molecules larger than the pores of the zeolite. Consequently, a measured flow through the membrane of molecules considerably larger than the pores of the zeolite is a direct proof of defects.

Polar molecules (such as water and ammonia) are strongly adsorbed in the zeolite pores, especially in zeolites with low Si/Al ratio. After drying in room air, such molecules block the pores of the zeolite. Furthermore, capillary condensation of water in defects in the mesopore range is also expected to occur under these conditions. The permeation of a weakly adsorbing gas such as He through a membrane which was dried under ambient conditions should therefore mainly occur through large defects not blocked by condensed water.

In the work presented in this thesis, the membranes were characterized by single gas permeation experiments as well as by mixture separations. In the former, a transmembrane pressure was employed as the driving force for diffusion through the membrane. In the latter, a Wicke-Kallenbach setup (section 1.5) was used.

1.7.3 X-ray Powder Diffraction (XRPD)

Powder diffraction can be used for qualitative/quantitative phase analysis, structure solution/refinement, determination of microstructure parameters (crystal size and microstrain) and texture analyses. In the work presented in this thesis, XRPD was used for identification of prepared materials, *in-situ* studies of

structure changes during calcination (paper V-VII), preferred orientation analyses (paper II, VII) as well as the preparation of crystallization curves (paper II). In the work described in paper VI, the apparent activation energy was calculated for the decomposition of the template in TPA-silicalite-1 using non-isothermal kinetic analysis methods of HT-XRPD data.

XRPD was of great importance for the work behind this thesis, and will therefore be discussed thoroughly in the following sections.

1.7.3.1 The Braggs law and the intensity of the diffracted beam

The phenomenon of diffraction was first described in 1912 by Sir W.L Bragg in terms of simultaneous reflection of the X-ray beam by lattice planes which belong to the same family. If θ is the angle between the primary beam and the family of lattice planes with Miller indices *hkl* and d_{hkl} is the interatomic distance (in ångström) of that family of planes, diffraction will occur at angle θ if the following relation holds (Braggs law);

$$n\lambda = 2d_{hkl}\sin\theta \qquad (1.2)$$

where *n* is an integer, set to 1 in experiments with a monochromatic beam.

In XRPD, the intensity of the diffracted beam from a powder can be recorded as a function of the scattering angle (2θ) (angular dispersive methods) or at a fixed angle using a polychromatic beam (energy dispersive methods). This results in a *powder diffraction pattern* (i.e. a set of diffraction angles or energy values converted into *d*-spacings), also called a *diffractogram*. The diffraction pattern is unique for each crystalline material. Hence, a qualitative analysis is thus possible simply by matching the observed pattern with the patterns of known structures from a database. However, this is not trivial in those cases where the sample is a mixture of crystalline materials.

The intensity of the diffracted beam from a lattice plane *hkl* at Bragg angle θ can be described by the following equation;

$$I_{hkl} = k \cdot A \cdot Lp_{hkl} \cdot P_{hkl} \cdot \left|F_{hkl}\right|^2 \tag{1.3}$$

where k is a constant related to the instrumental setting, A is the absorption factor, Lp is the Lorentz-polarization factor, P is the multiplicity factor and F is the structure factor. The intensity of the diffracted beam of a crystalline phase in a mixture is directly proportional to its weight fraction. Hence, XRPD is a powerful technique for quantitative phase analysis. Reflection does not only occur at the Bragg angle, but also at slightly deviating angles due to instrumental and sample broadening effects (further discussed in the next section). This results in intensity versus 2θ curves which are called diffraction peaks. The integrated area of the peak is statistically more convenient to use for quantitative phase analysis.

The absorption factor A of the incident and reflected X-ray beams is dependent on many factors such as the geometry used for the experiment (reflection vs. transmission), the wavelength λ and the linear absorption coefficient of the sample.

The use of non-polarized X-ray beams has an effect on the reflected beam intensity according to:

$$f_p = 0.5\left(1 + \cos^2 2\theta\right) \tag{1.4}$$

Trigonometric factors influencing the intensity of the reflected beam are combined in the Lorenz factor:

$$f_L = \frac{1}{\left(4\sin^2\theta \cdot \cos\theta\right)} \tag{1.5}$$

The combination of f_P and f_L results in the Lorentz-polarization factor;

$$Lp = \frac{\left(1 + \cos^2 2\theta\right)}{\left(\sin^2\theta \cdot \cos\theta\right)} \tag{1.6}$$

and the constant 1/8 is included in the proportionality factor k (which involves some instrumental parameters and is constant for a certain experimental setup).

Depending on the crystal symmetry, the reflected beams from some planes may superimpose, resulting in a diffraction peak with higher intensity than if it resulted from a single plane. This intensity increase is taken into account by the multiplicity factor *P*.

The structure factor *F* is the key factor, which rules the interaction of X-rays with crystals and contains the structural information. The structure factor can be described by the following equation;

$$F_{hkl} = \left[(\sum f_n p_n e^{-2M} A_n)^2 + (\sum f_n p_n e^{-2M} B_n)^2 \right]^{1/2} \tag{1.7}$$

where n is the number of scattering atoms in the asymmetric unit; f_n is the scattering factor of the n-th atom of the asymmetric unit occupying the lattice position (x_n, y_n, z_n); A_n and B_n are the geometrical structure factors which are a complex function of (h,k,l) and the lattice positions (x_n,y_n,z_n) of the scattering atoms in the asymmetric unit; P_n is the so-called site multiplicity which is the number of the n-th atoms of the asymmetric unit in the crystallographic unit cell; M is the Debye-Waller temperature factor of the n-th atom of the asymmetric unit occupying the lattice position (x_n,y_n,z_n).

The atomic scattering factor (f_n) depends on the atomic number of the element as well as θ and λ. The scattering efficiency decreases with increasing $sin\theta$ and decreasing λ. The thermal vibrations of the atoms in a crystal affects the peak intensity, which is considered in the temperature factor M commonly expressed as;

$$M = b\frac{\sin^2\theta}{\lambda^2} \tag{1.8}$$

where b is a complex function which takes into account that the thermal motion of an atom and the consequent displacement from its lattice point is dependent on the chemical environment (i.e. nature of atoms in neighboring sites) as well as the crystal structure. Consequently, each atom in the asymmetric unit has its own temperature factor.

1.7.3.2 Peak broadening

The observed diffraction line profile, *h(x),* is the result of the *convolution* of the instrumental profile, *g(x)* (which includes aberrations introduced by the diffractometer and wavelength dispersion), and the sample profile, *f(x,)* in addition to the background. The instrumental profile is fixed for a particular instrument/target system. The contributions to the width of the specimen function include the Darwin width (which is simply the result of the uncertainty principle) and possibly the size of the crystallites and microstrain. Peak broadening can be characterized by the integral breadth β, which is the width of a rectangle having the same area and height as the peak. According to Scherrer [139] the peak broadening due to crystallite size, expressed as the integral breadth β_{size}, is;

$$\beta_{size} = \frac{\lambda}{D_v \cos\theta} \tag{1.9}$$

where D_v is the volume-weighted domain size, λ is the wavelength and 2θ is the Bragg angle. For spherical crystallites, the broadening due to size is isotropic (i.e. independent on crystallographic direction). Microstrain also broadens the specimen profile according to [140];

$$\beta_{strain} = 4\varepsilon \tan\theta \tag{1.10}$$

where ε represents the upper limit of microstrain. Microstrain is the result of variation in interatomic distances due to internal stresses or non-stoichiometry, micro-twinning, stacking faults, dislocations and other forms of atomic disorder.

1.7.3.3 Microstructure analysis

The presence of sample broadening is easily confirmed by plotting the Full Width at Half Maximum (FWHM) versus 2θ for the sample profiles as well as the profiles from a standard reference material (which show no sample broadening and thus represents the instrumental broadening). If the instrumental

broadening is sufficiently small, so that the sample broadening due to size and/or microstrain is a significant part of the total, information about the microstructure can be extracted by *Line Profile Analysis*. Generally, the first step is performed by *pattern decomposition* which involves the fitting of analytical *reflection profile functions* (ϕ) [141] to the various identified Bragg reflections without reference to a crystal structure model [142]. Frequently, the experimental profiles are modeled as Voigtian, which means that the shape is an intermediate between Lorentzian and Gaussian (the Voigt, the pseudo-Voigt and the Pearson VII functions belong to this category). Profile fitting gives the position, intensity, width and shape of individual reflections. However, the observed profile broadening must be corrected for the contribution from the instrument. In the second step, the information extracted from pattern decomposition is used to estimate the crystallite size and shape as well as the strain [143].

As a first approximation of the nature of the sample broadening, the method of Williamson and Hall [144] can be used. In this method, the "size" and "strain" contributions to the sample profile breadths are separated on the basis of their order dependence. Size broadening is order independent while strain broadening is not. Under the assumption that the integral breadth due to size and strain are Lorenzian, the following holds:

$$\beta = \beta_{size} + \beta_{strain} \tag{1.11}$$

Combining equation (1.9), (1.10) and (1.11) gives;

$$\beta^* = \frac{1}{D_v} + 2\varepsilon d^* \tag{1.12}$$

where $\beta^* = \frac{\beta \cos\theta}{\lambda}$ and $d^* = \frac{2\sin\theta}{\lambda}$. A plot of β^* versus d^* results in the so-called Williamson-Hall plot. The intercept gives an estimate of D_v and the slope is a measure of ε.

A major drawback of this method is that it is based on the approximation that the line profiles due to size and strain are Lorentzian which is unlikely to occur in practice. Nevertheless, the method gives valuable information about the nature of any structural imperfections in the sample and hence the procedure to be used in a subsequent detailed analysis [143,145].

1.7.3.4 The Rietveld method

About thirty years ago, Hugo Rietveld proposed a revolutionary method for extraction of structure information from powder diffraction data [146-147]. The method is appropriately called "*The Rietveld method*" and has become a powerful tool for crystallographers [148]. In the Rietveld method, all factors contributing to the intensity y_i at point i in the powder pattern may be simultaneously refined by a least-square procedure until the best fit is obtained between the entire observed powder diffraction pattern and the entire calculated pattern. Since the method is a structure refinement procedure, a reasonably good starting model is required. The strength of the method is that no effort is made to resolve overlapping peaks.

The quantity that is minimized by the least-square procedure is the residual S_y which is defined as [149];

$$S_y = \sum \frac{1}{y_i} \left(y_i - y_{ci} \right)^2 \tag{1.13}$$

where y_i and y_{ci} is the observed and calculated intensity at the i th step, respectively. The sum is over all data points in the powder pattern. The calculated intensity at point i (y_{ci}) is determined according to [149];

$$y_{ci} = y_{bi} + A \sum_{J,hkl} s_J \cdot Lp_{J,hkl} \cdot P_{J,hkl} \cdot \phi\left(2\theta_i - 2\theta_{J,hkl}\right) \cdot O_{J,hkl} \cdot \left| F_{J,hkl} \right|^2 \tag{1.14}$$

where y_{bi} is the background intensity, *J,hkl* denotes the Miller indices for the Bragg reflection *hkl* of phase *J,* s_J is the scale factor for phase *J* and O_{hkl} is the preferred orientation function. *Preferred orientation* of the crystallites results in

a higher diffraction intensity of the preferentially oriented planes with respect to the intensity of the same planes in a randomly oriented sample. In thin film analysis, a large deviation of the relative intensities of the diffraction peaks from a randomly oriented powder may give indications of preferred orientation of the sample crystallites. Effects of preferred orientation can be accounted for by models of different complexity. The most frequently used models are the expression of March [150] revised by Dollase [151] and the spherical harmonics [152]. In this work, the March-Dollase model was used to evaluate the preferred orientation in a MFI film.

The model parameters that may be refined include not only the structure (atom positions, thermal and site-occupancy parameters) but also parameters for the background, lattice constants, instrumental geometrical-optical features, specimen aberrations, scale factor and peak broadening due to the sample microstructure. Multiple phases may be refined simultaneously and based on the refined scale factor for each constituent, the composition of the mixture may be calculated. The scale factor for component J in a polyphasic mixture (s_J) is proportional to the weight fraction of that component in the mixture (w_J) according to;

$$w_J = \frac{s_J M_J V_J}{\sum_k s_k M_k V_k} \tag{1.15}$$

where M_J and V_J is the unit cell mass and volume, respectively. The sum is over all crystalline components (k) in the mixture. However, as this algorithm is based on the normalization equation $\sum w_k = 1$, the presence of an amorphous component leads to an overestimation of the weight fractions. However, the problem can be resolved by adding a known amount of internal standard which is considered as a component itself [147,153-159]. The refined weight fractions of the sample crystalline components can then be rescaled with respect to the added standard.

1.7.3.5 In-situ X-ray Powder Diffraction

X-ray powder diffraction data collected *in-situ* at non-ambient temperatures, i.e. High Temperature (HT) XRPD, is a powerful tool in studies of temperature induced structure changes such as phase transformations, phase transitions, crystallite growth and thermal expansion. Another important application of HT-XRPD is kinetic analysis, which will be further discussed in section 1.8. The instrument can be a conventional X-ray diffractometer equipped with a heating chamber and a high-speed detector such as a Position Sensitive Detector (PSD). However, due to the low brightness of in-house X-ray sources, long data collection times are required to obtain adequate data for structure refinements. Consequently, the time resolution is strongly limited and structure changes due to fast reactions become difficult to study. In addition, weakly scattering samples (such as zeolites) and small sample volumes (such as thin films) further reduce the possibilities with in-house instrumentation. In such cases, a synchrotron source may be necessary. The main advantage of synchrotron radiation is the high brightness, which allows the collection of full powder patterns in seconds. Furthermore, the resolution is considerably higher which provides more detailed structural information including the possibility of line broadening analyses, which gives information regarding the microstructure (crystallite size and strain) of the sample.

1.8 Kinetic analysis

Kinetic analysis using HT-XRPD data can be used for calculation of empirical coefficients which give indication about the reaction mechanism (generally interface or diffusion controlled reaction) and the rate limiting step of the reaction. The Arrhenius parameters, i.e. the apparent activation energy E_a of the reaction and the frequency factor A (also called pre-exponential factor), can be determined. The rate of reaction is followed by the conversion factor α, a

normalized factor proportional to the integrated intensity of diffraction peaks whose variation is in turn proportional to the advancement of the reaction. Such an effect can be the growth or disappearance of a peak as a function of temperature at a constant heating rate (non-isothermal kinetic analyses) or time at a constant temperature (isothermal kinetic analyses).

In this work, non-isothermal kinetic analyses were performed for the template removal reaction in silicalite-1 (Paper VI). Therefore, the following paragraph will give a short theoretic background to non-isothermal kinetic analyses [160]. In addition, the methods used for the kinetic analysis presented in paper IV will be described.

The rate of the kinetic process can be expressed as;

$$\frac{d\alpha}{dt} = kf(\alpha) \tag{1.16}$$

or in the integrated form;

$$g(\alpha) = kt \tag{1.17}$$

where α is the conversion factor, k is the rate constant, $f(\alpha)$ is the kinetic model function which depends on the mechanism of the reaction and g(α) is the integral of $\frac{1}{f(\alpha)}$. There are many different kinetic model functions that describes solid state reactions [160]. However, the most frequently used function for nucleation and crystal growth in solids was first formulated by Avrami [161], and can be written in the following form:

$$g(\alpha) = [-\ln(1-\alpha)]^{\frac{1}{n}} \tag{1.18}$$

The value of n depends on the mechanism and dimensionality of nucleation and growth. For an interface-controlled growth n is an integer, for a diffusion-controlled growth n takes either integer or half-integer values. Many methods, such as the one proposed by Kissinger [162] (see below) for kinetic analysis were derived especially for the Avrami equation.

The reaction rate is temperature dependent and is assumed to follow the Arrhenius equation;

$$k = A\exp\left(\frac{-E_a}{RT}\right) \tag{1.19}$$

where T is the absolute temperature, R is the gas constant, E_a is the apparent activation energy of the reaction and A is the frequency factor. Non-isothermal data is collected during a constant change in temperature. Hence, the temperature at any point during heating/cooling can be written as;

$$T = \beta t + T_0 \tag{1.20}$$

or in the differentiated form;

$$dT = \beta dt \tag{1.21}$$

where T_0 in equation (1.20) is the reaction onset temperature.

Various expressions can be derived from the above equations. One that forms the basis of many kinetic analysis methods can be derived by combining equations (1.16), (1.19) and (1.21), integrating and substituting $X = \frac{E_a}{RT}$;

$$g(\alpha) = \int_0^\alpha \frac{d\alpha}{f(\alpha)} = \frac{AE_a}{R\beta}\int_{X0}^{X} e^{-X}X^{-2}dX \tag{1.22}$$

where

$$p(X) = \int_{X0}^{X} e^{-X}X^{-2}dX \tag{1.23}$$

$p(X)$ is called "the temperature integral" and can not be integrated analytically. Commonly used approximating formulas for $p(X)$ are those proposed by either Doyle [163] or by Murray and White [164].

Two main analysis approaches exist: i) the determination of the kinetic model function which best describes the experimental data, followed by calculation of the kinetic parameters. ii) so-called "isoconversional" methods which allow the determination of the kinetic parameters without a prior knowledge of the kinetic model function. Such methods consider points of the same α on several α versus

T-curves, collected at various heating rates, so that f(α) has identical magnitude and can be cancelled out.

Many kinetic models may provide a similar description of the reaction process but the calculated kinetic parameters can differ significantly. Therefore, the determination of the appropriate kinetic model is facilitated if the value of E_a is determined first using isoconversional methods [165].

The apparent activation energy (E_a) of the template decomposition in silicalite-1 was calculated (Paper VI) using the following methods for kinetic analysis of non-isothermal data; i) the Kissinger method [162], ii) the method of Flynn-Wall-Ozawa [166-167] and iii) the method proposed by Kennedy and Clark [168]. According to Kissinger [162], the slope of a plot of ln (β/T_p^2) versus $1/T_p$ is proportional to E_a according to the following equation;

$$\ln\left(\frac{\beta}{T_p^2}\right) = -\frac{E_a}{RT_p} + k \tag{1.24}$$

where β is the heating rate, T_p is the temperature (expressed in Kelvin) at which the reaction rate is maximum, R is the molar gas constant and k is the rate constant. The method of Flynn-Wall-Ozawa is based on the Doyle's approximation of the temperature integral:

$$\ln \beta = \ln \frac{AE_a}{R} - 1.052\frac{E_a}{RT} - 5.33 - \ln g(\alpha) \tag{1.25}$$

Under the assumption that the kinetic model function is invariant for all the runs, a plot of lnβ versus $1/T$ for a chosen value of α should be a straight line with a slope proportional to E_a.

According to the method of Kennedy and Clark [168], the following relation holds:

$$\ln\left(\frac{\beta g(\alpha)}{T - T_0}\right) = \ln(A) - \frac{E_a}{RT} \tag{1.26}$$

A plot of the left side of equation (1.26) versus 1/*T* should result in a straight line with the slope proportional to E_a. Kennedy and Clark [168] also showed that equation (1.27) can be used for the determination of the parameter *n* in the Avrami equation;

$$\ln\left(h(\alpha)\right) = n\left(\ln(A) - \frac{E_a}{RT}\right) + n\ln\left(\frac{T - T_0}{\beta}\right) \tag{1.27}$$

where $h(\alpha)$ is $(-\ln(1-\alpha))$. For a fixed temperature, α is determined for various heating rates. Since the quantity $n\left(\ln(A) - \frac{E_a}{RT}\right)$ is constant at constant *T*, a plot of $\ln(h(\alpha))$ versus $\ln\left(\frac{T - T_0}{\beta}\right)$ will have gradient *n*.

2. AIM OF THIS WORK

The seed film method has been developed for the preparation of thin continuous molecular sieve films on various supports [169]. The first part of this work aimed at the development of the method for films of other zeolite types. A further objective was to utilize template free precursor gels in order to avoid a calcination procedure which might introduce defects in the film. During the course of the work, cracks were however frequently encountered in the synthesized films. No clear model for crack formation in zeolite films was found in the literature, and the second part of this work was therefore devoted to this issue. TPA-MFI films supported by porous α-alumina discs were chosen for the investigation since previous work by our group demonstrated that the reproducibility was high in this system and that defective as well as defect-free membranes could be prepared. In addition, this system is well characterized by our and other groups and also very interesting from an industrial point of view.

3. EXPERIMENTAL

3.1 Zeolite film synthesis

The films and membranes characterized in this work were prepared according to the seed-film method [169]. The method is described in section 1.6.1 (Figure 4). In the first step, the support is immersed in a solution containing cationic polymer molecules (0.4 wt% Redifloc 4150, Eka Chemicals). In the second step, the support is treated in a sol containing colloidal zeolite crystals. The result of this procedure is a layer of seed crystals attached to the support surface.

The seed crystals were synthesized using a method developed by our group [21]. Clear homogeneous solutions were hydrothermally treated in the presence of organic additives. After completion of the crystallization, the crystals were purified by repeated centrifugation followed by redispersion in a dilute ammonia solution to obtain a seed sol. The dry content was adjusted to 1.0 wt% and the pH to 10.0.

Following seeding, the support was hydrothermally treated in a synthesis mixture in order to grow a dense zeolite film. The compositions of the synthesis mixtures for the preparation of the films in this work are reported in Table 1, together with the size of the seed crystals.

Table 1. Molar composition of the zeolite synthesis gels.

Topology of films and seeds	Seed size (nm)	Molar composition of synthesis gel	Paper
FAU	70	$14Na_2O:Al_2O_3:10SiO_2:798H_2O$	I-II
MFI	120	$30Na_2O:Al_2O_3:100SiO_2:4000H_2O$	III
LTA	140	$2Na_2O:Al_2O_3:2SiO_2:35H_2O$	IV (S1)
LTA	140	$4.3Na_2O:Al_2O_3:2.5SiO_2:111H_2O$	IV (S2)
MFI	60	$3TPAOH:25SiO_2:1500H_2O:100EtOH$	V-VII

During growth of films of FAU (paper I-II) and LTA (paper IV), the gel separated in a clear upper part and a turbid lower part. An exception is the synthesis gel S2 used for the preparation of LTA membranes, where no separation occurred. The film growths were carried out in the clear top part if not stated otherwise.

In the preparation of FAU and LTA films (paper I-II and IV, respectively) synthesis parameters such as time and temperature were varied in order to control the thickness and quality of the films. The growth of FAU type films (paper I-II) was carried out both in the turbid and clear part of the synthesis mixture. For the preparation of LTA membranes (paper IV), a so-called repeated synthesis was also performed where fresh synthesis solution was added periodically to the cooled and rinsed samples.

The FAU films presented in paper I-II, were synthesized on polished α-alumina supports. In later work, porous α-alumina asymmetric discs with a thickness of 3 mm were used as supports (Inocermic GmbH, Germany), see Figure 5. The top layer was 30 μm thick with an average pore size of 100 nm. The MFI film used for the synchrotron diffraction experiment, presented in paper VII, was prepared on a slice (20×3×1 mm), cut from the original asymmetric α-alumina disc.

To avoid adsorption of dust particles on the supports, all solutions (for rinsing and surface charge modification) as well as the seed sol were filtered in the later work (papers III-V, VII).

3.2 Instrumentation

3.2.1 General

The thickness and morphology of the films were investigated using a Philips XL 30 Scanning Electron Microscope (SEM) equipped with a LaB_6 emission

source. Furthermore, an Oxford Ge X-ray detector attached to the SEM was used to determine the Si/Al ratio of a few samples by energy dispersive X-ray analysis (EDX). Due to the relatively large sampling area for the EDX technique, the determination of the Si/Al ratio in the films prepared on α-alumina supports was not possible due to the low film thickness (i.e. interference by the Al signal from the support material). Hence, such analyses were restricted to powders.

A Siemens D5000 powder X-ray diffractometer were used for X-ray Powder Diffraction (XRPD) data collection at room temperature.

A TEM analysis was performed on the MFI coated α-alumina support subjected to the SR experiment. The support surface was delicately grinded, and the resulting powder was deposited on a Cu grid. Bright field TEM images were recorded using a JEOL JEM 2010 instrument operating at 200 kV equipped with a Link energy dispersive X-ray spectrometer and a Gatan energy filter.

3.2.2 Permeation measurements

The membranes were dried at 100 °C (Paper III) or at room temperature (Paper IV). Such mild drying is not expected to activate the zeolite pores, as discussed in the introduction. Following drying, the membranes were mounted in a stainless steel cell and a rubber o-ring was used to obtain a gas tight connection.

Single gas permeation measurements were performed at room temperature with a feed gas applied at 5 bar absolute pressure (Paper III-IV). The permeate pressure was kept at 1 bar absolute pressure. The permeance was calculated from the measured flow of the permeate.

Permeation measurements for gas mixtures were performed using a Wicke-Kallenbach apparatus (Paper III). Helium was used as sweep gas. The membranes were mounted in a stainless steel cell equipped with graphite gaskets. The pressure was kept at 1 bar on both sides of the membrane. The temperature in the membrane cell was monitored during measurements. An

online connected gas chromatograph (GC) equipped with a thermal conductivity detector (TCD) and a flame ionization detector (FID) was used for quantitative analyses of the gas mixtures.

3.2.3 High Temperature X-ray Powder Diffraction (HT-XRPD)

3.2.3.1 TPA-MFI powder

The HT-XRPD data from the TPA-MFI powder (Paper VI and VII) were collected using a Panalytical θ/θ diffractometer (Cu radiation), equipped with an Anton Paar HTK 16 resistance heating chamber and a RTMS X'Celerator. Four different heating rates were used (3, 5, 10 and 20 °C/min). Data were collected with 50 °C steps during heating up to 500 °C. This temperature was held for 1 h during which data was collected every 15 min. For the heating rate 10 °C/min, data was collected also during cooling and during a second heating/cooling ramp. The data acquisition time for each experimental point was 3 minutes. All experiments were performed in air. The use of a standard silicon powder (NIST640c) directly mixed in the MFI powder allowed to determine the absolute cell parameters at each investigated temperature and correct for thermal expansion of the sample holder.

3.2.3.2 TPA-MFI membrane

A MFI coated α-alumina support as well as a non-coated support were investigated *in-situ* using the same in-house instrument as the one used for the powders (see previous section). The sample temperature was calibrated using known phase transitions. The temperature induced vertical shift of the sample holder was calibrated using the thermal expansion of a standard silicon powder (NIST640c). The samples were investigated during heating up to 500 °C as well as during cooling back to RT, with a heating/cooling rate of 3 °C/min. Diffraction data was collected every 50 °C in the range 23-45 °2θ.

A MFI film prepared on a porous α-alumina support with the dimensions 20×3×1 mm, was investigated using *in-situ* powder diffraction data collected at the Italian beamline BM08 (GILDA) at the European Synchrotron Radiation Facility (ESRF), Grenoble (France). The beamline configuration is described in detail by Meneghini et al. [171]. The specific experimental setup used in this work is shown in Figure 6. The sample was mounted in a metal tube with an inner diameter of 3.5 mm. After sample insertion, the end of the tube was sealed and the holder was mounted on a goniometric head. A hole (1 mm high and 12 mm width) in the tube allowed the SR beam to hit the sample, oriented with the zeolite membrane faced down, from the side (Figure 6). The sample was heated using a hot air stream generated by a heating gun placed vertically under the sample. Data collection was accomplished in parallel beam Debye geometry

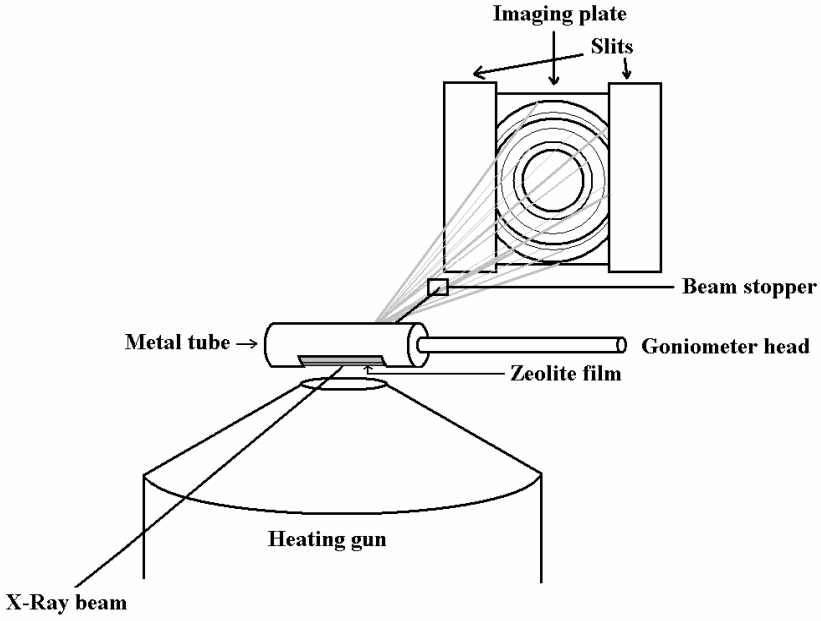

Figure 6. A sketch of the experimental set-up for HT-SRPD (see text for details).

using a monochromatized fixed wavelength of 1.0405 Å, calibrated using a standard. During heating, the temperature was monitored with a thermocouple positioned about half a mm below the sample. A heating/cooling gradient of 3 °C/min was applied. Full diffraction rings were recorded every 50 °C ± 3° with an exposure time of 2 min using an image plate (IP) detector mounted perpendicular to the incoming beam. The images stored in the IP were recovered using a Molecular dynamics scanner. The part of the image which corresponds to the diffracted X-rays from the planes parallel to the support surface was extracted using specific software (FIT2D).

3.3 Data evaluation

3.3.1 Kinetic analysis of TPA decomposition in MFI

The conversion factor α for the template decomposition in TPA-MFI powder was calculated according to;

$$\alpha = \left(\frac{I_c^T - I_c^{T=25°C}}{I_c^{\max} - I_c^{T=25°C}} \right) \tag{3.1}$$

where I_c^T is the sum of the 101/011 and the 200/020 diffraction peak areas divided by two at temperature T and I_c^{max} corresponds to the maximum value of I_c.

The apparent activation energy (E_a) of the template decomposition in silicalite-1 was calculated using the Kissinger method [162], the isoconversional method of Flynn-Wall-Ozawa [166-167] and the method proposed by Kennedy and Clark [168]. These methods were described in section 1.8. In the present work, the Avrami equation [161] was used as the kinetic model function f(α) (see section 1.8). The reaction order (n) for the Avrami equation was determined according to equation (1.27) [168]. Several plots, using different temperatures, were drawn in order to have several estimates of n.

3.3.2 Rietveld refinements

Rietveld refinements (Paper V-VII) of the XRPD patterns were carried out using GSAS [172]. The structure model reported by van Koningsveld [24] derived from single crystal XRD data was used in the refinements of the MFI phase. The structure model for the α-alumina was taken from a publication by Ishizawa et al. [173]. For all refinements, the atom positions and the thermal parameters were kept fixed at the literature values. However, the occupancy of the atoms in the TPA molecules present in the as-synthesized MFI structure was refined. The background, scale factor and some profile parameters were refined together with the cell parameters and the zero shift. The use of an internal standard with a known thermal expansion coefficient allowed to determine the absolute cell parameters of the investigated phases. In the case of the MFI powders and the α-alumina support, the internal standard was a Si powder. For the MFI film, the α-alumina support was used.

The preferred orientation of the crystals in the MFI film was refined using the March-Dollase model implemented in GSAS [172].

The template removal could be followed using the refined site occupancy of the atoms in the template molecules during heating of the TPA-MFI film. For the TPA-MFI powder systematically investigated in Paper VI, the template decomposition was followed by another approach: The powder was considered to be a mixture of TPA-MFI and HMFI which were refined as two separate phases. In these refinements, only the background and the scale factors were modeled. Based on the refined scale factors, the weight fractions of the phases were calculated (equation (1.15)).

3.3.3 Calculation of strain

The refined unit cell parameters of the phases in the MFI membrane (Paper V and VII) where based on data collected from planes parallel to the film surface and should therefore mirror the *d*-spacings of these planes. Consequently, the

out-of plane strain (i.e. the strain in the direction perpendicular to the film surface) along different crystallographic directions *l* of the crystallites in the composite could be calculated at each investigated temperature *T* using the following equation;

$$strain = \frac{(l^T_{membrane} - l^T_{reference})}{l^T_{reference}} \tag{3.2}$$

where MFI powder and a blank α-alumina support were used as references (i.e. represent the non-strained bulk lattice).

3.3.4 Line broadening analysis

Synchrotron radiation powder diffraction data collected *in-situ* for the MFI membrane (see section 3.2.3.2) was used to investigate the peak broadening of the α-alumina support by pattern decomposition. The pseudo-Voigt function (pV) was used to fit each peak. The function is defined as the weighted sum between a Lorentzian (L) and a Gaussian (G) curve according to;

$$pV(2\theta) = (1-\eta)G(2\theta) + \eta L(2\theta) \tag{3.3}$$

where η is the so-called mixing parameter. The pseudo-Voigt mimic the behavior of the Voigt function (the convolution of a Lorentzian and a Gaussian function), with the advantage of being mathematically more simple. The refined values of the integral breadth (β) and the mixing parameter (η) are used in the subsequent analysis.

The integral breadth of the Lorenzian (β_L) and Gaussian (β_G) components of the Voigt function corresponding to the pV function can be determined according to the following empirical formulas [174]:

$$\frac{\beta_L}{\beta_{pV}} = 0.017475 + 1.500484\eta - 0.534156\eta^2 \tag{3.4}$$

$$\frac{\beta_G}{\beta_{pV}} = 0.184446 + 0.812692(1 - 0.998497\eta)^{1/2} - 0.659603\eta + 0.44542\eta^2 \tag{3.5}$$

The microstructural information contained in the integral breadth of a measured peak profile $h(2\theta)$ is usually mixed with instrumental effects $g(2\theta)$. A deconvolution of those effects is necessary to obtain the pure microstructure-broadened peak profile $f(2\theta)$. An efficient way is to apply equation (3.4) and (3.5) to each peak profile collected from the specimen and to the profiles of a suitable standard (LaB_6 NIST SRM 660a, powder showing no microstructure broadening) in order to obtain the total measured breadths (β_L^h, β_G^h) and the contribution from the instrument (β_L^g, β_G^g). From the additive properties of the breadth for the Lorentz and Gauss functions, the microstructure-related Gaussian and Lorenzian breadths (β_L^f, β_G^f) can be obtain according to:

$$\beta_L^f = \beta_L^h - \beta_L^g \tag{3.6}$$

$$\left(\beta_G^f\right)^2 = \left(\beta_G^h\right)^2 - \left(\beta_G^g\right)^2 \tag{3.7}$$

Equations (3.4) and (3.5) can then be used again to obtain the total integral breadth of the $f(2\theta)$ function corresponding to the given peak.

4. RESULTS AND DISCUSSION

4.1 Template-free zeolite films and membranes

4.1.1 Film growth and morphology

The position of the support in the reaction vessel was shown to affect the FAU film growth. Films prepared in the clear upper part of the synthesis solution were thinner than films prepared in the bottom part of the reaction vessel. This was also observed by others [175]. Figure 7 shows SEM images of FAU films prepared in the top part (a, b) and bottom part (c, d) of the synthesis solution under otherwise identical conditions (6 h thermal treatment at 100 °C).

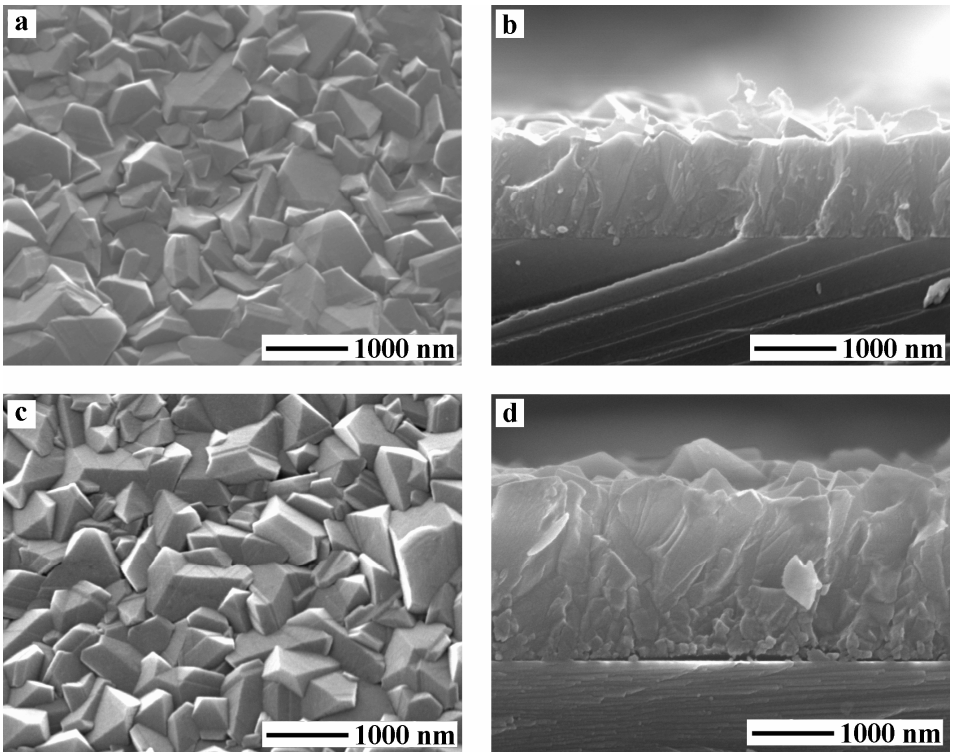

Figure 7. Top- and side view SEM images of FAU films prepared in the upper part (a, b) and the lower part (c, d) of the synthesis medium under otherwise identical conditions.

The film prepared in the bottom part is 1700 nm thick whereas the film prepared in the top part is 1000 nm thick. In addition, the films prepared in the bottom part are composed of two layers. Opposite to the single columnar layer observed for films synthesized in the clear upper solution (Figure 7b), the films synthesized in the bottom part have an additional layer, composed of small grains (Figure 7d). A possible explanation for these observations is the attachment of crystals formed in the bulk of the synthesis mixture on the growing film. This should be more extensive in the bottom part of the reactor as the concentration of crystals formed in the bulk should be higher in this area.

Figure 8 shows the film thickness as a function of synthesis duration for FAU films synthesized at various temperatures in the top part of the synthesis mixture. In addition, the obtained curve for films prepared in the bottom part of the reactor at 100 °C is also shown. In the beginning of film growth, the growth rate is constant and dependent of synthesis temperature. Furthermore, the film thickness reaches a maximum after a certain time which depends on the

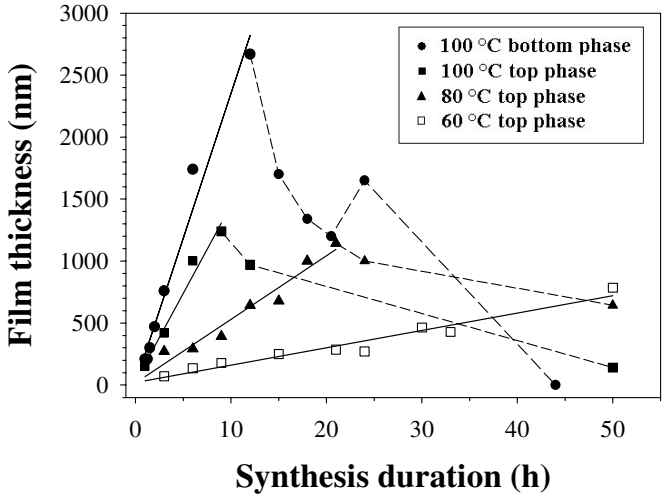

Figure 8. The film thickness as a function of synthesis duration for FAU-type films synthesized at different temperatures and positions (bottom, top) in the reaction vessel.

temperature. To investigate this phenomenon, XRPD analyses were performed on the bulk product formed after different synthesis times. It was found that the fraction of FAU decreases whereas the amount of zeolite P (GIS) increases as a function of synthesis time. Hence, the FAU type crystals are not stable in the precursor gel upon prolonged thermal treatment. These results lead to the conclusion that the dissolution of the FAU crystals and simultaneous growth of zeolite P is the likely cause of the observed decrease in film thickness. The same trend was observed by Covarrubias et al. who studied the intermediate and final phases during hydrothermal treatment of natural mordenite in alkaline medium [176]. The authors found the following phase transformation sequence: mordenite →FAU→GIS→hydroxysodalite.

NaA films were prepared on porous α-alumina supports (paper IV). It was found that a multi-step approach, i.e. periodical addition of fresh synthesis gel to the cleaned sample, was preferable in order to obtain films of high quality. In fact, this approach was previously adapted in the synthesis of zeolite A membranes in order to improve the separation performance [33]. The film thickness increased with each periodical exchange of the synthesis gel.

The NaA zeolite did not only grow as a film on top of the support, but a substantial amount was also found in the support pores. This is clearly observed in Figure 9 which shows a side-view SEM image of a NaA membrane formed after hydrothermal treatment at 75 °C for 6h.

ZSM-5 films with a low Si/Al ratio (ca 10) were prepared on porous α-alumina supports and tested as membranes in gas separation experiments (paper III). This particular system was previously investigated by our group [95]. Hence, the synthesis conditions of the membranes investigated here were adopted from that work. Figure 10 shows SEM images of a ZSM-5 membrane. The film thickness was in the range 1400-1800 nm for all membranes. As for the NaA membranes, substantial growth of zeolite in the pores of the top layer of the support was observed (Figure 10b).

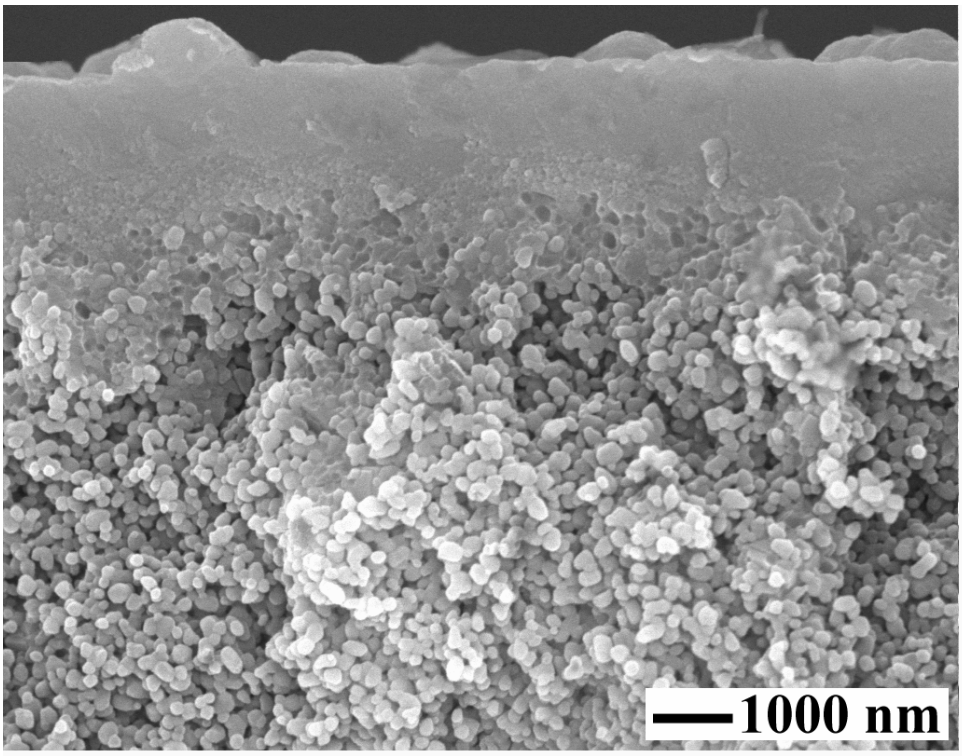

Figure 9. Side-view SEM image of a NaA film prepared at 75 °C for 6 h (without the addition of fresh synthesis gel). The image clearly shows that the pores of the support are plugged close to the interface between the support and the film.

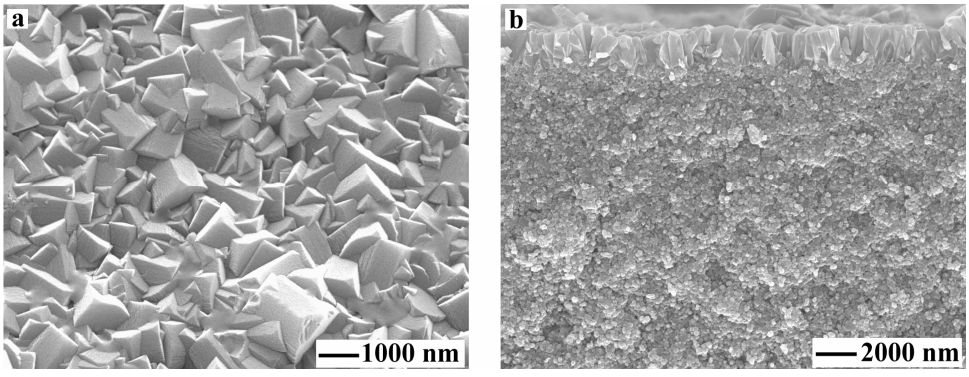

Figure 10. Top-view (a) and side-view (b) SEM images of a ZSM-5 membrane.

4.1.2 Determination of the zeolite film quality

The NaA films (Paper IV) as well as the ZSM-5 films (Paper III) were prepared on porous α-alumina supports which enabled single gas permeation tests (SF_6, He, N_2, H_2) in order to evaluate the quality of the films. The membranes were dried at room temperature (NaA membranes) or at 100 °C (ZSM-5 membranes) prior to single gas permeation experiments. After drying, the NaA zeolite is fully hydrated and no permeance is expected through the zeolite pores. Thus, weakly adsorbing gas molecules should permeate solely through defects. It was shown that a multi-step approach (see previous section) was necessary in order to obtain a gas-tight membrane. A high permeance was observed for all probe molecules for all LTA films prepared using one step (i.e. without exchange of synthesis gel) and it was concluded that these membranes were defective. A possible explanation is that the simultaneous growth of crystals in the bulk quickly consumed the nutrients before the film was fully closed in the one-step syntheses. On the contrary, the multi-step approach enabled the preparation of gas-tight membranes. Kumakiri et al. used a seeding technique to synthesize zeolite A and Y membranes [33]. The growth of the seeds was performed within the induction period of a clear solution. Hence, the nutrients in the synthesis solution were only consumed by the growing seeds attached to the support. However, the authors reported that repeated synthesis improved the water/ethanol separation factor in pervaporation experiments, in accordance with the work presented here.

Low or even undetectable permeances of SF_6 were found for the ZSM-5 membranes, indicating the absence of defects as the gas is expected to permeate mainly through defects. However, the permeances of N_2, He and H_2 were also low, indicating that the zeolite pores were blocked by adsorbed molecules even after drying at 100 °C. A completely dry membrane would have resulted in much higher permeances of these gases, considering that the kinetic diameter of these molecules are much smaller than the pores of ZSM-5 [69]. In fact,

separation experiments of a *n*-butane/*i*-butane mixture showed that it was necessary to dry the membrane at 220 °C in order to remove the molecules adsorbed in the zeolite pores (paper III). Noack et al. studied ZSM-5 membranes similar to the ones studied in this work [68]. The separation of *n*-butane/*i*-butane mixtures was investigated in the temperature range 25-130 °C. Low separation factors (<2) were obtained. However, the membrane was dried under mild conditions (150 °C at 10^{-3} mbar for 16 h) prior to measurement. Hence, it is possible that the zeolite pores were still blocked by adsorbed molecules and that the isomers permeated mainly through non-selective defects, resulting in poor separation factors.

4.1.3 Film stability during drying and thermal cycling

The thicker FAU films prepared in this work (Paper I-II) tend to detach from the dense support during rinsing of the as-synthesized samples. The weak adherence of the film to the support could in part be responsible. However, the relaxation of residual stressed may result in detachment of the film from the support. The risk of such effects is higher in thicker films since stored elastic strain energy per unit area of interface is increasing with film thickness. Since detachment of the FAU films were only observed for thick films, it is reasonable to assume that this effect is due to relaxation of residual stress.

The LTA membranes were very sensitive. Even membranes that were defect free after drying at room temperature according to gas permeation experiments, had cracks when the samples were investigated by SEM. These defects were probably formed during sample preparation for the SEM investigation or even in the microscope. Thicker films (>1000 nm) even detached from the support during drying prior to SEM analysis. In fact, formation of cracks were sometimes observed during recording of the SEM images. Straight cracks, that run both through and between crystals, were observed by SEM. Figure 11 shows a top-view SEM image of a LTA membrane with a typical crack. This particular

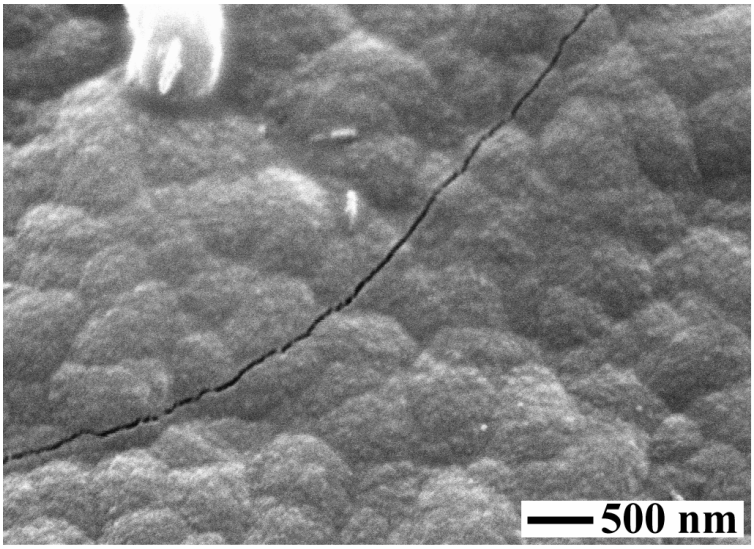

Figure 11. Top view SEM image of a crack in a NaA film formed after drying at moderate temperature (40 °C).

sample was gas-tight at room temperature. The formation of defects in these membranes is most likely due to drying, as the preparation procedure of samples for SEM investigation generally involved treatment at 40 °C.

The high sensitivity of the LTA membranes is further demonstrated in Figure 12, which shows the permeance of various gases as a function of temperature for an as-synthesized membrane dried at room temperature for some days. An instant rapid increase in the permeance of all gases is observed. The high permeance and low permeance ratios indicate that the film is defective and that the mass transport resistance is dominated by the support. In fact, numerous wide cracks were detected by SEM after the permeation experiment. The cracks were straight, intersecting perpendicular to each other and the film was partly detached from the support. The cracks even penetrate through the top layer of the support. The low temperature stability of the zeolite A membranes prepared in this work may be partly related to the shrinkage of the zeolite crystals upon drying as discussed in the introduction (1.1).

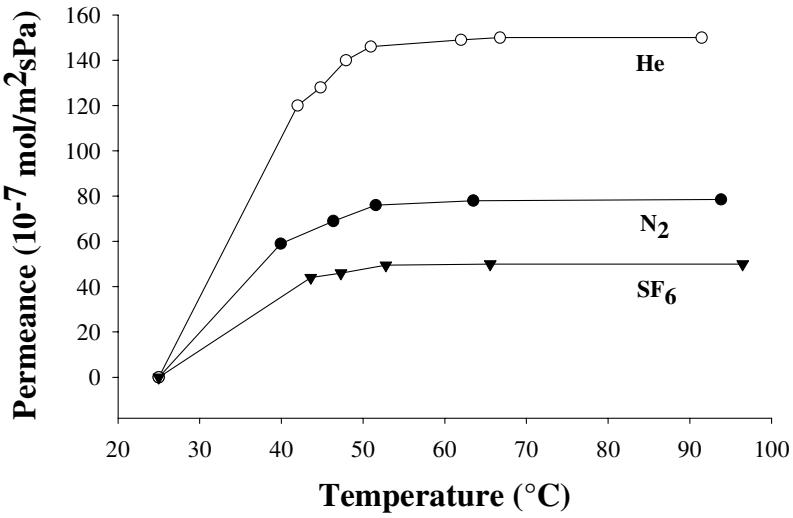

Figure 12. The permeance of He, N_2 and SF_6 measured *in-situ* during heating of a 1000 nm thick NaA film prepared at 100 °C for 6 h in synthesis gel S2 (see experimental). Prior to the experiment, the membrane was dried under ambient conditions for some days.

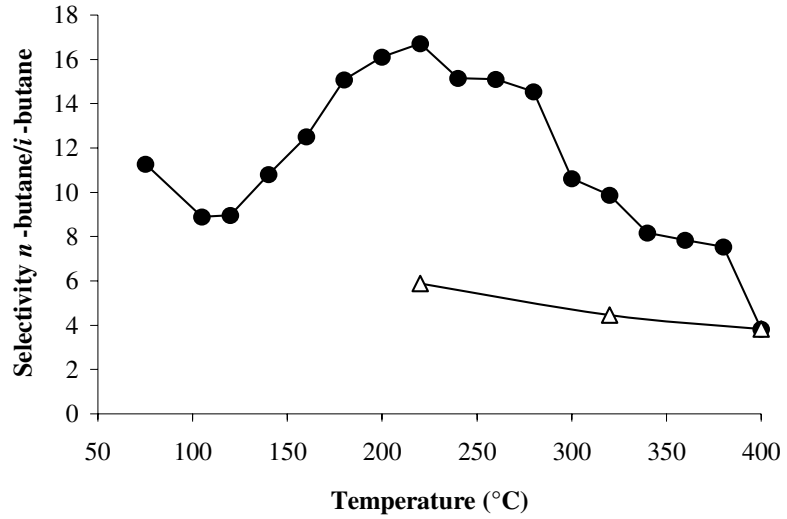

Figure 13. The separation selectivity for a 50/50 kPa *n*-butane/*i*-butane mixture of a ZSM-5 membrane (prepared from a template free synthesis gel) during heating (filled circles) and cooling (empty triangles).

The performance and thermal stability of template-free ZSM-5 membranes were investigated by *n*-butane/*i*-butane separation experiments (Paper III). Figure 13 illustrates the selectivity obtained for a membrane as a function of temperature during heating to 400 °C followed by cooling. The results presented in the Figure were obtained from a membrane that was dried for 12 h at 220 °C. This was shown to be necessary in order to remove adsorbed molecules (such as water and ammonia) which otherwise block the pores of the zeolite (Paper III).

During heating, the selectivity increased and reached a maximum of 16.7 at 220 °C. Further heating resulted in a decrease in selectivity, mainly in the ranges 280-300 °C and 380-400 °C. At these particular temperature intervals, defects were probably formed. At 400 °C the selectivity had dropped to 3.8. In order to confirm the cracks were formed during heating, permeation measurements were performed during cooling back to 200 °C. The high selectivities obtained during heating were not regained. These results indicate that cracks were formed during heating.

The temperature stability of the ZSM-5 membranes was further investigated by measuring the permeance of SF_6 as a function of temperature (Figure 14). The permeance remained low up to about 250 °C. Further heating resulted in a large increase of the permeance. After cooling back to room temperature, the permeance remained high. In addition, SEM images of the sample after the experiment showed large cracks with a width in the range 50-200 nm (Figure 15). Thus, it is likely that the sudden permeance increase is a direct consequence of the formation of those cracks. The temperature of crack formation for this membrane and the one subjected to the *n*-butane/*i*-butane separation experiment is in good agreement.

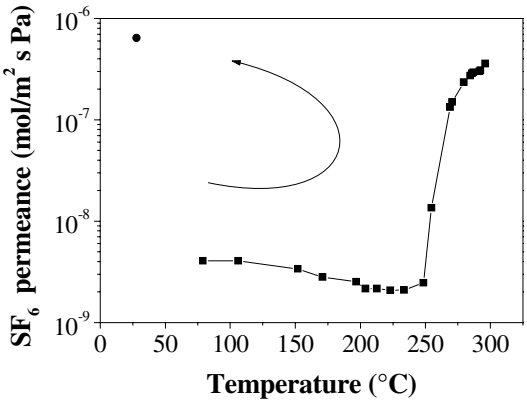

Figure 14. Permeance of SF_6 for a ZSM-5 membrane as a function of temperature. The arrow indicates the permeance after cooling back to ambient temperature.

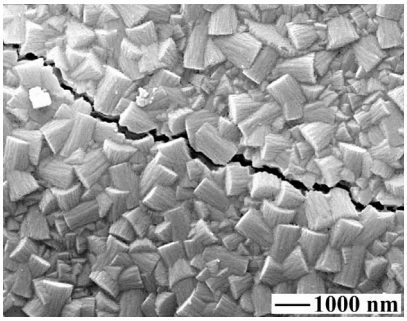

Figure 15. Top view SEM image of the ZSM-5 membrane subjected to the *in-situ* SF_6 permeance experiment.

4.2 TPA-MFI zeolite powder studied by HT-XRPD

Earlier work at the division showed that the heating/cooling rate during calcination of MFI membranes did not have a significant effect on the quality of the membranes [136]. In order to study this further, the thermal behavior of silicalite-1 (powder) during template removal using various heating rates was investigated by HT-XRPD. The data were evaluated by the Rietveld method. Figure 16a shows the low-angle diffraction peaks as a function of temperature for as-synthesized TPA-MFI powder. The intensity increases significantly in the range 275-500 °C. Figure 16b shows I_C (see equation (3.1)) and the refined wt% HMFI as a function of temperature. The agreement between the curves is very good. Hence, the template removal can be followed by the intensities of these peaks, which are readily extracted from the powder patterns. A sharp increase in intensity of the low-angle peaks during template removal was also observed by Milanesio et al. who performed a *in-situ* XRPD investigation of TS-1 and FeS-1 during template removal [16]. Although not demonstrated, the authors attributed

the change in intensity to the template removal. As observed in Figure 16, the template is decomposed and removed from the structure in the temperature range 275-500 °C, in accordance with previous work [14,43]

Figure 17 shows the MFI unit cell volume as a function of temperature during thermal cycling (25-500-25-500-25 °C in that order) in air. During heating, a first contraction peak is observed at about 175 °C. This is attributed to dehydration which occurs before template decomposition, as already reported [14]. A large contraction is observed in the temperature range 275-500 °C and is attributed to the template removal as discussed above. During cooling, the unit cell expands but at RT, the unit cell of the calcined MFI is smaller compared to the as-synthesized phase. These results are in concert with a previous study [17].

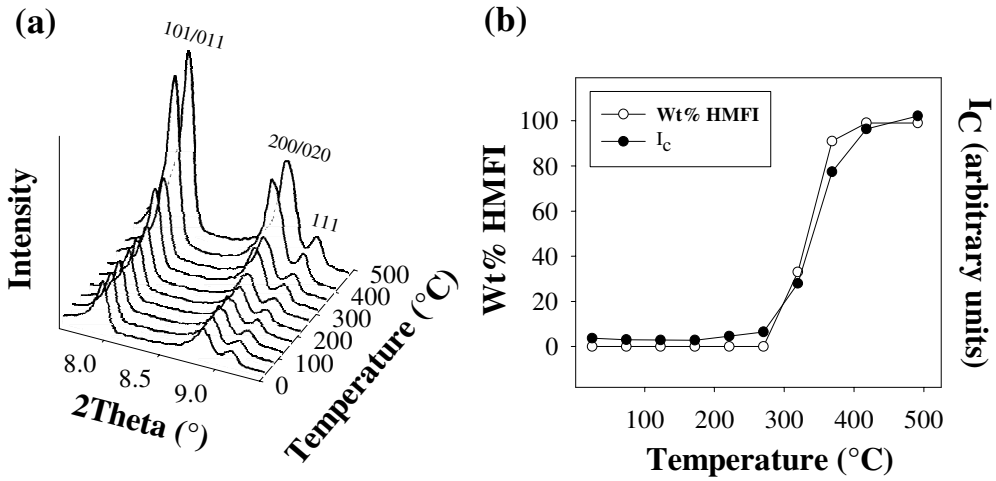

Figure 16. The low-angle diffraction peaks of TPA-MFI as a function of temperature is shown in (a). The refined wt% (empty circles) of the empty MFI structure as well as I_c (filled circles) are plotted against temperature in (b).

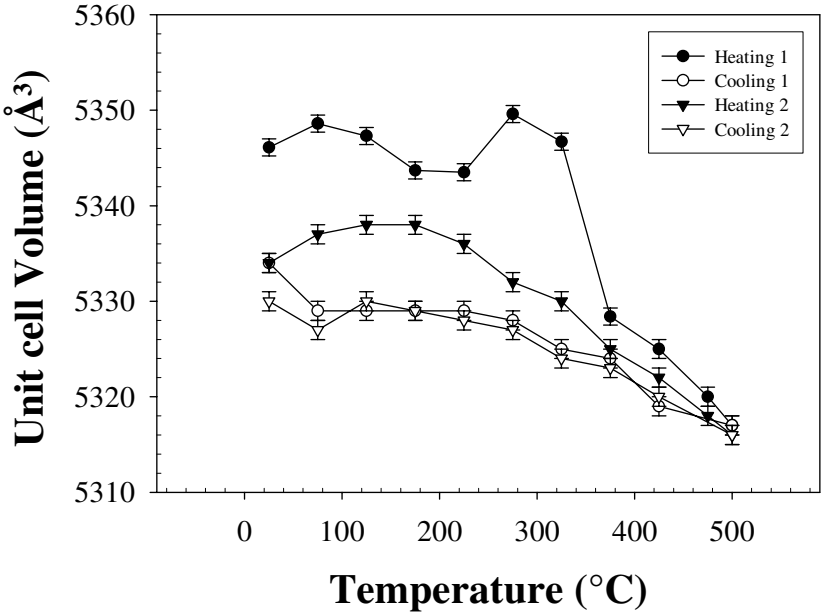

Figure 17. Unit cell volume of the as-synthesized TPA-silicalite-1 as a function of temperature during heating to 500 °C (heating 1) followed by cooling to RT (cooling 1). The temperature ramp was repeated on the calcined material and the data are included in the figure (heating 2 followed by cooling 2).

During heating of the calcined MFI powder (heating 2 in Figure 17), NTE is observed in the temperature range 175-500 °C. Hence, the NTE in TPA-silicalite-1 during calcination is not only due to the removal of the template molecules. A structure intrinsic mechanism is also present, which can be explained by the rigid-unit modes (RUM) theory, i.e. temperature-induced transverse vibrations of two-coordinate bridging oxygen atoms which causes a decrease in the distance between the Si atoms in adjacent tetrahedral sites [18].

Figure 18 shows the MFI unit cell volume (a) and the conversion factor α (b) (see equation (3.1)) as a function of temperature during the first heating ramp using various heating rates. As can be observed in this Figure, the cell volume of MFI is not sensitive to the heating rate. On the contrary, the heating rate affects the template removal (Figure 18b). Hence, a dependence of thermal contraction

on the heating rate should be observed for the NTE caused by template removal. This was not observed, probably due to masking by the structure intrinsic NTE mechanism (see Figure 17) which is not dependent on the kinetics.

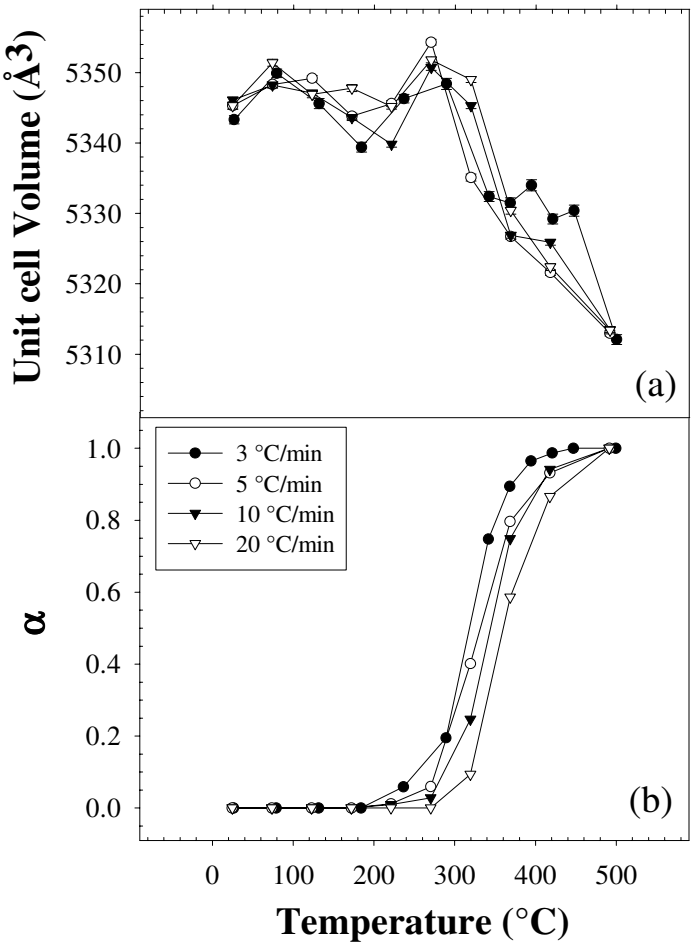

Figure 18. The MFI unit cell volume (a) and α (b) as a function of temperature for various heating rates during heating of an as-synthesized powder.

4.2.1 Kinetics of TPA removal

The apparent activation energy (E_a) for the template decomposition in silicalite-1 was determined using the Kissinger and the Flynn-Wall-Ozawa methods (equations (1.24) and (1.25), respectively). The method of Kennedy and Clark, with the Avrami equation as a kinetic model, was also used to determine both the E_a and the reaction order (equations (1.26) and (1.27), respectively). The Kissinger and the Flynn-Wall-Ozawa methods gave an E_a of 138 (±25) and 138 (±29) kJmol^{-1}, respectively. The E_a determined with the method of Kennedy and Clark was 140 (±30), in good agreement with the results obtained with the other methods. The reaction order was estimated to be 0.5, which indicates that the rate-limiting step is one-dimensional diffusion [160]. This result is in agreement with Milanesio et al. [16], who studied the kinetics of template removal in Ti-silicalite-1. The reaction order of 0.5 was explained with preferred diffusion of the reaction products in the straight channels running along b, which offers the shortest way out of the crystals.

4.3 TPA-MFI membranes

4.3.1 SEM characterization of the TPA-MFI membranes

Figure 19 shows top- and side view SEM images of a calcined MFI membrane synthesized in the presence of organic template molecules. The MFI film appears to consist of three layers. The 700 nm thick top layer consists of crystals with columnar character. The next layer, defined as the intermediate layer in [82] is about 500 nm thick and is composed of small grains. Zeolite is also formed in the pores of the support. This zeolite-support composite layer (defined as the bottom layer in [82]) is about 500 nm thick. Opposed to the as-synthesized membrane, cracks with a width of about 30 nm are found after

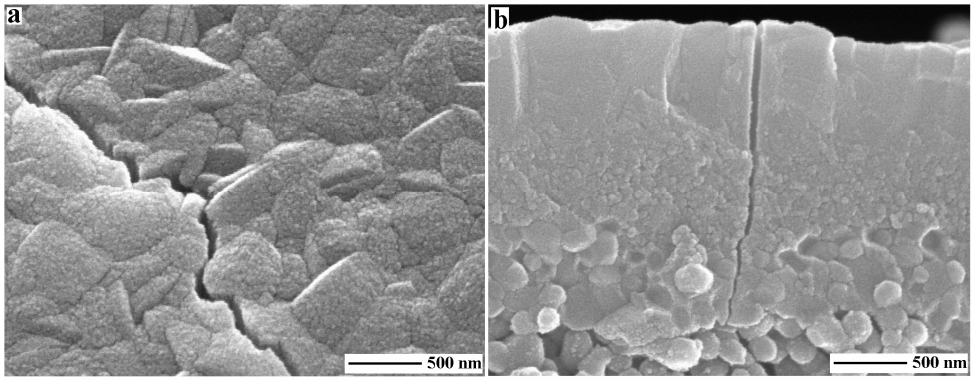

Figure 19. Top-view (a) and side-view (b) SEM image of a calcined MFI membrane synthesized at 100 °C for 72 h in the presence of TPA^+.

calcination [82], see Figure 19. The penetration of the MFI film in the pores of the support assures a strong anchoring of the film to the support. The crystals in the film appears to be well intergrown, an observation that is further supported by the fact that the cracks formed after calcination do not preferably run between crystals but also within crystals (Figure19).

4.3.2 Thermal behavior of TPA-MFI membranes studied by HT-XRPD

Figure 20 shows the refined a-axis (a) and c-axis (b) of the MFI coated α-alumina support as a function of temperature. For comparison, the refined unit cell parameters for a blank support are also included in the Figure. The unit cell expands as the temperature increases. The isotropic linear thermal expansion coefficient was $8.12 \cdot 10^{-6}$ and $8.25 \cdot 10^{-6}$ K^{-1} for the MFI coated support and the blank support, respectively. These values are in good agreement with literature data for α-alumina powder ($7.9 \cdot 10^{-6}$ K^{-1} [177]). However, comparing the non-coated and coated support, a slightly lower expansion was observed for the latter. This difference is mainly due to a lower thermal expansion along the c-

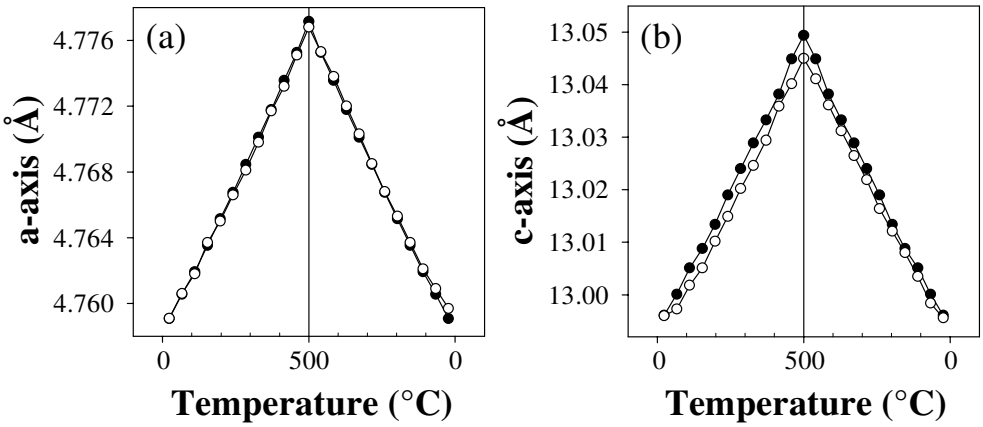

Figure 20. The refined a-axis (a) and c-axis (b) as a function of temperature for a MFI coated α-alumina support (empty symbols) and a blank α-alumina support (filled symbols) in the temperature cycle 25-500-25 °C.

direction in the MFI coated α-alumina support, compared to the blank support (Figure 20 b). Hence, the presence of the zeolite film affects the thermal expansion of the support. This will be discussed later in this section.

Figure 21 reports the refined a-axis (a), b-axis (b) and c-axis (c) of the MFI film in the temperature cycle 25-500-25 °C. For comparison, the cell parameters of the MFI powder are also included in the Figures. The unit cell in the MFI film is distorted with respect to the powder during the entire temperature cycle. The b-axis is always longer in the film whereas the a- and c-axes are shorter. From Figure 20 and 21 it is clear that the thermal expansion of MFI and α-alumina differs significantly. The α-alumina support expands while the MFI film contracts. The film should therefore experience an isotropic in-plane tensile stress (i.e. stress in the plane parallel to the film surface) which increases during heating. Consequently, an out-of-plane strain (i.e. strain in the direction perpendicular to the film surface) would build up as a result of Poisson's ratio. Here it should be remarked that the refined unit cell parameters of the phases in

the membrane are based on data collected from planes parallel to the film surface (see section 3.2.3.2) and should therefore mirror the *d*-spacings of these planes. Consequently, the out-of-plane strain of crystals in the MFI film could be calculated at each investigated temperature using the MFI powder as reference. The results are shown in Figure 22. As the majority of the crystals are

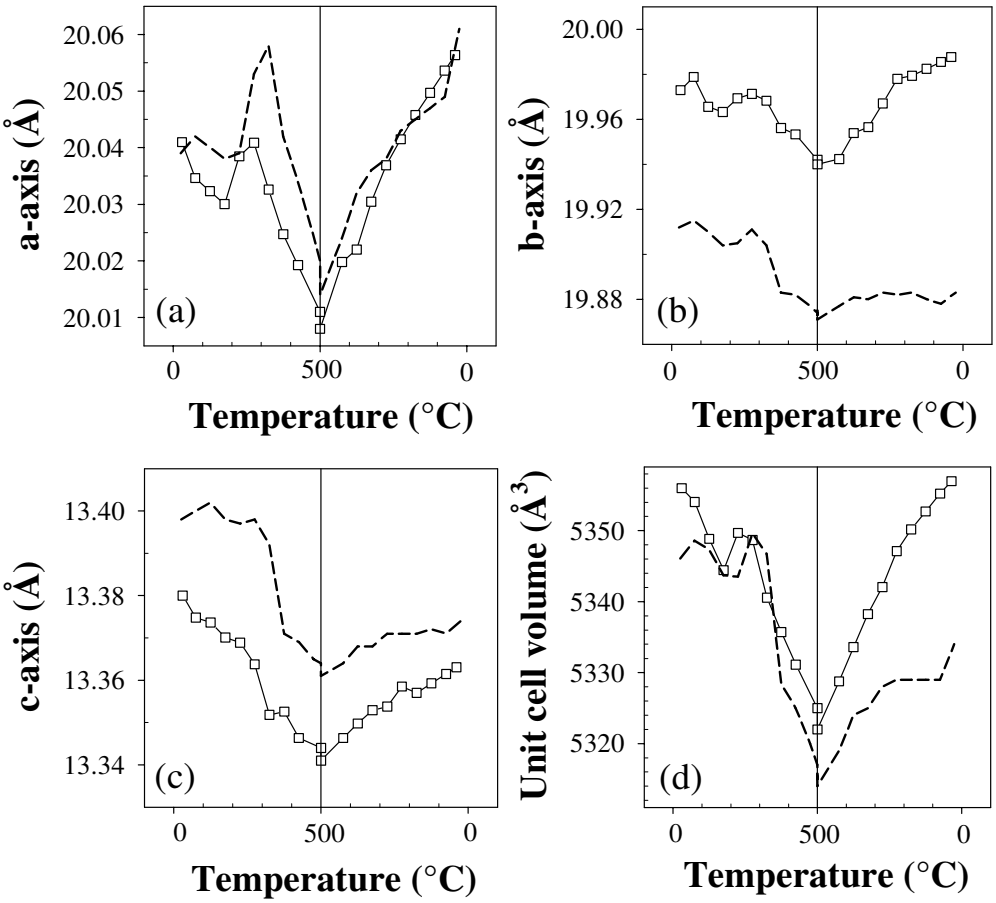

Figure 21. The refined a-axis (a), b-axis (b), c-axis (c) and unit cell volume (d) as a function of temperature for the MFI film (connected symbols) as well as MFI powder (dashed line) in the temperature cycle 25-500-25 °C.

oriented with the a-axis perpendicular to the film surface (see Paper VII), the strain along this crystallographic direction (out-of-plane strain) should be most representative for the MFI film. The strain is overall compressive along the a-direction (Figure 22). An out-of-plane compressive strain would be expected for a film with a positive Poisson's ratio which is exposed to an in-plane tensile stress [178]. The strain in the a-direction increases with temperature up to about 325 °C after which it is decreased gradually, probably due to formation of cracks

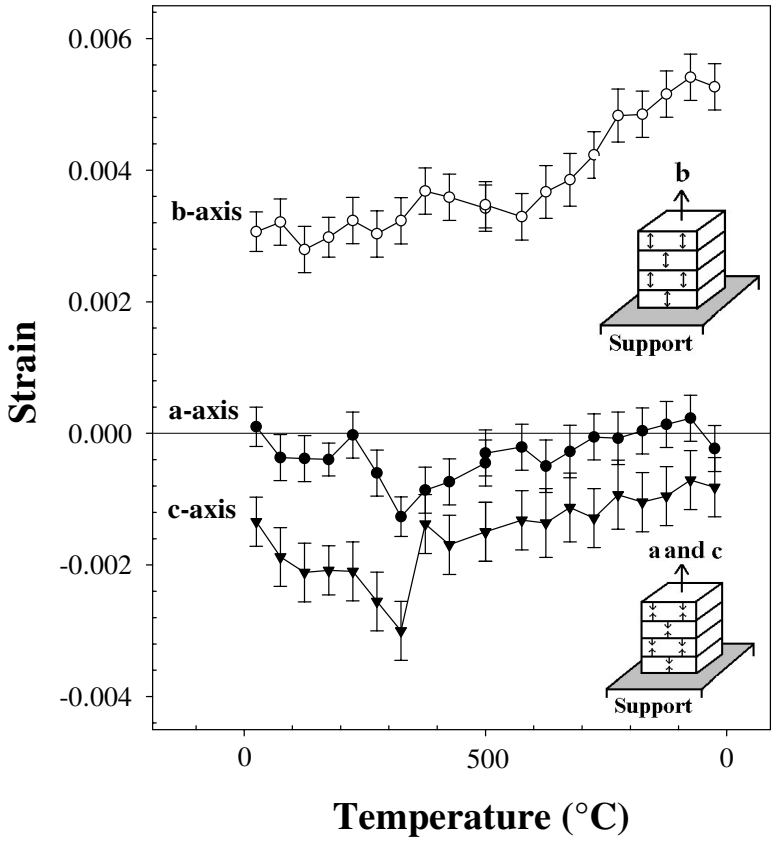

Figure 22. The out-of-plane strain as a function of temperature along different crystallographic directions in the MFI film. The inserted sketches show that the crystallographic planes along b are under tensile strain while the ones along a and c are under compressive strain.

in the zeolite film during further heating up to 500 °C. In fact, the work presented in this thesis showed that cracks were formed in ZSM-5 membranes in the temperature range 220-400 °C (see section 4.1.3). The decrease in strain during cooling is reasonable considering that the thermal in-plane strain decreases as the difference in volume between the film and the support is reduced.

An overall compressive out-of-plane strain is also observed for the c-axis. Furthermore, the variation in strain for the c-axis with temperature is qualitatively the same as the one observed for the a-axis.

A more surprising result is the large out-of-plane tensile strain along the b-direction (Figure 22), which actually increases during cooling. This apparently odd behavior is difficult to explained on the basis of the data presented here, and should be investigated further in the future.

The out-of-plane strain in the MFI coated α-alumina support was also calculated, using the blank support as a reference. The results are shown in Figure 23. A compressive strain is observed for the c-axis during the entire temperature cycle. The strain increases during heating, which is explained by an increased difference in unit cell volume between the support and the MFI zeolite. However, a larger increase in strain would probably have been observed if no cracks were formed in the zeolite film. During cooling, the strain decreases as the thermal expansion mismatch between the zeolite and the support decreases. The strain along the a-axis barely exceeds the experimental error. However a slight compressive and tensile strain is observed during heating and cooling, respectively. It should be remarked that the strain in the α-alumina support is at least one order of magnitude smaller than that observed in the zeolite film. It is improbable that the overall out-of-plane compressive strain observed in the α-alumina support is caused by the thin zeolite layer on top of the support (ca 1200 nm, see section 4.3.1). However, the film extends into the pores of the support, thus forming a zeolite-support composite layer (ca 500 nm,

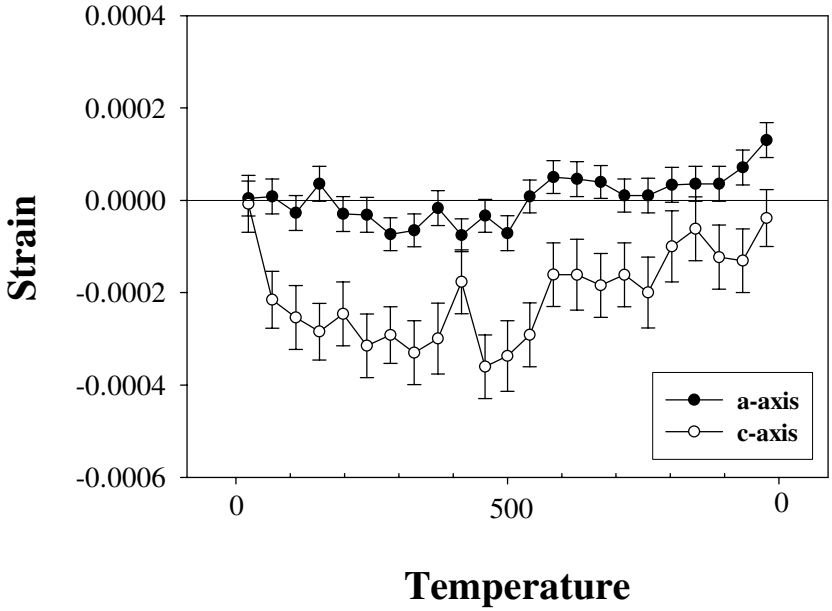

Figure 23. The out-of-plane strain along the a- and c- direction in the MFI coated α-alumina support as a function of temperature.

see section 4.3.1). It is possible that the negative thermal expansion of the zeolite surrounding the α-alumina grains in this layer causes a net in-plane tensile strain which is mirrored in the observed out-of-plane compressive strain.

4.3.3 The microstructure of the α-alumina support

The microstructure of the α-alumina support as a function of temperature was studied using the method of Williamson and Hall (equation (1.12)) (Paper VII). The isotropic size and microstrain at RT was 89 nm and 0.0124 %, respectively. Hence, defects are already present in the support of the as-synthesized membrane. The defects are probably dislocations, considering the nature of the α-alumina structure (Paper VII). However, it should be emphasized that the method of Williamson and Hall (equation (1.12)) should not be used

quantitatively [179]. It should only serve as a first approximation of the nature of the line broadening effects. Figure 24 shows the microstrain of the α-alumina support as a function of temperature. A large increase in microstrain is observed during heating which may suggest the formation of structural defects in the support. It is possible that the defects are formed in order to release the thermal stress induced in the support during heating. The stabilization of the microstrain at 500 °C is possibly due to the fact that the thermal stress decreases during cooling (as the difference in thermal expansion between the zeolite and the support decreases) and does no longer induce the formation of structural defects in the support. In order to confirm the results from the line broadening analysis, bright field TEM images were recorded from the support subjected to the *in-situ* experiment, see Figure 25. In fact, structural defects (likely dislocations) were observed. The SAED diffraction pattern in the insert confirms that the signal comes from a single crystal of α-alumina.

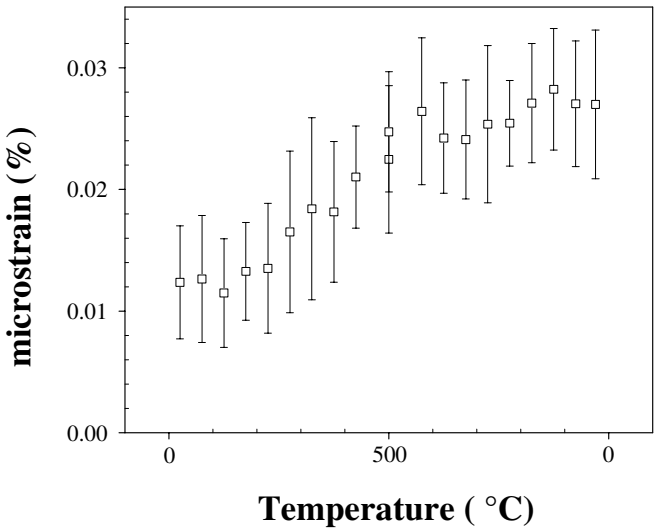

Figure 24. Microstrain of the MFI coated α-alumina support as a function of temperature.

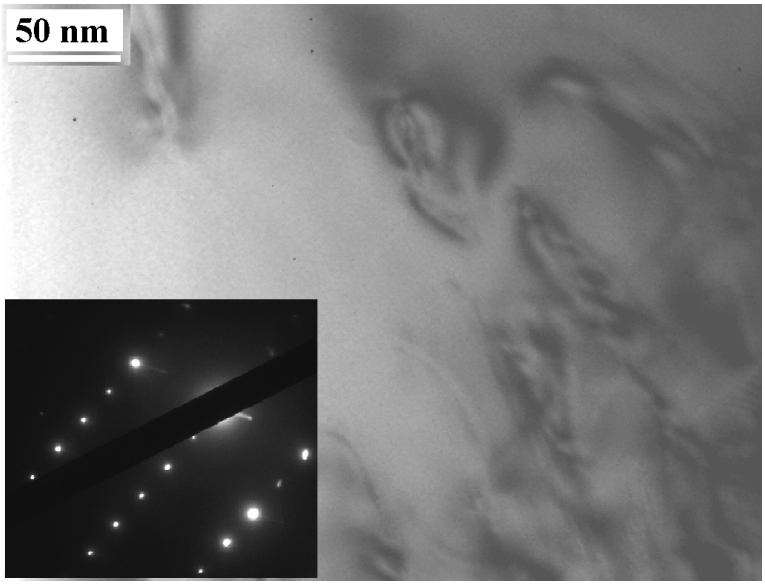

Figure 25. A bright field TEM image, of a sample taken from the membrane that underwent the *in-situ* synchrotron experiment, showing structural defects in the α-alumina support. The SAED diffraction pattern in the insert confirms that the signal is transmitted by a single crystal of α-alumina.

4.3.4 Crack formation model

A model for crack formation was postulated on the basis of the results presented in this thesis and previous work at our division [82]. However, some important assumptions, which are supported by SEM images (section 4.3.1 and [82]), have to be made: (a) The crystals are strongly bonded to the support. (b1) Relatively thick MFI films, as the one studied here and in previous work by our group (membrane type U-72 in [82]), are composed of well intergrown crystals. (b2) In the case of thinner films (500 nm, membrane type M30 in previous work [82]), the crystals are less intergrown compared to thicker films.

Our models for crack formation is described as follows: During heating, the MFI crystals experience a weak contraction at about 175 °C (dehydration) and a strong contraction in the temperature range 275-500 °C (template removal). At

the same time, the α-alumina support expands. The difference in thermal behavior between the film and support induces thermal stress in the relatively thick film (b1), which eventually is released mainly via crack formation. Dislocations in the support are also formed, possibly to release part of the stress. In the case of a thin film (b2), less or no stress develops and the grain boundaries are opened, as also suggested by Dong et al. ([15]). In fact, defects with a width of a few nanometers is present in this kind of membrane [116] which may be open grain boundaries formed during calcination, according to our model. During cooling, the support contracts and the MFI film expands. Hence, the width of the defects formed at high temperature is likely to decrease as also suggested by Dong et al. [15].

The crystal intergrowth should be the main factor determining the type of defects (cracks or open grain boundaries). In the case of highly intergrown crystals, the bonds between crystals and within crystals are of similar strength and cracks may develop even within crystals (b1). Less or no intergrowth should result in the formation of open grain boundaries upon calcination (b2).

The model (b1) can be generalized to explain the crack formation observed in the template-free ZSM-5 and NaA membranes (Paper III and IV, respectively), The permeation results for these membrane types showed that cracks were formed during heating. In addition, SEM observations of these membranes showed that the films extend into the support pores and that cracks do not preferably run between crystals. Hence, the films are strongly bonded to the support and the crystals are well intergrown. Negative thermal expansion for the hydrated forms of NaA and ZSM-5 ([20], [180]) has been reported. Based on these experimental results and literature reports, the model for crack formation should be applicable for all membrane systems studied in this thesis.

Finally, earlier work has indicated that the heating rate [14] and the orientation of the crystals in the film [134] may influence the crack formation, and these two parameters will now be discussed in relation to our model for crack

formation. In this work (Paper VI), the effect of heating rate on the thermal behavior of silicalite-1 powder during calcination was investigated. It was found that the variation of the heating rate has no effect on the thermal expansion curves (see Figure 18). Hence, under the assumption that the crystallites constituting a supported MFI film has the same thermal behavior as the crystallites in the powder, the thermal expansion mismatch at a certain temperature during calcination of a supported film is independent of heating rate. Hence, the crack formation should not be influenced by the heating rate as opposed to an early recommendation [14] to calcine zeolite membranes very slowly in order to avoid crack formation. In fact, previous work at our division showed no correlation between the heating/cooling rate and membrane quality [136]. The work presented here (papers VI-VII) showed that MFI has an anisotropic thermal behavior. Hence, the orientation of the crystals in the film should influence the thermal behavior of the film, as already suggested [134]. Based on data for MFI powder presented in this thesis (Figure 21), the in-plane thermal expansion would be largest for b- and c-oriented films. Hence, such films would have a thermal behavior closest to the one for the support and should be more crack resistant. As discussed in the introduction, b-oriented MFI films with high performance in xylene isomer separation has been prepared by Lai et al. [67]. The high quality of the membranes was partly attributed to absence of cracks, due to the presence of an intermediate layer of mesoporous silica between the support and the zeolite film which eliminate thermal stresses [67]. However, considering the results presented in this thesis, a contributing factor to the crack resistance of these membranes could be the specific preferred orientation, which reduces the thermal expansion mismatch between the materials in the composite, or weakly intergrown crystals.

5. CONCLUSIONS

Conditions were established for the preparation of FAU films on dense alumina supports and LTA films on porous α-alumina supports. The thickness of the films was linearly dependent on the synthesis duration. However, a maximum in the FAU film thickness was observed after prolonged hydrothermal treatment due to dissolution of the FAU crystals and simultaneous growth of GIS. Furthermore, the position of the support in the reactor during growth of FAU films was shown to affect the film thickness. Thicker films were obtained when the supports were placed in the bottom part of the reactor. The quality of the LTA membranes could be improved by applying several growth steps were fresh synthesis gel was periodically added to the cleaned samples.

ZSM-5 films with low Si/Al ratio were prepared on porous α-alumina supports according to a procedure previously developed by our research group. In butane isomer mixture separation experiments, a maximum separation factor of 17.8 was obtained at 220 °C. It was shown that drying of the membrane at high temperature was crucial to obtain high fluxes and separation factors.

Common for both the MFI and the LTA films prepared in this work was that cracks were readily formed during heating as determined by *in-situ* gas permeation measurements. The MFI membranes with low Si/Al ratio cracked after exposure to temperatures higher than 250 °C. The zeolite NaA films cracked already at 40 °C. These results prompted a study of the crack formation with the aim to develop a model. Relatively thick α-alumina supported TPA-MFI films (ca 1800 nm) which reproducibly crack during calcination, according to previous work by our group, were chosen for the study. The crystals in these films are well intergrown. The proposed model explains the crack formation in membranes studied in this thesis as well as the lack of cracks in thinner MFI membranes (ca 500 nm) developed by our research group. The latter type of

membrane is composed of less intergrown crystals, compared to thicker MFI films. In addition, nano-sized defect are formed in these membranes during calcination, according to permporosimetry measurements previously performed at our division. According to the model, the zeolite contracts and the support expands. In the case of films composed of well intergrown crystals, stress develops in the composite as a result of the thermal expansion mismatch. The stress is eventually released via crack formation in the film and dislocations in the α-alumina support. For films in which the crystals are less intergrown, the grain boundaries are opened during heating and no cracks are formed, in accordance with models already presented in the literature. These open grain boundaries are probably the nano-sized defects observed by permporosimetry in previous work.

The model for crack formation was developed based on results from various experimental techniques such as HT-XRPD (utilizing both synchrotron radiation and in-house sources) in combination with the Rietveld method, SEM, TEM and gas permeation measurements. The MFI powder experiences a large contraction in the temperature range 275-500 °C, in accordance with literature. The contraction was shown to be related to template removal and possibly a structure intrinsic mechanism. The MFI film also contracts during heating while as the α-alumina support expands. The thermal expansion mismatch between the film and the support caused in-plane tensile strain which increased during heating. This was mirrored in a compressive out-of-plane strain of most crystals in the film, due to the effect of Poisson's ratio. In fact, the strain was found to increase during heating up to about 325 °C, as the difference in volume between the film and the support increased. Further heating caused a decrease in strain, which was attributed to the formation of cracks in the membrane which released the strain. The thermal behavior of the MFI coated α-alumina support was shown to be different from the blank support. This was explained by an overall thermal compressive out-of-plane strain, probably due to the presence of zeolite in the

pores of the support. Furthermore, a microstructure analysis of the MFI coated support using *in-situ* synchrotron diffraction data showed that structural defects were formed during heating up to 500 °C. These defects were possibly due to the accumulated thermal stress.

This thesis work also showed that the contraction behavior of TPA-MFI powder was independent on heating rate. Therefore, the difference in thermal expansion between the support and the TPA-MFI film should not vary with heating rate. This implies that the crack formation can not be influenced by the heating rate, according to the model presented in this thesis. In fact, earlier work at our division showed that no correlation exists between heating rate and crack formation.

6. IDEAS FOR FUTURE INVESTIGATIONS

New experiments to further optimize the synthesis conditions for the preparation of high quality membranes should be performed, taking into consideration the model for crack formation presented in this thesis. The risk of crack formation in zeolite membranes could basically be reduced by (i) minimizing the difference in thermal expansion between the film and the support and (ii) minimizing the intergrowth between the crystals in the film without compromising the film continuity. The first criteria could be achieved by choosing a support material with a thermal behavior similar to the one of the zeolite film or deposit intermediate layers of for example mesoporous silica as discussed in the introduction. Furthermore, as the thermal expansion of some zeolites (such as MFI) is anisotropic, the orientation of the crystals in the film should have an influence on the thermal stress. Based on the results of the present work, b- and c-oriented MFI films should have higher crack resistance. In order to fulfill the second criteria, synthesis conditions in general such as properties and orientation of seed crystals, temperature, synthesis time and chemistry of synthesis solution are factors to consider.

7. ACKNOWLEDGEMENTS

My deepest gratitude to my supervisor Prof. Jonas Hedlund for his encouragement and support during this work. I am also grateful to Prof. Johan Sterte, for giving me the opportunity to begin my PhD studies at his division. Currently, Prof. Sterte is the president of Växjö university. I am especially grateful to Prof. Alessandro Gualtieri, for patiently teaching me the Rietveld method and for kindly sharing his expertise in XRPD. Hopefully, I will gain a deeper knowledge about the Rietveld method in our future collaboration. I thank Dr. Fredrik Jareman for all the fruitful scientific discussions, for our collaboration in some of the papers and for all the laughs in the lab. I thank Lic. Eng. Charlotte Andersson for our collaboration in paper VII. I am grateful to our Secretary Ingrid Granberg for all the administrative help, and also for all the nice chats. I would like to thank Dr. Lubomira Tosheva and Lic.Eng. Vania Engström, for always taking the time to help me, both at work and in private. Thank you for being such good friends. I thank Dr. Zheng Wang, Dr. Olov Öhrman, Mr. Olle Niemi, Dr. Valeri Naidenov, Dr. Derek Creaser, Ms. Maria Edin, Dr. Ingrid Nohlgren, Dr. Peter Sedin and Dr. Margareta Lidström-Larsson for their companionship. A special thank to my "big sister" Dr. Qinghua Li, for her contagious enthusiasm for science and also for being such a good friend. Dr. Li has now started a wonderful carrier at the University of Shanghai, China and is also the mother of two beautiful girls. I wish her all the best.

I would like to thank Tina Giliberti for her help in the laboratory during the second part of this work. I thank Dr. Monica Dapiaggi, Dr. Carlo Meneghini and Dr. Matteo Leoni for participating in the work presented in some of the papers. I thank Prof. Maria Prudenziati, my current employer, for allowing me to do the final preparations for this thesis on working hours.

Financial support from the Swedish Research council (VR) as well as the foundation Blanceflor Boncompagni-Ludovisi, born Bildt is acknowledged.

Jag skulle vilja tacka mina underbara föräldrar, Bengt och Gertrud Lassinantti, samt mina syskon, Simon och Matilda Lassinatti, for allt det stöd ni har gett mig under dessa år.

Grazie mio amore per tutto quello che hai fatto per me. Senza di te, questa tesi non avrebbe mai stato realizzato. Ti adoro per chi sei e come sei.

I dedicate this thesis to my children, Ania and Isak, and to my husband, Alessandro. I hope my modest accomplishment will make you proud of me.

Magdalena Gualtieri
August 2006

8. REFERENCES

[1] R. Szostak, Molecular Sieves, Blackie Academic & Professional, London, 2nd ed.,1998, pp. 20, 158.

[2] D.W. Breck, Zeolite Molecular Sieves, John Whiley & sons, New York, 1974, p. 350.

[3] D.W. Breck, Zeolite Molecular Sieves, John Whiley & sons, New York, 1974, p. 348.

[4] R. Szostak, Handbook of molecular Sieves, Van Nostrand Reinhold, New York, 1992.

[5] G. Vezzalini, S. Quartieri, E. Galli, A. Alberti, G. Cruciani, and Å. Kvick, Zeolites, 19 (1997) 323.

[6] D.W. Breck, Zeolite Molecular Sieves, John Whiley & sons, New York, 1974, p. 351.

[7] H. van Koningsveld, J.C. Jansen and H. van Bekkum, Zeolites, 7 (1987) 564.

[8] B.F. Mentzen, J.-M. Letoffe and P. Claudy, Thermochimica Acta, 288 (1996) 1.

[9] H. Van Koningsveld and J.H. Koegler, Micropor. Mesopor. Mater., 9 (1997) 71.

[10] W.M. Meier and D.H. Olson, Atlas of Zeolite Structure Types, Butterworths, London, 1987.

[11] P. Tschaufeser and S.C. Parker, J. Phys. Chem., 99 (1995) 10609.

[12] P. Lightfoot, D.A. Woodcock, M.J. Maple, L.A. Villaescusa and P.A. Wright, J. Mater. Chem., 11 (2001) 212.

[13] S.H. Park, R.W. Grosse-Kunstleve, H. Graetsch and Gies, in “Progress in Zeolite and Microporous Materials, Studies in Surface Science and Catalysis”, 105 (1997) 1989.

[14] E.R. Geus and H. van Bekkum, Zeolites, 15 (1995) 333.

[15] J. Dong, Y.S. Lin, M.Z.-C. Hu, R.A. Peascoe and E.A. Payzant, Micropor. Mesopor. Mater., 34 (2000) 241.

[16] M. Milanesio, G. Artioli, A.F. Gualtieri, L. Palin and C. Lamberti, J. Am. Chem. Soc., 125 (2004) 14549.

[17] R. Millini, G. Perego, D. Berti, W.O. Parker Jr. A. Carati and G. Bellussi, Micropor. Mesopor. Mater., 35-36 (2000) 387.

[18] M.P. Attfield and A.W. Sleight, Chem. Commun., (1998) 601.

[19] J.W. Couves, R.H. Jones, S.C. Parker, P. Tschaufeser and C.R.A. Catlow, J. Phys. Condens. Matter, 5 (1993) L329.

[20] A. Colantuono, S. Dal Vecchio, G. Mascolo and M. Pansini, Thermochimica Acta 296 (1997) 59.

[21] B.J. Schoeman, Doctoral thesis, Chalmers University of Technology, Göteborg, 1994.

[22] H. Lechert, P. Staelin and C. Kuntz, Zeolites, 16 (1996) 149.

[23] B.J. Schoeman, J. Sterte and J.-E. Otterstedt, Zeolites, 14 (1994) 110.

[24] H. Van Koningsveld, H van Bekkum and J.C. Jansen, Acta Cryst., B43 (1987) 127.

[25] S. Henga, P.P.S. Laua, K.L. Yeung, M. Djafer and J.-C. Schrotter, J. Membr. Sci., 243 (2004) 69.

[26] Q. Li, M.L. Amweg, C.K. Yee, A. Navrotsky and A.N. Parikh, Micropor. Mesopor. Mater., 87 (2005) 45.

[27] H. Lee, S.I. Zones and M.E. Davis, Micropor. Mesopor. Mater., 88 (2006) 266.

[28] Q. Li, B. Mihailova, D. Creaser and J. Sterte, Micropor. Mesopor. Mater., 43 (2001) 51.

[29] H. Robson (Ed), Verified syntheses of zeolitic materials, second ed., Elsevier Science B.V, Amsterdam, 2001.

[30] R.I. Walton, R.I. Smith and D. O'Hare, Micropor. Mesopor. Mater., 48 (2001) 79.

[31] T. Cetin, M. Tather, A. Erdem-Senatal, U. Demirler and M. Ürgen, Micropor. Mesopor. Mater., 47 (2001) 1-14.

[32] C. Bebon, D. Colson, B. Marrot, J.P. Klein and F. Di Renzo, Micropor. Mesopor. Mater., 53 (2002) 13.

[33] I. Kumakiri, T. Yamaguchi and S.-I. Nakao, Ind. Eng. Chem. Res., 38 (1999) 4682.

[34] H. Kacierk and H. Lechert, J. Phys. Chem., 79 (1975) 1589.

[35] V.N. Romannikov, V.M. Mastikhin, S. Hočevar and B. Držaj, Zeolites, 3 (1983) 311.

[36] L.M. Parker, D.M. Bibby and J.E. Patterson, Zeolites, 4 (1984) 168.

[37] G. Debras, A. Gourgue, J.B. Nagy and G. De Clippeleir, Zeolites, 5 (1985) 377.

[38] M. Soulard, S. Bilger, H. Kessler and J.L. Guth, Zeolites, 7 (1987) 463.

[39] J.B. Nagy, P. Bodart, H. Collette, J. El Hage-Al Asswad, Z. Gabelica, R. Aiello, A. Nastro and C. Pellegrino, Zeolites, 8 (1988) 209.

[40] J. El Hage-Al Asswad, N. Dewaele, J.B. Nagy, R.A. Hubert, Z. Gabelica, E.G. Derogane, F. Crea, R. Aiello and A. Nastro, Zeolites, 8 (1988) 221.

[41] M. Soulard, S. Bilger, H. Kessler and J.L. Guth, Zeolites, 11 (1991) 107.

[42] S. Bilger, M. Soulard, H. Kessler and J.L. Guth, Zeolites, 11 (1991) 784.

[43] K.H. Gilbert, R.M. Baldwin and J.D. Way, Ind. Eng. Chem. Res., 40 (2001) 4844.

[44] M. Nowotny, J.A. Lercher and H. Kessler, Zeolites, 11 (1991) 454.

[45] M. Soulard, S. Bilger, H. Kessler and J.L. Guth, Zeolites, 11 (1991) 107.

[46] O. Pachtová, M. Kocirik, A. Zikánová, B. Bernauer, S. Miachon and J.-A. Dalmon, Micropor. Mesopor. Mater., 55 (2002) 285.

[47] A.S.T. Chiang and K.-J. Chao, J. Phys. Chem. Solids, 62 (2001) 1899.

[48] T.C. Bowen, R.D. Noble and J.L. Falconer, J. Membr. Sci., 245 (2004) 1.

[49] J. Caro, M. Noack, P. Kölsch and R. Schäfer, Micropor. Mesopor. Mater., 38 (2000) 3.

[50] L. Cot, A. Ayral, J. Durand, C. Guizard, N. Hovnanian, A. Julbe and A. Larbot, Solid State Sciences, 2 (2000) 313.

[51] J.G. Tsikoyiannis and W.O. Haag, Zeolites, 12 (1992) 126.

[52] H. Sakai, T. Tomita and T. Takahashi, Sep. Pur. Tech., 25 (2001) 297.

[53] S. Miachon, E. Landrivon, M. Aouine, Y. Sun, I. Kumakiri, Y. Li, O. Pachtov Prokopová, N. Guilhaume, A. Giroir-Fendler, H. Mozzanega, and J.-A. Dalmon, J. Membr. Sci., in press.

[54] A. Giroir-Fendler, J. Peureux, H. Mozzanega and J.-A. Dalmon, Stud. Surf. Sci. Catal., 101A (1996) 127.

[55] G.E. Romanos, T.A. Steriotis, E.S. Kikkinides, N.K. Kanellopoulos, V. Kasselouri, J.D.F. Ramsay, P.Langlois and S. Kallus, J. Eur. Ceram. Soc., 21 (2001) 119.

[56] D. Uzio, J. Peureux, A. Giroir-Fendler, J.-A. Dalmon and J.D.F. Ramsay, Stud. Surf. Sci. Catal., 87 (1994) 411,

[57] W.J.W. Bakker, F. Kapteijn, J. Poppe and J.A. Moulijn, J. Membr. Sci., 117 (1996) 57.

[58] K. Kusakabe, T. Kuroda and S. Morooka, J. Membr. Sci., 148 (1998) 13.

[59] I. Kumakiri, T. Yamaguchi and S.-I. Nakao, Ind. Eng. Chem. Res., 38 (1999) 4682.

[60] S. Nair, Z. Lai, V. Nikolakis, G. Xomeritakis, G. Bonilla and M. Tsapatsis, Micropor. Mesopor. Mater., 48 (2001) 219.

[61] X. Xu, W. Yang, J. Liu and L. Lin, Micropor. Mesopor. Mater., 43 (2001) 299.

[62] J.J. Jafar and P.M. Budd, Microporous Mater., 12 (1997) 305.

[63] M. Kondo, M. Komori, H. Kita and K.-I. Okamoto, J. Membr. Sci., 133 (1997) 133.

[64] Z. Gao, Y. Yue and W. Li, Zeolites, 16 (1996) 70.

[65] K. Aoki, K. Kusakabe and S. Morooka, AIChE J., 46 (2000) 221.

[66] N. Nishiyama, T. Matsufuji, K. Ueyama and M. Matsukata, Microporous Mater., 12 (1997) 293.

[67] Lai, G. Bonilla, I. Diaz, J.G. Nery, K. Sujaoti, M. A. Amat, E. Kokkoli, O. Terasaki, R. W. Thompson, M. Tsapatsis and D. G. Vlachos, Science, 300 (2003) 456.

[68] M. Noack, P. Kölsch, J. Caro, M. Schneider, P. Toussaint and I. Sieber, Micropor. Mesopor. Mater., 35-36 (2000) 253.

[69] J. Hedlund, M. Noack, P. Kölsch, D. Creaser, J. Caro and J. Sterte, J. Membr. Sci., 159 (1999) 263.

[70] C.J. Gump, X. Lin, J.L. Falconer and R.D. Noble, J. Membr. Sci., 173 (2000) 35.

[71] K. Keizer, A.J. Burggraaf, Z.A.E.P. Vroon and H. Verweij, J. Membr. Sci., 147 (1998) 159.

[72] J. Coronas, R.D. Noble and J.L. Falconer, Ind. Eng. Chem. Res., 37 (1998) 166.

[73] J. Hedlund, J. Sterte, M. Anthonis, A.J. Bons, B. Carstensen, E.W. Corcoran, H.W. Deckman, W. de Gijnst, P.P. de Moor, F. Lai, J. McHenry, W. Mortier and J. Reinoso, Micropor. Mesopor. Mater., 52 (2002) 179.

[74] J.B.Nagy, P. Bodart, I. Hannus and I. Kiricsi, Synthesis, characterization and use of zeolitic microporous materials, DecaGen Ltd., Szeged, Hungary, 1998, p. 133.

[75] S. Li, V. A. Tuan, J. L. Falconer and R. D. Noble, Micropor. Mesopor. Mater., 58 (2003) 137.

[76] V. A. Tuan, S. Li, J. L. Falconer and R. D. Noble, Journal of Membr. Sci., 196 (2002) 111.

[77] H. Kalipcilar, S.K. Gade, R.D. Noble and J.L. Falconer, J. Membr. Sci., 210 (2002)113.

[78] E.E. McLeary, J.C. Jansen and F. Kapteijn, Micropor. Mesopor. Mater., 90 (2006) 198.

[79] G. Saracco, H.W.J.P. Neomagus, G.F. Versteeg and W.P.M. van Swaaij, Chem. Eng. Sci., 54 (1999) 1997.

[80] J.M. van de Graaf, M. Zwiep, F. Kapteijn and J.A. Moulijn, Chem. Eng. Sci., 54 (1999) 1441.

[81] J.M. van de Graaf, M. Zwiep, F. Kapteijn and J.A. Moulijn, Applied Catalysis A: General, 178 (1999) 225.

[82] J. Hedlund, F. Jareman, A-J. Bons and M. Anthonis, J. Membr. Sci., 222 (2003) 163.

[83] J. Coronas and J. Santamaria, Chem. Eng. Sci., 59 (2004) 4879.

[84] Y. S.S. Wan, J. L. H. Chau, A. Gavriilidis and K. L. Yeung, Micropor. Mesopor. Mater., 42 (2001) 157.

[85] M. Vilaseca, J. Coronas, A. Cirera, A. Cornet, J.R. Morante and J. Santamaría, Catalysis Today 82 (2003) 179.

[86] O. Hugon, M. Sauvan, P. Benech, C. Pijolat and F. Lefebvre, Sensors and Actuators B, 67 (2000) 235.

[87] M. Grahn, Z. Wang, M. Lidström-Larsson, A. Holmgren and J.Hedlund, Micropor. Mesopor. Mater., 81 (2005) 357.

[88] J.C. Jansen, J.H. Koegler, H. van Bekkum, H.P.A. Calis, C.M. van den Bleek, F. Kapteijn, J.A. Moulijn, E.R. Geus and N. van den Puil, Micropor. Mesopor. Mater., 21 (1998) 213.

[89] J.L.H. Chau, C. Tellez, K.L. Yeng and K. Ho, Journal of Membr. Sci., 164 (2000) 257.

[90] W. Xu, J. Dong, J. Li and F. Wu, J. Chem. Soc., Chem. Commun., (1990) 755.

[91] E. Kikuchi, K. Yamashita, S. Hiromoto, K. Ueyama and M. Matsukata, Micropor. Mater., 11 (1997) 107.

[92] N. Nishiyama, K. Ueyama and M. Matsukata, Micropor. Mater., 7 (1996) 299.

[93] S. Mintova, V. Valtchev, B.J. Schoeman and J. Sterte, J. Porous Mater., 3 (1996) 143.

[94] J. Hedlund, B.J. Schoeman and J. Sterte, in: H. Chon, S.-K. Ihm and Y.S. Uh (Eds), Progress in Zeolites and Microporous Materials, Elsevier, Amsterdam, 1997, p. 2203.

[95] S. Mintova, J. Hedlund, V. Valtchev, B.J Schoeman and J. Sterte, J. Mater. Chem., 8 (1998) 2217.

[96] J. Sterte, S. Mintova, G. Zhang and B.J. Schoeman, Zeolites, 18 (1997) 387.

[97] J. Hedlund, B.J. Schoeman and J. Sterte, Chem. Commun., (1997) 1193.

[98] V. Valtchev, B.J. Schoeman, J. Hedlund, S. Mintova and J. Sterte, Zeolites, 17 (1996) 408.

[99] M.C. Lovallo and M. Tsapatsis, AlChE J., 42 (1996) 3020.

[100] A. Gouzinis and M. Tsapatsis, AlChE J., 44 (1998) 1903.

[101] L. Boudreau and M. Tsapatsis, Chem. Mater., 9 (1997) 1705.

[102] S. Mintova, V. Valtchev, V. Engström, B.J. Schoeman, J. Sterte, Micropor. Mater., 11 (1997) 149.

[103] J. Hedlund, S. Mintova and J. Sterte, Micropor. Mesopor. Mater., 28 (1999) 185.

[104] Z. Wang, J. Hedlund and J. Sterte, Micropor. Mesopor. Mater., 52 (2002) 191.

[105] Q. Li, J. Hedlund, D. Creaser and J. Sterte, Chem. Commun. 6 (2001) 527.

[106] Q. Li, J. Hedlund, J. Sterte, D. Creaser and A.-J. Bons, Micropor. Mesopor. Mater., 56 (2002) 291.

[107] O.G.W. Öhrman, Licentiate thesis, Luleå University of Technology, 2003:35.

[108] K. Kusakabe, T. Kuroda, A. Murata and S. Morooka, Ind. Eng. Chem. Res., 36 (1997) 649.

[109] K. Ha, Y.J. Lee, H.J. Lee and K.B. Yoon, Adv. Mater. 12 (2000) 1114.

[110] Z. Lai, M. Tsapatsis and J.P. Nicolich, Adv. Funct. Mater., 17 (2004) 716.

[111] C.S. Tsay and A.S.T. Chiang, AIChE J., 46 (2000) 616.

[112] S. M. Lai, L. T. Y. Au and K. L. Yeung, Micropor. Mesopor. Mater., 54 (2002) 63.

[113] Z. Wang and Y. Yan, Chem. Mater., 13 (2001) 1101.

[114] J. Hedlund and F. Jareman, Curr. Opin. Coll. Interface Sci., 10 (2005) 226.

[115] A.-J. Bons and P.D. Bons, Micropor. Mesopor. Mater., 62 (2003) 9.

[116] F. Jareman, J. Hedlund, D. Creaser and J. Sterte, J. Membr. Sci., 236 (2004) 81.

[117] W.J.W. Bakker, F. Kapteijn, J. Poppe and J.A. Moulijn, J. Membr. Sci., 117 (1996) 57.

[118] Á. Berenguer-Murcia, J. García-Martínez, D. Cazorla-Amorós, Á. Linares-Solano and A.B. Fuertes, Micropor. Mesopor. Mater. 59 (2003) 147.

[119] J. Coronas, J.L. Falconer and R.D. Noble, Aiche J., 43 (1997) 1797.

[120] E. Piera, A. Giroir-Fender, J.A. Dalmon, H. Moueddeb, J. Coronas, M. Menèndez and J. Santamarìa, J. Membr. Sci., 142 (1998) 97.

[121] Y. Yan, M.E. Davis and G.R. Gavalas, Ind. Eng. Chem. Res., 34 (1995) 1652.

[122] Y. Yan, M.E. Davis and G.R. Gavalas, J. Membr. Sci., 126 (1997) 53.

[123] Y. Yan, M.E. Davis and G.R. Gavalas, J. Membr. Sci., 123 (1997) 95.

[124] M.P. Bernal, J. Coronas, M. Menéndez and J. Santamaría, Micropor. Mesopor. Mater., 60 (2003) 99.

[125] B.S. Kang and G.R. Gavalas, Ind. Eng. Chem. Res., 41 (2002) 3145.

[126] J. Dong, K. Wegner and Y.S. Lin, J. Membr. Sci., 148 (1998) 233.

[127] Z.A.E.P Vroon, K. Keizer, A.J. Burggraaf and H. Verweij, J. Membr.Sci., 144 (1998) 65.

[128] J.M. van de Graaf, F. Kapteijn and J.A. Moulijn, Chem. Eng. Sci., 54 (1999) 1081.

[129] F. Jareman and J. Hedlund, Micropor. Mesopor. Mater., 82 (2005) 201.

[130] F. Jareman, Doctoral thesis, Luleå university of technology, 2004:11

[131] H.W. Deckman, D.M. Cox, A.J. Bons, B. Carstensen, R.R. Chance, E.W. Corcoran, W.D. Gijnst, J.A. McHenry, J.J. Reinoso, R.B. Saunders and P.J. Tindall, Characterization of zeolite membrane quality and structure, IWZMM2001 Book of Abstracts, 2001, p. 9.

[132] F. Jareman, J. Hedlund and J. Sterte, Sep. Purif. Technol., 32 (2003) 159.

[133] G. Bonilla, M. Tsapatsis, D.G. Vlachos and G. Xomeritakis, J. Membr. Sci., 182 (2001)103.

[134] M.J. den Exter, H. van Bekkum, C.J.M Rijn, F. Kapteijn, J.A. Moulijn, H. Schellevis and C.I.N. Beenakker, Zeolites, 19 (1997) 13.

[135] L.V.C. Rees and R. von Ballmoos, Zeolites 10 (1990) 442.

[136] F. Jareman, C. Andersson and J. Hedlund. Micropor. Mesopor. Mater.,79 (2005) 1.

[137] R. Lai and G.R. Gavalas, Micropor. Mesopor. Mater., 38 (2000) 239.

[138] M. Pan, Y.S. Lin, Micropor. Mesopor. Mater., 43 (2001) 319.

[139] P. Sherrer, Göttinger Nachrichten, 2 (1918) 98.

[140] D. Balzar and H. Ledbetter, J. Appl. Cryst., 26 (1993) 97.

[141] R. A. Young in: R.A. Young (Ed), The Rietveld Method, Oxford University Press, New York, 1993, p. 9.

[142] J.I. Langford and D. Louër, Rep. Prog. Phys., 59 (1996) 131.

[143] J.I. Langford in: E. Prince and J.K. Stalick (Eds.), Accuracy in Powder Diffraction II, NIST Spec. Pub. No. 846., US Dept of Commerce, Gaithersburg MA, 1992, p. 110.

[144] G.K. Williamson and W.H. Hall, Acta Metall., 1 (1953) 22.

[145] R. Delhez, T.H. de Keijser, J. I. Langford, D. Louër, E.J. Mittemeijer and E.J. Sonneveld in: R.A. Young (Ed), The Rietveld Method, Oxford University Press, New York, 1993, p. 132.

[146] H.M. Rietveld, Acta Cryst., 22 (1967) 151.

[147] H.M. Rietveld, J. Appl. Cryst., 2 (1969) 65.

[148] R.A. Young (Ed), The Rietveld Method, Oxford University Press, New York, 1993

[149] R.A. Young in: R.A. Young (Ed), The Rietveld Method, Oxford University Press, New York, 1993, p. 4.

[150] A. March, Z. Kristallogr., 81 (1932) 285.

[151] W.A. Dollase, J. Appl. Cryst., 19 (1986) 267.

[152] R.B. Von Dreele, J. Appl. Cryst., 30 (1997) 517.

[153] D.L. Bish and J.B. Post, Am. Min., 78 (1993) 932.

[154] A.G. De La Torre, S. Bruque and M.A.G. Aranda, J. Appl. Cryst., 34 (2000) 196.

[155] A.F. Gualtieri, Powder Diff., 11 (2) (1996) 97.

[156] A.F. Gualtieri, J. Appl. Cryst., 33 (2000) 267.

[157] A.F. Gualtieri and G. Artioli, Powder Diff., 10 (4) (1995) 269.

[158] P. Riello, G. Fagherazzi and P. Canton, Acta Cryst., A54 (1998b) 219.

[159] M. Lassinantti Gualtieri, M. Prudenziati and A.F. Gualtieri, Surf. Coat. Technol., in press.

[160] C.H. Bamford and C.F.H. Tipper, Comprehensive Chemical Kinetics, Elsevier, New York, 1980, vol. 22, pp 41-113.

[161] M. Avrami, J. Chem. Phys., 7 (1939) 1103.

[162] H.E. Kissinger, Anal. Chem., 29 (1957) 1702

[163] C.D. Doyle, J. Appl. Pol. Sci., 5 (1961) 285.

[164] P. Murray and J. White, Transactions of the British Ceramic Society, 54 (1955) 204.

[165] F. Baitalow, H.-G. Schmidt, G. Wolf, Thermochimica Acta, 337 (1999) 111.

[166] J.H. Flynn, L.A. Wall, J. Polym. Sci. Part B 4 (1966) 323.

[167] T. Ozawa, Bull. Chem. Soc. Jpn. 38 (1965) 1881.

[168] J.A. Kennedy and S.M. Clark, Thermochimica Acta, 307 (1997) 27.

[169] J. Hedlund, Doctoral thesis, Luleå university of technology, 1998:33.

[170] E. Piera, J. Coronas, M. Menéndez and J. Santamaría, Chem. Commun., (1999) 1309.

[171] C. Meneghini, G. Artioli, A. Balerna, A.F. Gualtieri, P. Norby and S. Mobilio, J. Synchrotron Rad., 8 (2001) 1162.

[172] A.C. Larson and R.B. von Dreele (1994) "*GSAS Generalized strucure analysis system*" Laur 86-748, Los Alamos National Laboratory, Los Alamos, New Mexico.

[173] N.Ishizawa, T. Miyata, I. Minatio, F. Marumo and S. Iwai, Acta Cryst., B36 (1980) 228.

[174] T.H. Keijser, E.J. Mittemeijer and H.C.F. Rozendaal, J. Appl. Cryst., 16 (1983) 309.

[175] S.P. Davis, E.V.R. Borgstedt and S.L. Suib, Chem. Mater., 2 (1990) 712.

[176] C. Covarrubias, R.García, R. Arriagada, J. Yánez and M.T. Garland, Micropor. Mesopor. Mater., 88 (2006) 220.

[177] M. Dapiaggi, G. Artioli and L. Petras, The Rigaku Journal, 19 (2002) 35.

[178] M. Ohring, Materials Science of Thin Films, Academic Press, New York, 2002.

[179] J.I. Langford, A. Boultif, J.P. Auffréic and D. Louër, J. Appl. Cryst., 26 (1993) 22.

[180] P.M. Jardim, B.A. Marinkovic, A. Saavedra, L.Y. Lau, C. Baehtz and F. Rizzo, Micropor. Mesopor. Mater., 76 (2004) 23.

PAPER I

Synthesis of thin zeolite Y films on polished α-alumina wafers using a seeding technique

---

Magdalena Lassinanti, Jonas Hedlund and Johan Sterte,
Porous Materials in Environmentally Friendly Processes, Editors. I. Kiricsi, G. Pál-Borbély, J.B.Nagy and H.G. Karge, Elsevier, Amsterdam, 181-187 (1999).

I. Kiricsi, G. Pál-Borbély, J.B. Nagy, H.G. Karge (Editors)
Porous Materials in Environmentally Friendly Processes
Studies in Surface Science and Catalysis, Vol. 125

Synthesis of thin zeolite Y films on polished α-Alumina wafers using a seeding technique

M. Lassinantti, J. Hedlund and J. Sterte

Division of Chemical Technology, Luleå University of Technology, SE-971 87 Luleå, Sweden

Zeolite Y films were synthesized on polished α-alumina wafers by using a seeding technique which includes surface modification, seed adsorption and growth of the seed crystals into a dense film. The film thickness was found to be a linear function of synthesis duration up to a certain point. Further treatment reduced the film thickness. Continuous and crack free films with thicknesses in the range 210 to 2670 nm were synthesized in this work.

1. INTRODUCTION

The synthesis of thin, dense and continuous molecular sieve films is of great interest in various applications, for instance for molecular sieve membranes. Zeolite films used in membrane applications must have high quality. Cracks in the film are detrimental for the selectivity of the membrane. Moreover, to obtain a high flux through the membrane, the molecular sieve film should be thin. Most films are synthesized in the presence of organic template molecules. In order to render these films useful, a calcination step after the synthesis is performed to remove the template molecules which otherwise block the channels in the zeolite. This treatment is often accompanied by crack formation. A convenient way to avoid this problem may be to synthesize the films in the absence of template molecules and thereby avoid the calcination step. For zeolite Y, which has an open pore structure, ion exchange of the template molecules can also be an option. The seed film method has been previously used to synthesize films of a number of zeolites on various supports [1-3]. In the present work, this method is adapted to the synthesis of thin, nearly template free, zeolite Y films on α-alumina wafers.

2. EXPERIMENTAL

Colloidal seed crystals of zeolite Y were synthesized in a clear homogeneous solution. The molar composition of the synthesis mixture was 2.46 $(TMA)_2O$: 0.032 Na_2O: Al_2O_3: 3.40 SiO_2: 400 H_2O [4]. The silica source was tetraethoxysilane (TEOS, > 98 %, Merck) and the aluminum source was aluminum isopropoxide (Sigma). The alkali sources were a tetramethylammonium hydroxide (TMAOH, Sigma) and a 0.10 M sodium hydroxide solution prepared from pellets (Riedel-deHaën). The synthesis mixture was prepared by adding a

mixture of aluminum isopropoxide, water, TMAOH and a 0.10 M sodium hydroxide solution to a mixture of TEOS and water under vigorous stirring. Following hydrolysis for 18h, crystallization was executed under reflux in an oil bath at a temperature of 100°C. After a synthesis time of 168 h, the crystals were purified by centrifugation and redispersion in a 0.1 M ammonia solution. The purification steps were repeated twice. The solid content and pH of the sol were adjusted to 1.0 % and 10.0. In order to investigate the ion exchange properties of the seed crystals, two as-synthesized seed sol samples were centrifugated and redispersed (three times) at room temperature in the following media; (i) distilled water and (ii) 0.1 M ammonia solution.

One side polished α-alumina (0001) substrates were placed vertically in Teflon holders and cleaned according to the procedure described previously [1]. Following cleaning, the substrates were treated for five minutes in a solution of cationic polymer molecules (0.4 wt% Redifloc 4150, Eka Chemicals), adjusted to pH 8.0 by addition of ammonia. The substrates were rinsed in an 0.1 M ammonia solution to remove excess polymer. In the following step, the modified substrates were treated with the seed sol for five minutes. After adsorption of seed crystals, the substrates were rinsed in a dilute ammonia solution to remove excess seed crystals. To increase the amount of adsorbed seed crystals, the polymer and seed adsorption was repeated. Following seeding, the substrates (still mounted in holders) were immediately placed in a synthesis solution of the molar composition 14 Na_2O: Al_2O_3: 10 SiO_2: 798 H_2O [5]. The gel was prepared by mixing an aqueous solution of sodium metasilicate ($Na_2SiO_3 \cdot 9H_2O$ > 98 %, Sigma) with aluminumsulfate-18-hydrate (Riedel-deHaën) dissolved in a 1.00 M sodium hydroxide solution. The mixture was homogenized for two hours. Film growth was effected at 100°C and atmospheric pressure under reflux. Synthesis times were in the range 1 to 44 h. After cooling, the samples were treated a few seconds in an ultrasonic bath and finally rinsed in a dilute ammonia solution.

Dynamic light scattering (DLS) was used to follow the growth of the zeolite Y seed crystals using a Brookhaven Instruments ZetaPlus instrument. The thickness and morphology of the zeolite Y films were investigated using a Philips XL 30 Scanning Electron Microscope (SEM). Prior to the SEM characterization, the samples were coated with a thin layer of gold. A Siemens D5000 powder X-ray diffractometer (XRD) equipped with a Göbel mirror was used to collect XRD data. Theta:two theta scans were performed in the 2θ range from 5° to 35°. Fourier transform infrared (FTIR) spectroscopy measurements were performed using a Perking Elmer 2000 FTIR spectrometer. Gas adsorption data were recorded, at liquid nitrogen temperature, on calcined (450°C, 1 h) seed crystals with a Micromeritics ASAP 2010 instrument. The sample was outgassed at 300°C for 24 hours prior to the measurement. Nitrogen was used as the adsorbate and the BET equation was employed to calculate the surface area.

3. RESULTS AND DISCUSSION

DLS-measurements during the synthesis of the seed crystals showed that the final average crystal size was 81 nm. After synthesis, the seed crystals were separated from the mother liquid by repeated centrifugation and redispersion in a 0.1 M ammonia solution. The purpose was to separate the crystals from amorphous material present in the mother liquid and to exchange the TMA^+ ions to ammonium ions. FTIR measurements were used to monitor the

progress of the ion exchange. Figure 1 a illustrates the spectrum of a zeolite Y seed sol sample washed in water. The most intense peak originating from the zeolite structure appears at 1006 cm^{-1} (asymmetric stretch of Si-O-Al chains) [6]. The TMA^+ ions incorporated in the pore structure of the zeolite give an intense peak at 1489 cm^{-1} (C-H-bending vibration) [7]. The spectrum collected from zeolite Y seed crystals purified in a dilute ammonia solution is shown in Figure 1 b. The intensity ratio of the two peaks mentioned above is much larger for this spectrum than for the spectrum collected from the seeds purified in water. This indicates that most of the TMA^+ ions originally present in the pore structure of the zeolite has been exchanged to ammonium ions. The peak at 1422 cm^{-1} that can be seen in Figure 1 b is due to ammonia.

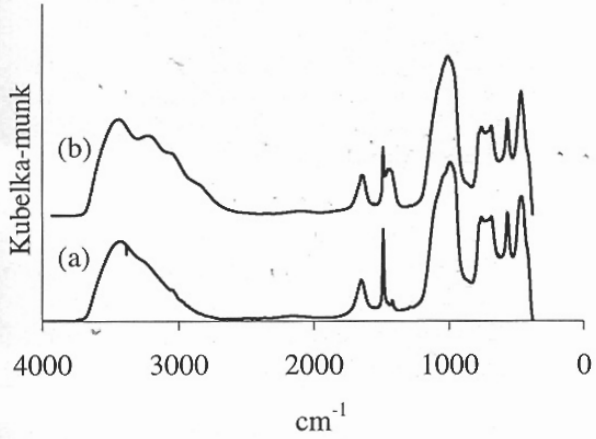

Figure 1. FTIR spectra from seed sol sample washed in water (a) and ammonia solution (b).

Gas adsorption data was collected from a calcined sample of the zeolite Y seed sol. The specific surface area was calculated to 526 m^2/g in accordance with previous results [4].

Figure 2 shows seeded α-alumina wafers. After one adsorption step (a) the distance between the seeds is of the order 100 nm. After two adsorption steps (b) the distance has decreased significantly.

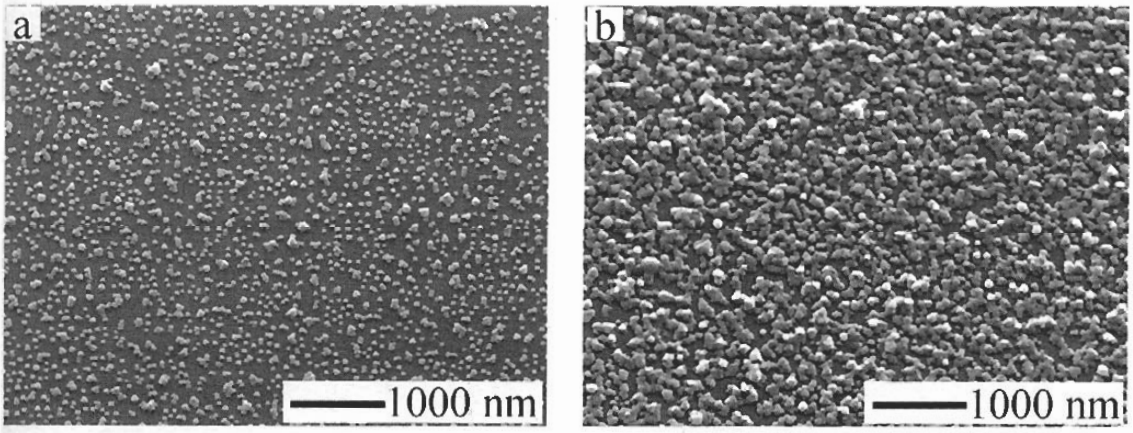

Figure 2. Seeded wafer after one adsorption step (a), and two adsorption steps (b).

The seeded substrates were hydrothermally treated in a synthesis solution in which the adsorbed crystals were grown to form films. The thickness and morphology of the films were investigated by SEM, see Figure 3. The top view images show that the films are dense and

appear to be free of pinholes and cracks. The crystals are intergrown. The film thickness is constant and the results are reproducible. After treating a seeded substrate in a synthesis solution, the seeds grow both laterally and vertically. After 1 h of synthesis, a continuous film

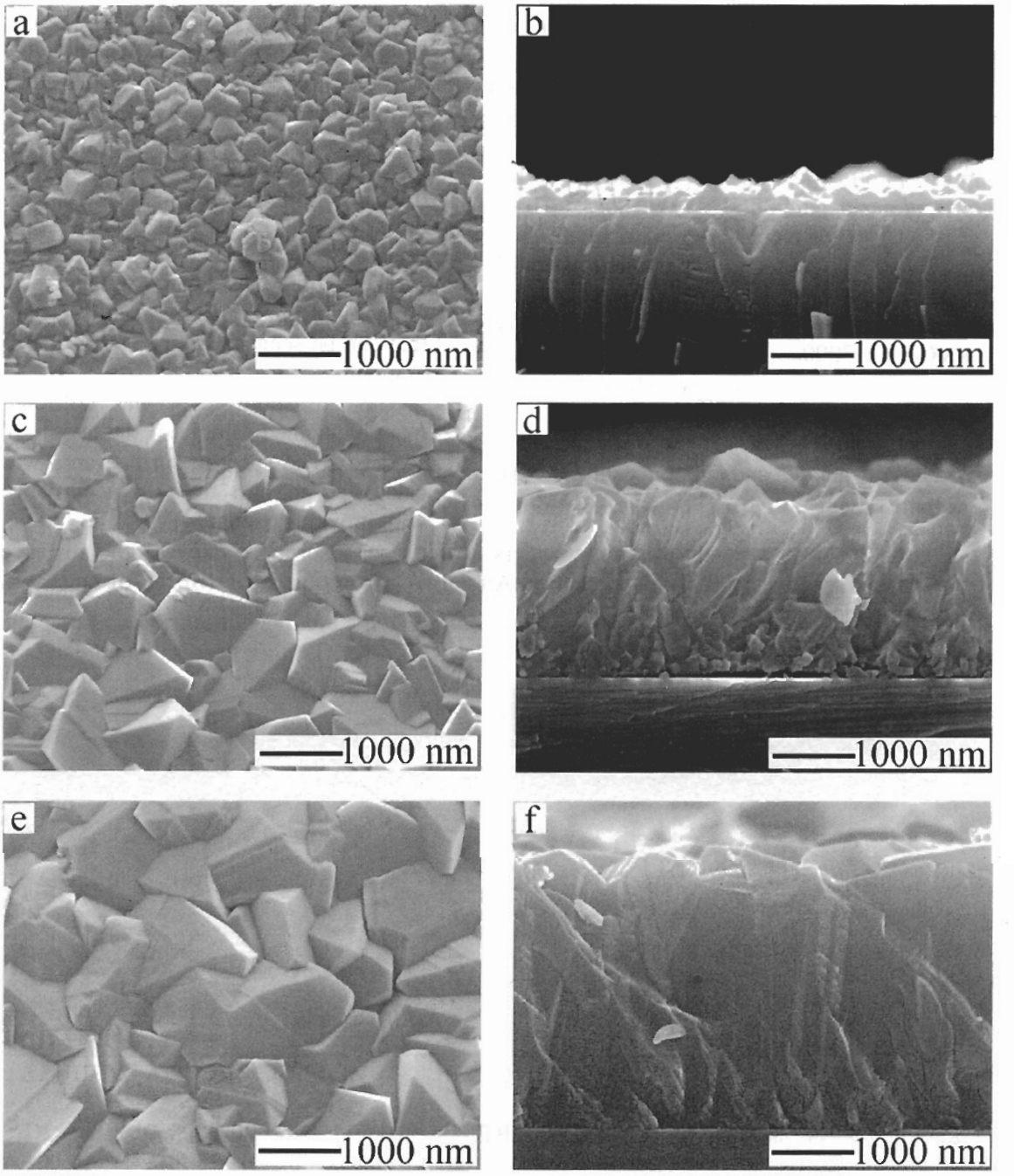

Figure 3. SEM images of films synthesized for 1 h (a,b), 6 h (c,d) and 12 h (e,f).

with a thickness of about 210 nm was formed, see Figure 3 (a) and (b). Prolonged exposure of the seeded substrate to the synthesis solution gives a thicker film with more well developed crystal faces, see Figure 3 (c) and (d). After 12 h of synthesis, the film thickness is estimated to 2670 nm, see Figure 3 (e) and (f). Note, that the number of crystals per unit area decreases with increasing film thickness, probably due to the fact that some of the crystals have been encapsulated by other faster growing crystals.

The film thickness as a function of synthesis time is shown in Figure 4. The growth rate is first constant, but seems to decrease after about 6 h, probably due to consumption of nutrients in the synthesis gel. After approximately 12 hours of synthesis, the film thickness has reached a maximum value. Films left in contact with the synthesis solution for longer periods show a decrease in thickness, accompanied by a change in morphology. After 24 h of crystallization

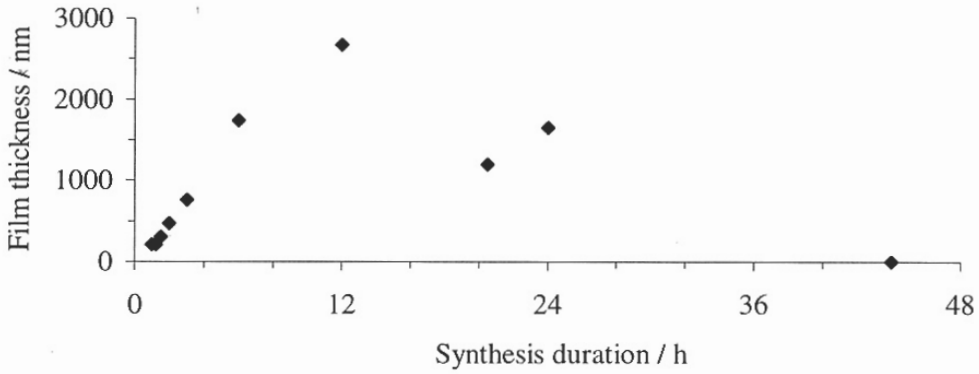

Figure 4. Film thickness as a function of synthesis duration.

the film is smooth and the crystals have lost their typical morphology. After 44 h of hydrothermal treatment, the film has no resemblance with the original zeolite Y film. The gel-like layer appears to be speckled with some unknown material. An estimation of the thickness was difficult because the layer was too thin. Thus, the film thickness was set to zero for this sample in Figure 4. The reproducibility of events taking place after 12 h of synthesis was poor. In order to rule out the possibility of film formation without seeding the substrate, an experiment was carried out where a cleaned substrate was placed in the synthesis solution for 20 h. No zeolite film formed on the substrate. Only a few, several micron large crystals were attached to the wafer surface, somewhat more densely on the unpolished side.

XRD-data were collected from purified and dried crystals formed in the bulk of the synthesis solution during film synthesis as well as from films. The diffractograms showed the peaks characteristic of zeolite Y, see Figure 5. Some of the film samples also contained unidentified peaks at the d values 11.98 and 14.92. The preferred orientation of the crystals constituting the film was investigated using the XRD data collected from the films. A powder sample of the purified seed sol was used as a reference and considered to have a random orientation, see Figure 5 (c). Figure 5 (a) shows the XRD diffractogram from a sample with adsorbed seed crystals (average size 154 nm) on an alumina wafer. Major peaks are the (111) peak and the (555) peak indicating a preferred orientation of the seed crystals with the {111} prism parallel to the substrate surface. The crystals in the films seem to be randomly oriented,

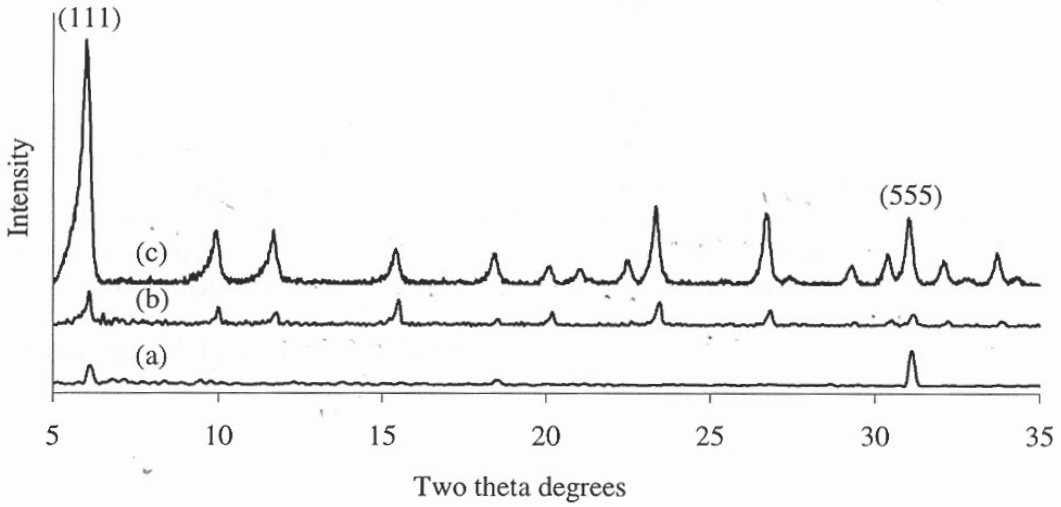

Figure 5. XRD diffractogram recorded from adsorbed seed crystals (a), a film synthesized for 6 h (b) and a powder reference sample (c).

see Figure 5 (b), since the relative peak intensities are approximately the same for the films as for the reference sample. Thus the orientation is changing during the growth of the film. This can be explained by attachment of crystals formed in the bulk to the growing film or secondary nucleation. The change in the preferred orientation of the crystals in the film should not be due to sedimentation, and subsequent attachment of crystals, formed in the bulk of the synthesis gel since random orientation is also obtained when the substrate is facing downward.

The stability of the films was controlled by subjecting them to ultrasound treatment for two hours. Films synthesized for less than 9 h show no signs of film detachment after this treatment, as judging from SEM images. Thicker films tend to peal off. Cracks could however be detected for all the films that were still attached to the substrate except for the thinnest one. These cracks developed straight through the crystals which indicates that the crystals constituting the film were intergrown. The thickness of the zeolite films has decreased after the treatment, indicating that crystals originally attached to the surface has detached. The relative decrease is more pronounced for thicker films. The fact that all zeolite films on the non polished sides of the wafers are still attached to the wafer after ultrasound treatment indicates that the roughness of the substrate surface is an important factor when it comes to the adhesion of the film. XRD data was recorded for treated films, and the patterns indicate random orientation of the crystals constituting the films. Thus the random orientation of the crystals constituting the films seems not to be a result of improper rinsing of the as-synthesized films.

4. CONCLUSIONS

A seeding technique has been used to synthesize thin zeolite Y films on α-alumina substrates. Seed crystals were synthesized in the presence of organic template molecules.

Most of the template molecules were exchanged with ammonium ions during the purification of the seed crystals. The synthesis mixture used for film growth was free from organic templates. The film thickness was shown to be approximately a linear function of synthesis duration up to a certain point. Further treatment caused the film thickness to decrease. Continuous films with thicknesses in the range 210 to 2670 nm were grown using synthesis times in the range 1 h to 12 h. XRD patterns recorded from adsorbed seeds indicate a preferred orientation with the {111} prism parallel to the substrate surface. XRD patterns collected from selected films indicate random orientation of the crystals constituting the films. The change in orientation is probably due to secondary nucleation or attachment of crystals formed in the gel. The adhesion of the films was shown to be relatively poor. Films synthesized for more than 6 h were partly pealed off during ultrasonic action, and all films showed a decrease in thickness after this treatment. Films synthesized in this work are thin and intergrown, thus good candidates for use in membrane applications.

REFERENCES

1. J. Hedlund, B.J. Schoeman and J. Sterte, in H. Chon, S.-K. Ihm and Y.S. Uh (Eds), Progress in Zeolites and Microporous Materials, Elsevier, Amsterdam, (1997) 2203.
2. S. Mintova, J. Hedlund, B.J. Schoeman, V. Valtchev and J. Sterte, Chem. Commun. (1997) 15.
3. J. Hedlund, B. Schoeman and J. Sterte, Chem. Commun. (1997) 1193.
4. B.J. Schoeman, J. Sterte and J.-E. Otterstedt, Zeolites (1994) 110
5. K. Kusakabe, T. Kuroda, A. Murata and S. Morooka, Ind. Eng. Chem. Res. 36 (1997) 649.
6. R. Szostak, Handbook of Molecular Sieves, Van Nostrand Reinhold, New York,1992, p. 287.
7. R. Szostak, Handbook of Molecular Sieves, Van Nostrand Reinhold, New York,1992, p. 442.

PAPER II

Faujasite-type films synthesized by seeding

Magdalena Lassinantti, Jonas Hedlund and Johan Sterte

Microporous and Mesoporous Materials, 38 (2000) 25-34.

ELSEVIER

Microporous and Mesoporous Materials 38 (2000) 25–34

MICROPOROUS AND MESOPOROUS MATERIALS

www.elsevier.nl/locate/micromeso

Faujasite-type films synthesized by seeding

Magdalena Lassinantti, Jonas Hedlund, Johan Sterte *

Division of Chemical Technology, Luleå University of Technology, SE-971 87 Luleå, Sweden

Received 5 July 1999; received in revised form 4 October 1999; accepted 5 October 1999

Abstract

Thin and continuous Faujasite-type films were synthesized on α-alumina wafers using a seeding technique. Surface modified wafers were seeded with colloidal zeolite Y crystals prior to film growth in a synthesis mixture. The effects of hydrothermal treatment on film thickness, morphology and preferred orientation of the crystals constituting the film were investigated using scanning electron microscopy and X-ray diffraction. During hydrothermal treatment a precipitate formed rapidly, leaving an almost clear solution in the upper part of the reactor. Experiments at 60–100°C were performed with the sample placed in the upper part of the synthesis solution. An increase in the film growth rate with increasing temperature was observed. Adsorbed seeds were shown to be oriented with the {1 1 1} pyramid, parallel to the substrate surface. A change in the orientation with film growth was noted, probably due to the attachment of secondary crystals to the growing film surface. In one experimental series, film growth was effected at the bottom of the tube at 100°C. Faster film growth and multilayered films were obtained. A decrease in the film thickness after prolonged hydrothermal treatment was observed in all experimental series. This is probably due to the dissolution of the film and formation of zeolite P in the synthesis solution. The thicknesses of the films synthesized in this work are in the range of 150–2700 nm. The films are promising candidates for use in membrane applications.

Keywords: Faujasite; Film; Seeding; Membrane; Ion exchange

1. Introduction

Thin molecular sieve films are of great interest in a number of potential industrial applications, the most interesting one probably being the membranes of various types. Zeolite films for membrane applications must be of an extremely high quality. Even a small number of defects in the film is detrimental to the selectivity of the membrane. Moreover, to obtain a high flux through the membrane, the molecular sieve film should be thin. Molecular sieve membranes of Faujasite may be of particular interest due to their high aluminum content, i.e. their hydrophilicity. The channel system in Faujasite-type structures is three dimensional with equidimensional channels intersecting in a perpendicular fashion. The free aperture diameter for the channels is 7.4 Å in NaY [1].

Reports concerning the synthesis of zeolite films bring about three different strategies. (i) the method of direct crystallization, (ii) the vapor phase method, and (iii) methods involving seeding

* Corresponding author. Tel.: +46-920-72314; fax: +46-9-209-1199.

E-mail address: johan.sterte@km.luth.se (J. Sterte).

1387-1811/00/$ - see front matter
PII: S1387-1811(99)00296-6

of the substrate surface prior to film synthesis. Applying the third approach, several methods for the attachment of seeds to the surface have been proposed. Zeolite Y films were synthesized on tubular α-alumina supports, using a seeding technique in which the support was rubbed with NaX zeolite crystals that acted as growth centers [2]. The seeding step was shown to be crucial for the film formation. In the synthesis of highly oriented films of zeolite A, glass supports were immersed in a colloidal zeolite A suspension to obtain seed crystal layers [3]. This step was repeated several times in order to obtain a high coverage of the support with seed crystals. Silicalite membranes were synthesized by allowing the silicalite particles in a precursor silicalite/alumina film to grow under appropriate synthesis conditions [4]. In this way, the interzeolitic spacing in the film was closed, forming a continuous molecular sieving layer. Kita et al. synthesized a NaY zeolite membrane using a seeding approach [5]. A porous alumina substrate was subjected to a water suspension of NaY seed crystals. Following seeding, the film growth was effected by hydrothermal treatment in a synthesis solution. The resulting film was 20 μm thick and consisted of intergrown, randomly oriented crystals. A synthesis procedure known as "the seed film method" [6–11] has been developed. According to this method, the substrate surface is modified in order to facilitate seed adsorption from a seed crystal sol. The modification required is determined by the type of the surface. For example, negatively charged surfaces are modified by the adsorption of a cationic polymer. The seed film technique enables the preparation of very thin films and has shown to be applicable to many types of supports. Coatings of zeolite Y synthesized using this technique have been reported on fibers of cotton, linen and chemi-thermo mechanical pulp (CTMP)-fluff [11]. No systematic investigation of the preparation of Faujasite-type films on inorganic substrates has however been reported. The scope of the present work was to study the effects of various synthesis parameters on the crystallization of Faujasite-type films with the objective of developing preparative procedures suitable for membrane preparations.

2. Experimental section

Colloidal crystals of zeolite Y used as seeds were synthesized in a clear homogeneous solution. The molar composition of the synthesis mixture was $2.46(TMA)_2O{:}0.032Na_2O{:}Al_2O_3{:}3.40SiO_2{:}400H_2O$ [12]. The silica source was tetraethoxysilane (TEOS > 98%, Merck) and the aluminum source was aluminum isopropoxide (Sigma). The alkali sources were tetramethylammonium hydroxide (TMAOH, Sigma) and a 0.10 M sodium hydroxide solution (Riedel-deHaën). The synthesis mixture was prepared by adding a mixture of aluminum isopropoxide, water, TMAOH and a 0.10 M sodium hydroxide solution to a mixture of TEOS and water under vigorous stirring. Following hydrolysis for 18 h, crystallization was effected under reflux in a polypropylene reactor placed in an oil bath at a temperature of 100°C. After 192 h of hydrothermal treatment, the crystals were purified by centrifugation and redispersion in a 0.10 M ammonia solution. After each redispersion, the seed sol was allowed to equilibrate for 24 h. The purification procedure was repeated twice. Following a final redispersion in distilled water, the solid content and the pH of the sol were adjusted to 1.0% and 10.0, respectively (the latter by addition of a dilute ammonia solution). In order to investigate the ion exchange properties of the seed crystals, two as-synthesized seed sol samples were purified in the following different media. (i) 0.10 M ammonia solution and (ii) distilled water. The purification sequence was the same as that described above but without the adjustment of the pH and the solid content. An additional sample purified in a dilute ammonia solution for four months was also investigated. Following purification, the samples were air dried for 18 h at 100°C.

One side polished α-alumina (0 0 0 1) substrates were mounted vertically in Teflon holders. The substrates were rinsed in acetone for 5 min in ultrasound. After ultrasonification, the substrates were boiled for 5 min in an alkaline solution having the volume composition $5H_20{:}1H_2O_2{:}1NH_3$ (30% H_2O_2 and 25 wt.% NH_3 solution) and in an acidic solution with a volume composition $6H_2O{:}1H_2O_2{:}1HCl$ (30% H_2O_2, 37% HCl). Following cleaning, the substrates were treated for

5 min in a solution containing cationic polymer molecules (0.4 wt.% Redifloc 4150, Eka Chemicals), adjusted to pH 8.0 by addition of a dilute ammonia solution. The substrates were rinsed in a 0.1 M ammonia solution to remove excess polymer. In the following step, the modified substrates were immersed in the seed sol for 5 min. After the adsorption of seed crystals, the substrates were rinsed in a dilute ammonia solution to remove excess crystals. To increase the amount of adsorbed seed crystals, the polymer and the seed adsorption steps were repeated once more. Following seeding, the substrates (still mounted in holders) were immediately placed in a synthesis gel with the polished side almost vertical but leaning slightly downwards in order to avoid sedimentation of crystals formed in the bulk onto the surface. The molar composition of the synthesis solution was $14Na_2O{:}Al_2O_3{:}10SiO_2{:}798H_2O{:}3Na_2SO_4$. This solution was prepared by mixing an aqueous solution of sodium metasilicate ($Na_2SiO_3 \cdot 9H_2O > 98\%$, Sigma) with aluminum-sulfate-18-hydrate (Riedel-deHaën) dissolved in a 1.0 M sodium hydroxide solution. The gel was homogenized under stirring for 2 h. A precipitate formed rapidly in the reactor during film synthesis, leaving a clear solution in the upper part of the synthesis gel. Film growth in the upper part of the synthesis gel was studied at the temperatures 60°C, 80°C and 100°C. Film growth with the substrates placed in the lower part of the gel was studied at 100°C. All the films were grown under static conditions at an atmospheric pressure and under reflux. After cooling, the samples were rinsed in a dilute ammonia solution. In order to investigate the events taking place in the bulk of the film synthesis solution, the bulk product was purified by sedimentation and redispersion in dilute ammonia solution. The purification step was repeated twice, and the dispersion was air dried at 100°C. Commercial powders of zeolite Y and zeolite P (Eka Nobel) were used as references. The relative amount of each zeolite in the bulk product was calculated by dividing the sum of the areas of the most intense peaks in the sample, originating from the zeolite investigated, with the same sum obtained from the reference sample. As the bulk product is a mixture of zeolites Y and P, this simple equation is applicable because the absorption coefficients are similar for zeolites Y and P, since a calibration curve based on different mass ratios of the two zeolites gives a straight line.

Dynamic light scattering (DLS) was used to follow the growth of the seed crystals using a Brookhaven Instrument BI200SM light scattering system. The thickness and morphology of the films were investigated using a Philips XL 30 scanning electron microscope (SEM) equipped with a LaB_6 emission source. Top view images were recorded with a 20° tilt of the specimen. Elemental analyses of seed crystals and crystals formed in the bulk during film synthesis were performed using an energy dispersive X-ray spectrometer (EDX, Link Isis) attached to the SEM. Prior to the SEM characterization, the samples were coated with a thin layer of gold. A Siemens D5000 powder X-ray diffractometer (XRD) running in the Bragg–Brentano mode and equipped with a Göbel mirror, was used to collect the XRD data in the 2θ range of 5°–35°. Fourier transform infrared (FTIR) spectroscopy measurements were performed using a Perkin–Elmer 2000 FTIR spectrometer.

3. Results and discussion

Seed crystals, 70 nm as measured by DLS, were adsorbed on α-alumina wafers in order to facilitate zeolite growth. After one adsorption step, approximately 30% of the substrate is covered with seed crystals, see Fig. 1(a). An additional adsorption step results in a substantially improved seeding, see Fig. 1(b), with a coverage of about 60%. A seeding procedure involving two steps was used to grow the films. In order to investigate the possibility of the film growth without seeding the wafer, an experiment was made where a nonseeded α-alumina wafer was immersed in a synthesis gel for 20 h. From the top view of the SEM images (not shown here), it was concluded that no film was formed on nonseeded substrates.

The influence of synthesis temperature on films grown in the upper part of the synthesis gel was investigated using three different temperatures: 60°C, 80°C and 100°C. The top and side view

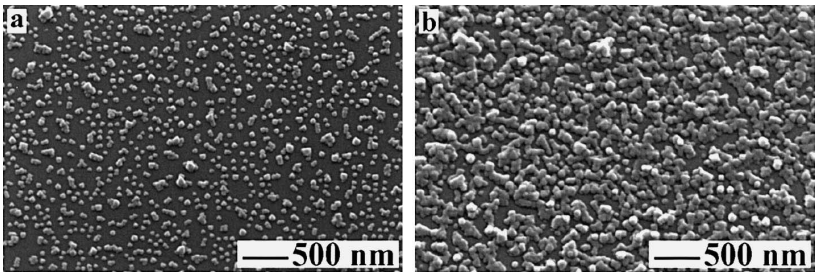

Fig. 1. A seeded wafer after (a) one and (b) two adsorption steps.

SEM images were used to study the morphology and thickness of the films. The film surface morphology follows a similar trend during growth in each of these series synthesized in the upper part of the synthesis vessel. After a short synthesis time, before a continuous film has been formed, the size distribution of the crystals is narrow. Upon prolonged hydrothermal treatment however, some crystals are larger. Further exposure of the film to the synthesis solution causes these larger crystals to encapsulate the surrounding crystals. In Fig. 2, this process can be followed for films synthesized at 80°C. Also, the amount of crystals per unit area decreases with increasing thickness. The processes described above however, take place at different synthesis times due to the different growth rates in each series, see Fig. 3. The relationship between the initial film growth rate, measured as a change in the film thickness, and the synthesis temperature appears to be exponential. A plot of the natural logarithm of the film growth rate (estimated by linear regression of the initial part of each curves shown in Fig. 3) against $1/T$ results in a straight line. Although on the basis of three data points only, this indicates that the growth reaction follows the Arrhenius equation, as can be expected. The activation energy was calculated to be 60 kJ/mol. Even though this value is uncertain, it agrees well with the results obtained previously [13]. During the hydrothermal treatment of the film synthesis solution, an aluminosilicate gel is rapidly precipitated. At 80°C and 100°C, an almost clear solution is formed in the upper part of the synthesis mixture. At 60°C, the upper phase is somewhat cloudy. In order to investigate the film growth in the lower part, one experimental series was performed with the substrates placed in the lower part of the synthesis mixture during film growth at a temperature of 100°C. After 1 h of synthesis, a continuous film with a thickness of 210 nm had formed. After 12 h, the film thickness had reached a maximum of 2740 nm. Films synthesized at 100°C in the lower part of the synthesis mixture were thicker than the films synthesized in the upper part using the same synthesis duration and temperature, see Figs. 3 and 4. Davis et al. obtained similar results when growing zeolite Y coatings on copper foils [14]. They found that thinner coatings were formed in the upper part of the gel precursor. The results obtained in the present study can probably be explained by the attachment of crystals formed in bulk on the growing film. This is more likely to happen when the film is grown at the bottom of the synthesis gel, as the concentration of crystals formed in bulk should be higher in this area. The higher nutrient concentration at the bottom of the synthesis solution can also promote secondary nucleation processes that could affect the film thickness. A secondary nucleation process is also supported by the fact that the film thickness is approximately the same as the surface crystal size, estimated by SEM top view images, for all films synthesized in the upper part of the synthesis solution. For films hydrothermally treated at the bottom of the synthesis solution, on the contrary, a deviation between these two values is obtained, which increases with the film thickness. A film synthesized in the upper part of the tube at 100°C for 6 h is 1000 nm thick, see Fig. 4(a) and (b), which is about the same as the length of the larger crystals. A film synthesized at 100°C in the lower part of the tube

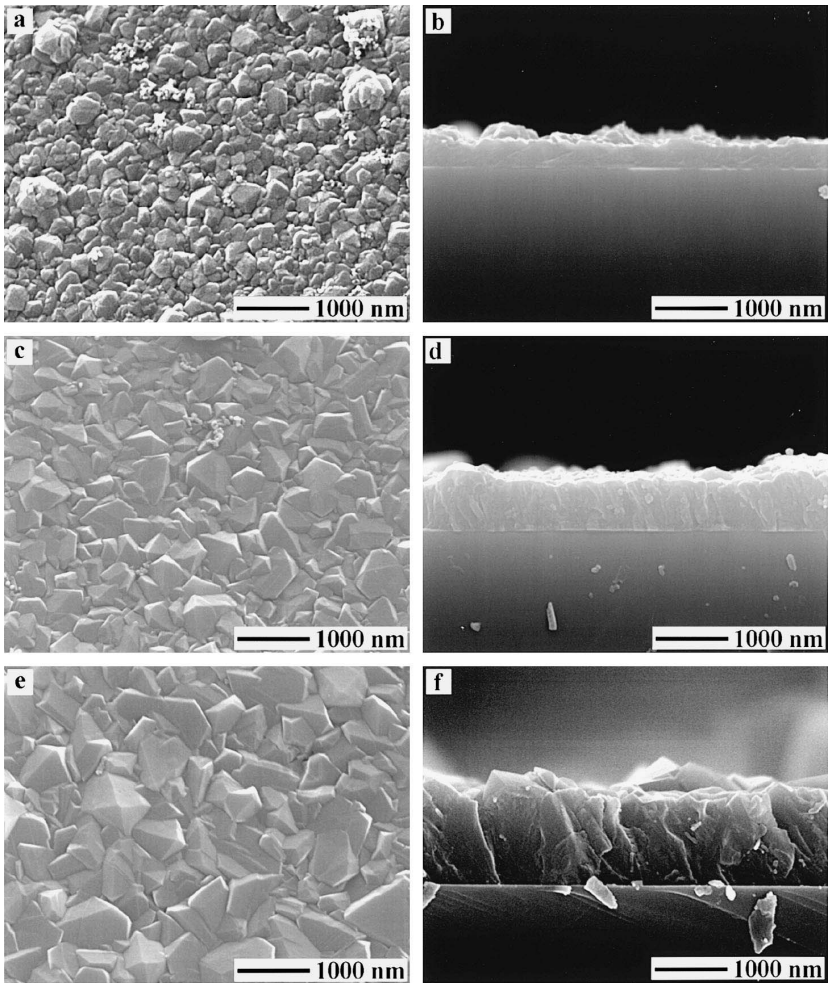

Fig. 2. SEM images of films synthesized at 80°C in the upper part of the synthesis mixture for (a, b) 3 h, (c, d) 12 h and (e, f) 21 h.

for 6 h, has a crystal size of about 1000 nm, whereas the film thickness is about 1700 nm, see Fig. 4(c) and (d). Moreover, subjecting films synthesized at the lower part of the synthesis solution at 100°C to ultrasound treatment causes the film thickness to decrease. The relative decrease is more pronounced for thicker films. Thus, crystals originally attached to the surface seem to have detached during ultrasound treatment. This indicates that multilayered films are synthesized in the bottom part of the synthesis solution, due to the attachment of bulk crystals on the surface of the growing film or the secondary nucleation reactions. In a few films, a thin gel layer can be seen on the film surface, probably due to inadequate rinsing.

Thicker films synthesized at 100°C, tend to peel off during rinsing. A partial explanation of this phenomenon could be the small number of surface hydroxyl groups (<1 OH/nm^2) on the single

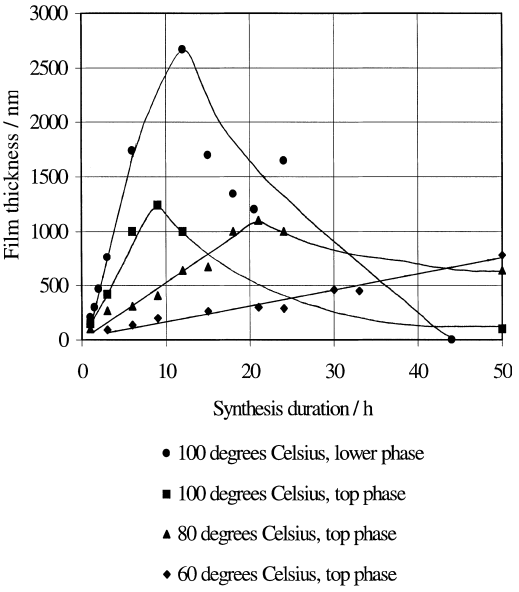

Fig. 3. Film thickness of Faujasite-type films as a function of the synthesis time.

crystal α-alumina wafer [15], which weakens the electrostatic adsorption between the wafer surface and the cationic polymer, i.e. the adhesivity of the zeolite film. However, this does not explain why thinner films do not peel off during rinsing.

From Fig. 3, for films synthesized at 100°C and 80°C, it is quite clear that the film thickness increases up to a certain time of hydrothermal synthesis and then decreases upon a prolonged treatment. This should also be the case for films synthesized at 60°C, but the experimental series was probably not sufficiently extended. This phenomenon has previously been reported for the preparation of ZSM-5 films [8], although it was not further investigated. In order to do so, purified crystals formed in the bulk of the synthesis solution after different periods of synthesis times were investigated by XRD. Successive transformation of the bulk product during hydrothermal treatment is often encountered in the zeolite synthesis. Fig. 5 shows the amount of Faujasite and zeolite P in the crystalline bulk product as a function of synthesis duration. It is clear that the fraction of Faujasite decreases, whereas the amount of zeolite P increases. The same kind of behavior can be expected of the crystals constituting the film, i.e. it is likely that the zeolite P crystals formed after prolonged hydrothermal treatment grows at the expense of the crystals in the bulk as well as of the crystals constituting the film. Thus, the reason for the decrease in the film thickness is likely to be the formation of zeolite P. However, the crystals constituting the films seem to dissolve more rapidly than the crystals formed in the bulk of the synthesis solution. After 44 h of hydrothermal treatment at 100°C in the lower part of the synthesis solution, no film can be detected on the wafer despite a rather high relative amount of Faujasite in the crystalline bulk product, see Fig. 5. A possible explanation for this is that the smaller crystals constituting the film are more quickly dissolved than the larger crystals (1800 nm) in the bulk. It is also observed in the Figure, that the fractions of Faujasite and zeolite P does not add up to 100% after about 340 h of synthesis. This may be due to the crystallinity difference between the reference sample of zeolite P and the zeolite P formed in the bulk of the synthesis solution. For example, the crystallinity for the bulk product consisting of Faujasite, obtained after 12 h of synthesis, is higher than the reference sample (see Fig. 5).

The preferred orientation of the crystals constituting the films was investigated using XRD data. A powder sample of Faujasite, obtained after 12 h of synthesis, was used as a reference and considered to have random orientation of the crystals. An XRD diffractogram of adsorbed seed crystals is shown in Fig. 6(a) along with patterns obtained from films synthesized at 100°C (b) and (c) and the pattern obtained from the powder reference (d). Major peaks in the diffractogram obtained from the adsorbed seed crystals are the (1 1 1) peak and the (5 5 5) peak indicating a preferred orientation of the seed crystals with the {1 1 1} pyramid parallel to the substrate surface. The seed crystals seem to be adsorbed in a "flat" manner, with the {1 1 1} pyramid facing the flat wafer. The crystals in the film samples seem to have an orientation quite different from the refer-

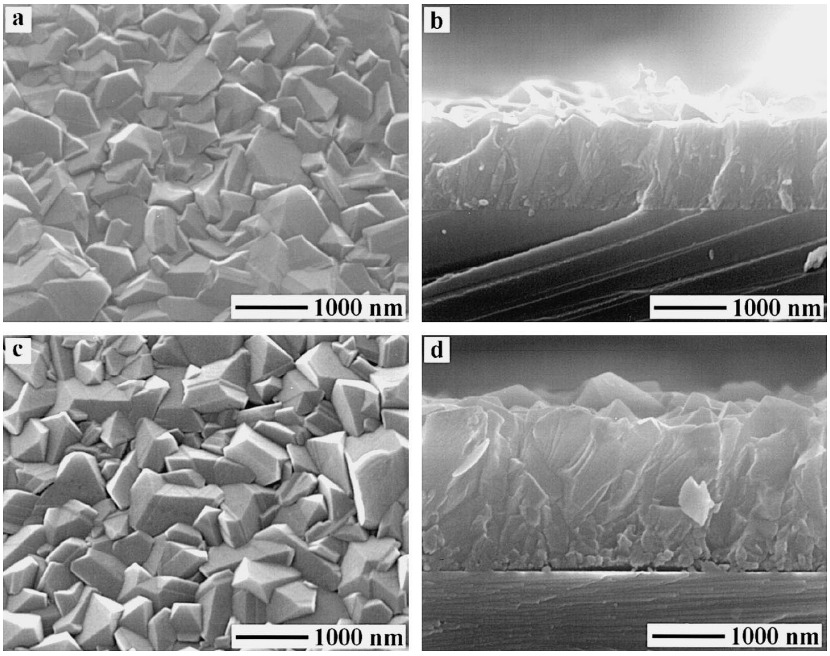

Fig. 4. SEM images of films synthesized at 100°C for 6 h in (a, b) the upper part and (c, d) the lower part of the synthesis solution.

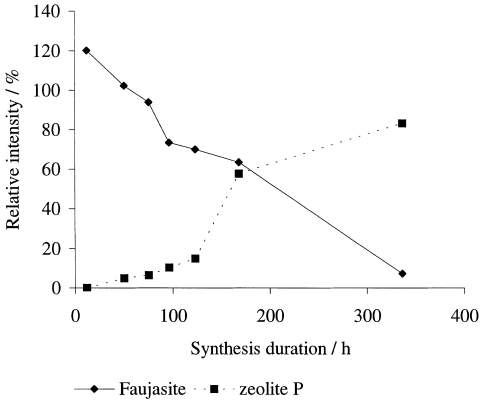

Fig. 5. The fraction of Faujasite and zeolite P of the bulk product as a function of synthesis duration.

ence sample, indicating a preferred orientation of the crystals constituting the films. To further investigate the change in orientation of the films crystallographic preferred orientation based on the

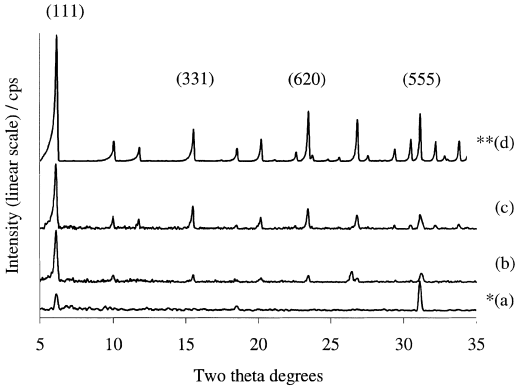

* The intensity has been multiplied with two.
** The intensity has been divided by ten.

Fig. 6. XRD diffractograms recorded from (a) adsorbed seed crystals; films synthesized at 100°C in the upper part of the synthesis mixture for (b) 3 h and (c) 6 h, (d) along with a pattern collected from a powder sample.

X peak and the Y peak (CPO(X)/(Y)) was defined in the following way [16]:

$$\mathrm{CPO(X)/(Y)} = \frac{A_S^{(X)}/A_S^{(Y)} - A_P^{(X)}/A_P^{(Y)}}{A_S^{(X)}/A_S^{(Y)}},$$

where A refers to the peak area, S to the film sample and P to the powder reference sample. The (1 1 1) peak was chosen as the reference peak as it is intense in all the diffractograms. The (3 3 1) peak and the (6 2 0) peak have a relatively high intensity in all the diffractograms, and are thus suitable for the CPO calculations as well. If the CPO value is zero, the crystals are randomly oriented. A value of one means that the crystals are oriented with the (1 1 1) plane parallel to the substrate surface and that the⟨1 0 0⟩ direction is oriented 55° from the normal to the substrate surface. A value of CPO(1 1 1)/(3 3 1) equal to $-\infty$ implies a preferred orientation with the (3 3 1) plane parallel to the substrate surface. A value of CPO(1 1 1)/(6 2 0) equal to $-\infty$ indicates a preferred orientation with the (6 2 0) plane parallel to the substrate surface. A {1 1 1} orientation of the crystals in the film means that two of the channel assemblages run parallel to the film surface, whereas one runs perpendicular to it. Fig. 7 shows the change in CPO with the film thickness. The series at 60°C is not represented in the figure due to low intensity and uncertainty of the XRD data from this series. However, similar trends were found in this series. From Fig. 7(a), it is clear that the value of CPO(1 1 1)/(3 3 1) is near unity for thin films according to previous discussions. The CPO value decreases with increasing film thickness in each series. Fig. 7(b) shows CPO(1 1 1)/(6 2 0) as a function of film thickness. The trend is similar as for CPO(1 1 1)/(3 3 1) also. The results presented in Fig. 7 indicates that the orientation of the crystals constituting the films proceeds towards a random orientation during film growth. A possible explanation for the change in orientation from the (1 1 1) plane parallel to the substrate surface is the secondary nucleation taking place on the film surface during film growth or attachment of bulk crystals onto the surface of the growing film. These crystals are less likely to be attached with the {1 1 1} pyramid parallel to the substrate surface because the film surface is uneven

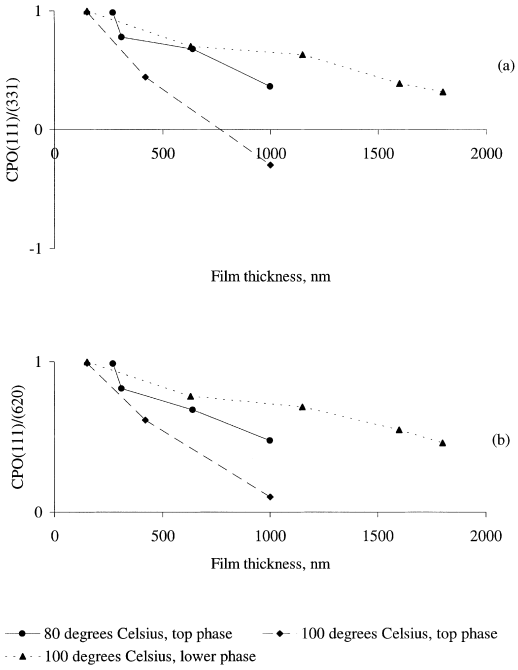

Fig. 7. (a) CPO (1 1 1)/(3 3 1) and (b) CPO (1 1 1)/(6 2 0) as a function of Faujasite-type film thickness.

as opposed to the flat support. As mentioned previously, the number of crystals per unit area decreases with increasing film thickness. This indicates a competitive growth of the crystals constituting the films. Competitive growth has in previous work explained the preferred orientation of crystals in MFI-type films [8]. Although a competitive growth can be concluded from SEM images in the present study, the secondary nucleation process or the attachment of crystals formed in the bulk of the synthesis solution onto the growing surface is probably too extensive to allow a preferred orientation to develop.

The Si/Al ratio of the crystals constituting the film can affect the permeation properties in a membrane. The zeolite films are too thin to be analyzed by EDX. However, the Si/Al ratio for the crystals formed in the bulk of the synthesis solution was measured with EDX: a Si/Al ratio of 1.5 was obtained.

A problem associated with the preparation of MFI-type zeolite films is that they tend to crack upon calcination, thus imposing difficulties in membrane applications. For MFI-type materials synthesized using tetrapropylammonium hydroxide as a template, a calcination procedure is necessary to remove the template ions and to open up the pore structure. However, in Faujasite-type zeolites, the pores are substantially larger and hence, it should be possible to remove the templating ions (TMA^+) by ion exchange. This was investigated for the zeolite Y seed crystals synthesized in the presence of TMA^+ ions. The progress of the exchange of TMA^+ ions for NH_4^+ ions in the seed crystals during purification in dilute ammonia solution was followed by FTIR spectroscopy (Fig. 8). The most intense band originating from the zeolite structure is located at 1015 cm^{-1} [17]. The TMA^+ ions incorporated in the pore structure of the zeolite result in an intense band at 1489 cm^{-1} and a weaker one at 1420 cm^{-1} [18]. Ammonia and water present in the pore structure of the zeolite give intense bands at about 1450 and 1640 cm^{-1}, respectively [19]. Fig. 8(a) shows the spectrum obtained from zeolite Y seeds purified in distilled water. Spectra collected from seed crystals purified in a dilute ammonia solution, equilibrated for 72 h and 4 months are shown in Fig. 8(b) and (c), respectively. The intensity ratio between the bands at 1015 and 1489 cm^{-1} was calculated for each spectrum. The spectrum collected from the seed crystals purified in a dilute ammonia solution for 72 h has a much higher intensity ratio between the two bands than the crystals purified in distilled water (2.2 and 1.5, respectively). This indicates that most of the TMA^+ ions originally present in the pores have been exchanged by ammonium ions. The intensity ratio increased even more (4.4), when equilibrating for 4 months. EDX analysis show that the molar Si/Na ratio is lower for the seed crystals washed in water than for the seed crystals purified in a dilute ammonia solution, 4.9 and 7.1, respectively. This indicates that some of the sodium counter ions have been exchanged by ammonium ions as well. As no TMAOH was used in the film growth step, the resulting films were essentially free from organic template ions.

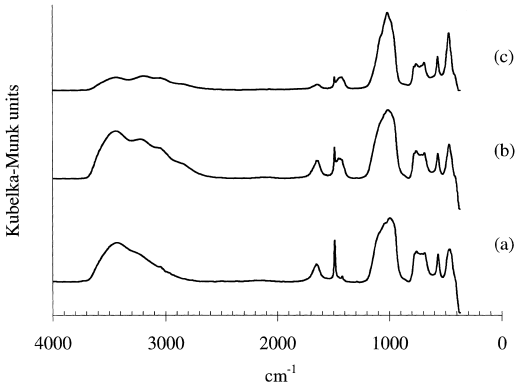

Fig. 8. FTIR spectra from seed sol samples washed in (a) water and in a dilute ammonia solution for (b) 72 h and (c) 4 months.

4. Conclusions

Continuous films of Faujasite were synthesized on polished α-alumina wafers seeded with colloidal zeolite Y crystals synthesized in a clear solution in the presence of template molecules. Most of the template molecules were however ion exchanged to ammonium ions during the purification steps of the seeds making the films synthesized essentially template free. During hydrothermal treatment, a precipitate formed, leaving a clear solution in the upper part of the synthesis vessel. The rate of film growth in the lower part of the synthesis solution was found to be higher than that in the clear upper part. This was most likely due to secondary attachment or nucleation of crystals on the growing film surface for films prepared in the lower part of the gel. The final film thickness could be controlled using a suitable synthesis duration. Also, lowering the synthesis temperature results in a decrease in the film growth rate. The film thickness was shown to decrease upon a prolonged hydrothermal treatment. This behavior can be explained by the formation of zeolite P that grows at the expense of the Faujasite-type crystals formed in the synthesis solution as well as the crystals constituting the film. Films with thicknesses ranging from 150 to 2740 nm were synthesized using the method described in this work. Seeds adsorbed on the wafers

were oriented with the {1 1 1} pyramid parallel to the substrate surface. A change leading to random orientation of the crystals constituting the films could be detected during synthesis. This was probably due to the attachment of secondary crystals on the growing film. Films synthesized in this work were continuous and free from defects observed by SEM. They are currently being evaluated as membranes, using a porous alumina ultrafiltration membrane as a substrate.

Acknowledgements

The Swedish Research Council for Engineering Sciences (TFR) is acknowledged for supporting this work financially.

References

[1] D.W. Breck, Zeolite Molecular Sieves, Krieger, NY, USA, 1974, p. 77.
[2] K. Kusakabe, T. Kuroda, A. Murata, S. Morooka, Ind. Engng. Chem. Res. 36 (1997) 649.
[3] L. Boudreau, M. Tsapatsis, Chem. Mater. 9 (1997) 1705.
[4] M.C. Lovallo, M. Tsapatsis, AIChE journal 42 (1996) 3020.
[5] H. Kita, T. Inoue, H. Asamura, K. Tanaka, K. Okamoto, Chem. Commun. (1997) 45.
[6] V. Valtchev, B.J. Schoeman, J. Hedlund, S. Mintova, J. Sterte, Zeolites 17 (1996) 408.
[7] J. Hedlund, B.J. Schoeman, J. Sterte, in: H. Chon, S.-K. Ihm, Y.S. Uh (Eds.), Progress in Zeolites and Microporous Materials, Elsevier, Amsterdam, Stud. Surf. Sci. Catal. 105 (1997) 2203.
[8] S. Mintova, J. Hedlund, V. Valtchev, B.J Schoeman, J. Sterte, J. Mater. Chem. 7 (1997) 2341.
[9] J. Sterte, S. Mintova, G. Zhang, B.J. Schoeman, Zeolites 18 (1997) 387.
[10] J. Hedlund, B.J. Schoeman, J. Sterte, Chem. Commun. (1997) 1193.
[11] S. Mintova, V. Valtchev, B.J. Schoeman, J. Sterte, Porous Mater. 3 (1996) 143.
[12] B.J. Schoeman, J. Sterte, J.-E. Otterstedt, Zeolites 14 (1994) 110.
[13] R.M. Barrer, Hydrothermal Chemistry of Zeolites, Academic Press, New York, 1982, p. 152.
[14] S.P Davis, E.V.R. Borgstedt, S.L. Suib, Chem. Mater. 2 (1990) 712.
[15] J.C. Jansen, J.H. Koegler, H. Van Bekkum, H.P.A. Calis, C.M. van den Bleek, F. Kapteijn, J.A. Moulijn, E.R. Geus, N. Van der Puil, Micropor. Mesopor. Mater. 21 (1998) 213.
[16] J.P. Verduijn, A.J. Bons, M.H. Anthonis, L.H. Czarnetzki, Int. Pat. Appl. PCT WO 96/01683, 1996.
[17] R. Szostak, Handbook of Molecular Sieves, Van Nostrand Reinhold, NY, 1992, p. 287.
[18] R. Szostak, Handbook of Molecular Sieves, Van Nostrand Reinhold, NY,1992, p. 442.
[19] M.W. Urban, Vibrational Spectroscopy of Molecules and Macromolecules on Surfaces, Wiley, New York, 1993, p. 197.

PAPER III

Preparation and evaluation of thin ZSM-5 membranes synthesized in the absence of organic template molecules

---

Magdalena Lassinantti, Fredrik Jareman, Jonas Hedlund, Derek Creaser and Johan Sterte

Catalysis Today, 67 (2001) 109-119.

ELSEVIER

Catalysis Today 67 (2001) 109–119

CATALYSIS TODAY

www.elsevier.com/locate/cattod

Preparation and evaluation of thin ZSM-5 membranes synthesized in the absence of organic template molecules

Magdalena Lassinantti*, Fredrik Jareman, Jonas Hedlund, Derek Creaser, Johan Sterte

Division of Chemical Technology, Luleå University of Technology, 971 87 Luleå, Sweden

Abstract

Porous α-alumina supports with a pore size of 100 nm were seeded with colloidal TPA-silicalite-1 crystals with a size of 120 nm. The seeded supports were calcined and treated in a synthesis solution free from organic template molecules to form ZSM-5 films on the supports. According to SEM images, the films were about 2 μm thick and no defects could be found on the as-synthesized membranes. Single gas permeation data was collected and good quality membranes (defined as having a non-detectable permeance of SF_6 after drying at 100°C) were further evaluated using binary/ternary gas mixtures. The selectivity for *n*-butane/*i*-butane had a maximum value of 17.8 at 220°C. Water was selectively separated from a helium-diluted vaporized water/ethanol azeotrope with a maximum selectivity of 12.4.

Keywords: α-Alumina; ZSM-5 film; TPA-silicate-1 crystal; Azeotrope

1. Introduction

Thin, supported zeolite membranes with well-defined pores of molecular dimensions have the potential to exhibit both high selectivity and high permeability and operate under harsh conditions, such as elevated temperatures and high pressure. The catalytic properties of zeolites are well known. Thus, zeolite membranes also have an excellent potential for applications in catalytic membrane reactors. In such a configuration, catalysis and separation of products can be performed in a single unit operation. Even though some work in this exciting field of research has been done [1,2], most papers published deal with separation only. The separation mechanisms are in many cases complex. However, Keizer et al. [3,4] classified the permeation results obtained for various two component gas mixtures on a silicalite-1 membrane by considering the occupancy on the external surface and the zeolite pores as well as the mobility in the pores.

Various zeolite species with different pore size and aluminum content, i.e. polarities, such as Faujasite type structures [5,6], A-type structures [2,7–10] and Ferrierite type structures [11] have been investigated in membrane applications. The majority of the work has however been on MFI-type structures, i.e. silicalite-1 and ZSM-5. Many industrially important species have a kinetic diameter similar to the pore opening of MFI-type structures. As a consequence, an MFI-type membrane has the potential to be a useful separation device.

Usually zeolite membranes are synthesized by direct hydrothermal treatment in a synthesis solution containing a templating agent which becomes incorporated in the pore structure. By a calcination procedure, the templating agent is removed in order to make the molecular sieve microporous. It is well known that this treatment may cause cracks, which makes the membrane less effective. In the present

* Corresponding author.

0920-5861/01/$ – see front matter
PII: S0920-5861(01)00270-X

work, a method comprised of seeding the porous support with colloidal seed crystals followed by growth of the seeds into a dense film was used to prepare thin ZSM-5 membranes without the use of organic template molecules in order to avoid the potentially detrimental calcination procedure. ZSM-5 membranes prepared in a similar way have previously been investigated by our group [12]. Low fluxes and poor selectivities were found for an *n*-butane/*i*-butane mixture in the temperature range investigated, probably due to blockage of zeolite channels by adsorbed molecules such as water and/or ammonia. In the present work, selectivities and fluxes for *n*-butane/*i*-butane were investigated at higher temperatures. Catalytic conversion of ethanol into diethylether and ethylene will also be discussed.

2. Experimental

2.1. Preparation of membranes

TPA-silicalite-1 seeds with an average size of 120 nm were prepared from a synthesis solution with the composition 9 TPAOH:25 SiO_2:360 H_2O:100 EtOH. The synthesis solution was hydrothermally treated for 2 days in an oil bath at a temperature of 100°C. The alkali source was tetrapropylammoniumhydroxide (Sigma, 1.0 M aqueous solution) and the silica source was tetraethoxysilane (Merck, >98%). The seed crystals were purified by repeated centrifugation followed by redispersion in a dilute ammonia solution to obtain a seed sol. The dry content was adjusted to 1.0 wt.% and the pH to 10.0. The zeolite membranes were grown on asymmetric α-alumina supports with an average pore size of 100 nm in the top layer (Inocermic GmbH). The supports were rinsed for 20 min in acetone and methanol and rinsed in filtered (0.1 μm filter) 0.1 M ammonia solution. Following cleaning, the supports were treated for 20 min in a solution containing cationic polymer molecules (0.4 wt.% Redifloc 4150, Eka Chemicals), adjusted to pH 8.0 by addition of a dilute ammonia solution. The solution was filtered with a 0.8 μm filter prior to use. The substrates were rinsed in a filtered (0.1 μm) 0.1 M ammonia solution to remove excess polymer. In the following step, the modified supports were immersed in the seed sol for 20 min. The sol was filtered with a 0.8 μm filter prior to use. No effort was made to limit seed adsorption to the top layer of the α-alumina disk. After adsorption of seed crystals, the supports were rinsed in a filtered (0.1 μm) 0.1 M ammonia solution to remove excess crystals. A calcination procedure (500°C for 4 h) was carried out to remove template molecules from the adsorbed seed crystals. Following calcination, the supports were immediately placed in a synthesis gel for 12 h at 180°C to form ZSM-5 films. The synthesis gel was prepared by dissolving sodium metasilicate ($Na_2SiO_3 \cdot 9H_2O$ > 98%, Sigma) and aluminum sulfate ($Al_2(SO_4)_3 \cdot 18$ H_2O, Riedel-deHaën) in water in separate beakers. The contents of the beakers were carefully mixed and a dilute silica sol (Bindzil 30/220, Eka Nobel AB) was added. The molar composition of the resulting synthesis gel was 30 Na_2O:Al_2O_3:100 SiO_2:4000 H_2O. Following hydrothermal treatment, the samples were rinsed thoroughly in 1 M NH_3 and treated in a ultrasonic bath in order to remove excess synthesis mixture and sediments from the porous support.

A synthesis gel was seeded (0.05 wt.% silicalite-1 seed crystals) and hydrothermally treated for 12 h at 180°C. The obtained product was purified and freeze dried and used for XRD and EDX analysis.

2.2. General characterization

A Philips XL 30 Scanning Electron Microscope (SEM) equipped with a LaB_6 emission source was used to study the thickness and morphology of the membranes. Elemental analysis of the product formed after seeding the membrane synthesis solution was performed using an energy dispersive X-ray spectrometer (EDX, Link Isis) attached to the SEM. All samples were gold coated prior to measurements. A Siemens D5000 powder X-ray diffractometer (XRD) running in the Bragg–Brentano mode was used to collect XRD data.

2.3. Permeation measurements

Gas permeation measurements were performed in a test facility based on the Wicke–Kallenbach technique. The membranes were mounted in a stainless steel cell equipped with graphite gaskets. The permeate and retentate pressures were controlled by a regulating

valve connected to a pressure transmitter through a PID controller. The gases were fed to the system by three mass flow controllers. The equipment allowed two gases to be chosen without restrictions via a gas manifold system containing magnetic valves. Helium was used as sweep gas in all measurements. Liquids were fed to the system with a syringe pump and vaporized in an evaporator located in a heated zone kept at 170°C. A thermocouple (type K) was connected to the membrane cell in order to record the temperature of the separation process. All control and measurement signals to and from the system were connected to a data acquisition interface, controlled and monitored by a commercial software package. An online Varian 3800 gas chromatograph (GC), with a column switching system allowing for separation of a wide range of samples, was used for quantitative analyses of the gas mixtures. The GC was equipped with a capillary column (J&W DB-1, 60 m, i.d. 0.32 mm, d.f. 5 μm) and two packed columns (molecular sieve 13×, $\frac{45}{60}$ mesh, 4 ft × $\frac{1}{8}$ in. and Chromosorb 107, $\frac{80}{100}$ mesh, 6 ft × $\frac{1}{8}$ in.). A thermal conductivity detector (TCD) and a flame ionization detector (FID) connected in series detected the separated components. In the case of single gas permeation measurements, a flowmeter (ADM 1000, J&W Scientific) was used to measure flow rates higher than 15 ml/min (STP). At lower fluxes, soap bubble flowmeters (1 and 25 ml) were used.

Single gas permeation measurements (H_2, N_2, He and SF_6) were performed at room temperature with a feed gas applied at 5 bar absolute pressure. The permeate pressure was maintained at 1 bar absolute pressure. No sweep gas was used and permeances were calculated from the measured flow. The membranes were dried in air at 100°C for 12 h prior to measurements. In one experiment, the permeance of SF_6 for an as-synthesized membrane was monitored as a function of temperature during drying in the stainless steel cell.

Butane isomers were mixed in a 50/50 kPa mixture which was fed to the membrane cell at a total volumetric flow rate of 200 ml/min (STP). No absolute pressure difference was applied over the membrane. Helium was used as sweep gas at a volumetric flow rate of 200 ml/min (STP). The permeate and retentate were analyzed with a GC. Three experimental series were performed with butane isomers. In the first series, referred to as Run 1, the membrane was slowly heated up to 80°C (1°C/min) after which permeation tests were performed at up to 220°C in 20°C intervals. After keeping the membrane at 220°C for 12 h, the temperature was reduced to 100°C. Subsequently, new permeation measurements at 20°C intervals at up to 400°C were performed. This series will be referred to as Run 2. During Run 2, pure isobutane was also fed to the membrane at 260, 300 and 400°C in order to investigate whether catalytic isomerization of *i*-butane occurred. In order to study the reproducibility of the results obtained in Run 2 (after the membrane had been exposed to elevated temperatures), new measurements were performed upon cooling back to 320 and 200°C. Run 3 will represent this final test series.

The volumetric flow rate of the ethanol/water azeotrope (96%/4%) from the syringe pump was 0.2 or 0.1 ml/min. The vaporized azeotrope was mixed with helium at a volumetric flow rate of 200 or 1000 ml/min (STP). The UNIFAC method was used to determine the partial pressures of the components in the feed stream yielding 4.3/25/71.7 and 0.58/3.4/97 kPa water/ethanol/helium mixtures, respectively. These two feeds were fed to the membrane that was held at a temperature varying from 100 to 200°C with 20°C intervals. Due to catalytic activity of the membrane at higher temperatures two different selectivities were calculated. One was calculated directly from the results of the gas chromatography analysis without any consideration of the reduction of ethanol permeances due to the reactions below [13]:

$$C_2H_5OH \rightarrow C_2H_4 + H_2O,$$

$$2C_2H_5OH \rightarrow C_2H_5OC_2H_5 + H_2O$$

The other selectivity accounted for the conversion of ethanol to diethylether and ethylene to give an alternative measure of the selectivity of the membrane. In this case, the quantities of ethanol and water were corrected for the reactions based on the measured amounts of diethylether and ethylene.

3. Results and discussion

3.1. Membrane morphology

Fig. 1(a) and (b) shows top and side view images of a membrane. No pinholes or cracks could be found on the as-synthesized films. Crystal aggregates were

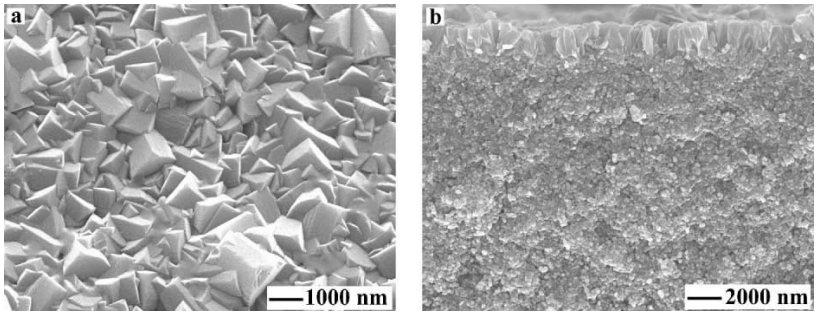

Fig. 1. Top (a) and side (b) view SEM images of an ZSM-5 membrane.

present on the film surfaces. Holes could be seen from top view SEM images (not shown here), probably resulting from detached crystal aggregates. It was however difficult to judge if these holes penetrated the film. No continuous film was formed on the back side of the support.

Even though the same synthesis procedure had been utilized for all membranes prepared in this work, the thickness of the zeolite layer varied between 1400 and 1800 nm. An exact determination was however difficult due to the rough support surface.

XRD patterns were collected from membranes prepared in this work. No other peaks than those expected from ZSM-5 and α-alumina were obtained. Fig. 2(a) shows XRD data from an ZSM-5 membrane along with data recorded from the product formed after hydrothermal treatment of a seeded synthesis solution. The relative intensities of the (1 3 3) peak and the (0 5 1) peak are larger for the membrane sample compared to the powder (which is considered to have a random orientation). This suggests a preferred orientation of the crystals constituting the membrane in accordance with findings previously reported [14]. For some membranes the effect was not as clear, probably due to randomly oriented crystal aggregates attached to the surface of the film.

The Si/Al ratio in the zeolite powder formed after hydrothermal treatment of a seeded synthesis solution was found to be 10 based on EDX analysis. The zeolite film may have an even lower ratio due to dissolution of the alumina support during membrane synthesis and incorporation of the leached aluminum

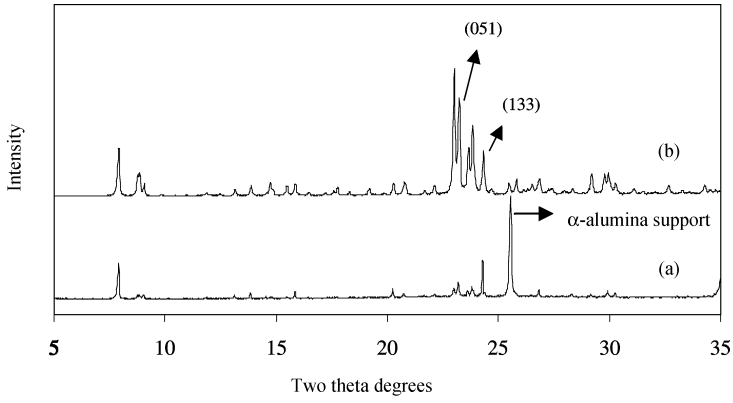

Fig. 2. XRD diffractograms for a zeolitic membrane (a); together with a powder reference sample (b).

into the zeolite layer [15,16]. Thus, a high content of adsorbed molecules such as water and ammonia in the as-synthesized membranes can be expected due to the polar nature of the formed zeolite. Since the membranes investigated in this work were not thermally pretreated, some of the adsorbed molecules can be expected to remain in the zeolite structure after drying at moderate temperatures. This might affect the permeation behavior of the membrane as demonstrated by Funke et al. [17].

3.2. Permeation measurements

3.2.1. Single gas permeation measurements

In order to crudely evaluate the membrane quality, each membrane was first tested in a single gas permeation experiment. Membranes with no measurable permeance of SF_6 after drying at 100°C for 12 h, were selected for further permeation experiments. Note that all membranes had been prepared by the same procedure. Thus, differences in permeation results are due to synthesis reproducibility difficulties. Table 1 gives a summary of the results obtained for selected membranes. Even an extremely low permeance of SF_6 dramatically affects the N_2/SF_6 ratio since the permeance of N_2 also remains very low in these cases (see M1, M2, M4 and M6 in Table 1). This is probably due to the blocking effects of adsorbed species present in the pore structure of the membrane. A much higher permeance ratio would have been expected from a completely dry membrane since the N_2 permeance probably would be much higher and the SF_6 would remain low, since SF_6 is expected to permeate mainly through defects.

Table 1
Single gas permeation measurements for selected membranes[a]

Sample	Permeance (10^7 mol/m^2 s Pa)				N_2/SF_6
	H_2	N_2	He	SF_6	
M1	8.4	3.9	4.1	0.9	4.4
M2	3.1	1.7	1.8	0.4	4.4
M3	3.9	2.0	1.9	<0.001[b]	>2000
M4	2.5	1.2	1.6	0.1	12
M5	1.2	0.62	0.7	<0.001[b]	>620
M6	3.2	1.2	1.6	0.1	12
M7	1.6	0.58	0.92	<0.001[b]	>580

[a] A transmembrane pressure difference of 4 bar was utilized.
[b] Undetectable.

Thus, the N_2/SF_6 ratio does not necessarily represent the quality of a membrane that is not fully dried even though Funke et al. [18] introduced the N_2/SF_6 ratio as criterion for a good MFI membrane. They postulate that a permselectivity higher than 80 indicates a good MFI membrane. Coronas et al. [16,19] also used N_2/SF_6 permselectivity measured at room temperature as an indication of ZSM-5 membrane quality. A permeation ratio as high as 259 was measured for zeolite membranes grown on tubular α-alumina support. The results presented here give permeation ratios greater than 580 (based on the detection limit of the SF_6 permeance) for good membranes, see Table 1. However, a direct comparison may be inappropriate since the membranes in this work were not thermally pretreated.

Table 2 shows previously reported N_2 and SF_6 permeances for MFI membranes. Even though the film thickness in the present work was as low as 2 μm the permeance was not very high compared to previously reported results for significantly thicker films [15,19–22]. Xomeritakis et al. [21] reported (for an MFI membrane with a thickness of 38 μm) a nitrogen permeance similar to the present work. Gump et al. [23] reported a nitrogen permeance four times larger than in the present work. These two reported results support our assumption that adsorbed species may be present inside the zeolite pores. However earlier reported ZSM-5 membranes synthesized in the absence of template molecules [12,24,25] show significantly lower permeances than in the present work, probably also due to adsorbed species in the zeolite channels.

The effect of temperature on membrane stability was investigated by studying the permeance of SF_6 at different temperatures. Fig. 3 shows the SF_6 permeance as a function of temperature for M7. As can be seen, the permeance was very low up to about 250°C after which it dramatically increased. After cooling the membrane back to ambient temperature the permeance remained very high, as indicated by the arrow in Fig. 3. A likely explanation for this result is the formation of defects in the film. In contrast to as-synthesized membranes, cracks with a width of 50–200 nm were found in the zeolite film after this test, see Fig. 4. Dong et al. [26] described template-removal associated crack formation in MFI membranes. The present work shows that cracks can form in MFI membranes even if no template was present in the as-synthesized membrane.

Table 2
Comparison of N_2, SF_6 and butane isomers permeational properties (the temperature in K is given within brackets, if nothing is noted the permeance was given at room temperature)

	Film thickness (1/μm)	Permeance (10^{10}/(mol/m^2 s Pa))					
		N_2	SF_6	N_2/SF_6	*n*-Butane	*i*-Butane	$\alpha_{n/i\text{-butane}}$
Present work	2	2000	<1	>2000	830 (493)	45	17.8
[25][a]	6	0.14	0.006	23	0.1[b] (423)	0.15[b]	–
[24][a]	3	3.7 (378)	0.099	37	0.099[b] (378)	0.074[b]	2
[12][a]	1.5	9.9 (418)	0.87	11.38	0.5[b] (418)	0.4[b]	0.7
[19]	–	400		6.00	700 (410)	60	11
[15]	100	270 (418)			120 (423)	90	1.3
[21]	38	1600	160	10.00	320[b]	8.6[b]	37[c]
[22]	50	–	–	–	756		48
[20]	–	8800		240.00	700 (350)	20	20

[a] Template free synthesized ZSM-5 membranes.
[b] Single gas measurements.
[c] Permselectivity.

3.2.2. Permeation of a 50/50 n-butane/i-butane mixture

Fig. 5 illustrates the *n*-butane/*i*-butane selectivity as a function of temperature for M3 and Fig. 6 shows the permeances obtained in Run 1. During the first heating cycle up to 220°C (Run 1) the selectivity was close to unity up to 160°C and the permeance of both gases was very low, approximately 5×10^{-10} mol/m^2 s Pa. Between 160 and 200°C the selectivity increased dramatically to 17.8. The permeance increased for both *n*-butane and *i*-butane, see Fig. 6, although the *n*-butane permeance increased much more resulting in the higher selectivities. In Run 2 the selectivity and the *n*-butane permeance were 6.7 and 13.7 times higher, respectively, than in Run 1 at 105°C (compare Runs 1 and 2 in Figs. 5 and 6). This clearly indicates that the zeolite pores were at least partly blocked by adsorbed species at low temperatures during Run 1, which reduced the permeance and selectivity. The isomers probably permeated mainly through defects or grain boundaries present in low quantities. The selectivity reached a maximum of 16.7 at 220°C. Higher temperatures resulted in a lower selectivity. In the temperature range 280–300 and 380–400°C some events took place, see Run 2 in Figs. 5 and 7, which led to particularly sharp drops in selectivity. Between these intervals, the permeance increased more for *i*-butane than for *n*-butane, which might

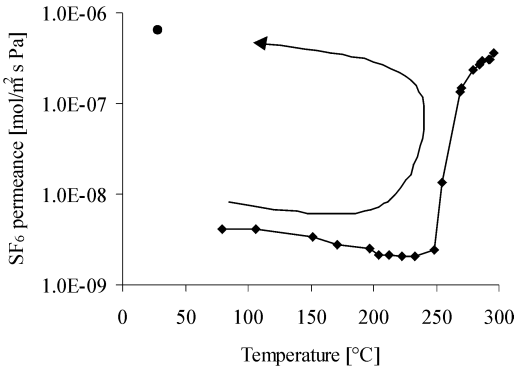

Fig. 3. Permeance of SF_6 for membrane M7 as a function of increasing temperature and after cooling the membrane to room temperature. A transmembrane pressure difference of 4 bar was utilized.

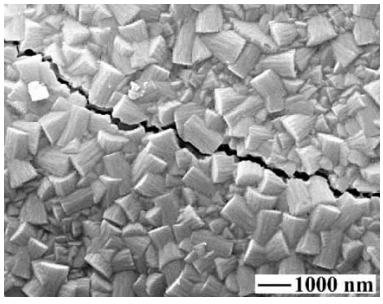

Fig. 4. Top view SEM image of membrane M7 taken after SF_6 permeation measurements conducted during drying up to 300°C.

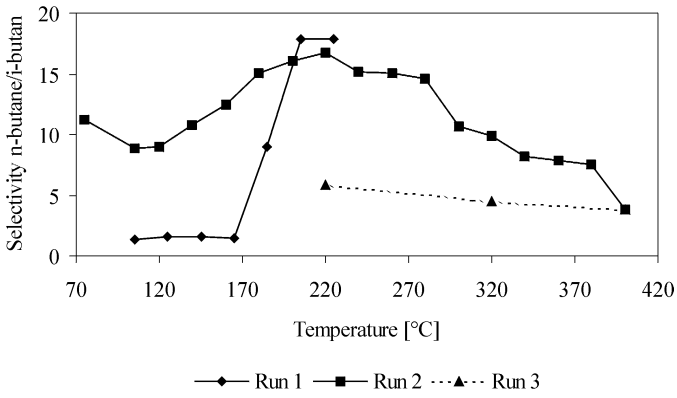

Fig. 5. Selectivities for a 50/50 kPa *n*-butane/*i*-butane mixture for membrane M3 using helium as sweep gas.

be due to the formation of cracks in the zeolite film or simply the effect of temperature on the transport mechanisms. Others have observed an optimal temperature for *n*-butane/*i*-butane selectivity with MFI based membranes [19,20]. At 400°C the selectivity had dropped to 3.8. When decreasing the temperature in Run 3 the high selectivities obtained in Run 2 were not regained, see Fig. 5. At 220°C the selectivity was only 5.8 which is considerably lower than the maximum of 16.7 found in Run 2. The permeation of both isomers was also much higher in Run 3 compared to Run 2, see Fig. 7. The lower selectivities of Run 3 indicate that the molecules increasingly permeated through paths larger than the zeolite pores at higher temperatures. However, these paths cannot be large and/or numerous since the membrane was still able to separate the two butane isomers. Even in Run 3 the selectivity decreased with temperature which suggests that part of the decrease in selectivity with temperatures greater than 220°C observed in Run 2 was caused by the effects of temperature on the transport mechanisms. However, the particularly large changes in selectivity between 280 and 300°C and between 380 and 400°C are mainly caused by crack/defect formation due to the thermal instability of the membrane.

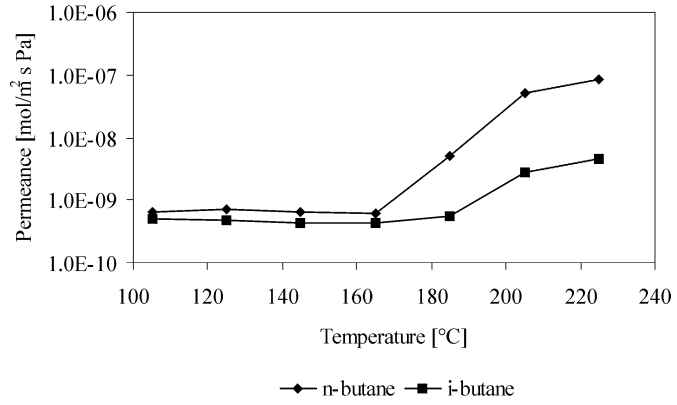

Fig. 6. The permeance of the butane isomers in Run 1 as a function of temperature. A 50/50 kPa mixture of butane isomers were fed to the membrane and helium was used as a sweep gas.

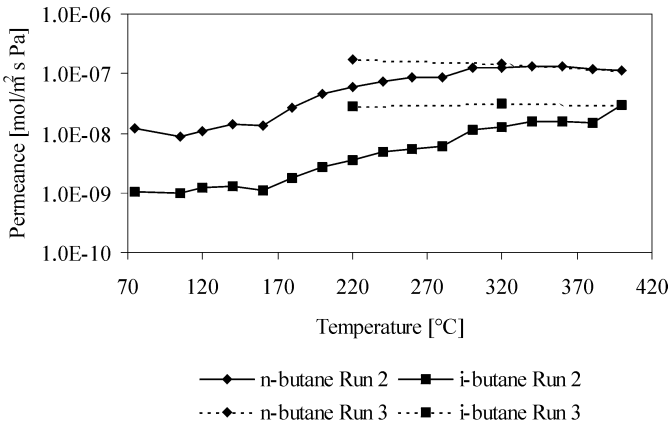

Fig. 7. Permeances of the butane isomers in Runs 2 and 3. A 50/50 kPa butane isomer mixture was used as feed and helium was utilized as a sweep gas.

A catalytic isomerization of *i*-butane to *n*-butane would have increased the apparent selectivities obtained. Pure *i*-butane was fed to the membrane at 260, 300 and 400°C during Run 2. At these conditions no *n*-butane was detected in the permeate. Thus, the selectivities presented in this work only represent the separation ability of the membrane.

Noack et al. [24] prepared template free ZSM-5 membranes on α-alumina disks using the same synthesis conditions as used in the present work as well as in earlier work [12,14]. Permeances of mixtures of *n*-butane and *i*-butane of two different compositions (90:10, 10:90 mol.%) were studied. Low (<2) selectivities were obtained. However, the temperature range under investigation was 25–130°C, and the membrane was dried at mild conditions (150°C at 10^{-3} mbar for 16 h) prior to measurement. Lai and Gavalas [25] also synthesized template free ZSM-5 membranes with similar synthesis conditions as in the present work with the exception that multiple hydrothermal treatments were used. The membranes were, in this case as well, dried under mild conditions (vacuum 160°C overnight). The permeation properties were similar to earlier reported results [12,24], see Table 2. These results suggest a pore blocking effect at low temperatures similar to what has been observed in the present study.

The results obtained in the present work can be compared with related studies as in Table 2. If nothing is mentioned about the membrane test facility, similar experimental conditions as in this study were utilized. This is worth mentioning since the experimental set up can have an influence on the results obtained [20]. Gump et al. [20] synthesized an MFI-type membrane on a tubular α-alumina support. The Si/Al ratio of the synthesis solution was 100 and it contained TPAOH molecules as templates. A maximum selectivity of about 20 and an *n*-butane permeance of around 7×10^{-8} mol/m^2 s Pa was measured at a temperature of 80°C. At ambient temperature the selectivity was about 10 with an *n*-butane permeance of approximately 2×10^{-9} mol/m^2 s Pa. These results are similar to ours with the exception that the maximum selectivity was found at 220°C in the present study. An MFI-type membrane (silicalite-1) was prepared on a porous α-alumina disk by Keizer et al. [3]. A selectivity of 52 at 25°C was achieved with an *n*-butane permeance of around 3.2×10^{-8} mol/m^2 s Pa. After heating the membrane to 200°C, the selectivity had dropped to 11, whereas the permeance increased to about 4.2×10^{-8} mol/m^2 s Pa. The thickness of the membrane was around 3 μm. These results are similar to the ones found in the present work. Butane isomer separation measurements were performed on ZSM-5 membranes prepared on porous α-alumina supports [19]. In contrast to the experimental methods used by other groups mentioned above, a pressure drop of 138 kPa was applied over the membrane and no

sweep gas was utilized. The maximum selectivity for these membranes was 11 and 6.2 at 135°C. The Si/Al ratio in the synthesis solution was 600 and 100 and the synthesis was carried out in the presence of template molecules. The selectivity dropped to 5.7 and 2 at about 240°C. The permeances at maximum selectivity were 6.5×10^{-8} and 1.1×10^{-7} mol/m^2 s Pa. One should keep in mind that the mass transport through defects in the membrane probably increases as a result of transmembrane pressure difference, thus giving lower selectivities and higher fluxes. Gora et al. [22] reported a separation selectivity of 48 and an *n*-butane permeance of 756×10^{-10} mol/m^2 s Pa for a 50/50 *n*/*i*-butane mixture at room temperature for a non-supported 50 μm silicalite-1 membrane. Although the zeolite film thickness was approximately 25 times greater, the *n*-butane permeance was higher than in the present work. This inconsistency may be due to the presence of species, such as sodium in the zeolite pore structure that partly block the micropores in the present work. Xomeritakis et al. [21] used seeds and prepared a ~38 μm thick silicalite-1 membrane. The permeation flux ratio of a 50/50 *n*/*i*-butane mixture was 37 with an *n*-butane permeance of 318×10^{-10} mol/m^2 s Pa, i.e. similar to the results in the present work. On the other hand, Xomeritakis et al. [21] reports a very different N_2/SF_6 flux ratio of 10. This discrepancy may be due to the high aluminum content in the film in the present work or simply due to the fact that the membrane was not completely dry when the N_2 and SF_6 permeances were measured.

3.2.3. Permeation of a ternary ethanol/water/He mixture

Due to its polar nature, a ZSM-5 membrane with high aluminum content is water selective in a water/ethanol system in contrast to its aluminum free analog silicalite-1 that is ethanol selective [27]. Thus, the main separation mechanism in the system is differences in polarities rather than molecular sieving. Fig. 8 shows the selectivity for the separation of the water/ethanol azeotrope diluted with helium as a function of temperature. True separation was observed below 150°C, whereas at higher temperatures it was found that the membrane catalyzed the dehydration of ethanol to form diethylether and ethylene, see Fig. 9. At 200°C the flux of diethylether and ethylene even exceeds the flux of ethanol. To rule out the support as responsible for the catalysis the same experimental conditions were used, but a support without zeolite film was mounted in the cell. No diethylether or ethylene could be found in the permeate in this case. In the case of a poor quality zeolite membrane, low product concentrations were found in the permeate, probably due to dilution with unreacted feed. No products could be detected in the retentate from a good quality membrane, which indicates that the reaction mainly takes place in the zeolite pores.

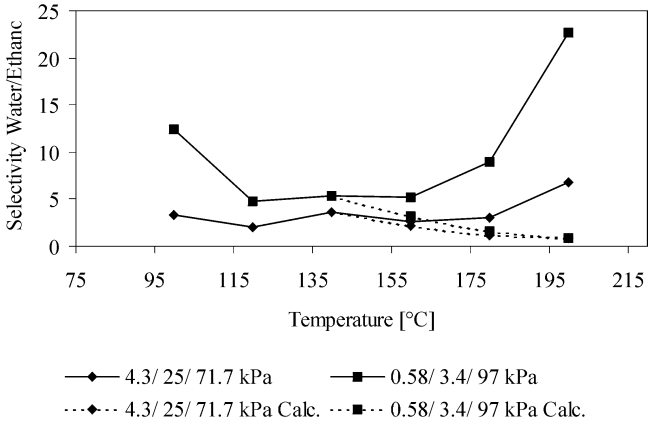

Fig. 8. Separation selectivities for two different compositions of water/ethanol/helium mixtures. The dashed lines show the selectivities after compensating for products (ethylene, diethylether and water) formed by dehydration of ethanol catalyzed by the membrane.

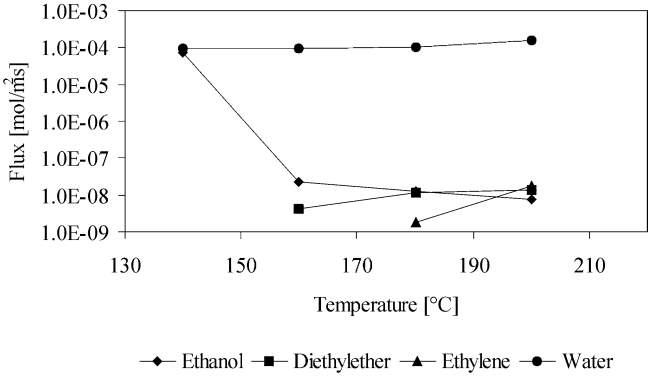

Fig. 9. Fluxes of ethanol, ether, ethylene and water as a function of temperature. The composition of the feed mixture was 0.58/3.4/97 kPa water/ethanol/helium. Helium was used as a sweep gas.

The catalyzed reactions misleadingly increased the selectivity based on ethanol and water. The dashed lines show the calculated selectivity after compensating for the formation of diethylether, ethylene and water. From about 95 to 150°C the selectivity dropped with increased temperature. The selectivities calculated from the reaction products indicate that the large increase in selectivity obtained beyond 150°C was simply due to the consumption of ethanol by the reactions. The selectivities calculated from the reaction products cannot be considered to represent the true water/ethanol selectivity. Lower selectivities were obtained for the less diluted azeotrope mixture, see Fig. 8. This trend may be caused by pore blockage by ethanol at lower dilution and/or effects of saturation of water already at high dilution. Permeances of water and ethanol are presented in Fig. 10. It can be seen that the water permeance is higher at lower partial pressures compared with the run with higher partial pressures. The permeance of ethanol seems to be independent of the partial pressure.

As far as we know, this is the first time gas phase separation of the ethanol/water azeotrope has been investigated using MFI-type membranes.

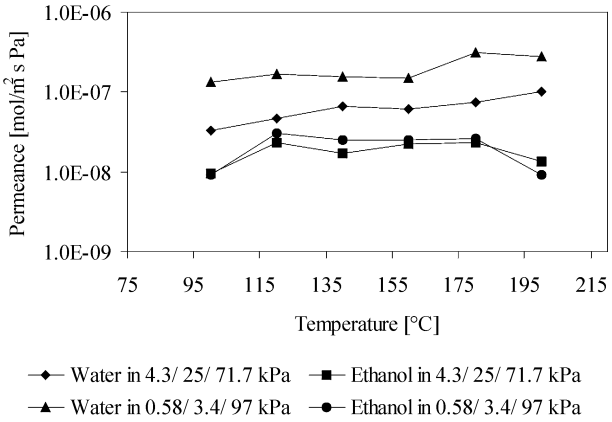

Fig. 10. Permeances of water and ethanol for two different water/ethanol/helium mixtures. A sweep gas (helium) was used.

4. Conclusions

A seeding technique was used to synthesize ZSM-5 membranes on porous α-alumina supports. The synthesis was carried out in a gel free from organic templates, making a calcination step unnecessary. The as-synthesized membranes were dried at 100°C for 12 h prior to single gas permeation measurements at room temperature. Membranes with no measurable flux of SF_6 were considered to be of high quality. In a series of seven membranes, three were found to meet this standard. From the permeation measurements of an *n*-butane/*i*-butane mixture it was concluded that a high drying temperature (>200°C) is necessary to make the zeolite pores available for gas permeation. A maximum selectivity of 16.7 was measured at 220°C. Beyond about 270°C crack formation severely deteriorated the performance of the membranes. The formation of defects is at least partly responsible for lower selectivities at elevated temperatures. All membranes that were exposed to higher temperatures showed the same tendency to form cracks. Experiments with vaporized ethanol/water azeotrope diluted with different amounts of helium were conducted. At temperatures higher than 150°C, the zeolite film catalyzed the formation of diethylether and ethylene. Higher selectivities were found for the more diluted azeotrope, the selectivity was 12.4 at 100°C.

Acknowledgements

The authors acknowledge the Swedish Research Council for Engineering Sciences (TFR) for financially supporting this work.

References

[1] J.M. van de Graaf, M. Zwiep, F. Kapteijn, J.A. Moulijn, Chem. Eng. Sci. 54 (1999) 1441.
[2] Z. Gao, Y. Yue, W. Li, Zeolites 16 (1996) 70.
[3] K. Keizer, A.J. Burggraaf, Z.A.E.P. Vroon, H. Verweij, J. Memb. Sci. 147 (1998) 159.
[4] Z.A.E.P. Vroon, K. Keizer, M.J. Gilde, H. Verweij, A.J. Burggraaf, J. Memb. Sci. 113 (1996) 293.
[5] K. Kusakabe, T. Kuroda, S. Morooka, J. Memb. Sci. 148 (1998) 13.
[6] I. Kumakiri, T. Yamaguchi, S.-I. Nakao, Ind. Eng. Chem. Res. 38 (1999) 4682.
[7] H. Kita, K. Horii, Y. Ohtoshi, K. Tanaka, K.-I. Okamoto, J. Mater. Sci. Lett. 14 (1995) 206.
[8] J.J. Jafar, P.M. Budd, Micropor. Mater. 12 (1997) 305.
[9] M. Kondo, M. Komori, H. Kita, K.-I. Okamoto, J. Memb. Sci. 133 (1997) 133.
[10] K. Aoki, K. Kusakabe, S. Morooka, AICHE J. 46 (2000) 221.
[11] N. Nishiyama, T. Matsufuji, K. Ueyama, M. Matsukata, Micropor. Mater. 12 (1997) 293.
[12] J. Hedlund, M. Noack, P. Kölsch, D. Creaser, J. Caro, J. Sterte, J. Memb. Sci. 159 (1999) 263.
[13] C.N. Satterfield, Heterogeneous Catalysis in Industrial Practice, Krieger Publishing Company, Malabar, Florida, 1996.
[14] S. Mintova, J. Hedlund, V. Valtchev, B.J. Schoeman, J. Sterte, J. Mater. Chem. 8 (1998) 2217.
[15] E.R. Geus, M.J. Den Exter, H. Van Bekkum, J. Chem. Soc., Faraday Trans. 88 (1992) 3101.
[16] J. Coronas, J.L. Falconer, R.D. Noble, AICHE J. 43 (1997) 1797.
[17] H.H. Funke, K.R. Frender, K.M. Green, J.L. Wilwerding, B.A. Sweitzer, J.L. Falconer, R.D. Noble, J. Memb. Sci. 129 (1997) 77.
[18] H. Funke, M. Kovalich, J. Falconer, R. Noble, Ind. Eng. Chem. Res. 35 (1996) 1575.
[19] J. Coronas, R.D. Noble, J.L. Falconer, Ind. Eng. Chem. Res. 37 (1998) 166.
[20] C.J. Gump, X. Lin, J.L. Falconer, R.D. Noble, J. Memb. Sci. 173 (2000) 35.
[21] G. Xomeritakis, A. Gouzinis, S. Nair, T. Okubo, H. Mingyan, R.M. Overny, M. Tsapatsis, Chem. Eng. Sci. 54 (1999) 3521.
[22] L. Gora, J.C. Jansen, T. Maschmeyer, Chem.-A Eur. J. 6 (2000) 2537.
[23] C.J. Gump, X. Lin, J.L. Falconer, R.D. Noble, J. Memb. Sci. 173 (2000) 35.
[24] M. Noack, P. Kölsch, J. Caro, M. Schneider, P. Toussaint, I. Sieber, Micropor. Mesopor. Mater. 35–36 (2000) 253.
[25] R. Lai, G.R. Gavalas, Micropor. Mesopor. Mater. 38 (2000) 239.
[26] J. Dong, Y.S. Lin, M.Z.-C. Hu, R.A. Peascoe, E.A. Payzant, Micropor. Mesopor. Mater. 34 (2000) 241.
[27] Q. Liu, R.D. Noble, J.L. Falconer, H.H. Funke, J. Memb. Sci. 117 (1996) 163.

PAPER IV

Effects of synthesis parameters on intra-pore zeolite formation in zeolite A membranes

---

Magdalena Lassinantti, Jonas Hedlund, Johan Sterte

Studies in Surface Science and Catalysis 135. Proceedings of the 13th international zeolite conference, Montpellier, France, 8-13 July, 20-P-10, 2001.

Effects of synthesis parameters on intra-pore zeolite formation in zeolite A membranes

M. Lassinantti, J. Hedlund and J. Sterte

Division of Chemical Technology, Luleå University of Technology, 971 87 Luleå, Sweden

Na-A films were synthesized on porous α-alumina substrates using a seeding technique. Effects of synthesis temperature, synthesis duration and gel composition on the morphology of the films were evaluated. Higher synthesis temperature resulted in relatively more growth of zeolite *into* the porous support compared to the film growth *on top of* the support. By using a multi-step synthesis procedure at low temperature, thicker films with less growth into the support could be prepared. Single gas permeation data indicates that as-synthesized films prepared using the multi step synthesis procedure at low temperature are defect-free in contrast to the other films prepared in the present work. The films prepared were all very sensitive to temperature and crack formation was observed even when drying samples at temperatures below 100^{o}C.

1. INTRODUCTION

Zeolite membranes exhibit the unique property of having well defined pores of molecular dimension. Thus high selectivity may be attained in separation applications. A high flux through the membrane increases the efficiency and is therefore desirable. A thin membrane, which offers less resistance to permeating species, is thus of great interest. However, such a membrane has to be grown on a porous support, in order to achieve the required mechanical strength. During the synthesis of supported membranes, siliceous species or zeolite may form within the pores of the support and reduce the flux through the membrane. Thus, synthesis methods limiting the zeolite formation to a thin film on top of the support surface is desired. Both the n-butane flux and selectivity in the separation of a mixture of n-butane and i-butane was improved for ZSM-5 membranes where the internal siliceous layer was assumed to be both thinner and more crystalline [1]. A diffusion barrier was also used during ZSM-5 membrane synthesis. In this way, the thickness of the internal siliceous layer was decreased and the crystallinity was increased [2, 3]. Both flux and selectivity in n-butane/i-butane separation experiments were improved. Tsay et al. used a vapor phase regrowth to limit the support pore plugging [4]. The present paper reports on the effect of temperature and synthesis time as well as the composition of the synthesis gel on the growth of zeolite A into and on top of porous supports.

2. EXPERIMENTAL

A synthesis solution with the molar composition 8 $(TMA)_2O$: 0.2 Na_2O: Al_2O_3: 5 SiO_2: 406 H_2O was used to prepare seed crystals at 60 °C for 96 h. The as-synthesized crystals were purified and the solid content and pH in the final sol were adjusted to 1.0 % and 10.0, respectively. Two-layered α-alumina discs with an average pore diameter of 100 nm in the top layer were used as supports. The substrates were cleaned and treated for 25 min in a solution containing cationic polymer molecules (0.4 wt% Redifloc 4150, Eka Chemicals), adjusted to pH 8.0. The solution was filtered with a 0.8 µm filter prior to use. After rinsing in filtered (0.1 µm) 0.1 M ammonia solution, the modified substrates were immersed in the seed sol for 25 min and rinsed again. Following seeding, the samples were calcined in order to remove the template molecules present in the seed crystals. Two different synthesis gels were used, denoted S1 and S2. The molar composition of S1 and S2 was 2 Na_2O: Al_2O_3: 2 SiO_2: 35H_2O and 4.3 Na_2O: Al_2O_3: 2,5 SiO_2: 111 H_2O, respectively. S1 was prepared by mixing an aqueous solution of sodium metasilicate ($Na_2SiO_3 \cdot 9H_2O$ > 98 %, Sigma) with a suspension of aluminum hydroxide (Riedel-deHaën). Aluminum metal (Riedel-deHaën) and sodium hydroxide were dissolved in distilled water and then mixed with an aqueous solution of sodium metasilicate ($Na_2SiO_3 \cdot 9H_2O$ > 98 %, Sigma) to obtain S2. The samples were treated for 1, 3 and 6 h at 100 °C using S1. The synthesis temperatures and duration were 50 °C for 20.5-96 h, 75 °C for 1-12 h and 100 °C for 1-3 h, respectively, when S2 was used. A repeated synthesis procedure was also carried out at 50 and 75 °C, where fresh synthesis gel S2 was added periodically to the cooled and rinsed samples. The samples were characterized by Scanning Electron Microscopy (SEM) and X-ray diffraction (XRD). Single gas permeation experiments (H_2, N_2, He, SF_6) were carried out at room temperature with a feed pressure of 5 bar, the permeate pressure was 1 bar.

3. RESULTS AND DISCUSSION

The main objective of this work was to investigate the possibility of applying the seed-film approach [5] for the preparation of thin continuous films of zeolite A on porous substrates, i.e. effective zeolite A membranes. The initial approach involved seeding of α-alumina substrates with colloidal zeolite A crystals of 140 nm to facilitate growth of the film. The seeding resulted in a monolayer coverage of seed crystals which were situated solely on the surface of the support. A SEM image of the seeded support is shown in Figure 1. No penetration of crystals into the top layer of the support was observed. Neither was such a penetration expected since the nominal pore size of the surface layer of the support is about 100 nm, i.e. smaller than the size of the seed crystals. Seeded substrates were subjected to the synthesis gels at various temperatures and for various duration. Some results of these experiments are listed in Table 1 together with sample designations and the conditions used in the specific preparations.

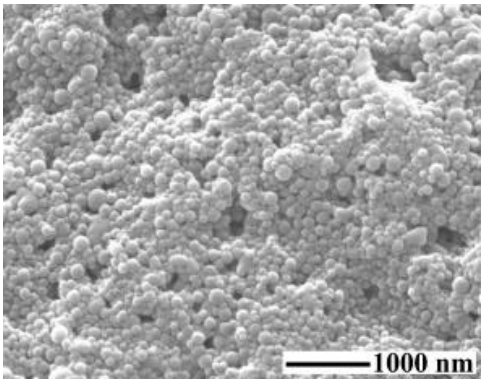

Fig. 1. A SEM image of a seeded support.

Table 1
Experimental details, film thickness and H_2 permeance (10^{-7} mol / $m^2 \cdot s \cdot Pa$)

Sample code (synthesis gel code)	Synthesis temp / °C	Synthesis duration / h	Average film thickness / nm	Average penetration depth / nm	H_2 Permeance
M1 (S1)	100	3	600	2400	18
M2 (S1)	100	6	1000	5400	0.13
M3 (S2)	50	24	500	280	16
M4 (S2)	50	48	250	750	200
M5 (S2)	50	24+24	850	350	1.7
M6 (S2)	50	24+24+24+24	1450	700	0.62
M7 (S2)	75	3	400	1440	21
M8 (S2)	75	6	500	1500	0.14
M9 (S2)	75	9	600	1200	130
M10 (S2)	75	3+3	1000	2300	0*
M11 (S2)	75	3+3+3	1700	1000	0*
M12 (S2)	100	1	600	2500	0.26
M13 (S2)	100	3	500	3000	860

* Not detectable

Use of synthesis gel S1 and a synthesis time of 3 h at 100°C resulted in a smooth continuous film with a thickness of 600 nm (M1) as estimated from the side-view SEM image of this sample shown in Figure 2. After 6 h of synthesis using this gel, the film thickness reached 1000 nm. XRD showed that both the film and the material crystallized in the bulk phase consisted mainly of zeolite A with minor amounts of FAU-type zeolite and sodalite (bulk only). Using synthesis gel S2, a temperature of 75°C and a synthesis time of 3 h resulted in the formation of a continuous film with an approximate thickness of 400 nm (M7). Prolonging the synthesis time to 6h and 9 h, resulted in a further growth of the films to a thickness of about 500 (M8) and 600 nm (M9), respectively. A SEM side-view image of sample M8 is shown in Figure 2.

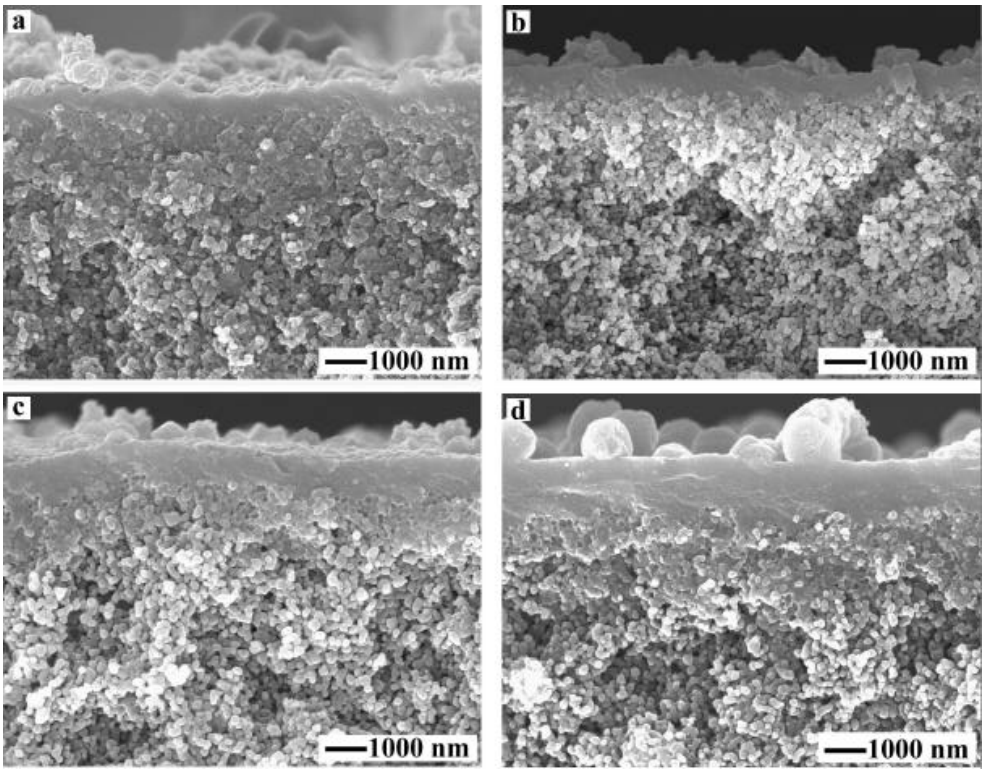

Fig. 2. Side view SEM images of membranes synthesized in S1 at 100 °C M1 (a), S2 at 50° M3 (b) 75° M8 (c) and 100 °C M12 (d). The thickness of the film on top of the support is in the range 500-600 nm for all samples.

Further prolongation of the synthesis time, beyond 9 h, resulted in a slight decrease in the film thickness. XRD analyses of these samples showed that the films consisted of zeolite A. Samples were also prepared using this synthesis gel (S2) and a synthesis temperature of 50^{o}C. A synthesis time of 24 h at this temperature (M3) resulted in a continuous film with a thickness of about 500 nm whereas a longer time, 48 h, resulted in a considerably thinner film, about 250 nm (Table 1). A side-view SEM image of the former sample is shown in Figure 2. XRD analyses of these films showed that they consisted of zeolite A, although traces of FAU type zeolite could be found after more than 24 h of hydrothermal treatment. An observation common for all these preparations is that they result not only in films on the surface of the support but also in a substantial growth of zeolite into its porous top-layer. The penetration dept for the preparations discussed above, estimated from SEM side-view analyses are given in Table 1. In most cases this penetration dept exceeds the film thickness, the only exception being the first sample prepared at 50^{o}C. Moreover, the penetration depth for a given film thickness increases with increasing synthesis temperature or if gel S1 is used, as demonstrated by Figure 2. Based on experience with the preparation of MFI-type

membranes it is strongly believed that excessive intergrowth of the zeolite and the support is detrimental in membrane applications, mainly because it affects the thermal stability of the resulting membrane and tends to result in the formation of cracks. Even if crack formation could be avoided, however, intergrowth is highly undesired since it limits the flux through the membrane. This in combination with the fact that the possibilities to control film parameters, such as thickness, in a one-step preparation turned out to be limited, led to the use of an alternative approach involving a multiple-step growth procedure.

Repeated synthesis at the temperatures 50° and 75°C were carried out using synthesis mixture S2. When applying syntheses in two or three steps at 75°C, samples M10 and M11, gradually thicker films were obtained. In this case, the zeolite penetration dept into the substrate did not follow the increase in film thickness. Figure 3 shows SEM side-view images of samples prepared using the multi-step approach with 2 and 3 steps of 3h at 75°C. For comparison, samples prepared using identical conditions and the same total synthesis times but in one single step are also shown in the Figure. Despite the fact that the three-step synthesis resulted in an almost threefold increase in film thickness compared with the one-step sample, the penetration dept of the two samples were essentially the same.

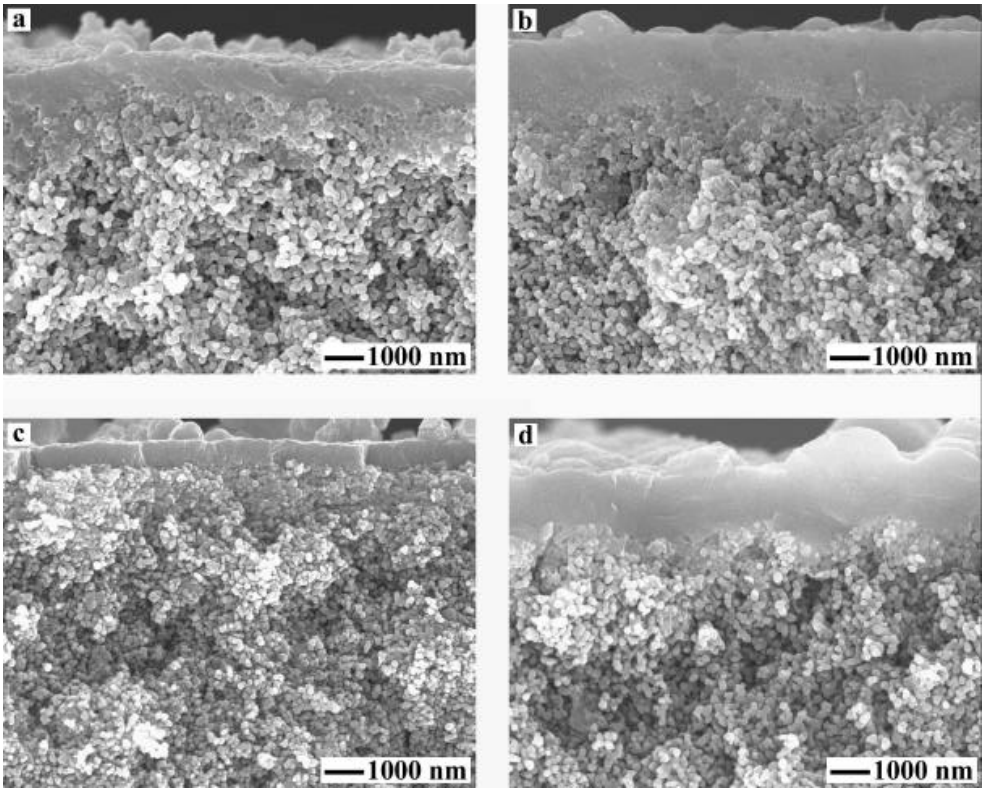

Fig. 3. Side view SEM images of membranes synthesized for 6 and 9 h in one step M8 (a), M9 (c) and in several steps M10 (b), M11 (d).

The samples prepared using the two types of procedures also differed significantly in surface morphology. Whereas the sample prepared using a single step showed a rather rough surface, see Figure 4 (a), the one prepared according to a two-step procedure was considerably smoother (b).

Repeated syntheses, in two or four steps, were also performed at a crystallization temperature of 50°C. In analogy with the observations for the 75° samples the film thickness increased with an increasing number of steps whereas the growth of the zeolite into the support remained at the same level or was even smaller than that of the single-step sample. Four steps of 24 h each at 50°C resulted in a film with a thickness of about 1450 nm and a penetration dept of ca 700 nm compared with a corresponding thickness of 250 nm and a penetration dept of 750 nm for the sample prepared in one step of 48 h. No defects in the form of pinholes or cracks could be observed in the SEM images of any of the samples prepared using a multi-step procedure at 50°C. Cracks were sometimes observed in films synthesized by the multi-step procedure at 75°C, as illustrated by Figure 4 (b). XRD of all the samples prepared using this technique showed that they mainly consisted of zeolite A, only traces of FAU type zeolite were found. The relative intensities of the zeolite A peaks in all film samples were essentially identical with those recorded for a powder reference sample, indicating a random orientation of the crystals constituting the films.

In order to further evaluate the existence of defects in the films, single gas permeance was measured on as-prepared samples, dried in air at room temperature. It should be noted that the samples were not dried at elevated temperatures or calcined prior to the measurements wherefore the zeolite is expected to be fully hydrated and blocked by adsorbed water. Thus, gases are expected to permeate solely through defects. A low or non-detectable gas flow through the films is therefore an indication of a continuous film with a low density of defects. Results of single gas permeation measurements for selected samples are reported in Table 1. For both synthesis gels and for all synthesis temperatures used in the single step procedure a trend can be observed. The gas permeance generally decreases with increasing thickness of the film on the surface of the substrate. All samples prepared in this manner (possibly with the exception of M2 and M8) do, however, show a significant permeance indicating the existence of a substantial density of defects in the zeolite layer.

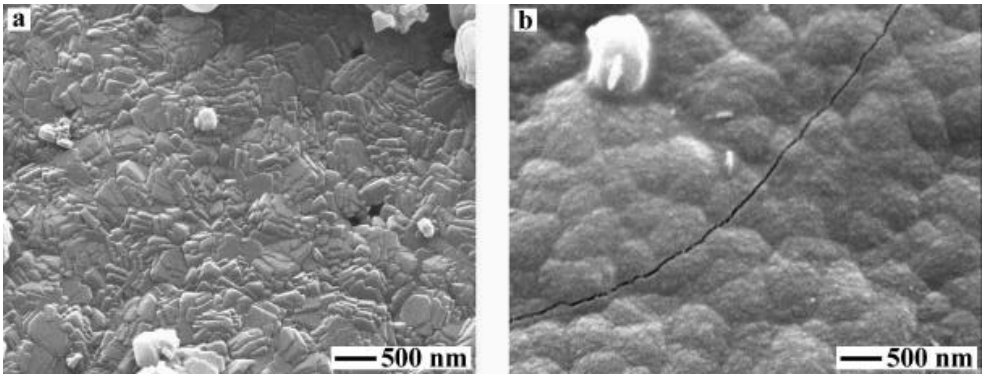

Fig. 4. SEM images of films synthesized at 75 °C in S2 for 6 h by one-step synthesis M8 (a) and repeated synthesis (3+3 h) M10 (b).

The samples prepared using multiple-step growth, on the other hand, all show a relatively low or even undetectable permeance. The results presented in Table 1 indicate that the permeance decreases with increasing number of steps and that a synthesis temperature of 75°C is preferential, yielding in both cases a virtually non-permeable zeolite layer. These results are in agreement with the findings of Kumakiri et al. [6] who found that the selectivity for dehydration of ethanol in pervaporation could be improved by repeating the membrane synthesis procedure. Permeances for both hydrogen and SF_6 were measured for all samples in the present study. The ratio H_2/SF_6 was in all cases within a range 3.1-5.3. This indicates that the assumption of permeance through defects larger than the zeolite pores is valid since a considerably higher ratio would be expected if mass transport through zeolite pores would predominate. In order to test the actual membrane performance of some of the materials, attempts were made to remove adsorbed water prior to or during evaluation. Figure 5 shows the permeance of SF_6, N_2 and He for sample M2 as a function of temperature in the membrane cell. Due to blockage by water, all permeances are very low at 25°C. A rapid increase of the permeance of all gases was then observed indicating permeance through non-selective passages through the membrane. The selectivities obtained are in fact lower than those expected assuming a Knudsen type flow through the membrane. This, in combination with the high fluxes clearly indicates that defects (cracks) are formed in the membrane upon drying. From these experiments it is thus obvious that membranes prepared by the application of the methods used in the present work are very sensitive to moderately high temperatures. In fact they appear to be so sensitive that mere drying at below 100°C may induce crack formation, sometimes crack formation was even observed during recording of SEM images. Although the multi-step synthesis approach resulted in less crystallization within the pores of the substrate the intergrowth was still significant. This may explain the low thermal stability of the membranes.

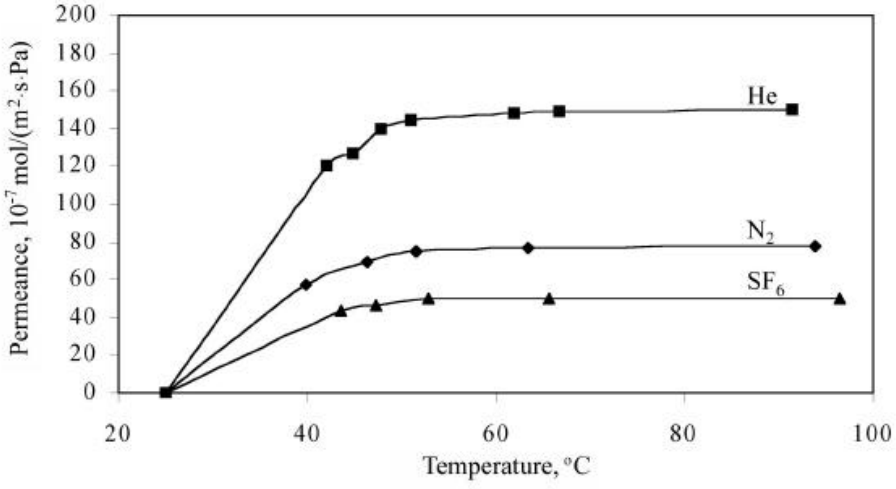

Fig. 5. Permeance of He, N_2 and SF_6 upon drying membrane M2 at elevated temperature.

4. CONCLUSIONS

Zeolite NaA films were synthesized on porous α-alumina supports. It was found that the tendency for the films to grow inwards into the support could be suppressed by application of a repeated synthesis strategy. Conditions were established for the preparation of relatively thin films virtually free from macroscopic defects. The materials were however very sensitive to elevated temperatures as signified by crack formation upon drying. This may be associated with the fact that the intergrowth of the zeolite with support pores still remained substantial. Further precautions would be needed in order to prevent such intergrowth. A possibility would be to combine the results of this study with recently developed masking techniques [7]. This may make it possible to prepare highly efficient zeolite A membranes applicable for high-flux gas-phase separations.

5. ACKNOWLEDGEMENTS

The authors acknowledges the Swedish Research Council for Engineering Sciences (TFR) for financial support of this work.

REFERENCES

1. Y. Yan, M. E. Davis and G. R. Gavalas, Ind. Eng. Chem. Res., 34 (1995) 1652.
2. Y. Yan, M. E. Davis and G. R. Gavalas, J. Membr. Sci., 123 (1997) 95-103.
3. Y. Yan, M. E. Davis and G. R. Gavalas, J. Membr. Sci., 126 (1997) 53-65.
4. C. S. Tsay and A. S. T. Chiang, AIChE J., 46 (2000) 616-625.

5. J. Hedlund, B.J. Schoeman and J. Sterte, in H. Chon, S.-K. Ihm., Y.S. Uh (eds.), Progress in Zeolites and Microporous Materials 105, Amsterdam, Elsevier Science 1997, 2203.
6. I. Kumakiri, T. Yamaguchi and S.- I. Nakao, Ind. Eng. Chem. Res. 38 (1999) 4682-4688.
7. M. H. C. Anthonis, A-J. Bons, H. W. Deckman, J. Hedlund, W. F. Lai, and J. A. Peters, PCT application, WO 00/53298, 2000.

PAPER V

Accurate measurement of the thermal expansion of MFI zeolite membranes by *in-situ* HT-XRPD

Magdalena Lassinantti Gualtieri, Alessandro F. Gualtieri, Jonas Hedlund, Fredrik Jareman, Johan Sterte and Monica Dapiaggi

Proc. 14th International Zeolite Conference. E. van Steen et al. Eds (2004) 703.

ACCURATE MEASUREMENT OF THE THERMAL EXPANSION OF MFI ZEOLITE MEMBRANES BY *IN SITU* HTXRPD

Gualtieri, L.M.[1], Gualtieri, A.F.[2], Hedlund, J.[1], Jareman, F.[1], Sterte, J.[1] and Dapiaggi, M.[3]

[1]Department of Chemical and Metallurgical Engineering, Luleå University of Technology, 971 87 Luleå, Sweden.
[2]Dipartimento di Scienze della Terra, Università di Modena e Reggio Emilia, Via S. Eufemia 19, I-41100 Modena, Italy.
[3]Dipartimento di Scienze della Terra, Università di Milano, Via Botticelli 23, I-20133 Milano, Italy.

ABSTRACT

Template removal by calcination of MFI type membranes is often accompanied by crack formation. The thermal behavior of MFI type membranes, synthesized with and without masking, was studied to understand the mechanism. Masking prevents growth of zeolite in the interior of the support during membrane synthesis. Rietveld refinements of powder diffraction data collected in situ at high temperature allowed to accurately determine the change in thermal expansion of the MFI film and the porous α-alumina support. During heating, a relatively large contraction of the cell volume during template removal occurred in the zeolite powder and in the film of the membrane prepared with masking. The much smaller decrease in the non-masked sample indicates that this membrane is under stress during heating and as a consequence, cracks are formed. The stress imposed in the membrane prepared without masking may be due to the opposite thermal behavior of the substrate in combination with strong bonds between the membrane and the support.

Keywords: MFI zeolite membrane; calcination; High temperature X-ray diffraction;crack formation

INTRODUCTION

MFI zeolite membranes are extensively studied due to their outstanding separation capability for compounds of industrial importance. Almost without exception, the MFI type membranes are synthesized in the presence of organic template molecules that are removed by calcination to obtain a microporous structure. The membranes are synthesized on porous supports, commonly α-alumina, which add mechanical strength to the thin zeolite layer. Conventional membrane synthesis methods often result in silicious deposits in the support pores. Recently, a two-step masking procedure, which protects the support during membrane synthesis and thereby inhibits the formation of intra support deposits was reported [1]. MFI membranes synthesized using this method were compared with membranes synthesized by omitting masking [2] and it was observed that the masked membranes had higher selectivity and permeance (i.e. less defects and intra-support zeolite growth, respectively).

During calcination of the as-synthesized MFI membranes, cracks in the zeolite layer may form [2-5]. Cracks are detrimental for the separation performance of the membrane [2]. Crack formation within single crystals of MFI during template removal has been under investigation [6-7]. However, the crystals were very large (hundreds of microns). Thus, intra crystal cracks should not be considered as a problem in membrane applications since the crystals constituting the membranes usually are smaller than 1 μm. It is well known that a thermal expansion mismatch between bonded materials may result in stress development and consequently cracks within the composite. Furthermore, the as-synthesized MFI framework is larger than the calcined form [7-9]. The difference is due to the contraction of the b- and c-axis which is only partly compensated by an expansion of the a-axis in the calcined form [8]. The largest change in the framework coincides with the template degradation [7, 9] at around 300 °C. The orientation of the crystals constituting the membrane may influence the thermal behavior, due to the anisotropic contraction of the MFI lattice upon template removal. This factor was addressed by den Exter et al. who concluded that the change in the zeolite film during calcination was strongly dependent on the orientation of the crystals [10]. Hence, the thermal behavior of the crystal-support composite is correlated to the crystal orientation and certain preferred orientations may increase the stress imposed on the layer by the substrate.

Proceedings: 14th International Zeolite Conference
Editors: E. van Steen et al
ISBN: 0-958-46636-X

25 – 30 April 2004
Cape Town, South Africa
Produced by: Document Transformation Technologies

It is commonly stated that the template degradation is responsible for crack formation in zeolite membranes since the largest difference in the thermal expansion between the support (which expands during heating) and the zeolite can be found in that temperature interval. However, in order to better understand the crack formation process in MFI membranes, the thermal behavior of the porous support as well as the zeolite film must be accurately investigated. An appropriate technique is high temperature X-ray powder diffraction (HTXRPD) which allows to follow the evolution of the cell parameters in real time during heating. This experimental technique has recently been applied for the investigation of MFI films prepared on porous ceramic supports [9] by a direct synthesis approach. However, the curves of the thermal expansions were built with only a few points and needed further revision. This work is a thorough investigation of the change of the cell parameters of MFI membranes and the α-alumina support as well as MFI zeolite powder in-situ during the entire calcination procedure. Membranes synthesized with and without masking are evaluated.

EXPERIMENTAL SECTION

The supports used were porous α-alumina asymmetric discs (Inocermic GmbH, Germany), with a pore size of 100 nm in the 30 μm thick top layer. The supports were carefully washed (acetone, ethanol and dilute ammonia solution) and dried prior to use. MFI type nanocrystals were adsorbed on the cleaned supports as described previously [11]. In some cases, a two-step masking procedure recently described by Hedlund et al. [1] was applied prior to seeding. A viscous polymer solution is applied on the top surface of the support. After drying, this polymer forms a protective layer. In the next step, the pores of the support are filled with molten wax. No wax will cover the top of the support due to the protective polymer layer. Finally, the polymer layer is dissolved in acetone and MFI type seed crystals are adsorbed on the exposed support top surface. Following seeding, the substrates (masked as well as non-masked) were placed in a synthesis solution with the molar composition 3TPAOH: $25SiO_2$: $1500H_2O$: 100EtOH for 72 h in an oil bath holding a temperature of 100 °C. The chemicals used were tetrapropylammoniumhydroxide (TPAOH; 40% water solution, AppliChem) and tetraethylortosilicate (TEOS; >98%, Merck). After the synthesis, the samples were carefully washed in dilute ammonia solution and dried. Hereafter, the membranes synthesized using masking are denoted M72 (masked substrate, 72 h synthesis) while the non-masked samples are denoted N72 (non-masked, 72 h synthesis). The zeolite formed in the bulk of the synthesis solution used for N72 was washed and dried. The wax in the masked sample (M72) was dissolved in xylene prior to membrane characterization in order to avoid smoke formation during the HTXRD measurements. SEM images were collected with a Philips XL30 scanning electron microscope. XRPD data in the range 7-80 °2θ was collected at room temperature using a conventional Bragg-Brentano geometry. The use of standard reference silicon powder (NIST 640b), applied on top of the membranes and mixed in the MFI powder, respectively, allowed exact determination of the cell parameters. The in situ data was collected using a Philips X'Pert PW 3701 powder diffractometer equipped with a PMP 1600 hot chamber. A θ/2θ scan was accomplished in the ranges 7-10, 22.5-25 (intense peaks of the MFI structure), 25-27.5 and 34-39 °2θ (intense peaks of the α-alumina). A heating/cooling gradient of 2 °C/min was applied. The temperature was held constant at 500 °C for 5 h before cooling. The data collection was repeated two times. Accurate cell parameters (room temperature data) and thermal expansion (in situ data) of the zeolite phase and α-alumina substrate were determined with the Rietveld method using GSAS software [12]. The structure model reported by van Koningsveld [13] derived from single crystal XRD data was used in the refinements for the MFI phase. The structure model for the α-alumina was taken from a publication by Ishizawa et al.[14].

RESULTS AND DISCUSSION

Estimated from side view SEM images, the as-synthesized sample N72 is composed of two layers, see Figure 1a. The top layer is a zeolite film with a thickness of about 700 nm The bottom layer is about 1 μm and appears to be zeolite grown in the pores of the support, thus forming a zeolite-support composite layer. Hence, the total membrane thickness in this sample was about 1700 nm. In sample M72 on the contrary, the total membrane thickness was about 800 nm and the zeolite-support composite layer was considerably thinner, see Figure 1b. No cracks or larger defects could be observed (within the detection limit of the microscope) in the as-synthesized samples. However, after the HTXRPD measurements, minor cracks with a width of about 20 nm were found in both samples. At this point it should be clarified that the quality of the membranes cannot be determined only by a SEM investigation. Rather, it should be viewed as a complementary tool to porosimetry data, single gas permeation measurements and mixture separations [2].

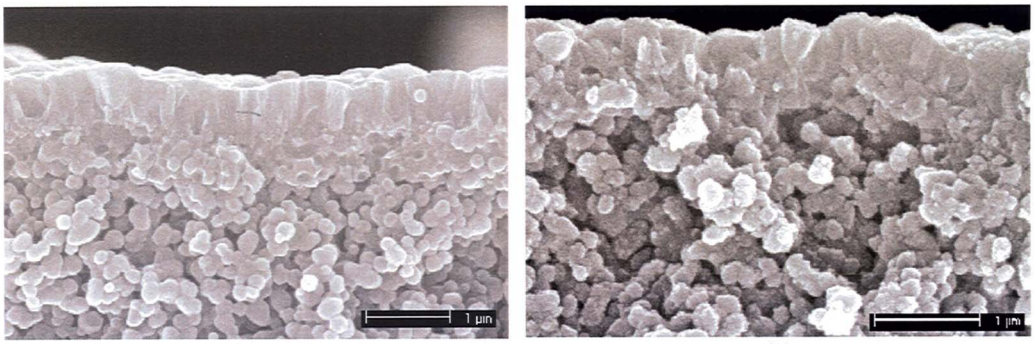

(a) (b)

Figure 1. Side view SEM images of a non-masked (a) and a masked (b) MFI membrane.

Table 1. Cell parameters of the MFI crystals constituting the non-masked (N72) membrane, the masked (M72) membrane as well as the MFI powder. Values from the literature are also shown for comparison.

Structure	Cell parameters of TPA-MFI				
	a-axis (Å)	b-axis (Å)	c-axis (Å)	Cell volume (Å^3)	Reference
N72	20.044 (2)	19.940 (3)	13.385 (1)	5349.9 (9)	This work
M72	20.050 (3)	19.985 (4)	13.375 (2)	5359 (1)	This work
MFI powder	20.031 (2)	19.914 (3)	13.395 (1)	5343.3 (9)	This work
MFI film on porous α-alumina substrate	20.034	19.927	13.388	5345	[9]
MFI film on porous YZ substrate	20.074	19.965	13.421	5379	[9]
MFI powder	20.009 (5)	19.886 (6)	13.363 (3)	5317	[9]
MFI single crystal	20.022(2)	19.899(2)	13.383(1)	5332 (4)	[13]
MFI powder	20.0402(6)	19.9348 (6)	13.4075 (4)	5356.2 (2)	[8]
MFI powder	20.101 (1)	19.872 (1)	13.365 (1)	5339	[17]

Table 1 shows the refined cell parameters of the MFI crystals constituting the membranes as well as MFI powder. Values of powder/single crystal MFI (Si/Al = 319 – ∞) as well as MFI membranes found by other authors are also shown for comparison. From Table 1, it is clear that the unit cell volume of the MFI phase constituting the films are significantly larger than the unit cell volume of the powder. Obviously, the unit cell parameters in MFI increase linearly with decreasing Si/Al ratio [15]. Due to the alkaline leaching of the α-alumina support, the Si/Al ratio of the synthesis mixture may decrease significantly during hydrothermal treatment [16]. Thus, incorporation of aluminum in the MFI framework is expected in the membrane N72 as well as the zeolite powder formed in the bulk, to a higher extent in the former case. Hence, the larger unit cell volume of N72 (compared to the MFI powder) may be explained by a lower Si/Al ratio. Using the masking technique, the support is protected by the wax during the hydrothermal synthesis and aluminum leaching should be limited. The large unit cell volume in M72 is therefore difficult to explain, especially considering the very large value of the b-axis. However, comprehensive mapping of the aluminum content in the different samples is required. The refined cell parameters of the α-alumina in sample N72 were; a = 4.76002 (6) Å, c= 12.9946 (3) Å and V= 254.98(2) Å^3. The values for M72 were a= 4.75960 (7) Å, c= 12.9937 (3) Å and V= 254.92 (1) Å^3. The almost identical values found for the α-alumina in the different samples demonstrates the accuracy of the refinements for alumina.

The expansion of α-alumina is linear in the whole temperature range for a substrate without a zeolite coating and for sample M72 were the substrate was protected by wax during zeolite synthesis, see Figure 2. In sample N72 however, a change in the slope is observed in the expansion curve at about 125 °C during both heating and cooling (Figure 2 and 3). Besides, it should be remarked that the overall thermal expansion is clearly lower in the entire temperature range investigated for this sample. In this case, the substrate was exposed to the zeolite synthesis solution during the thermal treatment. This result has never been reported so

far and is not yet explained. Because of the deep penetration of the X-rays in the substrate (>100 μm), it is very unlikely that a change in the α-alumina microstructure at the interface with the zeolite layer could be monitored. Thus, it is unlikely that the effect is caused by the presence of the relatively thin zeolite film. However, the interior of the substrate in the non-masked membranes contains zeolite (or siliceous species) which may affect the thermal expansion of the α-alumina.

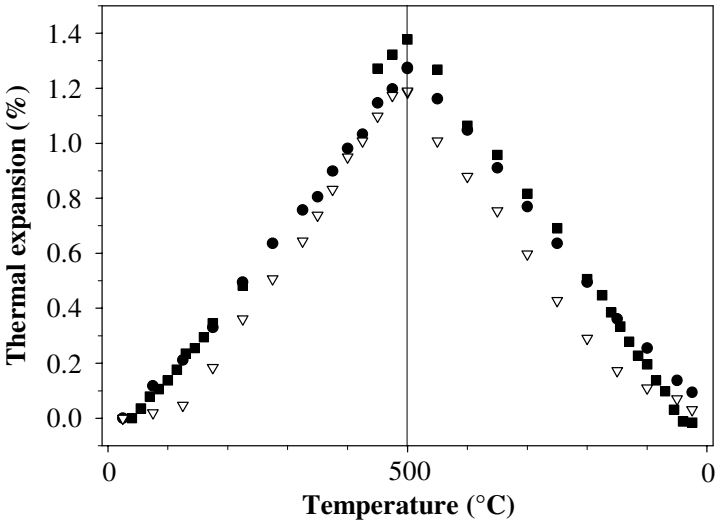

Figure 2. Change in the cell volume of the α-alumina substrate without a zeolite coating (black circles), in sample N72 (white triangles) and in sample M72 (black squares) during heating and cooling.

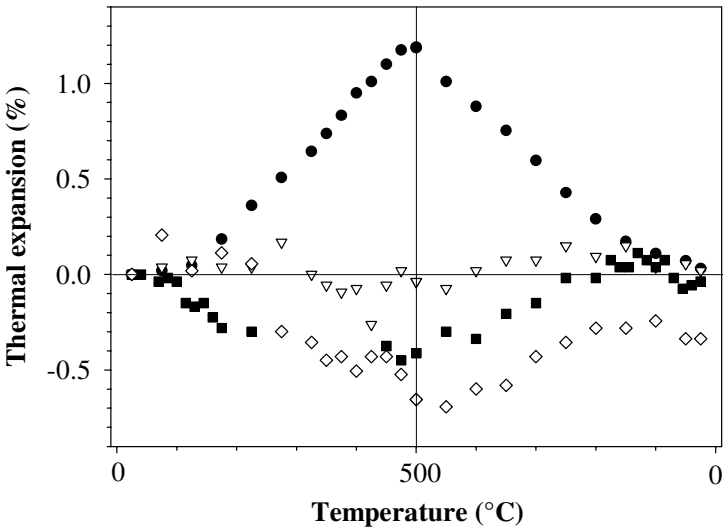

Figure 3. Change in the cell volume of the MFI powder (white diamonds), the MFI phase in sample N72 (white triangles), the MFI phase in sample M72 (black squares) and the α-alumina in sample N72 (black circles) during heating and cooling.

The zeolite framework in the zeolite powder and sample N72 slightly expands in the temperature interval ~ 25-225 °C (Figure 3). At about 300 °C there is a relatively large decrease in the cell volume due to the template removal. However, the decrease is more striking in the zeolite powder. The membrane prepared by a masking technique has a quite different thermal behavior. The expansion at moderate temperature, observed in the zeolite powder and sample N72, is absent. Instead, the framework has a more or less linear negative expansion in the investigated temperature interval. No sharp decrease in the cell volume due to template removal is observed. During cooling, all three samples expand and a maximum is observed at around 100-200 °C. The calcined zeolite membranes (both N72 and M72) have virtually the same volume as the as-synthesized zeolite at 25 °C (see again Figure 3 and Table 2). The calcined zeolite powder however, is 0.3 % smaller than the as-synthesized form showing a sort of a hysteresis effect (Figure 3). These results are in concert with the literature data [7-9]. Millini et al. compared the unit cell volume variation between the as-synthesized form and the calcined form of TS-1 [8]. The authors found that the decrease in cell volume in the calcined form (compared to the as-synthesized samples) was less with increased Ti content. They suggested that in very high Ti loadings, the effect of the increased lattice volume due to Ti incorporation prevails over the volume decrease due to template removal. Although Ti substitution with Si in the MFI framework results in a larger increase in cell volume than the corresponding Al substitution, the results of Millini et al. indicates that a low Si/Al ratio would be expected to have a smaller decrease in cell volume due to template removal. Therefore, it can not be excluded that the larger decrease in cell volume during template removal in the powder zeolite and M72 (compared to N72) may at least partly be due to a higher Si/Al ratio in these samples. Another explanation for the different behavior of the zeolite powder and the zeolite membranes may be found on a more mechanical basis. The negative volume expansion of the zeolite phase in N72 during template removal may be hindered by bonds between the crystals constituting the film and the alumina substrate. These bonds may be much stronger, both mechanically and chemically, than in M72 since the penetration of the zeolite film in the pores of the support in N72 results in a larger contact area between the two phases. As a result, a tensile stress develops in the film during heating. During cooling the zeolite membrane is forced to retain its original volume due to strong bonds within the film and with the substrate. Hence the film may be under tensile stress even after cooling back to room temperature. M72 on the other hand, is less bonded to the support (due to lack of support pore penetration). Hence, the crystals may have more degrees of freedom on the support surface and contract without strain. Of course, the zeolite crystals in M72 may be less attached to each other, which might contribute to the higher contraction tendency during template removal. During cooling, M72 behaves more like N72, retaining the volume of the as-synthesized form. Hence, also in this case, the zeolite phase is under tensile stress at room temperature after template removal. However, the results presented here show that the masked membrane, compared to the unmasked one, is under less stress during the heating cycle. This difference may explain the fact that non-masked membranes have a higher tendency to crack during calcination compared to masked ones [2]. Furthermore, the fact that the masked membrane (M72) is thinner than the unmasked sample (N72) may also contribute to the higher flexibility of the former. In fact, Hedlund et al. have shown that thinner membranes (both masked and non-masked membranes) are less likely to form cracks during the calcination procedure [2]. The main source of the tensile stress developing in the membranes, mostly in N72, is the large expansion of the α-alumina substrate (shown clearly in Figure 3). This fact was not properly underlined in previous work [9]. The decrease in cell volume of the zeolite phase is negligible compared to the expansion of the α-alumina substrate. At 400 °C the cell volume decreased 0.07 % for the zeolite phase in N72 whereas the volume of the α-alumina increased with 0.95 %. In a highly inter-grown zeolite film, firmly bonded to the support after synthesis, this large difference in expansion (mainly because of the α-alumina) causes tensile stress in the zeolite film during heating. This stress might cause cracks even at temperatures lower than 350 °C (the temperature for template removal). In fact, cracks formed at about 250 °C during heating of a MFI type membrane synthesized at 100 °C without template molecules and masking [11]. Dong et al. found that the crack formation temperature of an alumina supported MFI type membrane was higher than 350 °C [3]. However, this membrane was synthesized at 185-190 °C. Hence, the deviation in cell volume (of the alumina substrate and the MFI film) with respect to the volume at the synthesis temperature (where the substrate as well as the zeolite film should be under zero stress) was much less in this case which might result in a higher crack formation temperature. The high stability during thermal cycling of a stainless steel supported silicalite-1 membrane (synthesized at 180°C) could partly be explained likewise [18].

Table 2. The % change of the unit cell dimensions of the MFI membranes and the powder reference before and after calcination (room temperature).

Sample	% change (at 25 °C) of the MFI after template removal			
	a-axis	b-axis	c-axis	Cell volume
N72	+0.09	-0.03	-0.06	+0.02
M72	+0.15	±0	-0.22	-0.04
MFI powder	+0.05	-0.21	-0.18	-0.34

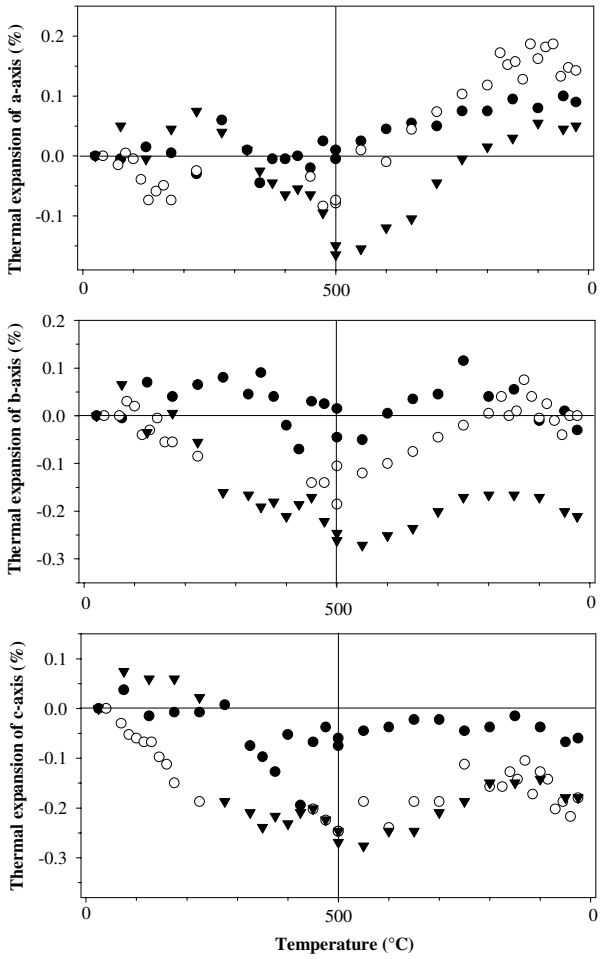

Figure 4. Change in the length of the unit cell axes of the MFI phase in N72 (black circles), M72 (white circles) and zeolite powder (black triangles) during heating and cooling.

Figure 4 shows the thermal expansion of the MFI unit cell axes during the heating cycle. Due to template removal, there is a contraction of the cell parameters in all investigated samples during heating. However, the contraction is larger in the powder zeolite and M72. During cooling (after template removal) the unit cell axes expand in all the samples. However, compared to the as-synthesized phase, the calcined MFI structure shows a contraction along the b- and c-axes and an expansion along the a-axis (see Table 2 and Figure 4), in agreement with the literature [7, 9]. There are, however, some differences between the samples. As seen in

table 2, the a-axis is considerably longer in the membranes (compared to the powder) after calcination and the b-axis is much shorter in the powder (compared to the membranes). Furthermore, c is much longer in N72. As discussed previously, the volume of the calcined zeolite film is approximately the same as the as-synthesized phase. This is due to a much larger expansion of the a-axis in the membranes (and the c-axis in sample N72) and a much larger contraction of the b-axis in the powder. It should be noted that, like in the as-synthesized sample, the b-axis in sample M72 is much longer than expected (i.e. no contraction after template removal).

CONCLUSIONS

For the first time, the change in the cell parameters with temperature was accurately determined with the Rietveld method for MFI membranes and the α-alumina support as well as a zeolite reference powder during the entire calcination procedure. Membranes synthesized with and without masking were evaluated. During heating, a relatively large contraction of the cell volume was found in the powder zeolite and the membrane prepared with masking. The much smaller decrease in the non-masked sample indicates that the membrane is under stress during heating. The main source of stress is the large expansion of the α-alumina substrate which contributes most to the difference in thermal expansion between the zeolite phase and the substrate. This different thermal behavior between membranes prepared with and without masking may explain the fact the masked membranes show less tendency to crack during calcination. However, in can not be ruled out that the different thermal behavior of the samples may, at least partly, be due to differences in the Si/Al ratio. Therefore, a determination of the aluminum content in the MFI structure in the different samples are planned. Furthermore, the role of the film thickness on the thermal behavior of the membranes will be investigated in the future.

ACKNOWLEDGEMENTS

The authors are grateful to the Swedish Research Council as well as the foundation Blanceflor Boncompagni-Ludovisi, born Bildt for the financial support.

REFERENCES

1. J. Hedlund, J. Sterte, M. Anthonis, A.J. Bons, B. Carstensen, E.W. Corcoran, H.W. Deckman, W. de Gijnst, P.P. de Moor, F. Lai, J. McHenry, W. Mortier and J. Reinoso, Micropor. Mesopor. Mater., 52 (2002) 179-189.
2. J. Hedlund, F. Jareman, A-J. Bons and M. Anthonis, J. Membr. Sci., in press.
3. J. Dong, K. Wegner and Y.S. Lin, J. Membr. Sci., 148 (1998) 233-241.
4. Z.A.E.P Vroon, K. Keizer, A.J. Burggraaf and H. Verweij, J. Membr.Sci., 144 (1998) 65-76.
5. J.M. van de Graaf, F. Kapteijn and J.A. Moulijn, Chem. Eng. Sci., 54 (1999) 1081-1092.
6. O. Pachtová, M. Kocirik, A. Zikánová, B. Bernauer, S. Miachon and J.-A. Dalmon, Micropor. Mesopor. Mater., 55 (2002) 285-296.
7. E.R. Geus and H. van Bekkum, Zeolites 15 (1992) 333-341.
8. R. Millini, G. Perego, D. Berti, W.O. Parker Jr. A. Carati and G. Bellussi, Micropor. Mesopor. Mater., 35-36 (2000) 387-403.
9. J. Dong, Y.S. Lin, M.Z.-C. Hu, R.A. Peascoe and E.A. Payzant, Micropor. Mesopor. Mater., 34 (2000)241-253.
10. M.J. den Exter, H. van Bekkum, C.J.M Rijn, F. Kapteijn, J.A. Moulijn, H. Schellevis and C.I.N. Beenakker, Zeolites, 19 (1997) 13-20.
11. M. Lassinantti, F. Jareman, J. Hedlund, D. Creaser and J. Sterte, Catalysis Today, 67 (2001) 109-119.
12. A.C. Larson, R.B. von Dreele (1994) "GSAS Generalized strucure analysis system" Laur 86-748, Los Alamos National Laboratory, Los Alamos, New Mexico.
13. H. van Koningsveld, H. van Bekkum and J.C. Jansen, Acta Cryst., B43 (1987) 127-132.
14. N.Ishizawa, T. Miyata, I. Minatio, F. Marumo and S. Iwai, Acta Cryst., B36 (1980) 228-230.
15. B.L. Meyers, S.L. Ely, N.A. Kutz, J.A. Kaduk and E. van den bossche, J. Catal., 91 (1985) 352.
16. E.R. Geus, M.J. den Exter and H. van Bekkum, J. Chem. Soc. Faraday Trans., 88 (1992) 3101-3109.
17. B.F. Mentzen and F. Lefebvre, Mat. Res. Bul., 32 (1997) 813-821.
18. Wridzer J.W. Bakker, F. Kapteijn, J. Poppe, J.A. Moulijn, J. Membr. Sci., 117 (1996) 57-78.

PAPER VI

The influence of heating rate on template removal in silicalite-1: an *in situ* HT-XRPD study

---

Magdalena Lassinantti Gualtieri, Alessandro F. Gualtieri and Jonas Hedlund
Microporous and Mesoporous Materials, 89 (2005) 1-8.

Available online at www.sciencedirect.com
SCIENCE DIRECT®
Microporous and Mesoporous Materials 89 (2006) 1–8
MICROPOROUS AND MESOPOROUS MATERIALS
www.elsevier.com/locate/micromeso

The influence of heating rate on template removal in silicalite-1: An in situ HT-XRPD study

Magdalena Lassinantti Gualtieri [a,*], Alessandro F. Gualtieri [b], Jonas Hedlund [a]

[a] Department of Chemical Engineering and Geosciences, Luleå University of Technology, 971 87 Luleå, Sweden
[b] Dipartimento di Scienze della Terra, Università di Modena e Reggio Emilia, Via S. Eufemia 19, I-41100 Modena, Italy

Received 8 June 2005; accepted 29 September 2005
Available online 16 November 2005

Abstract

The effect of heating rate on thermal behavior of TPA-silicalite-1 during calcination and the reaction kinetics for TPA decomposition were investigated. The cell parameters of the TPA-silicalite-1 during the heating cycles were determined with the aid of high temperature X-ray diffraction data and the Rietveld method. The template decomposition is accompanied by a large contraction of the unit cell. The unit cell dimensions during template removal are not affected significantly by the heating rate. Consequently, the rate of contraction is approximately proportional to the heating rate. The intensity of some diffraction peaks changes during heating, especially the 101/011 and the 200/020 peaks. The intensity change of those peaks shows the same dependence with temperature as the TPA occupancy, indicating that these parameters are related. An analysis of the kinetics for TPA decomposition based on the intensity change of the 101/011 and the 200/020 peaks was performed. The apparent activation energy (E_a) of the template decomposition in silicalite-1 determined with the Kissinger and the Flynn–Wall–Ozawa methods was 138 (±25) and 138 (±29) kJ mol^{-1}, respectively. The reaction order, determined with the method of Kennedy and Clark, was close to 0.5 indicating that the rate-limiting step is mono-dimensional diffusion. E_a was 140 (±30) kJ mol^{-1}, in good agreement with the results obtained with the other methods.

With the results presented here, it is possible to discuss possible effects of the heating rate on the crack formation frequently observed in zeolite membranes during calcination.

Keywords: MFI zeolite; High temperature X-ray diffraction; Kinetic analysis; Membrane; Crack formation

1. Introduction

The MFI zeolite structure, including ZSM-5 and the aluminum-free analog silicalite-1, has a two-dimensional pore system consisting of sinusoidal channels running in the [100] direction and intersecting straight channels running along the [010] direction [1]. MFI zeolite can be synthesized with Si/Al ratios in the range 5–∞ [2]. For crystallization of highly siliceous MFI, organic template molecules (usually tetrapropylammoniumhydroxide, TPAOH) are added to the synthesis mixture. These molecules are trapped in the pores of the as-synthesized material. In order to make the pores accessible to guest molecules, the organic templates are removed by thermal decomposition at high temperature, a process denoted calcination.

Zeolites often exhibit the unusual phenomenon of intrinsic negative thermal expansion (NTE), i.e. contraction heating, which seems to be correlated to the type of channel system [3,4]. Zeolites with two- or three-dimensional channel systems show NTE, which was suggested to result from structural expansion into the pores and channels during heating [4,5]. The positive thermal expansion observed in a few zeolite types seems to be related to their high density and one-dimensional pore systems [3,4]. Other factors affecting the thermal behavior of a specific zeolite are the Si/Al ratio [4], the extra-framework cations [4], the

* Corresponding author. Tel.: +39 059 2055293; fax: +39 059 2055235.
E-mail address: mgualtieri@unimore.it (M. Lassinantti Gualtieri).

1387-1811/$ - see front matter
doi:10.1016/j.micromeso.2005.09.022

sorption/desorption of water [6,7], phase transitions [8] and the removal of template molecules [9–12].

The thermal behavior of TPA-MFI during calcination was extensively studied in the past [9–12]. The structure contracts at temperatures above 300 °C. The temperature interval where the contraction occurs coincides with the template removal [9–12]. Furthermore, the unit cell of the calcined framework is smaller than the as-synthesized one [9,10,12,13].

Zeolites with MFI topology are often prepared in the form of membranes and studied in separation applications, due to their potential to separate compounds of industrial interest. Usually, the membranes are prepared in the presence of organic template molecules. During calcination of the as-synthesized MFI membranes, cracks in the zeolite layer may form [14,15], possibly due to a difference in the thermal behavior between the thin zeolite film (that contracts during heating) and the support (that expands during heating) [12]. Such a thermal expansion mismatch between bonded materials may result in stress and cracks within the composite. Cracks are not desired in membranes since they offer non-selective transport pathways.

The calcination of zeolite membranes is usually performed for several hours at 400–500 °C with a slow heating rate from ambient to the calcination temperature. It is common belief that a fast heating rate increases the risk of crack formation in MFI membranes. Cracks within large MFI crystals have been suggested to result due to strain caused by trapped gaseous products unable to diffuse out of the structure [9].

The effect of heating rate on template decomposition in MFI crystals was previously studied by Gilbert et al. [16]. TG/DTA was used to determine the rate of weight loss and temperature at maximum weight loss rate in order to identify the conditions were the stress in the individual crystals was at minimum. It was found that increased heating rate resulted in a higher temperature of reaction and a faster rate of weight loss. Hypothetically, such conditions increase the risk of intra-crystal cracks [16].

In the present work, the effect of heating rate on the MFI structure will be studied by HT-XRPD and the Rietveld method for the first time. On the basis of the results, possible effects of heating rate on crack formation in supported MFI zeolite membranes during calcination will be discussed. In addition, the apparent activation energy of the template decomposition will be calculated using classical kinetic analysis methods of non-isothermal data.

2. Experimental section

Tetrapropylammoniumhydroxide (TPAOH; 40% water solution, AppliChem), distilled water and tetraethylorthosilicate (TEOS; >98%, Merck) were mixed and stirred for 48 h. The molar composition of the resulting clear synthesis solution was $3TPAOH:25SiO_2:1500H_2O:100EtOH$. The clear synthesis solution was hydrothermally treated for 72 h under reflux in an oil bath holding a temperature of 100 °C. The product was carefully washed in distilled water by centrifugation and redispersion. The procedure was repeated three times. After washing, the crystals were dried at 50 °C for 24 h and stored at room temperature for one week before the HT-XRPD experiments. The crystals prepared by this procedure have a tablet habit, with well developed (0 1 0) faces and the other faces are curved (Fig. 1). The average size of the main crystal is approximately $0.8 \times 0.8 \times 0.4$ μm. In addition, considerably smaller 90° rotational intergrowths are present.

In situ XRPD data were collected using four heating rates (3, 5, 10 and 20 °C/min). The data for the experiment with a heating rate of 3 °C/min were collected using a Philips X'Pert PW 3701 powder diffractometer (Cu radiation) equipped with a PMP 1600 hot chamber and a gas proportional detector. The data acquisition time for each investigated temperature was 13.75 min. A Panalytical θ/θ diffractometer (Cu radiation), equipped with an Anton Paar HTK 16 resistance heating chamber and a RTMS X'Celerator, was used to collect data using higher heating rates (5, 10 and 20 °C/min). In these experiments, the data acquisition time for each experimental point was 3 min. In each series, the time to reach maximum temperature was determined not only by the heating rate but also by the data acquisition time and number of investigated data points. Hence, the average heating rate, defined as 475 °C divided by the total time from 25 °C to 500 °C was 1.53, 4, 6.6 and 9.96 °C/min for the series 3, 5, 10 and 20 °C/min. All experiments were performed in air and the sample temperature was calibrated using known phase transitions and thermal expansion of standard phases. The 2θ region 6–30° was investigated. Data were collected with 50 °C steps during heating up to 500 °C. This temperature was held for 1 h during which data were collected every 15 min. For the heating rate 10 °C/min, data were collected also during cooling and during a second heating/cooling ramp. The use of a standard silicon powder (NIST640c) directly mixed in the MFI powder allowed to determine the absolute

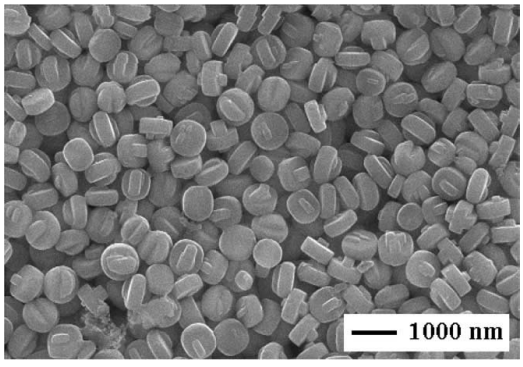

Fig. 1. SEM image of the as-synthesized silicalite-1 crystals.

cell parameters at each investigated temperature and correct for thermal expansion of the sample holder.

The MFI cell parameters at each temperature were refined with the Rietveld method using the GSAS [17] package and the EXPGUI graphical interface [18]. The orthorhombic structure described in [19] was used as structure model. The thermal expansion coefficient of standard silicon powder (640c) was taken from [20]. A multi-term Simpson's rule integration of the pseudo-Voigt profile function was used. The atom positions and the isotropic thermal parameters and occupancy factors were kept fixed during refinements. The 2θ zero shift, Lorentzian coefficients, scale factors and background were refined. The Gaussian coefficient was kept fixed at the value obtained for the RT data of the as-prepared sample. In order to follow the template decomposition, a quantitative phase analysis was performed in which the orthorhombic MFI with full and zero occupancy of the atoms in the template molecules, respectively, was refined as two separate phases. In these refinements, the cell parameters for both structure models were kept fixed at the previously obtained values. Hence, only the background and the scale factors were refined.

The kinetic analysis was performed using the α versus temperature data (non-isothermal mode), where α is the conversion factor defined as

$$\alpha = \left(\frac{I_c^T - I_c^{T=25\,^\circ C}}{I_c^{\max} - I_c^{T=25\,^\circ C}}\right), \tag{1}$$

where I_c^T is the sum of the 101/011 and the 200/020 peak areas divided by two at temperature T and $I_c^{\max}$ corresponds to the maximum value of I_c. Normally, the peak area under investigation should be divided by the area of a standard peak. However, the intensity of the standard peak in this case was too low with the risk to introduce a large error due to the uncertainty of the peak fit. However, no significant variation of the standard silicon peak intensity was observed in temperature. The Kissinger method [21], the isoconversional method of Flynn–Wall–Ozawa [22,23], and the method proposed by Kennedy and Clark [24] were used. The first two methods were chosen since the activation energy E_a of the template decomposition in silicalite-1 can be determined without prior knowledge of the reaction mechanism. In fact, according to the Kissinger method, the slope of a plot of $\ln(\beta/T_p^2)$ versus $1/T_p$ is proportional to the activation energy according to the following equation:

$$\ln\left(\frac{\beta}{T_p}\right) = -\frac{E_a}{RT_p} + k, \tag{2}$$

where β is the heating rate, T_p is the temperature (expressed in Kelvin) at which the reaction rate is maximum, R is the molar gas constant and k is the rate constant. Based on Doyle's approximation of the temperature integral, Flynn–Wall–Ozawa developed an alternative method to calculate the activation energy;

$$\ln\beta = \ln\frac{AE_a}{R} - 1.052\frac{E_a}{RT} - 5.33 - \ln g(\alpha), \tag{3}$$

where A is the frequency factor and $g(\alpha)$ is the integral of the kinetic model function $f(\alpha)$. Under the assumption that the kinetic model function is invariant for all the runs, a plot of $\ln\beta$ versus $1/T$ for a chosen value of α should be a straight line with a slope proportional to E_a.

Kennedy and Clark proposed a method to perform a kinetic analysis on a single set of non-isothermal data. According to the method described in [24], the following relation holds:

$$\ln\left[\frac{\beta f(\alpha)}{T - T_0}\right] = \ln(A) - \frac{E_a}{RT}. \tag{4}$$

A plot of the left side of Eq. (4) versus $1/T$ should result in a straight line with the slope proportional to E_a. The authors call this a "*ln–ln plot*". The Avrami equation [25] $[-\ln(1-\alpha)]^{1/n}$ was used as the kinetic model function $f(\alpha)$ in the present work, as it was previously determined as suitable to describe the template decomposition reaction kinetics in MFI type molecular sieves [11]. The reaction order for the Avrami equation was determined according to the following equation [24]:

$$\ln[g(\alpha)] = n\ln\left[\ln(A) - \frac{E_a}{RT}\right] + n\ln\left[\left(\frac{T - T_0}{\beta}\right)\right], \tag{5}$$

where $g(\alpha)$ is $[-\ln(1-\alpha)]$ and n is the reaction order. Since the quantity $n[\ln(A) - E/RT]$ is constant for any particular value of T, a plot of $\ln[g(\alpha)]$ versus $\ln[(T - T_0)/\beta]$ will have slope n. As the 3 °C/min data set contained most points in the α-range 0.2–0.8, which is most reliable for this kind of analysis [26], $\ln(A)$ determined from the intercept in the ln–ln plot was fixed for the linear fit of the ln–ln plots for the other series.

3. Results and discussion

Fig. 2 shows a sequence of XRPD patterns collected during heating of as-synthesized TPA-MFI ($\beta = 10$ °C/min). The relative intensity of several peaks changes with temperature. The intensity of some reflections increases whereas the intensity of others diminishes as the temperature increases. The strongest intensity increase is observed for the low angle peaks (i.e. 101/011 and 200/020). These intensity changes will be discussed later. A decreased intensity is observed for the 501 peak and the 051 peak.

The agreement factors of the Rietveld refinements (as defined in GSAS [17]) for the calculation of the cell parameters for the data collected with the heating rates 5, 10 and 20 °C/min were $R_{wp} = 0.11$–0.14 and $\chi^2 = 1.3$–1.9. The corresponding values for the series collected with a heating rate of 3 °C/min were $R_{wp} = 0.06$–0.08 and $\chi^2 = 4.1$–7.4.

Fig. 3 shows the cell parameters and the unit cell volume as a function of temperature during heating of the as-synthesized MFI powder. The cell parameters and volume during cooling in the series collected with $\beta = 10$ °C/min

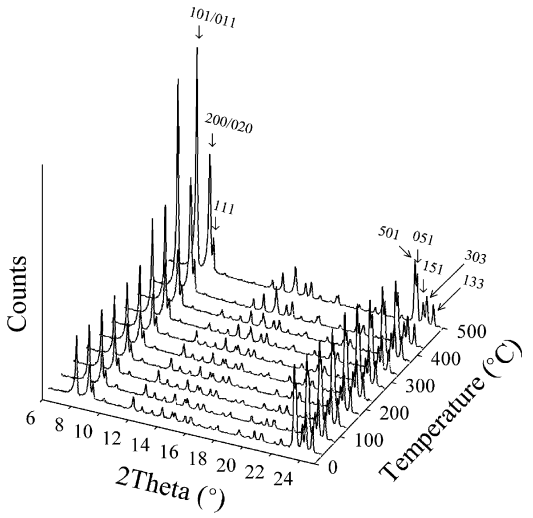

Fig. 2. XRPD patterns collected during heating ($\beta = 10$ °C/min) of TPA-MFI zeolite.

are also displayed. All unit cell parameters and the unit cell volume increase below 75 °C. In the temperature interval 75–275 °C, all unit cell parameters and the unit cell volume first decrease slightly and then increase. A relatively large contraction of all axes and the unit cell volume is observed above 275 °C. During cooling the unit cell expands, as observed for the 10 °C/min data set in Fig. 3 (dashed line).

Fig. 4 shows the evolution of the unit cell volume of the sample collected with a heating rate of 10 °C/min. For this particular sample, the heating cycle 25–500–25 °C was repeated on the calcined material. Hence, a comparison between the thermal behaviour of the TPA-MFI powder and the calcined MFI powder is possible. The curve of the TPA-MFI is shifted to higher cell volumes with respect to the others. The two cooling cycles overlap perfectly. It is interesting to observe that the second heating ramp is shifted to higher cell volumes in the temperature range 25–375 °C with respect to the cooling ramps. This difference could possibly be explained by hysteresis due to desorption and readsorption of water. A detailed discussion is beyond the scope of this paper. However, the matter is currently under investigation and will be reported in later work. As shown in Fig. 4 (heating 2), NTE is observed in the temperature range 175–500 °C in the calcined material.

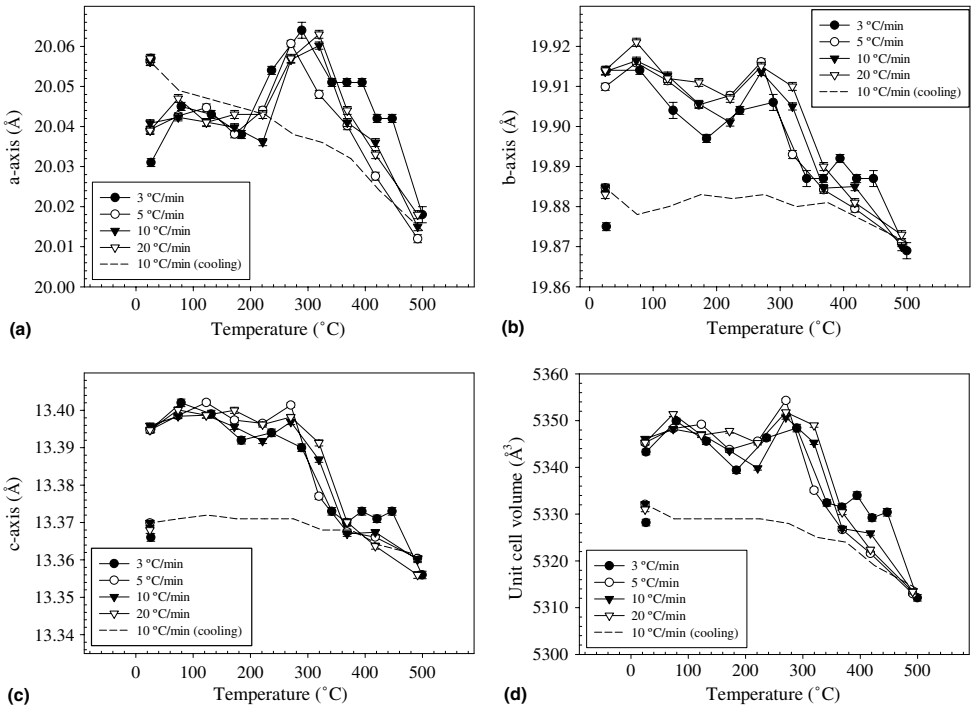

Fig. 3. The variation of the unit cell axes and volume during heating up to 500 °C of TPA-MFI powder using three different β's; 3 °C/min (filled circles), 5 °C/min (empty circles), 10 °C/min (filled triangles) and 20 °C/min (empty triangles). The variation of the unit cell dimensions during cooling with $\beta = 10$ °C/min is also shown (dashed line). The RT data after calcination for each series is indicated. Legend: (a) *a*-axis, (b) *b*-axis, (c) *c*-axis and (d) volume.

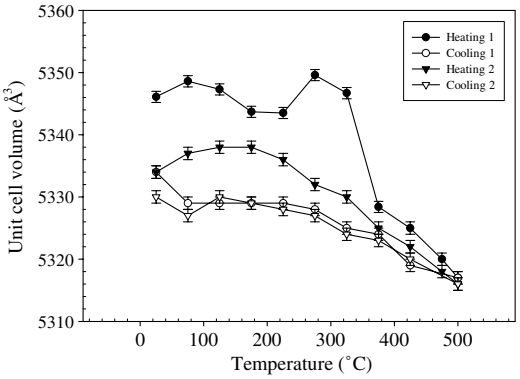

Fig. 4. The variation of the unit cell volume during heating to 500 °C (heating 1) of the as-synthesized TPA-silicalite-1 followed by cooling to RT (cooling 1). The heating ramp was repeated on the calcined material and the unit cell variations are included in the figure (heating 2 followed by cooling 2). The applied heating rate was 10 °C/min.

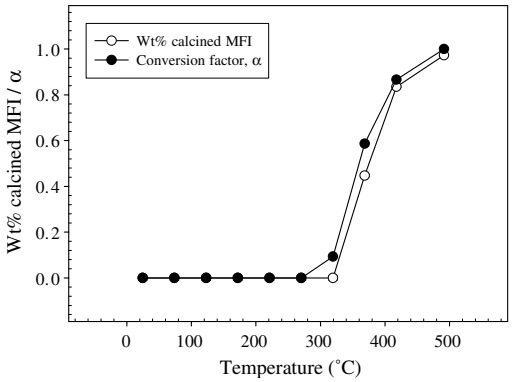

Fig. 5. The refined weight % of calcined empty MFI and the conversion factor α as a function of temperature for $\beta = 20$ °C/min.

Hence, the mechanisms causing NTE in TPA-silicalite-1 during calcination are probably not only due to the removal of the template molecules. As the heating rate affects the kinetics of the template removal reactions [16], a dependence of the heating rate for the NTE mechanism caused by template removal should be observed. However, no such trends are evident in axis lengths or unit cell volume (Fig. 3). It is possible that such an effect is masked by NTE which is not dependent on the kinetics, i.e. structure intrinsic mechanisms. Such a mechanism in zeolites is explained on the grounds of the rigid-unit modes (RUM) theory and is due to temperature-induced transverse vibrations of two-coordinate bridging oxygen atoms which causes a decrease in the distance between the Si atoms in adjacent tetrahedral [5]. As a result, the structure contracts during heating.

Since no clear trends in axis lengths or unit cell volume are observed between the various heating rates, the unit cell volume decreases faster when faster heating rates are applied.

Another interesting observation is that the cell volume of the calcined MFI is smaller than in TPA-MFI (see Fig. 3). RT data of the calcined MFI are shown as unconnected symbols. The difference is due to a contraction of the *b*- and *c*-axis which is only partly compensated by an expansion of the *a*-axis in the calcined form (Fig. 3). These results are in concert with previous results [12,13]. The change in % calculated for the 10 °C ramp is +0.077(5), −0.141(4), −0.189(5) and −0.194(7) for the unit cell axes (a, b, c) and cell volume, respectively. The standard deviations within brackets were derived from the ones given by the GSAS software. Qualitatively, the same result was obtained for the other series. The minor difference observed could be due to varying amount of adsorbed water molecules that affects the cell volume of the calcined material [6].

Fig. 5 shows the conversion factor α together with the refined weight fraction of the calcined MFI structure as a function of temperature for $\beta = 20$ °C/min. The agreement between the curves is very good indicating a connection between these separate observations. The refined occupancy factor for the TPA molecules during calcination was previously used as basis for a kinetic analysis of the template removal reaction in TS-1 and Fe-MFI zeolite [11]. In the present work, the kinetic analysis was based on a conversion factor α calculated from the intensity change of the low-angle peaks during template removal. Fig. 6 shows α versus T for the different heating rates. In this case, a clear trend is observed for varying heating rates since the value of α directly mirrors the TPA occupancy in MFI. In agreement with the results of Gilbert et al. [16], a slower heating rate decreases the temperature of reaction.

Fig. 7 shows a plot of $\ln(\beta/T_p^2)$ versus $1/T_p$. The apparent activation energy, calculated from the slope according

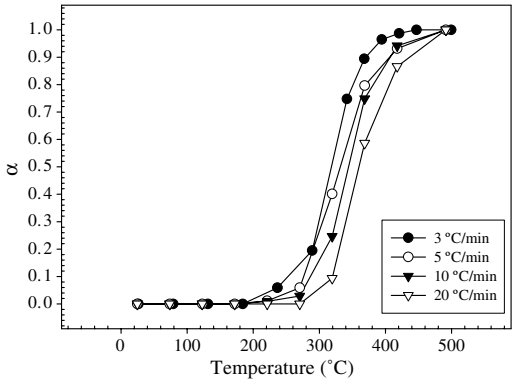

Fig. 6. The conversion factor α as a function of temperature for $\beta = 3$ °C/min (●), 5 °C/min (○), 10 °C/min (▼) and 20 °C/min (▽). The conversion factor was calculated on the basis of the integrated intensity of the low angle peaks (see Section 2 for details).

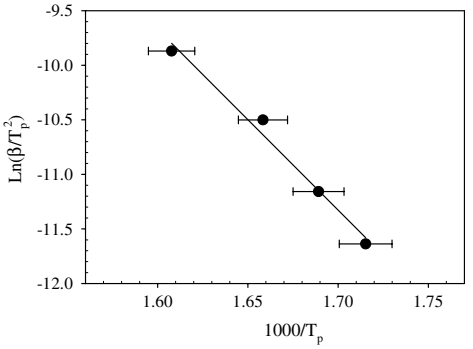

Fig. 7. A plot of $\ln(\beta/T_p^2)$ versus $1000/T_p$. According to the Kissinger method, the slope is proportional to E_a (see Eq. (2) in Section 2). The experimental error in the y-direction is within the plotted data points.

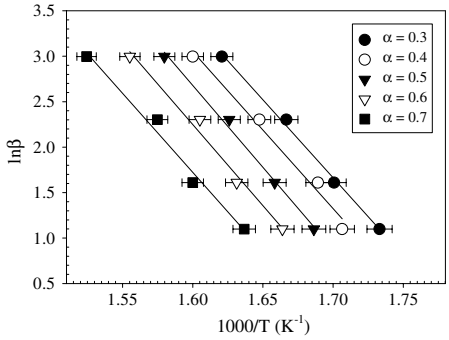

Fig. 8. A plot of $\ln\beta$ versus $1000/T$ for different values of α. The slope of each curve is proportional to E_a according to the method of Flynn, Wall and Ozawa (see Eq. (3) in Section 2).

to Eq. (2), is 138 (±25) kJ mol^{-1} with $R^2 = 0.985$. Fig. 8 shows a plot of $\ln\beta$ versus $1/T$ for different α. The apparent activation energy calculated from the slope of each curve according to Eq. (3) is shown in Table 1. The average value is 138 (±29) kJ mol^{-1}. An advantage of this method is that any changes in the mechanism of the reaction are immediately apparent as variations in the slope for different α. In fact, Maciejewski suggests to use an isoconversional method as a first test of reaction complexity [27]. The fitted curves in Fig. 8 are parallel, indicating only one rate limiting step.

Milanesio et al. successfully fitted the kinetic data using the well-known Avrami equation [11]. Under the assumption that the Avrami equation is valid for the reaction kinetics in the silicalite-1 powder studied here, Eq. (5) was used to determine the reaction order. The results are reported in Table 2. In concert with previous results [11], the obtained values for n (close to 0.5) indicate that the reaction is limited by mono-dimensional diffusion [26]. Milanesio et al. [11] explained this result in terms of

Table 1
The apparent activation energy, calculated from the slope of each curve in Fig. 8, according to Eq. (3)

α	E_a (kJ/mol)	R^2
0.3	136 (±26)	0.997
0.4	136 (±28)	0.985
0.5	142 (±29)	0.994
0.6	141 (±29)	0.985
0.7	137 (±26)	0.983

The R^2 value for each linear fit of the curves in Fig. 8 is also reported.

Table 2
The reaction order n for each data set, determined from the slope of $\ln[-\ln(1-\alpha)]$ versus $\ln[(T-T_0)/\beta]$

β (°C/min)	T_0 (°K)	n	R^2
3	483	0.32 (±2)	0.988
5	493	0.35 (±2)	0.992
10	520	0.43 (±3)	0.992
20	567	0.52 (±3)	0.997

T_0 as well as the regression coefficient from the linear fit are also shown.

preferred (mono-dimensional) diffusion of the reaction products out of the crystal along the b-axis, which provides the shortest diffusion path. The value of n will be set to 0.5 in the subsequent analysis. The plot of the left side of Eq. (4) against $1/T$ for the 3 °C/min series is shown in Fig. 9. From the slope of the plot for each β, the activation energy was calculated (see Table 3). The apparent activation energies E_a determined from each experimental series are nearly

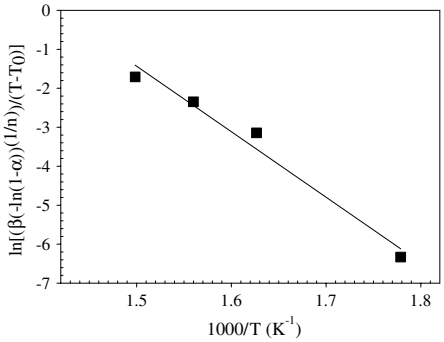

Fig. 9. The ln–ln plot (Eq. (5), Section 2) for the data set collected with $\beta = 3$ °C/min. The experimental error is within the plotted data points.

Table 3
The results from the kinetic analysis obtained by the method of Kennedy and Clark [24] (see Eq. (4) in Section 2)

β (°C/min)	E_a (kJ/mol)	R^2
3	140 (±16)	0.975
5	142 (±22)	0.944
10	139 (±26)	0.961
20	139 (±42)	0.936

the same within the experimental error. Furthermore, E_a determined in this way is in perfect agreement with that obtained with the isoconversional Flynn–Wall–Ozawa method as well as the Kissinger method.

On the basis of the results in the present work, it is possible to discuss potential effects of the heating rate on the formation of cracks in supported MFI membranes during calcination. Cracks are most likely formed during calcination as a consequence of accumulated thermal stress due to a thermal expansion mismatch between the MFI film and the support [12]. It is often assumed that a fast heating rate during calcination of MFI membranes increases the risk of crack formation [9]. However, Jareman et al. [28] reported no correlation between β (0.2–5 °C/min) and the quality of MFI membranes. In concert, cracks are also observed using slow heating rates such as 0.2–0.5 °C/min [14,15]. The present work shows that the unit cell dimensions of the MFI structure after template removal are practically independent on the heating rate. Furthermore, the unit cell dimensions at a certain temperature during calcination are independent on heating rate. Hence, under the assumption that the thermal behavior of the crystallites constituting a supported MFI film has the same thermal behavior as the crystallites in the powder, the residual stress at a certain temperature during calcination of a supported film is independent on heating rate. The stress cannot be minimized by optimization of the heating rate. Therefore, the results in [14,15,28] together with the results presented here strongly support the hypothesis that cracks in MFI membranes are a result of a thermal expansion mismatch between the MFI film and the support. If the cracks are formed as a consequence of a thermal expansion mismatch [12] and the contraction of the MFI unit cell is not affected by the heating rate during calcination, no correlation of the crack formation and heating rate is expected. This was in fact concluded in [28]. However, the present work shows that the rate of contraction is dependent on heating rate as expected. A possible effect of the contraction rate on the crack formation process cannot be excluded. Nevertheless, this factor did obviously not have an influence on the quality of the calcined membrane system studied by Jareman et al. [28].

4. Conclusions

The MFI framework contracts during the temperature-induced decomposition reactions of template molecules. The unit cell volume is independent on heating rate and consequently, the rate of contraction is dependent of heating rate. After complete template decomposition, the cell parameters approach the same value regardless of the heating rate. The cell volume of calcined MFI at RT is smaller than the TPA-MFI.

The intensity of some diffraction peaks is highly affected by the template molecules occluded in the as-synthesized structure. As the molecules are removed, the intensity of those peaks changes. The most spectacular change can be observed for the low-angle peaks (101/011, 200/020). The agreement between TPA occupancy and the intensity of the low angle peaks during heating indicates a dependency between template occupancy and peak intensity. A kinetic analysis based on the intensity change of the low angle peaks was performed using three separate methods. The calculated apparent activation energy for template decomposition in air was 138 (±25) and 138 (±29) kJ mol^{-1} for the Kissinger and Flynn–Wall–Ozawa approach, respectively. The reaction order and apparent activation energy were determined using the method of Kennedy and Clark. The reaction order was close to 0.5 which indicates a diffusion limited reaction with mono-dimensional advancement. The apparent activation energy E_a was determined to 140 (±30) kJ mol^{-1}, which is in good agreement with the results obtained with the other methods.

The results presented here show that the unit cell parameters of MFI are not very sensitive to the heating rate. In addition, the unit cell dimensions approach the same values after calcination regardless of heating rate. Therefore, assuming that the thermal behavior of MFI crystallites in a supported film is the same as for MFI crystallites in powder, the residual stress in the film at a certain temperature during calcination is independent on heating rate.

Acknowledgement

The authors are grateful to the foundation Blanceflor Boncompagni-Ludovisi, born Bildt for the financial support for MLG.

References

[1] W.M. Meier, D.H. Olson, Atlas of Zeolite Structure Types, Butterworths, London, 1987.
[2] R. Szostak, Handbook of Molecular Sieves, Van Nostrand Reinhold, New York, 1992.
[3] P. Lightfoot, D.A. Woodcock, M.J. Maple, L.A. Villaescusa, P.A. Wright, J. Mater. Chem. 11 (2001) 212.
[4] P. Tschaufeser, S.C. Parker, J. Phys. Chem. 99 (1995) 10609.
[5] M.P. Attfield, A.W. Sleight, Chem. Commun. (1998) 601.
[6] P.M. Jardim, B.A. Marinkovic, A. Saavedra, L.Y. Lau, C. Baehtz, F. Rizzo, Micropor. Mesopor. Mater. 76 (2004) 23.
[7] G. Cruciani, A.F. Gualtieri, Am. Mineral. 84 (1999) 112.
[8] S.H. Park, R.W. Grosse-Kunstleve, H. Graetsch, H. Gies, in: Progress in Zeolite and Microporous Materials, Studies in Surface Science and Catalysis, vol. 105, 1997, p. 1989.
[9] E.R. Geus, H. van Bekkum, Zeolites 15 (1992) 333.
[10] J. Dong, Y.S. Lin, M.Z.-C. Hu, R.A. Peascoe, E.A. Payzant, Micropor. Mesopor. Mater. 34 (2000) 241.
[11] M. Milanesio, G. Artioli, A.F. Gualtieri, L. Palin, C. Lamberti, J. Am. Chem. Soc. 125 (2004) 14549.
[12] M. Lassinantti Gualtieri, A.F. Gualtieri, C. Andersson, J. Hedlund, F. Jareman, M. Leoni, C. Meneghini, J. Membr. Sci., in preparation.
[13] R. Millini, G. Perego, D. Berti, W.O. Parker Jr., A. Carati, G. Bellussi, Micropor. Mesopor. Mater. 35–36 (2000) 387.
[14] J. Hedlund, F. Jareman, A.-J. Bons, M. Anthonis, J. Membr. Sci. 222 (2003) 163.
[15] Z. Lai, M. Tsapatsis, J.P. Nicolich, Adv. Funct. Mater. 17 (2004) 716.
[16] K.H. Gilbert, R.M. Baldwin, J. Douglas Way, Ind. Eng. Chem. Res. 40 (2001) 4844.

[17] A.C. Larson, R.B. von Dreele, GSAS Generalized strucure analysis system, Laur 86-748, Los Alamos National Laboratory, Los Alamos, New Mexico, 1994.
[18] B. Toby, J. Appl. Cryst. 34 (2001) 210.
[19] H. van Koningsveld, H. van Bekkum, J.C. Jansen, Acta Cryst. B43 (1987) 127.
[20] M. Dapiaggi, G. Artioli, L. Petras, The Rigaku J. 19 (2002) 35.
[21] H.E. Kissinger, Anal. Chem. 29 (1957) 1702.
[22] J.H. Flynn, L.A. Wall, J. Polym. Sci. Part B 4 (1966) 323.
[23] T. Ozawa, Bull. Chem. Soc. Jpn. 38 (1965) 1881.
[24] J.A. Kennedy, S.M. Clark, Thermochim. Acta 307 (1997) 27.
[25] M. Avrami, J. Chem. Phys. 7 (1939) 1103.
[26] C.H. Bamford, C.F.H. TipperComprehensive Chemical Kinetics, vol. 22, Elsevier, New York, 1980, pp. 41–113.
[27] M. Maciejewski, Thermochim. Acta 355 (2000) 145.
[28] F. Jareman, C. Andersson, J. Hedlund, Micropor. Mesopor. Mater. 79 (2005) 1.

PAPER VII

Crack formation in α-alumina supported MFI zeolite membranes studied by *in-situ* High Temperature Synchrotron Powder Diffraction

---

Magdalena Lassinantti Gualtieri, Alessandro F. Gualtieri, Charlotte Andersson, Jonas Hedlund, Fredrik Jareman, Matteo Leoni and Carlo Meneghini

Submitted to Journal of Membrane Science

Crack formation in α-alumina supported MFI zeolite membranes studied by *in-situ* High Temperature Synchrotron Powder Diffraction

Magdalena Lassinantti Gualtieri, Charlotte Andersson, Fredrik Jareman and Jonas Hedlund

Department of Chemical Engineering and Geosciences, Luleå University of Technology, SE-971 87 Luleå Sweden

Alessandro F. Gualtieri

Dipartimento di Scienze della Terra, Università di Modena e Reggio Emilia, Via largo S. Eufemia 19, I-41100 Modena Italy

Matteo Leoni

Dipartimento di Ingegneria dei Materiali, Università di Trento, I-38050, Mesiano (TN), Italy,

Carlo Meneghini

Dipartimento di Fisica 'E. Amaldi' Università di Roma Tre, Via della Vasca Navale 84, I-00146 Roma, Italy

Submitted to: **Journal of Membrane Science**

Word processor: Word MS OFFICE 2000

*Corresponding author: Mrs. M. Lassinantti Gualtieri Tel.: +39-059-2055293, Fax +39-059-2055235

E-mail address: mgualtieri@unimore.it

Abstract

Cracks are frequently formed in α-alumina supported MFI membranes during calcination. To better understand crack formation, *in-situ* powder diffraction data was collected during calcination of a type of MFI membrane (ca 1800 nm thick) which is known to crack reproducibly. In addition, data for MFI powder and a blank support were also collected. Both a synchrotron radiation facility and an in-house instrument were used. The unit cell parameters were determined with the Rietveld method, and the strain in the direction perpendicular to the film surface was calculated for the film as well as for the support. The microstrain in the support was also estimated. Based on the results obtained here, a model for crack formation in this type of MFI membrane was proposed. The lack of cracks in other types of MFI membranes (ca 500 nm) prepared in our laboratory is also explained by the model. In thicker MFI films, the crystals are well intergrown. During heating, the MFI crystals contract and the α-alumina support expands. Consequently, a thermal stress develops in the composite which eventually leads to formation of cracks in the film and structural defects in the support. In thinner films, the crystals are less well intergrown and the thermal expansion mismatch leads to opening of grain boundaries rather than cracks.

Keywords: MFI zeolite membrane; *in-situ* study; synchrotron powder diffraction; crack formation; Rietveld method.

1. Introduction

The potential industrial applications of polycrystalline zeolite membranes are not fully explored. This explains the increasing number of papers and patents on this specific topic. To this aim, MFI is a particularly interesting zeolite structure topology due to the pores with a size close to the kinetic diameter of many industrially important molecules. MFI zeolites with a high Si/Al ratio generally require the addition of organic template molecules for the synthesis. Frequently used organic templates are quaternary ammonium cations such as TPA^+ (tetrapropylammonium). The template molecules are trapped in the zeolite channels and are usually removed by calcination to activate the membrane.

For good separation performance, no alternative pathways in the form of defects such as open grain boundaries, pinholes and cracks should exist in the film [1-4]. Cracks are possibly the most troublesome type of defect and may form during calcination [1].

In an early work, crack formation during template removal of MFI single crystals (cube-shaped silicalite, fluoride-synthesized silicalite and vanadium-containing silicalite) was investigated [5]. In large crystals (> 300 μm average crystal size) some straight cracks along the c-axis developed at 260 °C. The occurrence of straight cracks seems to be related to the dehydration of the framework during the initial Hofmann elimination reaction of TPA. Random cracking was observed in cube-shaped crystals larger than 150 μm (more severe in larger crystals). These observations match the temperature interval in which degradation of tripropylamine via β-elimination reactions occurs. It was postulated that the development of random cracks was related to the formation of carbonaceous species within the zeolite framework. Pachtova et al. [6] studied the TPA removal in large silicalite-1 crystals of three different sizes. No cracks were observed in the smallest crystal (L_c = 130 μm) after calcination in air. In larger crystals, cracks developed in both air and nitrogen atmosphere. In

the medium-sized crystals (L_c = 190 μm), cracks were found after complete template removal, whereas in the largest crystals (L_c = 230 μm) they already appeared after partial calcination. Hence, in concert with the results of Geus and van Bekkum [5], the formation of cracks was apparently dependent on the crystal size.

It is well known that a thermal expansion mismatch between bonded materials may result in stress and consequently cracks in a composite. In fact, Geus and van Bekkum suggested that cracks in supported MFI membranes were due to thermal stress during calcination [5]. The MFI structure experiences a strong contraction during template removal, which occurs in the approximate temperature range 300-500 °C [5,7-9]. Instead, the α-alumina supports used for MFI films expand during heating [8-10]. Furthermore, the unit cell of the calcined framework is smaller than the as-synthesized one [5,7,9,11]. The difference is due to the contraction of the b- and c- axes which is only partly compensated by an expansion of the a-axis in the calcined form [7,9,11]. den Exter et al. [12] studied b-oriented silicalite-1 films on dense silicon wafers. Derived from crystallographic data for as-synthesized and calcined silicalite-1, the authors reported that the change (%) in the unit cell dimensions after calcination (*ex-situ* data) was –0.71, +1.05 and –0.105 for the a-, b- and c-axes, respectively. Based on these results and a quantitative estimation of the a-and b-oriented crystallites in the film, the calcined crystal layer would show an expansion with respect to the as-synthesized film. In fact, a buckling of the calcined crystal layer was evident. The cracks observed in the film were attributed to compressive stress in the calcined layer.

To better understand the crack formation process in MFI membranes, the thermal behavior of the porous support as well as that of the zeolite film must be investigated. An appropriate technique is high temperature X-ray powder diffraction (HT-XRPD) which allows to follow the *d*-spacings of the crystal planes as a function of temperature. Consequently, the strain in the sample can

be followed as a function of temperature by comparing the *d*-spacings in the film with those in a non-stressed sample.

Dong et al. [8] performed a HT-XRPD study of silicalite-1 films on porous yttria-doped zirconia (YZ) supports as well as ZSM-5 films on α-alumina supports. The films were composed of randomly oriented crystals. The MFI crystals formed in the bulk of the synthesis solution were also investigated. The films were defective after calcination. Open grain boundaries were present in the calcined ZSM-5 films whereas cracks were detected in the films of silicalite-1. Thermal expansion curves of the composites were determined during heating of the as-synthesized samples. It was shown that the MFI unit cell experiences a large contraction during template removal, while the support expands. During cooling, after template removal, the zeolite expands while the support contracts. In addition, the thermal expansion of the various samples was shown to be different. However, the strain in the films during the temperature ramp was not reported, possibly because the different Si/Al ratios in the samples masked the difference in unit cell dimension caused by strain in the film.

Crack-resistantant MFI membranes were recently studied by Jeong et al. [10]. The authors performed a HT-XRPD study (using synchrotron radiation (SR)) of a c-/(*h0h*) oriented MFI film with a thickness of about 10 μm. The film was prepared on a thin mesoporous silica layer deposited on a porous α-alumina support. They found that the crystals in the film experienced an in-plane compressive strain (i.e. in the direction parallel to the film surface) during the entire calcination procedure. It was speculated that this behavior possibly could explain the lack of cracks in this system.

No HT-XRPD study of α-alumina supported MFI films which crack during calcination had been reported. This recently prompted a preliminary HT-XRPD investigation of such a film [9]. In addition, MFI powder was also investigated. The Rietveld method was used to determine the unit cell parameters in the MFI

film and the α-alumina support as well as MFI powder *in-situ* during the entire calcination procedure (i.e. both heating and cooling) [9]. The different thermal behavior of the film and the powder was attributed to tensile stress in the film during heating. The results of the preliminary investigation were however not sufficient to formulate a conclusive model for the crack formation process observed in the α-alumina supported MFI films prepared in our laboratory [1,9]. The present work is a natural follow-up of the preliminary study. For the first time, the Rietveld method and high resolution HT-SRPD data were used to investigate a type of MFI membrane (ca 1800 nm thick) which reproducibly crack during calcination. The unit cell parameters of the MFI film as well as the TPA^+ occupancy were determined as a function of temperature during the entire calcination procedure. In addition, the microstructure of the α-alumina support was followed in temperature by pattern decomposition and Williamson-Hall plots. HT-XRPD data collected with an in-house instrument were used to determine unit cell parameters as a function of temperature for a blank α-alumina support and MFI powder, which where used as references to calculate the strain in the membrane. The information obtained in this study will be used to formulate a model for crack formation. The model also explains the lack of cracks in thinner MFI membranes (ca 500 nm) synthesized in our laboratory. The model will be compared to those existing in the literature.

2. Experimental

Zeolite films were prepared on graded α-alumina filters (Inocermic GmbH, Germany). The top layer is 30 μm thick with 100 nm pores and the bottom layer is 3 mm thick with 3 μm pores. The zeolite film investigated by synchrotron radiation was grown on a slice (20×3×1 mm) cut from the as-purchased α-alumina filters using a diamond saw (Discotomo cutter). A full-size filter (∅ 25

mm) was used for the preparation of the membrane investigated by an in-house HT-XRPD instrument.

All supports were carefully washed with acetone, ethanol and a dilute (0.1M) ammonia solution. Silicalite-1 seed crystals (with an average size of 60 nm) were adsorbed on the supports as described previously [1]. Following seeding, the supports were placed in a synthesis solution with the molar composition 3TPAOH: 25SiO_2: 1500H_2O: 100EtOH for 96 h in an oil bath holding a temperature of 100 °C. The chemicals used were tetrapropylammoniumhydroxide (TPAOH**;** 40% water solution, AppliChem) and tetraethylortosilicate (TEOS; >98%, Merck). After synthesis, the samples were carefully washed in a dilute ammonia solution. The samples used in the present work should be identical (apart for the size of the sample studied by HT-SRPD) to the ones labeled U-72 in a previous work by our research group [1]. The zeolite film in this membrane type has a maximum crystal size of 400 nm on the top surface and a total thickness of 1800 nm. After calcination, these membranes are reproducible defective and cracks with an average width of 30 nm are present in the zeolite film and support cracks are also present as has been described earlier [1]. This type of membrane is thus suitable for studies of defect formation and was selected for the present study.

The MFI crystals formed in the bulk of the synthesis solution during growth of the film were carefully washed and subsequently dried. The crystals have a tablet habit with well developed (010) faces and the other faces are curved. The average size of the main crystal is approximately 0.8×0.8×0.4 μm. In addition, considerably smaller 90° rotational intergrowths are present.

Powder diffraction data were collected at the Italian beamline BM08 (GILDA) at the European Synchrotron Radiation Facility (ESRF), Grenoble (France). The beamline configuration is described in detail elsewhere [13]. Figure 1 illustrates the experimental set-up. The sample was mounted in a metal tube with an inner diameter of 3.5 mm which allowed sample insertion without damage of the film

surface and allowed the sample to expand during heating. The film was facing downwards. The end of the tube was sealed using a cap with an insertion to hold the surface of the sample in a horizontal position during the measurement. A perforation (1 mm high and 12 mm wide) in the tube allowed the SR beam to hit the sample from the side. The sample was heated by a hot air stream from a heating gun placed vertically under the sample. The diameter of the hot air stream was about 10 mm. Following sample insertion, the sample holder was mounted on a goniometer head. Data was collected in parallel beam Debye geometry using a wavelength of 1.0405 Å calibrated with FIT2D [14] against the NBS-640b Si standard with a = 5.43094(4) Å at 298 K. The temperature was monitored with a thermocouple positioned about half a mm below the sample. A heating/cooling gradient of 3 °C/min was applied. The sample was heated to 500 °C followed by a hour long isotherm and cooling back to room temperature. Full diffraction rings were recorded at steps of 50 °C ± 3° with an exposure time of 2 min, using an image plate (IP) detector, mounted perpendicular to the incoming beam at a distance of 235.7 mm. The data acquisition was thus performed using the full-plate mode, i.e. the slits in front of the IP are removed and the whole diffraction pattern is recorded. The images stored in the IP were recovered using a scanner with a dynamical range of 16 bit/pixel with a minimum pixel size of 50 × 50 μm^2. The data were extracted using FIT2D [14] and corresponds to the diffracted x-rays from the planes parallel to the film surface.

The absolute cell parameters during heating of the α-alumina support alone and a support coated with a MFI film were determined in separate experiments using an in-house instrument. A Panalytical θ/θ diffractometer (Cu radiation), equipped with an Anton Paar HTK 16 resistance heating chamber and a RTMS detector, was used to collect data using the same temperature ramp as for the synchrotron experiment described above. The sample temperature and temperature induced vertical shift of the sample holder were calibrated using

known phase transitions/transformations of standard materials and the thermal expansion of standard Si NIST 640c, respectively. For each experiment, the powder of the standards was finely dispersed over the investigated samples to form a thin film of a few μm.

The same in-house equipment was used to collect *in-situ* data of the MFI powder. The RTMS detector allowed fast data collection (3 min total acquisition time for each investigated temperature). A θ/θ scan was carried out in the region 6-30 °2θ. The use of a standard silicon powder (NIST640c) directly mixed in the MFI powder allowed to determine the absolute cell parameters of the MFI phase at each investigated temperature. In this case, a heating/cooling gradient of 10 °C/min was applied, but the experimental approach was otherwise the same as for the membrane (i.e. heating up to 500 °C followed by an hour long isotherm and cooling back to room temperature).

Rietveld refinements were performed using both SR data and data collected with the in-house instrument. The refinements were performed with the GSAS package [15] and its graphical interface EXPGUI [16]. The orthorhombic MFI structure was used [17]. The structure model for α-alumina was taken from Ishizawa *et al.* [18]. In the refinements using SR data, the cell parameters of the α-alumina support at each investigated temperature were kept fixed at the absolute values obtained using the data collected with the in-house instrumentation. Hence, the absolute cell parameters of the MFI phase could be determined using the α-alumina as internal standard. The peak profiles were modeled using a pseudo-Voigt function with one Gaussian and one Lorentzian coefficient. The cell parameters, 2θ zero shift, scale factor and background (shifted Chebyshev function with 9 terms) were refined. The atom positions and the isotropic thermal parameters and occupancy factors were kept fixed during refinements of α-alumina. In the refinements of the MFI phase using SR data, an overall occupancy factor for the different atomic species (C and N) of the TPA^+ molecule was refined.

The thermal expansion ratio K_T of the α-alumina substrate and the MFI film was calculated (as defined earlier [8]):

$$K_T = \frac{(V_{cell}^{T} - V_{cell}^{T=25°C})}{V_{cell}^{T=25°C}} \cdot 100 \quad (1)$$

The strain (*s*) along crystallographic direction (*l*) was calculated for both the MFI film and the α-alumina support at each investigated temperature *T* according to;

$$s = \frac{(l_{membrane}^{T} - l_{reference}^{T})}{l_{reference}^{T}} \quad (2)$$

where the MFI powder and the blank α-alumina support were used as references (i.e. represent the non-strained bulk lattice).

To study the microstructure, the profiles of the α-alumina (SR data) were investigated by means of pattern decomposition. Each peak was modeled with a pseudo-Voigt (pV) function and the peak position, the Full width at Half Maximum (FWHM), the maximum intensity and the shape parameter (η, the mixing coefficient) for the pseudo-Voigt function were refined together with parameters for the background. The refined values of the integral breadth (β) and the mixing parameter (η) were used in a subsequent analysis. The integral breadth of the Lorentzian (β_L) and Gaussian (β_G) components of the Voigt function corresponding to the pV function can be determined according to the following empirical formulas [19]:

$$\frac{\beta_L}{\beta_{pV}} = 0.017475 + 1.500484\eta - 0.534156\eta^2 \quad (3)$$

$$\frac{\beta_G}{\beta_{pV}} = 0.184446 + 0.812692(1 - 0.998497\eta)^{1/2} - 0.659603\eta + 0.44542\eta^2 \quad (4)$$

Applying the above equations to the powder pattern collected from the sample (h(2θ)) and from a profile standard (LaB_6) with no imperfection broadening (g(2θ)), the line broadening due to the microstructure of the sample (f(2θ)) can be calculated due to the additive property of the breadths of the Lorentzian functions and the squares of the breadths of Gaussian functions:

$$\beta_L^f = \beta_L^h - \beta_L^g \quad (5)$$

$$\left(\beta_G^f\right)^2 = \left(\beta_G^h\right)^2 - \left(\beta_G^g\right)^2 \quad (6)$$

Equations (3) and (4) were used again to obtain the total integral breadth of the f(2θ) function corresponding to the given peak.

The integral breadth in reciprocal units, $\beta_f^* = \frac{\beta_f \cos\theta}{\lambda}$, was plotted versus $d^* = \frac{2\sin\theta}{\lambda}$ in a Williamson-Hall plot [20]. In the plot, the reciprocal of the intercept gives an estimate of the apparent size D_v of coherently-diffracting domains and the slope is a measure of microstrain ε as shown in the following equation:

$$\beta_f^* = \frac{1}{D_v} + 2\varepsilon d^* \quad (7)$$

Although this method is based on the approximation that the line profiles due to size and microstrain are Lorentzian, which is unlikely in practice, the plot can be used to give a qualitative indication of the sample microstructure [21].

The application of this method to the zeolite phase is prevented by peak overlap due to the low symmetry of MFI and poor peak resolution which is an intrinsic limit of the Imaging Plate configuration.

A sample for TEM analysis was prepared by mild grinding of the α-alumina support surface followed by suspension in distilled water and deposition on a Cu grid. A JEOL JEM 2010 instrument, equipped with a Link energy dispersive X-ray spectrometer and a Gatan energy filter, operating at 200 kV was used for a TEM study.

3. Results and Discussion

The agreement factors of the Rietveld refinements (defined in GSAS [14]) for the calculation of the unit cell dimensions (SR and conventional data) were: R_{wp}=0.09-0.15, R_p=0.06-0.09, $R(F^2)$=0.15-0.20, χ^2=1.5-2.0. These factors indicate a good fit [22].

The preferred orientation of the zeolite crystals in the film was refined using the March-Dollase model implemented in GSAS [15]. The best fit was obtained with a ratio of 0.92 for the (501) crystallographic plane. This indicates that the crystals in the sample exhibit a weak preferred orientation with the a-axis perpendicular to the substrate surface, in agreement with previous observations [1].

Figure 2 shows the refined a-axis (a), c-axis (b) and unit cell volume (c) as a function of temperature (25-500-25 °C) for a blank α-alumina support and the MFI coated support. In addition, literature data [23] for α-alumina powder is included for comparison. As observed in the figure, the thermal expansions for the α-alumina supports are in concert with data for powder. However, a slightly

lower expansion is observed in the c-direction for the coated support compared to the blank support, resulting in a smaller unit cell volume. Such a difference in thermal expansion was also observed earlier [9] and indicates that the thermal expansion of the support is affected by the presence of the zeolite.

Figure 3 shows the refined a-axis (a), b-axis (b), c-axis (c) and unit cell volume (d) as a function of temperature (25-500-25 °C) for the MFI film (SR data). For comparison, the refined cell parameters of the MFI powder (in-house instrument) are also included in the figure. During heating, a first contraction peak of the unit cell volume (see Figure 3d) is observed for both the MFI powder and the film at about 175 °C. This contraction is attributed to dehydration, which occurs before the template decomposition as reported by Geus and van Bekkum [5]. Both the MFI powder and the film show a second contraction of all the axes in the temperature range 275-500 °C (Figure 3). The refined overall occupancy factor for C atoms in the TPA^+ molecule in the MFI zeolite film is given as a function of temperature in Figure 4. As the template is removed in the same temperature range (275-500 °C) where the strong contraction is observed, these events are clearly related. However, the negative thermal expansion in the TPA-MFI during calcination is probably not only due to the removal of the template. An intrinsic structure mechanism may also be present as discussed in earlier work [7]. During cooling from 500 °C, the MFI unit cell expands in all crystallographic directions. From Figure 3, it is clear that the thermal behavior of the MFI film is different from that of the powder during the entire temperature cycle. The b-axis in the film is much longer compared to the powder. On the other hand, the c-axis as well as the a-axis in the film are shorter.

At room temperature, the calcined MFI powder shows a contraction along the b- and c-axes and an expansion along the a-axis resulting in a much smaller volume compared to the as-synthesized phase. On the contrary, at room temperature, the calcined MFI film retains the volume of the as-synthesized

form, mainly due to a considerably larger expansion of the b-axis compared to the powder. This peculiar behavior of the film was already reported in [9], and could perhaps be explained by a lower Si/Al ratio in the film. In fact, the Si/Al ratio of the synthesis mixture may decrease significantly during hydrothermal treatment due to alkaline leaching of the α-alumina support [24]. Therefore, some T sites could be occupied by Al even though no Al was added in the synthesis gel. Meyers et al. studied the influence of Al substitution on the unit cell volume in calcined ZSM-5 [25]. In the range 2.7-5.3 Al atoms/unit cell, the unit cell volume exhibit a linear increase of 0.06 % for every Si atom substituted for Al. The maximum number of TPA^+ ions/unit cell that can be accommodated in the MFI structure is 4 [17]. In the absence of other cations (as in the synthesis solution used for the MFI films prepared in this work), the TPA^+ ions must compensate for the negative charge introduced by substitution of Si for Al. Therefore, not more than 4 Al atoms/unit cell may be incorporated in the MFI film studied here. Hence, considering the extreme case where the powder and the film contain 0 and 4 Al atoms/unit cell, respectively, the maximum volume difference between the powder and the film possibly explained by a different Si/Al ratio should be 0.24 % according to the linear equation of Meyers et al. [25]. The difference observed in our work (see Figure 3d) in the calcined materials at RT is much larger (0.43 %) and can therefore not only be explained by an increased Si/Al ratio of the MFI film during synthesis. In addition, the results of Meyers et al. also showed that the length of all the MFI unit cell axes increases linearly with increasing substitution of Si with Al [25]. Instead, here we observe a longer b-axis and a shorter c-axis in the film compared to the powder (Figure 3). Therefore, the possible incorporation of Al in the film does not give a satisfactory explanation to the observed unit cell distortion nor the larger volume of the film with respect to the powder. Instead, these results are possibly explained by internal strain in the film. In Figure 5, the thermal expansion/contraction ratio K_T of the MFI coated α-

alumina support and the MFI film is shown as a function of temperature. It is clear that the MFI coated α-alumina support and the MFI film behaves very differently during calcination. The support experiences a large expansion while the MFI film shrinks during heating to 500 °C. Obviously, the film should experience an isotropic tensile stress in the plane parallel to the film surface with a consequent strain in the direction perpendicular to the film due to the effect of Poisson's ratio. Here, it should be remarked that the unit cell dimensions shown in Figure 3 were calculated based on diffraction data from planes parallel to the film surface (see experimental). Hence, the length of the unit cell axes mirrors the *d*-spacings of these planes and can therefore be used to calculate the strain in the MFI film in the direction perpendicular to the film surface using the length of the unit cell axes in the powder as a reference. The results are shown in Figure 6. As the majority of the crystals are oriented with the a-axis perpendicular to the film surface (see above), the strain along this crystallographic direction is most representative for the film. Compressive strain is observed for the a-axis, which increases with temperature up to about 325 °C where a sharp decrease in strain is observed. During further heating up to 500 °C and subsequent cooling down to RT, a steady decrease in strain is observed. A compressive strain in the direction perpendicular to the film surface would be expected for crystals with a positive Poisson's ratio which are exposed to a tensile stress in the direction parallel to the film surface [26]. The abrupt decrease in strain at 325 °C could be due to the formation of cracks in the film, which releases the thermal stress and consequently the strain in the direction perpendicular to the film surface. Additional cracks are probably formed during further heating up to 500 °C, as the strain continues to decrease. In fact, *in-situ* permeation experiments showed that cracks were formed in ZSM-5 membranes in the temperature range 220-400 °C [27]. The steady decrease in strain during cooling is attributed to a decreased thermal stress in the direction parallel to the film surface, as the difference in volume between

the film and the support is reduced (Figure 5). The variation in strain with temperature of c-oriented crystals shows more or less the same trend as the one observed for the a-oriented crystals (i.e. sharp decrease at 325 °C and a steady decrease during cooling). A more surprising result is the large out-of-plane tensile strain of b-oriented crystals in the film (Figure 6), that actually increases during cooling. This peculiar behavior is difficult to explained based on the data presented here and should be investigated further in the future.

In Figure 2, it was shown that the thermal behavior of the alumina support was effected by the zeolite film. In order to investigate this further, the strain in the MFI coated α-alumina support was calculated at each investigated temperature, using the non-coated support as reference. The results are shown in Figure 7. A compressive strain is observed in the c-axis during the entire temperature cycle. However, the strain increases during heating, which is explained by an increased difference in thermal expansion between the support and the MFI zeolite (see Figure 5). During cooling, the strain decreases as the thermal expansion mismatch between the zeolite and the support decreases (Figure 5). The strain along a hardly exceeds the experimental error. However a slight compressive and tensile strain is observed during heating and cooling, respectively. It should be remarked that the strain in the α-alumina support is at least one order of magnitude smaller than that observed in the zeolite film. Based on the available data, the observed overall compressive strain in the direction perpendicular to the support surface (see Figure 7) is difficult to explain. It is unlikely that the effect is caused by the thin zeolite layer on top of the support (ca 1200 nm [1]). However, the film extends into the pores of the support, forming a zeolite-support composite layer (ca 500 nm [1]). It is possible that the negative thermal expansion of the zeolite surrounding the α-alumina grains in this layer causes a net tensile strain in the support in the direction parallel to the film surface Consequently, a net compressive strain

should be observed (Figure 7) in the direction perpendicular to the film surface due to the effect of Poisson's ratio.

The microstructure (size and microstrain) for the α-alumina support in the membrane investigated by SR was evaluated using equation (7), proposed by Williamson and Hall [20]. Figure 8(a) shows the Williamson-Hall plot based on data collected at 25 and 500 °C. The miller indices for the evaluated peaks are indicated. A Williamson-Hall plot was constructed for each investigated temperature. Figure 8(b) shows the microstrain of the α-alumina substrate as a function of temperature. The linear fit of the plot based on room temperature data gave a regression coefficient (R^2) of 0.54. The calculated microstrain and isotropic size was 0.012 % and 89 nm, respectively. The microstrain in the as-prepared membrane indicates the presence of structural defects. Defects in general are classified as point defects, line defects (dislocations) and planar defects (such as stacking faults). Considering the nature of the crystal structure of α-alumina, point defects, twins and stacking faults are ruled out. Hence, only dislocations should occur here. The scatter of the points in the Williamson-Hall plot, as indicated by the low regression coefficient value (R^2=0.54), is another indication for dislocations [28]. The observed isotropic size is reasonable considering that the 30 μm thick top layer is composed of 100 nm grains. The accuracy of the microstrain as a function of temperature is sufficient to reflect an increase from ca. 0.014 % at 225 °C to about 0.025 % at 500 °C (figure 8b) in correspondence with the temperature range of the template removal from the MFI film. However, any significant line broadening anisotropy was not observed in the patterns even for the high temperature data. It can not be excluded that the anisotropic peak broadening, generally observed in materials with a high density of dislocations [28], is partly masked by other factors which contribute to the peak broadening and possibly to the poor peak resolution. Such factors could be (i) thermal gradients which give an apparent variation in the peak position because some grains have a variation in position and some

others not; (ii) core/surface effects commonly observed in a polycrystalline material with constraints of the grain boundaries to the grain movement itself. Thus, the non-zero slope in the Williamson-Hall plots lead only to speculative indications. Nevertheless, it is possible that part of the thermal stress, which increases with temperature (as the difference in the thermal expansion coefficients of the α-alumina substrate and the zeolite film increases), is released via nucleation of dislocations in the support, probably on pre-existing dislocations (as inferred by the occurrence of microstrain at room temperature). The stabilization of the microstrain at 500 °C is possibly due to the fact the stress decreases during cooling (as the difference in K_T between the film and the support decreases) and does no longer induce the formation of defects at a microscale.

Figure 9 shows a bright field TEM image taken on a specimen from the membrane that underwent the *in-situ* synchrotron experiment. The presence of structural defects (likely dislocations) in the α-alumina support is confirmed. The SAED diffraction pattern in the inset shows that the signal is transmitted through a single crystal of α-alumina.

3.1. Model for crack formation

Based on the results of the present work and previous work [1] a model for crack formation or absence of cracks in MFI membranes can be formulated. The model is based on the following assumptions: (a) The crystals constituting the MFI film are strongly bonded to the support. This assumption is supported by the observation that the MFI film penetrates into the pores of the support [1] which should result in a key-lock effect and a large contact area between the two phases. (b1) In the case of relatively thick films (1800 nm, in present work and membrane type U-72 in previous work [1]), the crystals in the film are well intergrown. This assumption is supported by the fact that the cracks observed in

the film after calcination does not only run between crystals but also within crystals [1]. The cracks observed in the thick films [1] are typical channel cracks (i.e. the lateral crack length is many times the film thickness) [29] which propagate vertically down in the support. This indicates that the cracks were the result of a tensile stress in the film [29]. (b2) In the case of thinner films (500 nm, membrane type M30 in previous work [1]), the crystals are less intergrown and no cracks are observed.

Our model for crack formation is described as follows: During heating, the MFI crystals experience a weak contraction at about 175 °C (dehydration) and a strong contraction in the temperature range 275-500 °C (template removal). Instead, the α-alumina support expands which results in a difference in the expansion coefficients K_T of the two phases inducing thermal stress in the composite. In the case of a relatively thick film (b1), the thermal stress is released mainly via crack formation. In addition, part of the stress is also released via formation of structural defects in the α-alumina support. Despite the formation of cracks, the thick zeolite film is not completely relaxed as a tensile stress is present in the film also at room temperature (Figure 6). In the case of a thin film (b2), less or no stress develops and the grain boundaries are opened, as also suggested by Dong et al. [8]. In fact, defect distribution calculations for this type of membrane showed that defects with a width of a few nanometers are present [30]. These nano-defects are probably open grain boundaries formed during calcination, according to our model. The type of defects (cracks or open grain boundaries) formed in MFI membranes during calcination should mainly be determined by the degree of intergrowth between adjacent crystals in the film. If the crystals are highly intergrown, the bonds between crystals and within crystals are equally strong and cracks may develop even within crystals (b1). Less or no intergrown crystallites should result in the formation of open grain boundaries upon calcination (b2) as also described by Dong et al. [8].

Dong et al. [8] proposed the following model for the formation of defects in α-alumina supported MFI films (about 3 μm thick): The MFI film is chemically bonded to the support after synthesis. The bonds to the support are stronger than those between the crystallites and the thermal stress imposed on the film during heating is released via opening of the grain boundaries. During cooling after template removal, the MFI zeolite framework expands while the substrate shrinks. The inter-crystallite gaps become narrower but will not return to the original size because the calcined zeolite crystallites are smaller than the as-synthesized ones. The inter-crystalline gaps in the activated α-alumina supported MFI films were suggested to constitute the non-zeolitic micropores obscuring the xylene separation performance of similar membranes [31]. This model for defect formation coincides with our model in the case of less intergrown films. However, it is important to point out that the thickness of the film is not the only possible factor responsible for the crystal intergrowth and the associated defect formation. In fact, Dong et al. [8] observed no cracks in films which were considerably thicker than the one studied here and in [1]. Therefore, the synthesis conditions are probably important. Another factor which probably has a large influence on the quality of the membrane after calcination is the type of support and its properties (grain size, degree of sintering etc). In fact, a large difference in the quality of calcined membranes was observed for MFI films prepared on porous supports of α-alumina and Yttria-doped Zirconia [8].

4. Conclusions

As-synthesized MFI membranes, which reproducibly crack during calcination, were investigated by *in-situ* diffraction experiments. In addition, *in-situ* data was collected for MFI powder and a non-coated support. The Rietveld method was used to determine the unit cell parameters as a function of temperature for

the MFI film and the powder as well as the MFI coated support and the non-coated support. Hence, the strain in the direction perpendicular to the film surface could be followed in temperature for both the MFI film and the support. In addition, the TPA^+ occupancy of the MFI film as well as the microstrain of the α-alumina support were determined for each investigated temperature. It was found that the unit cell of the MFI phase contracts during heating and the template is removed. At the same time the α-alumina support expands. Due to the thermal expansion mismatch, a thermal stress develops in the composite. The stress is released by the formation of cracks in the film. The microstrain for the α-alumina substrate increases during heating, in correspondence with the temperature range of the template removal, and remains during cooling. Such microstrain may be due to plastic deformation and subsequent strain relaxation via formation of structural defects in the support. The results presented in this work could also be used to explain the lack of cracks in thinner MFI membranes prepared in our laboratory.

5. Acknowledgements

The synchrotron experiment performed at beamline BM08 at ESRF (exp. ref. nr. 08-02-369) was granted by the Italian institutions CNR, INFM, and INFN. The authors are grateful to the Swedish Research Council as well as the foundation Blanceflor Boncompagni-Ludovisi, born Bildt for financial support to CA and MLG. Our friend Dr. M. Zapparoli is kindly acknowledged for the collection of the high resolution TEM images.

References

[1] J. Hedlund, F. Jareman, A-J. Bons and M. Anthonis, A masking technique for high quality MFI membranes, J. Membr. Sci., 222 (2003) 163.

[2] J. Dong, K. Wegner and Y.S. Lin, Synthesis of submicron polycrystalline MFI zeolite films on porous ceramic supports, J. Membr. Sci., 148 (1998) 233.

[3] Z.A.E.P Vroon, K. Keizer, A.J. Burggraaf and H. Verweij, Preparation and characterization of thin zeolite MFI membranes on porous supports, J. Membr. Sci., 144 (1998) 65.

[4] J.M. van de Graaf, F. Kapteijn and J.A. Moulijn, Permeation of weakly adsorbing components through a silicalite-1 membrane, Chem. Eng. Sci., 54 (1999) 1081.

[5] E.R. Geus and H. van Bekkum, Calcination of large MFI-type single crystals, Part 2: Crack formation and thermomechanical properties in view of the preparation of zeolite membranes, Zeolites 15 (1992) 333.

[6] O. Pachtová, M. Kocirik, A. Zikánová, B. Bernauer, S. Miachon and J.-A. Dalmon, A comparative study of template removal from silicalite-1 crystals in pyrolytic and oxidizing regimes, Micropor. Mesopor. Mater., 55 (2002) 285.

[7] M. Lassinantti Gualtieri, A.F. Gualtieri and J. Hedlund, The influence of heating rate on template removal in silicalite-1: An in situ HT-XRPD study, Micropor. Mesopor. Mater., 89 (2005) 1.

[8] J. Dong, Y.S. Lin, M.Z.-C. Hu, R.A. Peascoe and E.A. Payzant, Template-removal-associated microstructural development of porous-ceramic-supported MFI zeolite membranes, Micropor. Mesopor. Mater., 34 (2000) 241.

[9] M. Lassinantti Gualtieri, A.F. Gualtieri, J. Hedlund, F. Jareman, J. Sterte and M. Dapiaggi, Accurate measurement of the thermal expansion of MFI

zeolite membranes by *in situ* HTXRPD, In Proc. 14th International Zeolite Conference. E. van Steen et al. Eds (2004) 703.

[10] H.-K. Jeong, Z. Lai, M. Tsapatsis and J.C. Hanson, Strain of MFI crystals in membranes: An in situ synchrotron X-ray study, Micropor. Mesopor. Mater., 84 (2005) 332.

[11] R. Millini, G. Perego, D. Berti, W.O. Parker Jr. A. Carati and G. Bellussi, Structural characterization of as-synthesized B- and Ti-containing MFI-type molecular sieves, Micropor. Mesopor. Mater., 35-36 (2000) 387.

[12] M.J. den Exter, H. van Bekkum, C.J.M Rijn, F. Kapteijn, J.A. Moulijn, H. Schellevis and C.I.N. Beenakker, Stability of oriented silicalite-1 films in view of zeolite membrane preparation, Zeolites, 19 (1997) 13.

[13] C. Meneghini, G. Artioli, A. Balerna, A.F. Gualtieri, P. Norby and S. Mobilio, Multipurpose imaging-plate camera for *in situ* powder XRD at the GILDA beamline, J. Synchrotron Rad., 8 (2001) 1162.

[14] A.P. Hammersley, S.O. Svensson, M. Hanfland, A.N. Fitch and D. Häusermann, Two-dimensional detector software: from real detector to idealised image or two-theta Scan, High Pressure Res. 14 (1996) 235.

[15] A.C. Larson, R.B. von Dreele (1994) "*GSAS Generalized structure analysis system*" Laur 86-748, Los Alamos National Laboratory, Los Alamos, New Mexico.

[16] B.H. Toby, EXPGUI, a graphical user interface for GSAS, J. Appl. Cryst. 34 (2001) 210.

[17] H. van Koningsveld, H. van Bekkum and J.C. Jansen, On the location and disorder of the tetrapropylammonium (TPA) ion in zeolite ZSM-5 with improved framework accuracy, Acta Cryst., B43 (1987) 127.

[18] N.Ishizawa, T. Miyata, I. Minatio, F. Marumo and S. Iwai, A structural investigation of α-alumina at 2170 K, Acta Cryst., B36 (1980) 228.

[19] Th.H. de Keijser, E.J. Mittemeijer, and H.C.F. Rozendaal, The determination of crystallite size and lattice-strain parameters in conjunction

with the profile-refinement method for the determination of Crystal Structures, J. Appl. Cryst., 16 (1983) 309.

[20] G.K. Williamson and W.H. Hall, X-ray line broadening from filed aluminum and wolfram, Acta Metall., 1 (1953) 22.

[21] J.I. Langford, A. Boultif, J.P. Auffréic and D. Louër, The use of pattern decomposition to study the combined x-ray diffraction effects of crystallite size and stacking faults in ex-oxalate zinc oxide, J. Appl. Cryst., 26 (1993) 22.

[22] L.B. McCusker, R.B. Von Dreele, D.E. Cox, L. Louër and P. Scardi, Rietveld refinements guidelines, J. Appl. Cryst., 32 (1999) 36.

[23] M. Dapiaggi, G. Artioli and L. Petras, A newly developed high-temperature chamber for in situ x-ray diffraction: setup and calibration procedures, The Rigaku Journal, 19 (2002) 35.

[24] E.R. Geus, M.J. den Exter and H. van Bekkum, Synthesis and characterization of zeolite (MFI) membranes on porous ceramic supports, J. Chem. Soc. Faraday Trans., 88 (1992) 3101.

[25] B.L. Meyers, S.R. Ely, N.A. Kutz and J.A. Kaduk, Determination of structural boron in borosilicate molecular sieves via X-ray diffraction, J. Catal., 91 (1985) 352.

[26] M. Ohring, Materials Science of Thin Films, Academic Press, New York, 2002.

[27] M. Lassinantti, F. Jareman, J. Hedlund, D. Creaser and J. Sterte, Preparation and evaluation of thin ZSM-5 membranes synthesized in the absence of organic template molecules, Catalysis Today, 67 (2001) 109.

[28] T. Ungar and A. Borbely, The effect of dislocation contrast on x-ray line broadening: A new approach to line profile analysis, Appl. Phys. Lett., 69 (1996) 3173.

[29] Z. Suo, Fractures in thin films, in: Encyclopedia of Materials: Science and Technology, Elsevier Science, 2001, pp. 3290-3296.

[30] F. Jareman, J. Hedlund, D. Creaser and J. Sterte, Modelling of single gas permeation in real MFI membranes, J. Membr. Sci., 236 (2004) 81.

[31] K. Wegner, J. Dong and Y.S. Lin, Polycrystalline MFI zeolite membranes: xylene pervaporation and its implication on membrane microstructure, J. Membr. Sci., 158 (1999) 17.

FIGURE CAPTIONS

Figure 1 A sketch of the experimental set-up for HT-SRPD (see text for details).

Figure 2. The refined a-axis (a), c-axis (b) and unit cell volume (c) as a function of temperature for a blank α-alumina support and the MFI coated support. Data from the temperature cycle 25-500-25 °C is reported. The dashed line in each diagram represents α-alumina from the literature [23].

Figure 3. The refined a-axis (a), b-axis (b) and c-axis (c) as well as the unit cell volume (d) as a function of temperature for the MFI film as well as MFI powder in the temperature cycle 25-500-25 °C.

Figure 4. The refined TPA^+ occupancy in the MFI film as a function of temperature.

Figure 5. Thermal expansion ratio K_T of the α-alumina support (full circles) and the MFI film (empty squares) as a function of temperature.

Figure 6. The strain along different crystallographic directions in the MFI film as a function of temperature. The direction of the strain is perpendicular to the film surface. The inserted sketches show that the crystallographic planes along b are under tensile strain while the ones along a and c are under compressive strain.

Figure 7. The strain along the a- and c-direction in the MFI coated α-alumina support. The direction of the strain is perpendicular to the support surface.

Figure 8. (a) Williamson-Hall plots for the α-alumina support in the as-synthesized membrane at 25 °C (filled circles) and 500 °C (empty circles). (b) Microstrain in the α-alumina support as a function of temperature during the temperature cycle 25-500-25 °C.

Figure 9. A bright field TEM image of a specimen of the sample that underwent the *in-situ* synchrotron experiment, showing the presence of structural defects. The SAED diffraction pattern in the inset shows that the signal is transmitted by a single crystal of α-alumina.

Figure 1

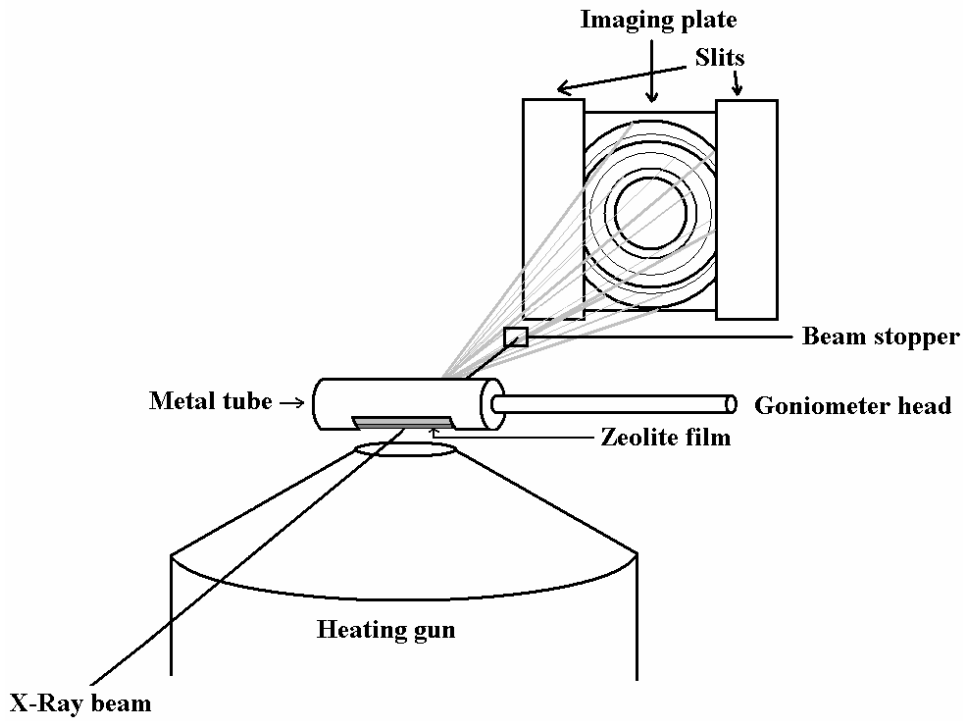
Imaging plate
Slits
Beam stopper
Metal tube →
Goniometer head
Zeolite film
Heating gun
X-Ray beam

Figure 2a

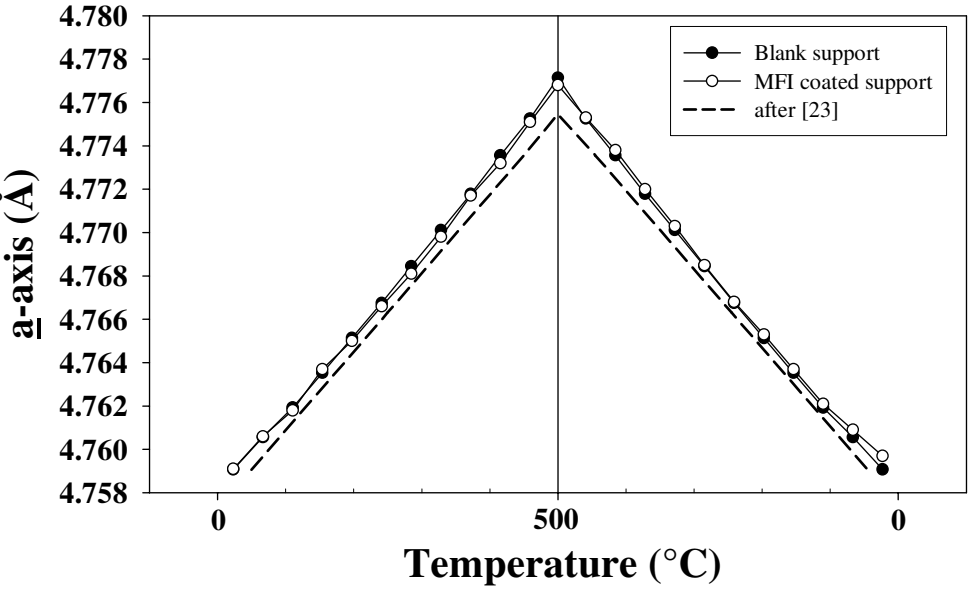
4.780
4.778
4.776
4.774
4.772
4.770
4.768
4.766
4.764
4.762
4.760
4.758
a-axis (Å)
0
500
0
Temperature (°C)
Blank support
MFI coated support
after [23]

Figure 2b

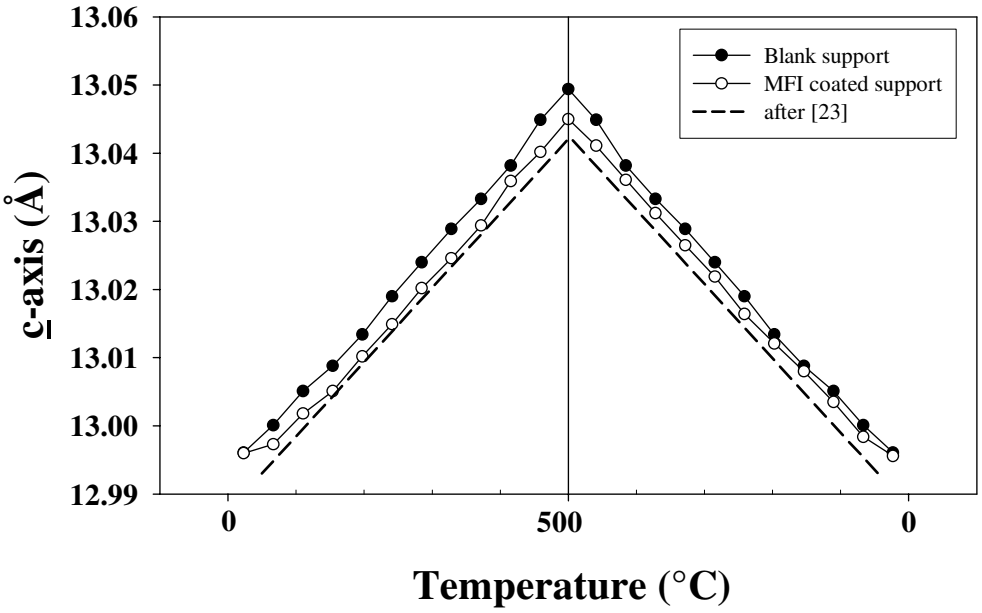
13.06
13.05
13.04
13.03
13.02
13.01
13.00
12.99
c-axis (Å)
0
500
0
Temperature (°C)
Blank support
MFI coated support
after [23]

Figure 2c

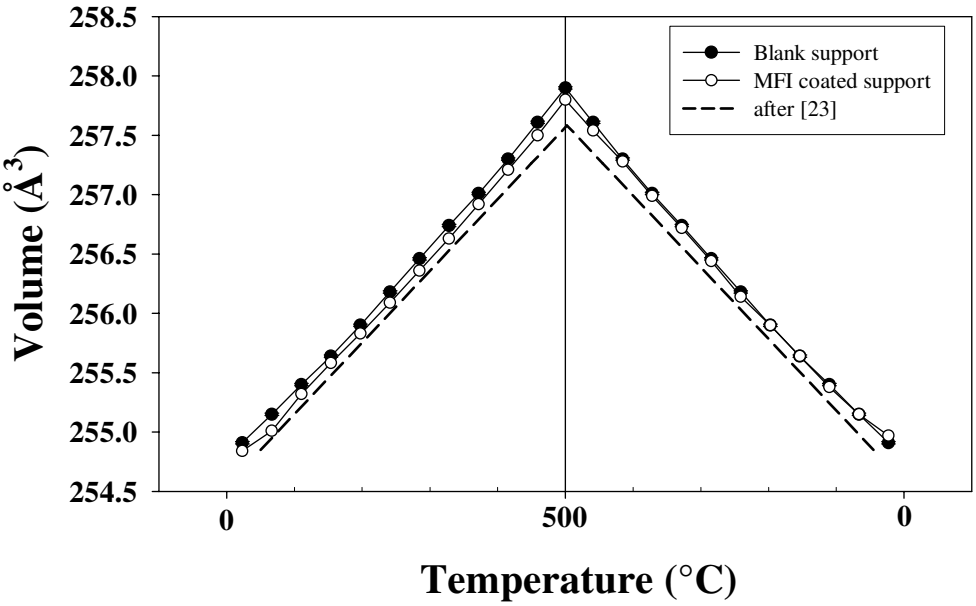
Blank support
MFI coated support
after [23]
Volume (Å^3)
258.5
258.0
257.5
257.0
256.5
256.0
255.5
255.0
254.5
0
500
0
Temperature (°C)

Figure 3a

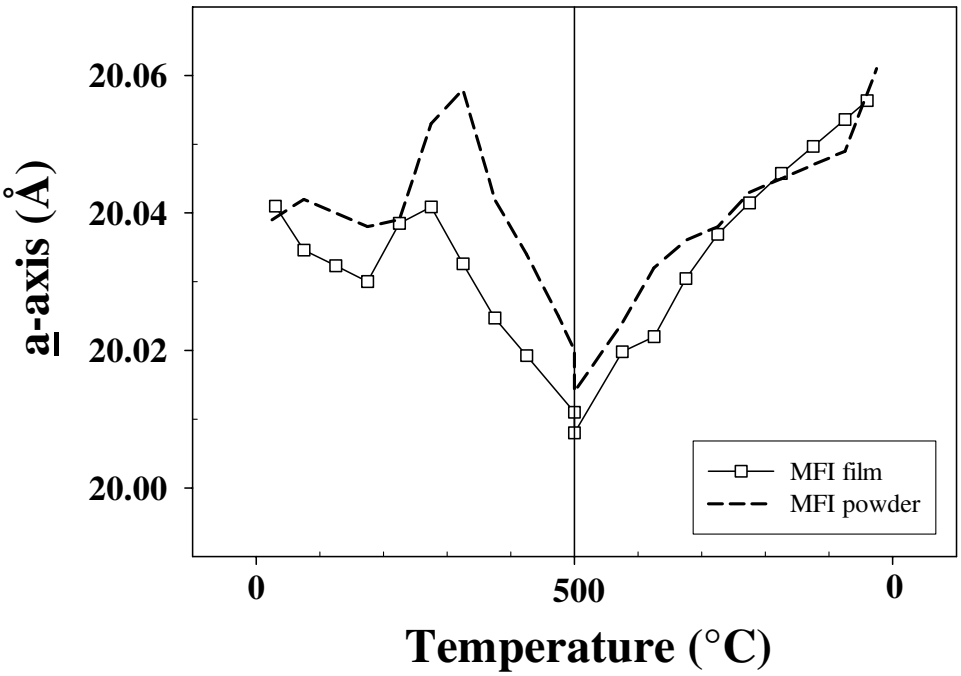
a-axis (Å)
20.06
20.04
20.02
20.00
0
500
0
Temperature (°C)
MFI film
MFI powder

Figure 3b

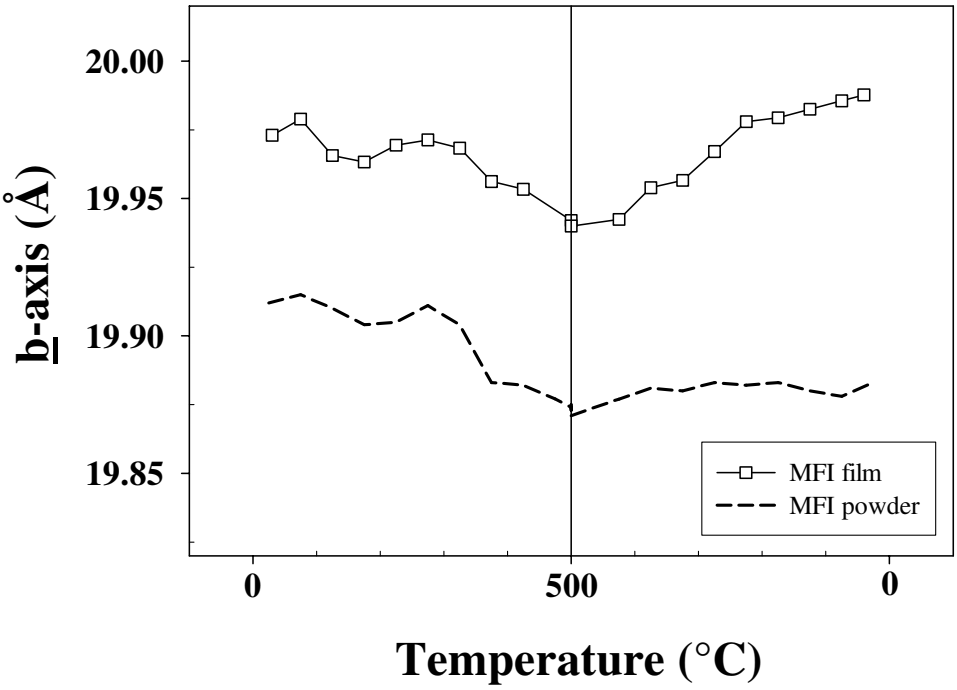
20.00
19.95
19.90
19.85
b-axis (Å)
0
500
0
Temperature (°C)
MFI film
MFI powder

Figure 3c

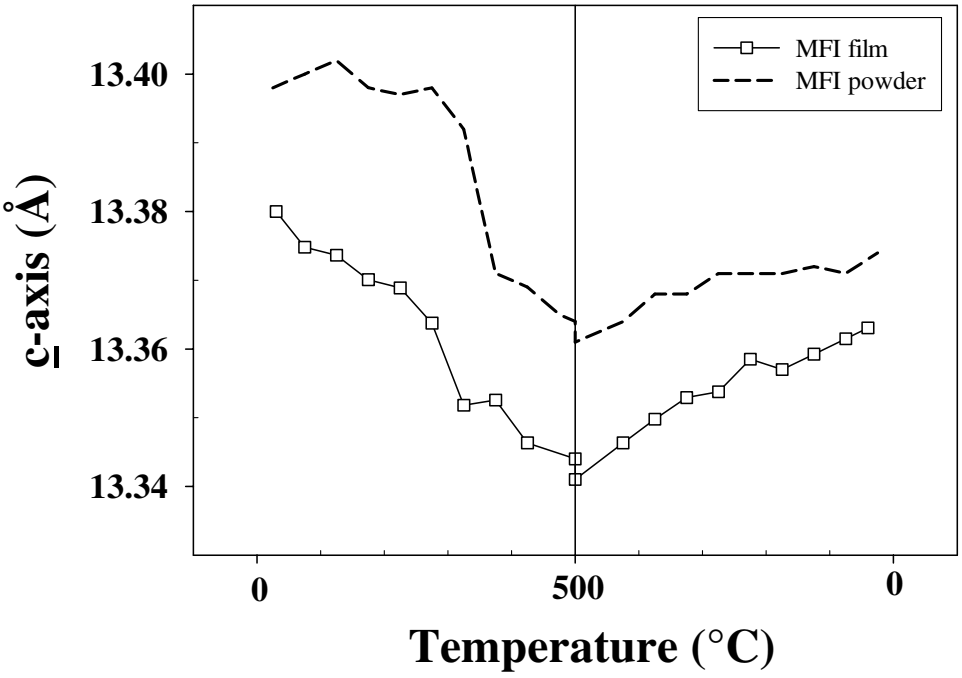
MFI film
MFI powder
13.40
13.38
13.36
13.34
c-axis (Å)
0
500
0
Temperature (°C)

Figure 3d

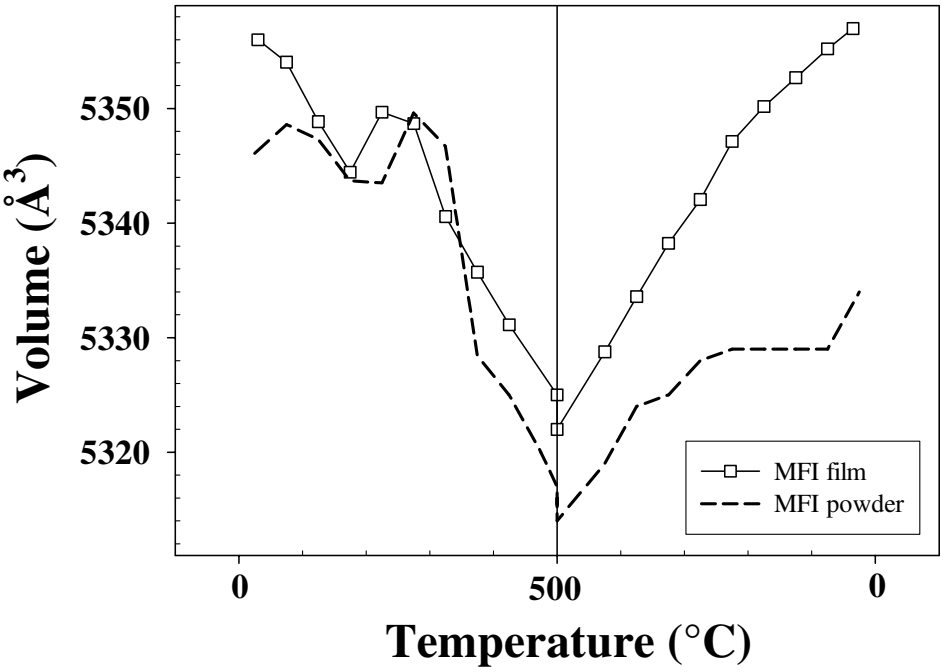
Volume (Å^3)
5350
5340
5330
5320
0
500
0
Temperature (°C)
MFI film
MFI powder

Figure 4

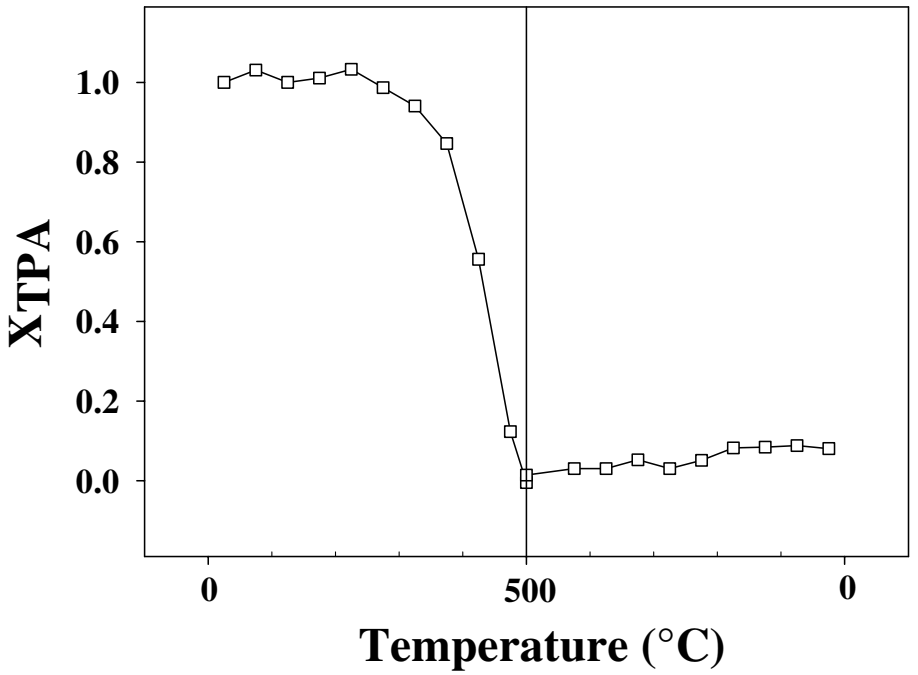

Figure 5

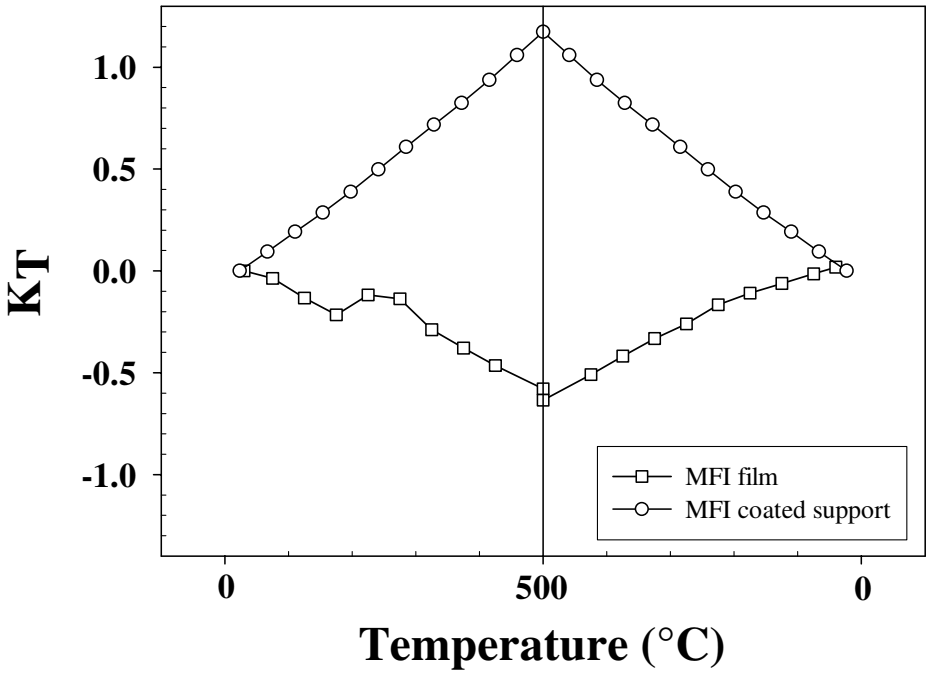
KT
1.0
0.5
0.0
-0.5
-1.0
0
500
0
Temperature (°C)
MFI film
MFI coated support

Figure 6

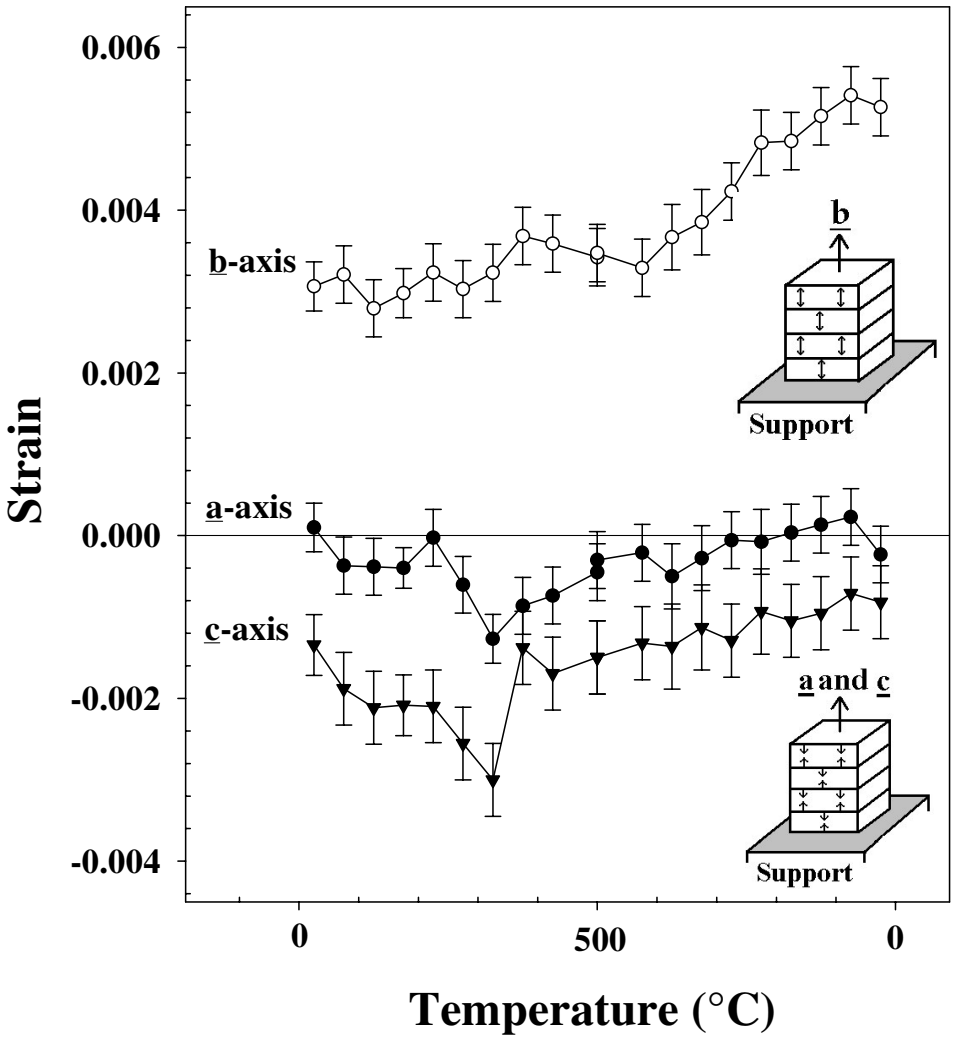
0.006
0.004
0.002
0.000
-0.002
-0.004
Strain
b-axis
a-axis
c-axis
b
Support
a and c
Support
0
500
0
Temperature (°C)

Figure 7

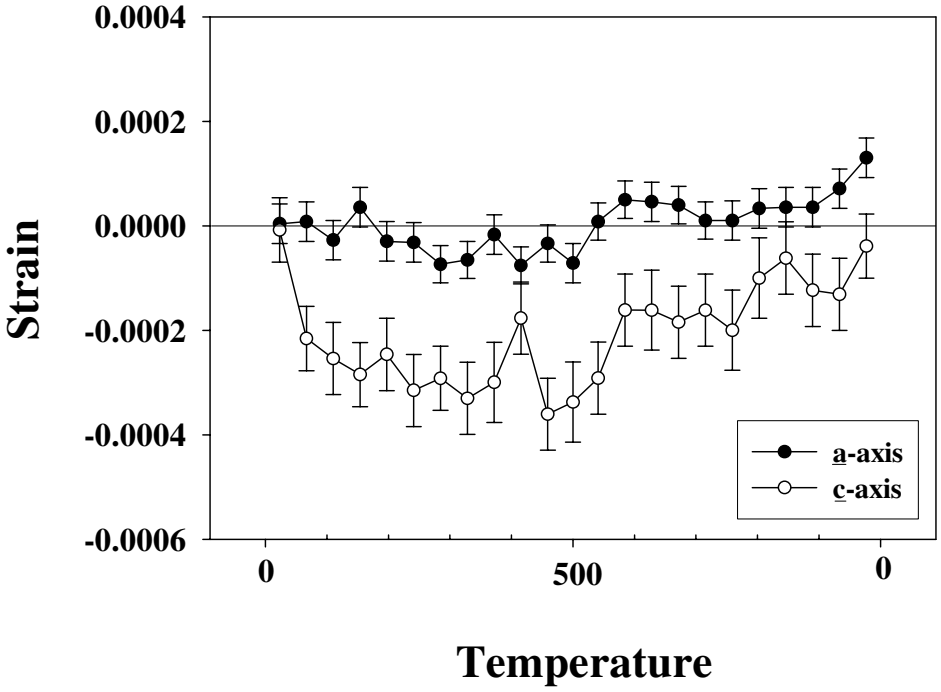
0.0004
0.0002
0.0000
-0.0002
-0.0004
-0.0006
Strain
0
500
0
Temperature
a-axis
c-axis

Figure 8a

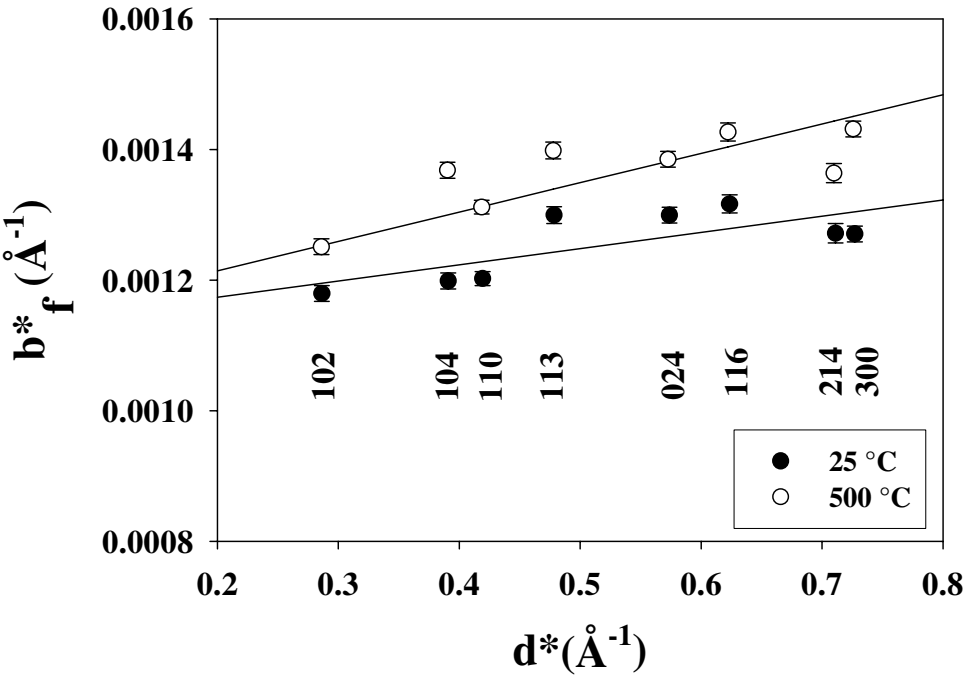
0.0016
0.0014
0.0012
0.0010
0.0008
b*f (Å-1)
0.2
0.3
0.4
0.5
0.6
0.7
0.8
d*(Å-1)
102
104
110
113
024
116
214
300
25 °C
500 °C

Figure 8b

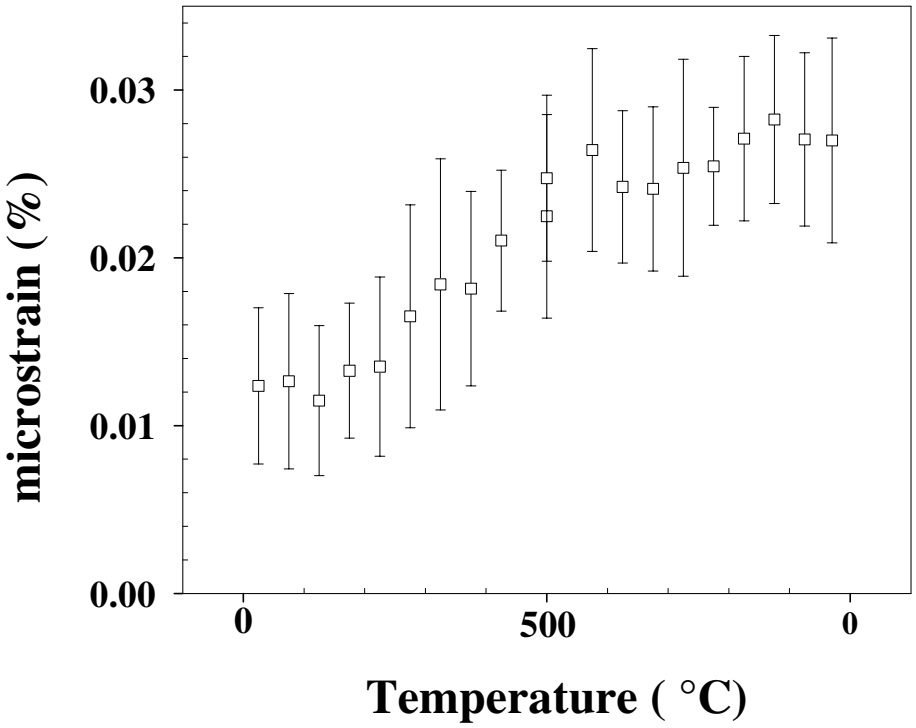

Figure 9